

NDOT Research Report

Report No: RDT 97-020

**PERMEABILITY CHANGES in
SOIL DUE TO FILL LOADING
and its EFFECT on the
GROUNDWATER FLOW
REGIME**

August 2001

Prepared by Research Division
Nevada Department of Transportation
1263 South Stewart Street
Carson City, Nevada 89712



TECHNICAL REPORT DOCUMENTATION PAGE

Report No. RDT 97-020		2. Government Accession No.	3. Recipient-s Catalog No.
4. Title and Subtitle Permeability Changes in Soil Due to Fill Loading and its Effect on the Groundwater Flow Regime		5. Report Date May 1997	
		6. Performing Organization Code	
7. Author(s) Gary Norris, Sherif Elfass, Rob Valceschini		8. Performing Organization Report No.	
9. Performing Organization Name and Address Department of Civil Engineering College of Engineering University of Nevada, Reno Reno, Nevada 89557		10. Work Unit No.	
		11. Contract or Grant No. P464-93-028	
12. Sponsoring Agency Name and Address Nevada Department of Transportation Research Division 1263 South Stewart Carson City, Nevada 89712		13. Type or Report and Period Covered July 1993 - To February 1997	
		14. Sponsoring Agency Code NDOT	
15. Supplementary Notes			
<p>16. Abstract</p> <p>The purpose of this research was to evaluate the need for a coupled field-lab test-analytical modeling program to successfully predict changes in the near surface groundwater flow conditions that occur as the result of planned highway fill construction. The study was proposed with the prospect of using the Zolezzi Lane site of the US 395 Extension as a test case. There is a controlling artesian layer that underlies the site at approximately twenty-foot depth that is fed from the west by snowmelt from the Carson Range. From piezometer reading from various depths along an east-west cross section at station 557+00 taken over a two year time span (one-half year before to one year after construction), it is clear that no change (beyond the six foot seasonal variation in water level) took place in the near surface soil of this alluvial deposit as the result of the construction of the north-south extension of US 395. Therefore, it is concluded that there is no particular need for such a coupled analysis in similar (cohesionless) soil and groundwater conditions. (However, there may still be a need to take piezometer reading to establish, from a legal standpoint that is only seasonal variations that occur.) A study of this type is still recommended for a cohesive soil site.</p> <p>However, during the course of the investigation there were a number of interesting and perplexing developments that occurred. It is these aspects that the report struggles to bring to light. Some of these issues are:</p> <ul style="list-style-type: none"> • The misinterpretation of soil type employing standard CPT data reduction and contradiction of said information with CPT piezo readings. • The very conservative (i.e. low) relative density and friction angle values obtained from CPT and SPT blow count correlations as compared with independent field density and lab strength determinations. • The disparate permeability values obtained from different field and lab tests. • The short lived two foot (or less) drop in piezometer water level (due to dilatant soil response) in piezometer readings immediately beneath the fill rather than the anticipated thirty to sixty foot rise (in a compressible soil) due to fill construction. <p>It is recommended that comparison of SPT/CPT assessed density and strength values with independently determined data be undertaken. Certainly such low blow count values are indicative of possible liquefaction and failure of the embankment over such loose cohesion less material and yet piezometer readings and undrained triaxial tests indicated a stable dilatant material.</p>			
17. Key Words Surface Groundwater Flow, Water Level, Dilatant Soil, Liquefaction of embankment		18. Distribution Statement Unrestricted. This document is available through the National Technical Information Service, Springfield, VA 21161	
19. Security Classif is report) Unclassified	20. Security Classif. (of this page) Unclassified	21. No. Of Pages 285	22. Price

NDOT Research Report

Report No: RDT 97-020

**PERMEABILITY CHANGES in
SOIL DUE TO FILL LOADING
and its EFFECT on the
GROUNDWATER FLOW
REGIME**

August 2001

Prepared by Research Division
Nevada Department of Transportation
1263 South Stewart Street
Carson City, Nevada 89712



TECHNICAL REPORT DOCUMENTATION PAGE

Report No. RDT 97-020	2. Government Accession No.	3. Recipient's Catalog No.
4. Title and Subtitle Permeability Changes in Soil Due to Fill Loading and its Effect on the Groundwater Flow Regime	5. Report Date May 1997	
	6. Performing Organization Code	
7. Author(s) Gary Norris, Sherif Elfass, Rob Valceschini	8. Performing Organization Report No.	
9. Performing Organization Name and Address Department of Civil Engineering College of Engineering University of Nevada, Reno Reno, Nevada 89557	10. Work Unit No.	
	11. Contract or Grant No. P464-93-028	
12. Sponsoring Agency Name and Address Nevada Department of Transportation Research Division 1263 South Stewart Carson City, Nevada 89712	13. Type or Report and Period Covered July 1993 - To February 1997	
	14. Sponsoring Agency Code NDOT	
15. Supplementary Notes		
<p>16. Abstract</p> <p>The purpose of this research was to evaluate the need for a coupled field-lab test-analytical modeling program to successfully predict changes in the near surface groundwater flow conditions that occur as the result of planned highway fill construction. The study was proposed with the prospect of using the Zolezzi Lane site of the US 395 Extension as a test case. There is a controlling artesian layer that underlies the site at approximately twenty-foot depth that is fed from the west by snowmelt from the Carson Range. From piezometer reading from various depths along an east-west cross section at station 557+00 taken over a two year time span (one-half year before to one year after construction), it is clear that no change (beyond the six foot seasonal variation in water level) took place in the near surface soil of this alluvial deposit as the result of the construction of the north-south extension of US 395. Therefore, it is concluded that there is no particular need for such a coupled analysis in similar (cohesionless) soil and groundwater conditions. (However, there may still be a need to take piezometer reading to establish, from a legal standpoint that is only seasonal variations that occur.) A study of this type is still recommended for a cohesive soil site.</p> <p>However, during the course of the investigation there were a number of interesting and perplexing developments that occurred. It is these aspects that the report struggles to bring to light. Some of these issues are:</p> <ul style="list-style-type: none"> • The misinterpretation of soil type employing standard CPT data reduction and contradiction of said information with CPT piezo readings. • The very conservative (i.e. low) relative density and friction angle values obtained from CPT and SPT blow count correlations as compared with independent field density and lab strength determinations. • The disparate permeability values obtained from different field and lab tests. • The short lived two foot (or less) drop in piezometer water level (due to dilatant soil response) in piezometer readings immediately beneath the fill rather than the anticipated thirty to sixty foot rise (in a compressible soil) due to fill construction. <p>It is recommended that comparison of SPT/CPT assessed density and strength values with independently determined data be undertaken. Certainly such low blow count values are indicative of possible liquefaction and failure of the embankment over such loose cohesion less material and yet piezometer readings and undrained triaxial tests indicated a stable dilatant material.</p>		
17. Key Words Surface Groundwater Flow, Water Level, Dilatant Soil, Liquefaction of embankment	18. Distribution Statement Unrestricted. This document is available through the National Technical Information Service, Springfield, VA 21161	
19. Security Classif is report) Unclassified	20. Security Classif. (of this page) Unclassified	21. No. Of Pages 285
		22. Price

ACKNOWLEDGMENT

This project was originally suggested to the authors by Ted Beeston, Head of the Geotechnical Section of NDOT, now retired. The supervision of this project was continued by Parviz Noori, Head of the Materials Division, and Alan Hilton, Manager of Research/Special Studies of NDOT. Their collective interest, assistance and ultimate patience is greatly appreciated.

Professor Raj Siddharthan and graduate students Hernan Perez, Jeffrey Palmer, Raghu Madhu, Mitch Burns, Mike Fordham, Frank Blackett, Mohamed Ashour, and Tung Nguyen all contributed to the project work. Their assistance was invaluable.

Mark Best from Pioneer Drilling helped with well installation on his own time in addition to the contracted piezocone work. His efforts are greatly appreciated.

Lastly, the senior author would like to thank audiences from AEG Great Basin and Southwest sections, Army Corps of Engineers at Vicksburg, Caltrans and NDOT for feedback from oral presentations of the material at technical meetings in a time span between draft and final versions of the report. Questions that were asked lead to considerable thought in fine tuning the content of the report.

TABLE OF CONTENTS

CHAPTER 1	1
INTRODUCTION	1
1.1. PREMISE OF CURRENT STUDY.....	1
1.2. FIELD STUDY SITE	3
1.3. OUTLINE OF SUCCEEDING CHAPTERS	5
CHAPTER 2	14
GENERAL FIELD AND LABORATORY WORK	14
2.1. PROPOSED APPROACH	14
2.2. PRE CONSTRUCTION FIELD WORK.....	16
2.2.1. <i>Installing Piezometers</i>	16
2.2.2. <i>Standard Penetration Testing</i>	19
2.2.3. <i>Well Installation</i>	20
2.2.4. <i>Cone Penetration Test</i>	21
2.2.5. <i>Monitoring the Piezometric Surface</i>	21
2.2.6. <i>In Place Hydraulic Conductivity</i>	22
2.3. DURING CONSTRUCTION.....	23
2.4. LABORATORY WORK	25
2.4.1. <i>Standard Geotechnical Tests</i>	26
2.4.2. <i>Field Density</i>	26

2.4.3. Specific Gravity and Water Content27

2.4.4. Particle Size Analysis28

2.4.5. Atterberg Limits29

2.4.6. Maximum and Minimum Dry Unit Weight and Void Ratio.....29

2.4.7. Consolidation Test.....30

2.5. SUMMARY31

CHAPTER 3.....55

LABORATORY TRIAXIAL HYDRAULIC CONDUCTIVITY TESTS.....55

3.1. HYDRAULIC CONDUCTIVITY55

3.2. SAMPLE PREPARATION55

3.3. SATURATION.....57

3.4. STRESS APPLICATION60

3.5. EQUIPMENT62

3.5.1. Stress Path62

3.5.2. Hydraulic Conductivity.....63

3.5.2.1. GDS.....63

3.5.2.2. Permeability Board.....64

3.6. HORIZONTAL HYDRAULIC CONDUCTIVITY65

3.7. HORIZONTAL HYDRAULIC CONDUCTIVITY TESTS67

3.8. SUMMARY70

CHAPTER 4.....74

FIELD HYDRAULIC CONDUCTIVITY TESTS	74
4.1. FIELD TESTS	74
4.2. CPT DISSIPATIONS	74
4.3. SLUG TEST.....	75
4.4. BAILING TEST.....	77
4.5. SUMMARY	78
CHAPTER 5.....	82
ANALYTICAL MODELING.....	82
5.1. STRESS MODELING	82
5.1.1. The Model.....	84
5.1.2. Initial Stresses	86
5.1.3. Embankment Loading Model	88
5.1.4. Results.....	89
5.2. SEEPAGE MODELING.....	90
5.2.1. The Model.....	91
5.2.2. Summary.....	92
CHAPTER 6.....	97
PIEZOMETRIC READINGS AND THEIR IMPLICATIONS.....	97
6.1. PREVIEW.....	97
6.2. PIEZOMETRIC READINGS AND THEIR IMPLICATION	97

6.3. SMALL CHANGES.....	101
6.4. SUMMARY	103
CHAPTER 7.....	127
COMPARISON OF LAB AND FIELD EVALUATION OF IN SITU STRENGTH AND DENSITY.....	127
7.1. OVERVIEW.....	127
7.2. COMPARISON FOR SAMPLES 1-4	128
7.3. CPT.....	129
7.4. SPT.....	132
7.5. LAB TRIAXIAL TEST STRENGTH.....	132
7.6. BROADER COMPARISON	141
7.7. OTHER LAB DATA	146
7.8. SUMMARY	148
CHAPTER 8.....	171
LAB AND FIELD PERMEABILITY TEST RESULTS	171
8.1. OVERVIEW.....	171
8.2. LAB TESTS.....	171
8.3. FIELD TESTS	174
8.4. LAB TESTS ON RECONSTITUTED SAMPLES AND GENERAL CONCLUSIONS.....	177
8.5. DISCUSSION.....	178

CHAPTER 9	184
FINITE ELEMENT AND STRESS PATH ANALYSIS	184
9.1. OVERVIEW.....	184
9.2. FINITE ELEMENT.....	184
9.3. STRESSES.....	189
9.4. SETTLEMENT.....	196
9.5. STRESS PATH TESTING.....	205
9.6. DISCUSSION.....	217
CHAPTER 10	231
CONCLUSIONS AND RECOMMENDATIONS	231
10.1. PROJECT RESPONSE AT A GLANCE.....	231
10.2. LESSONS LEARNED.....	232
10.3. IMPLEMENTATION AT FUTURE SITES.....	236
REFERENCES	238

APPENDICIES

APPENDIX 1	
Boring Logs for The Eight Holes Logged By NDOT.....	241
APPENDIX-2	
Interpreted Logs for the CPT Readings	252
APPENDIX-3	
Sample Test Data of In Place Hydraulic Conductivity Tests.....	257
APPENDIX-4	
A Complete Logging Description of Continuous Clear Tube Sample Obtained from Pz4 Location at a Depth of 8 to 21 ft.	260
APPENDIX-5	
Mathmatical Proof for the Equation Used In Calculating The Horizontal Hydraulic Conductivity.....	262
APPENDIX-6	
A Trial to Separate The Horizontal From The Vertical Hydraulic Conductivity Using The Faling Head Test Data.....	267
APPENDIX-7	
Initial Stress Conditions fr Various Elements for The Different Groundwater Conditions	270
APPENDIX-8	
Portion of FEADAM Output of The Stresses for The Undrained Case (All Layers Undrained Except for The Artesian).....	282
APPENDIX-9	
Portion of FEADAM Output of The Stresses for The Undrained Case (All Layers Below The Artesian Are Undrained)	***
APPENDIX-10	
Boring Log for The NDOT Sampling Operation Done on 9/11/96.....	***

LIST OF TABLES

TABLE 1.1	DESCRIPTION FROM THE SCS WASHOE COUNTY, NEVADA, SOUTH PART, P. 103	7
TABLE 1.2	DESCRIPTION FROM THE SCS WASHOE COUNTY, NEVADA, SOUTH PART, P. 264	8
TABLE 1.3	ENGINEERING INDEX AND PHYSICAL AND CHEMICAL PROPERTIES OF THE ROSE CREEK SERIES, WASHOE COUNTY, NEVADA, SOUTH PART, P.513	9
TABLE 2.1	PIEZOMETER LOCATIONS	32
TABLE 2.2	SOIL SAMPLE LOCATIONS	33
TABLE 2.3	STANDARD PENETRATION TESTING LOCATIONS	34
TABLE 2.4	FIELD DENSITY RESULTS	34
TABLE 2.5	SUMMARY OF THE SOIL PROPERTIES FOR EIFFERENT SAMPLES	35
TABLE 2.6	MAXIMUM AND MINIMUM DRY UNIT WEIGHT AND VOID RATIOS.....	36
TABLE 2.7	CONSOLIDATION TEST RESULTS.....	36
TABLE 4.1	PERMEABILITY VALUE RESULTING FROM CPT DISSIPATIONS	79
TABLE 5.1	PARAMETERS AND VALUES USED IN FEADAM MODEL	93
TABLE 5.2	RESULTS OF THE SENSITIVITY STUDY	94
TABLE 7.1	COMPARISON OF CPT, SPT AND LAB TEST STRENGTHS FOR SAMPLES 1-4	150
TABLE 7.2	DATA FROM TRIAXIAL TESTS FOR STRENGTH	151
TABLE 7.3	CORRELATIONS FROM SPT BLOW COUNTS	154
TABLE 7.4	COMPARISON OF SPT AND CPT, D, AND ϕ	155

TABLE 7.5	COMPARISON OF RANGE IN D_r FROM CPT AND LAB VOID RATIO.....	155
TABLE 8.1	PERMEABILITY RESULTS	181
TABLE 9.1	UNDRAINED AND DRAINED STRAINS AND SETTLEMENTS.....	220

LIST OF FIGURES

FIGURE 1.1	SITE MAP	10
FIGURE 1.2	MT. ROSE NE QUADRANGLE GEOLOGIC MAP	11
FIGURE 1.3	GENERAL DIRECTION OF GROUNDWATER MOVEMENT IN THE TRUCKEE MEADOWS (GATES AND WATTERS, 1992).....	12
FIGURE 1.4	SCS WASHOE COUNTY SOUTH PART, PART OF SHEETS 27 AND 28.....	13
FIGURE 2.1	ZOLEZZI LANE MAP FROM NDOT PLANS.....	37
FIGURE 2.2	VERTICAL CROSS SECTION SHOWING THE PIEZOMETER DEPTHS.....	38
FIGURE 2.3	PIEZOMETER INSTALLED IN THE BOREHOLE	39
FIGURE 2.4	LOCATION AND PROFILE FOR WELLS 1 AND 2.....	40
FIGURE 2.5	LOCATION AND PROFILE FOR WELL 3	41
FIGURE 2.6A	PIEZO CONE PLOTS FOR Pz3	42
FIGURE 2.6B	PIEZO CONE PLOTS FOR Pz4.....	43
FIGURE 2.6C	PIEZO CONE PLOTS FOR Pz5.....	44
FIGURE 2.6D	PIEZO CONE PLOTS FOR Pz6	45
FIGURE 2.7A	NDOT B1	46
FIGURE 2.7B	NDOT B2	47
FIGURE 2.8A	GRAIN SIZE CURVE FOR WELL 1 (D=5 FT), $D_{50}=0.10$ mm, $C_u=14$	48
FIGURE 2.8B	GRAIN SIZE CURVE FOR Pz3 (D=10 FT), $D_{50}=0.19$ mm, $C_u=10$	48
FIGURE 2.8C	GRAIN SIZE CURVE FOR WELL 2 (D=10 FT), $D_{50}=0.20$ mm, $C_u=13$	49
FIGURE 2.8D	GRAIN SIZE CURVE FOR WELL 2 (D=2 FT), $D_{50}=0.43$ mm, $C_u=8$	49
FIGURE 2.8E	GRAIN SIZE CURVE FOR WELL 2 (D=17.5 FT), $D_{50}=0.11$ mm, $C_u=6$	50

FIGURE 2.8F GRAIN SIZE CURVE FOR PZ4 (D=17.5 FT), $D_{50}=0.11$ mm, $C_u=6$	50
FIGURE 2.8G GRAIN SIZE CURVE FOR PZ4 (D=12 FT), $D_{50}=0.28$ mm, $C_u=11$	51
FIGURE 2.8H GRAIN SIZE CURVE FOR PZ4 (D=21.5 FT), $D_{50}=0.13$ mm, $C_u=10$	51
FIGURE 2.8I GRAIN SIZE CURVE FOR PZ4 (D=14.5 FT), $D_{50}=0.20$ mm, $C_u=10$	52
FIGURE 2.8J GRAIN SIZE CURVE FOR PZ3 (D=8.5 FT), $D_{50}=0.26$ mm, $C_u=7$	52
FIGURE 2.8K GRAIN SIZE CURVE FOR WELL 2 (D=8.5 FT), $D_{50}=0.26$ mm, $C_u=7$	53
FIGURE 2.8L GRAIN SIZE CURVE FOR PZ4 (D=21.5 FT), $D_{50}=0.13$ mm, $C_u=10$	53
FIGURE 2.9 STANDARD CONSOLIDATION DATA CURVE	54
FIGURE 3.1 TRIAXIAL TEST SET-UP FOR A) VERTICAL AND B) HORIZONTAL PERMEABILITY ASSESMENTS	71
FIGURE 3.2 A SCHEMATIC SKETCH OF PERMEABILITY BOARD	72
FIGURE 3.3 PERMEABILITY IN LAYERED SOIL	73
FIGURE 4.1 CONE DISSIPATION PLOT	80
FIGURE 4.2 AVERAGE VALUES OF LABORATORY DERIVED HORIZONTAL COEFFICIENT OF PERMEABILITY (k_h) AND CPTU t_{50} FOR U_2 PORE PRESSURE LOCATION (CONETEC INVESTIGATIONS LTD., 1990)	80
FIGURE 4.3 ANALYSIS OF PERMEABILITY BY VARIABLE HEAD TEST (DM-7)	81
FIGURE 5.1 SUBSURFACE AND ITS FINITE ELEMENT MESH	95
FIGURE 5.2A EMBANKMENT CROSS SECTION	96
FIGURE 5.2B FINITE ELEMENT MESH WITH EMBANKMENT	96
FIGURE 6.1 PZ1 READINGS	104
FIGURE 6.2 PZ2 READINGS	105
FIGURE 6.3 PZ3A READINGS	106
FIGURE 6.4 PZ3B READINGS	107

FIGURE 6.5	Pz3C READINGS	108
FIGURE 6.6	Pz4A READINGS	109
FIGURE 6.7	Pz4B READINGS	110
FIGURE 6.8	Pz4C READINGS	111
FIGURE 6.9	Pz4D READINGS	112
FIGURE 6.10	Pz5A READINGS	113
FIGURE 6.11	Pz5B READINGS	114
FIGURE 6.12	Pz5C READINGS	115
FIGURE 6.13	Pz6 READINGS	116
FIGURE 6.14	Pz7 READINGS	117
FIGURE 6.15	Pz8 READINGS	118
FIGURE 6.16	Pz2, Pz7 AND Pz8 READING PROFILES	119
FIGURE 6.17	Pz3A AND Pz4A READING PROFILES	120
FIGURE 6.18	Pz3A, Pz3B AND Pz3C READING PROFILES	121
FIGURE 6.19	Pz4A, Pz4B AND Pz4C READING PROFILES	122
FIGURE 6.20	Pz5A, Pz5B AND Pz5C READING PROFILES	123
FIGURE 6.21	Pz3C, Pz4C AND Pz6 READING PROFILES	124
FIGURE 6.22	ZONE OF FILL INDUCED NEGATIVE POREWATER PRESSURES	125
FIGURE 6.23	LATERAL DISTRIBUTION OF EXCESS POREWATER PRESSURE- TICKTON	126
FIGURE 7.1	CORRELATION BETWEEN GRAIN SIZE AND RATIO OF CONE BEARING AND STANDARD PENETRATION TEST RESISTANCE (AFTER ROBERTSON AND CAMPANELLA, 1983	156

FIGURE 7.2	CORRELATION BETWEEN DRAINED OR EFFECTIVE STRESS FRICTION ANGLE FROM STANDARD TRIAXIAL TESTS AND VOID RATIO.....	157
FIGURE 7.3	FRICTION ANGLE VERSUS VOID RATIO FOR SEVERAL GRANULAR SOILS FROM LAMBE AND WHITMAN (1969) WITH SUPERPOSED FIG. 7.2 RESULTS	158
FIGURE 7.4	PORE PRESSURE CURVES FOR UNDRAINED TESTS	159
FIGURE 7.5	NORMALIZED STRESS VERSUS STRAIN CURVES	160
FIGURE 7.6	DRAINED VOLUME CHANGE CURVES	161
FIGURE 7.7	ESTIMATION OF ϵ_{50} AS A FUNCTION OF e AND C_u	162
FIGURE 7.8	COMPARISON OF STANDARD TEST AND K_0 CONSOLIDATION TEST SHEAR RESPONSE	163
FIGURE 7.9	UNDRAINED TEST STRESS - STRAIN CURVES.....	164
FIGURE 7.10	DRAINED AND UNDRAINED EFFECTIVE STRESS PATHS FOR THE RECONSTITUTED SAMPLES 7 AND 8.....	165
FIGURE 7.11	ESTIMATED COMPACTNESS OF SAND FROM STANDARD PENETRATION TEST (DM-7).....	166
FIGURE 7.12	CORRELATIONS OF STRENGTH CHARACTERISTICS FOR GRANULAR SOILS (DM-7).....	166
FIGURE 7.13	CORRELATIONS OF N VALUES WITH SAND PARAMETERS (PH&T).....	167
FIGURE 7.14	STANDARD ONE - DIMENSIONAL AND K_0 CONSOLIDATION CURVES.....	168
FIGURE 7.15	ISOTROPIC CONSOLIDATION CURVES.....	169
FIGURE 7.16	CORRELATION BETWEEN STANDARD WATER CONTENT OR VOID RATIO AND PERCENT FINES	170
FIGURE 8.1	POSSIBLE MATERIAL VARIATION BASED ON CPT LOG INTERPRETATION.....	182
FIGURE 8.2	PERMEABILITY TEST DATA FROM LAMBE AND WHITMAN (1969).....	183

FIGURE 9.1	LOCATION OF ELEMENTS 302 AND 303 WITHIN THE FINITE ELEMENT MESH	221
FIGURE 9.2	POSSIBLE PORE PRESSURES AND UNDRAINED EFFECTIVE STRESS CIRCLES	222
FIGURE 9.3	PRESUMED A) STRESS AND B) COUNTERACTING VOLUME CHANGE RESPONSES (PZ4 AT 10 FT.) DUE TO UNDRAINED LOADING.....	223
FIGURE 9.4	PRESUMED STRESS CHANGES GOING FROM INITIAL (LEVEL GROUND) TO THE UNDRAINED TO THE DRAINED FILL LOADING CASE AT PZ4 AT 10 FT.	224
FIGURE 9.5	DRAINED CONDITIONING OF THE UNDISTURBED SAMPLE 12 PRIOR TO UNDRAINED TESTING.....	225
FIGURE 9.6	STRESS PATH SAMPLE RESPONSE DURING CONDITIONING PHASE	226
FIGURE 9.7	STRESS PATH SAMPLE RESPONSE DURING UNDRAINED LOADING	227
FIGURE 9.8	UNDRAINED STRENGTH AND STRESS LEVEL	228
FIGURE 9.9	UNDRAINED TO DRAINED FILL LOADING	229
FIGURE 9.10	DRAINED LOADING TO FAILURE	230

Chapter 1

Introduction

1.1. Premise of Current Study

A question arises as to the capability of the engineering profession to successfully predict changes in the near surface groundwater flow condition that occur as the result of planned highway fill construction. A case in point is the groundwater flow in a flat, grass covered, alluvial deposit underlain by a shallow gravelly artesian layer that is fed by spring snow melt from the Carson Range. The purpose of this research is to evaluate the need for a coupled field - lab test - analytical model to approach such prediction. The study was proposed with the prospect of using the Zolezzi Lane site of the US 395 Extension as a test case.

Currently, the geotechnical group of a highway department conducts a field investigation, performs laboratory tests, and undertakes an analysis with the objective of assessing the stability and settlement associated with planned or proposed highway fill construction. Given the desire to also assess changes in the near surface groundwater flow condition, the issue is whether this can be accomplished by simply performing additional field and laboratory work and undertaking a separate flow or seepage analysis. In this regard, the question is

how involved or coupled this work would have to be. In other words, could the test program be successfully accomplished by performing permeability tests in the field or in the lab on a few additional samples taken during field exploration and then the results applied in an independent seepage analysis, or would sample location, in situ tests, lab test setup and test pressures depend upon knowledge of the deformational and stability analysis results ahead of time. As is the nature of most Department of Transportation (DOT) work, different groups will work on a segment of a project, but each group will perform its work independently and pass its information on to the next group with little feedback from those that employ that information. While the work proposed here would be carried out entirely by the Geotechnical / Materials group, the question is whether the information required for such assessment can be carried out using information obtained during the exploratory subsurface investigation and the initial laboratory testing phase or whether a subsequent detailed field sampling / testing and laboratory test program would be required, one that can only be fashioned after first studying the results of analytical studies that are based on the exploratory work and standard lab test data as input. In other words, would a feedback loop be required as part of a coupled investigation.

Given this question, it was proposed by the Nevada Department of Transportation (NDOT) that a field case study be initiated with the stated objective

of ascertaining the need for undertaking a coupled field - lab - analytical program to assess changes in groundwater flow conditions resulting from highway fill construction.

1.2. Field Study Site

The Zolezzi Lane site along the extension of US 395 was proposed and accepted as a suitable field study site. See Fig. 1.1. At the start of this research project, there had been no construction at Zolezzi Lane, only staking, and there would be a half year's time span to establish seasonal piezometer readings before fill construction reached that location.

As shown on the geologic map for the Mt. Rose NE Quadrangle (Nevada Bureau of Mines and Geology, 1983), Zolezzi Lane east of South Virginia (old US 395) and its extension falls in a region of Quaternary alluvial bajada deposits (Qa). See Fig. 1.2. Such deposits are described on the geologic map as "thin sheet-like aprons of fine- to medium-grained clayey sand and intercalated muddy, medium pebble gravel; deposits of low gradient streams that are reworked older gravelly outwash and alluvial fan deposits; weakly weathered and largely undissected with little or no soil development (entisols)".

Figure. 1.3 taken from the "Geology of Reno and Truckee Meadows, Nevada" (Gates and Watters, 1992) shows that groundwater movement in the

Truckee Meadows region is at a near right angle to South Virginia Ave. and, therefore, virtually perpendicular to the planned alignment of the US 395 Extension. From the geologic map (Fig. 1.2), note that the deposit occurs immediately east of two channels of White's creek. As shown on the soils map (part of sheet 27 and 28) of the "Soil Survey of Washoe Co., South Part" (SCS, 1983) of Fig. 1.4, the northern channel of White's Creek feeds the agricultural ditch that passes through the west side of the site. From the "Reno Folio" (Nevada Bureau of Mines and Geology, 1976), it is stated that such quaternary alluvial sediment is poorly bedded to unbedded and displays a wide variation in physical properties. It has very low to moderate permeability, low to moderate compressibility, excellent to poor drainage, good to poor bearing and low to medium plasticity. The variability in physical properties necessitates careful on-site investigation.

According to the Soil Survey of Washoe County, South Part (SCS, 1983) the upper 5 ft. at the site (the depth of interest for Soil Conservation Service work) consists of soils of the Rose Creek Series, Unit # 810. See Fig. 1.4. Tables 1.1 and 1.2 provide the Soil Survey information relative to this series and particular unit. Highlights from these descriptions are that this upper 5 ft. of soil

- is alluvial material from mixed rock sources

- is poorly drained material of moderately rapid permeability of a flood plain deposit
- has a C horizon (16 to 60 in.) that is stratified sandy loam, fine sandy loam, very fine sandy loam or loam
- has fine to medium roots to a depth of 5 ft. and fine to medium pores
- has inclusions of other soil units (Holbrook and Truckee) and wet areas (wetlands)
- has altered drainage because of changes in the original course of streams or channel entrenchment
- exhibits a seasonal high water table at a depth of 4 to 6 ft. in spring and early summer

According to the soil survey the engineering index properties and the physical and chemical properties of the Rose Creek soils are as given in Table 1.3.

1.3. Outline of Succeeding Chapters

In ensuing chapters, the report will present the following:

- Chapter 2 General Field and Laboratory Work
- Chapter 3 Laboratory Triaxial Hydraulic Conductivity Tests
- Chapter 4 Field Hydraulic Conductivity Tests

- Chapter 5 Analytical Modeling
- Chapter 6 Piezometric Readings and Their Implication
- Chapter 7 Comparison of Lab and Field Evaluation of In Situ Strength and Density
- Chapter 8 Lab and Field Hydraulic Conductivity Test Results
- Chapter 9 Finite Element-Stress Path Studies
- Chapter 10 Conclusions and Recommendations

Table 1.1 Description from SCS Washoe County, Nevada, South Part, p. 103

810—Rose Creek fine sandy loam, drained. This very deep, poorly drained soil is on flood plains. Drainage has been altered. The soil formed in alluvium derived from mixed rock sources. Slopes are 0 to 2 percent. Elevation is 4,000 to 5,000 feet. The average annual precipitation is about 6 to 8 inches, the average annual air temperature is 47 to 50 degrees F, and the average frost-free period is 100 to 120 days.

Typically, the surface layer is grayish brown fine sandy loam about 16 inches thick. The underlying material to a depth of 60 inches is light brownish gray, stratified very fine sandy loam through gravelly loamy sand.

Included in this unit are Holbrook soils on narrow stringer channels, Truckee soils on lower flood plains, and wet areas. The unit is about 6 percent Holbrook soils, 5 percent Truckee soils, and 4 percent wet areas.

Permeability of this Rose Creek soil is moderately rapid. Available water capacity is moderate. Effective rooting depth is 60 inches for water-tolerant plants but is limited by the water table for water-sensitive plants.

Runoff is very slow, and the hazard of water erosion is slight. The hazard of soil blowing is slight. A seasonal high water table is at a depth of 48 to 72 inches in spring and early summer. Drainage has changed because the water table has dropped as a result of changes in the original course of streams or of channel entrenchment. This soil is subject to flooding during storms of prolonged high intensity. Channeling and deposition are common along streambanks.

This unit is used for urban development and crops.

Flooding is a limitation to use of this unit as sites for dwellings. This soil is subject to seasonal flooding that can be controlled only by major flood control structures. The use of this soil as septic tank absorption fields is moderately limited by flooding and the high water table. Dikes and channels that have outlets to bypass floodwater can be used to protect buildings and onsite sewage disposal systems from flooding. If the density of housing is too high, community sewage systems are needed to prevent contamination of water supplies as a result of seepage.

The main limitation to use of this soil as sites for roads is the susceptibility of the soil to frost heaving. Roads should be provided with drainage. Suitable material should be added to provide an adequate wearing surface.

If this unit is used for irrigated crops, the main limitation is the high water table. Under good management including a conservation cropping system, this soil will produce 5 tons per acre of alfalfa, 73 bushels per acre of barley, or 350 hundredweight per acre of potatoes. Applications of irrigation water should be adjusted to the available water capacity, the water intake rate, and the crop needs to avoid overirrigating and leaching of plant nutrients. Crops respond to nitrogen and phosphorus fertilizer.

This soil is in capability subclasses Iiw, irrigated, and VIw, nonirrigated.

Table 1.2 Description from SCS Washoe County, Nevada, South Part, p. 264

Rose Creek Series

The Rose Creek series consists of very deep, poorly drained soils on flood plains. Drainage has been altered. These soils formed in alluvium from mixed rock sources. Slopes are 0 to 2 percent.

Typical pedon of Rose Creek fine sandy loam, 2,000 feet west and 1,600 feet south of the northeast corner of sec. 17, T. 19 N., R. 20 E.

Ap1p—0 to 8 inches; grayish brown (10YR 5/2) fine sandy loam, very dark grayish brown (10YR 3/2)

moist; moderate fine subangular blocky structure; slightly hard, friable, slightly sticky and slightly plastic; many very fine to medium roots; common very fine to medium pores; 10 percent pebbles; effervescent; moderately alkaline; clear smooth boundary.

A12—8 to 16 inches; grayish brown (10YR 5/2) sandy loam, very dark grayish brown (10YR 3/2) moist; common medium prominent strong brown (7.5YR 5/6) mottles; massive; slightly hard, friable, slightly sticky and slightly plastic; many fine to medium roots; common very fine to medium pores; 10 percent pebbles; effervescent; moderately alkaline; clear smooth boundary.

C1—16 to 60 inches; light brownish gray (10YR 6/2) stratified very fine sandy loam, gravelly loamy sand, sandy loam, dark grayish brown (10YR 4/2) moist; common medium prominent strong brown (7.5YR 5/6) mottles; massive; slightly hard, friable, slightly sticky and slightly plastic; common very fine to medium roots; few very fine to medium pores; effervescent; moderately alkaline.

The soil profile is deeper than 60 inches. The mollic epipedon is 10 to 18 inches deep. Reaction throughout the profile ranges from mildly alkaline to moderately alkaline. The control section is stratified and has texture of sandy loam, fine sandy loam, very fine sandy loam, or loam. It is more than 15 percent fine or coarse sand and 5 to 18 percent clay. In pedons where texture is the coarser part of the range, the control section is 0 to 20 percent gravel.

Mottles are common below the upper part of the A horizon. The lower part of the C horizon is highly mottled or gleyed.

Table 1.3 Engineering Index and Physical and Chemical Properties of the Rose Creek Series, Washoe County, Nevada, South Part, p. 513

Soil name and map symbol	Depth <u>in</u>	USDA texture	Classification		Frag- ments > 3 inches <u>Pct</u>	Percentage passing sieve number--			Liquid limit <u>Pct</u>	Plas- ticity index	
			Unified	AASHTO		4	10	40			200
810----- Rose Creek	0-16 16-60	Pine sandy loam Stratified gravelly sand to silt loam.	SM, ML SM	A-4 A-2, A-4	0-5 0-5	90-100 85-100	80-95 70-95	65-80 50-70	45-55 30-40	25-30 20-25	NP-5 NP-5

Soil name and map symbol	Depth <u>in</u>	Clay <u>Pct</u>	Permeability <u>in/hr</u>	Available water capacity <u>in/in</u>	Soil reaction <u>pH</u>	Salinity <u>Mmhos/cm</u>	Shrink-swell potential	Erosion factors		Wind erodibility Group
								K	T	
806----- Truckee	0-12 12-30 30-60	5-12 18-25 3-10	2.0-6.0 0.2-0.6 6.0-20.0	0.10-0.12 0.14-0.17 0.08-0.12	>8.4 >8.4 >7.8	>16 >8 4-16	Low----- Moderate----- Low-----	0.20 0.24 0.24	5	4

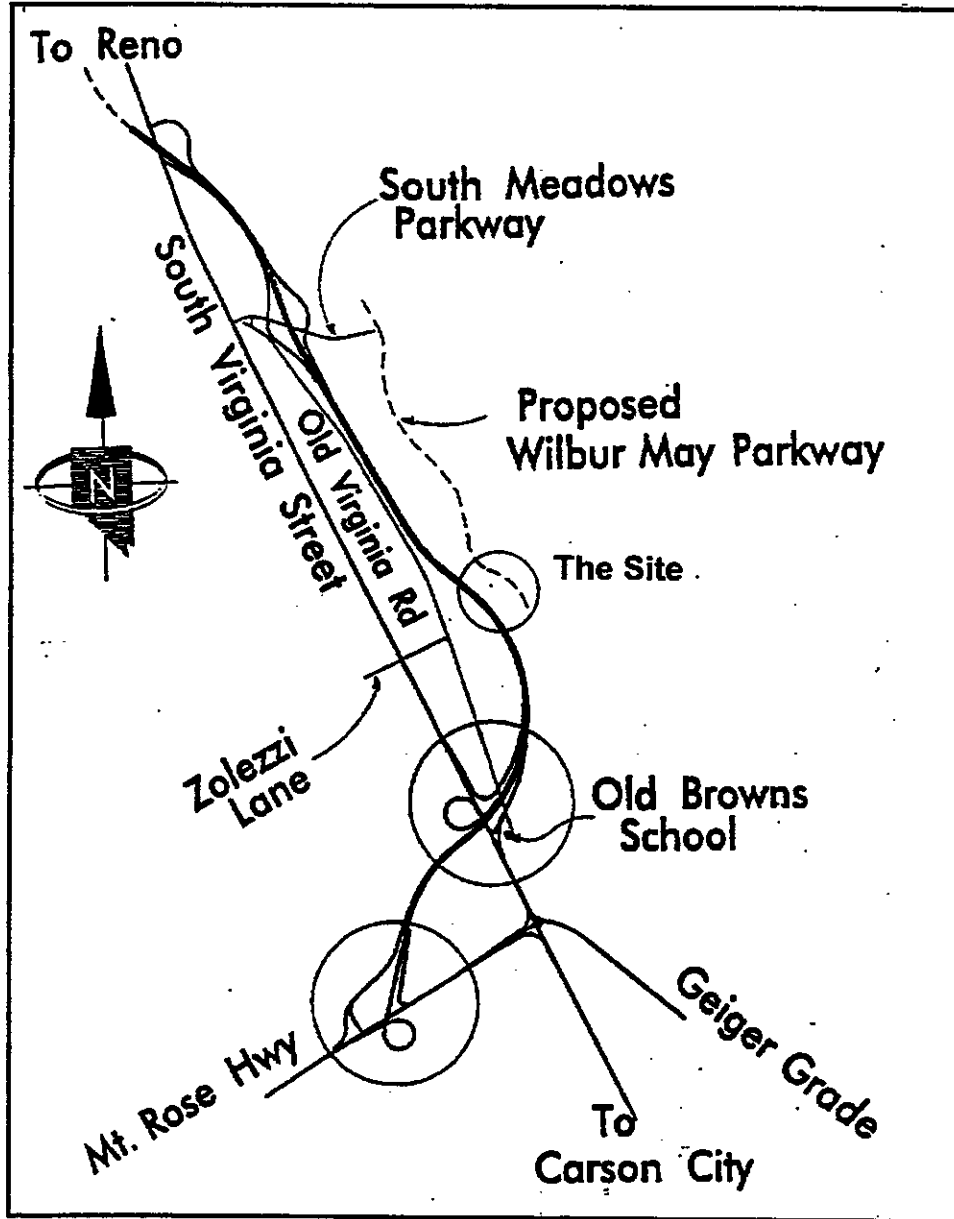


Fig. 1.1 Site Map

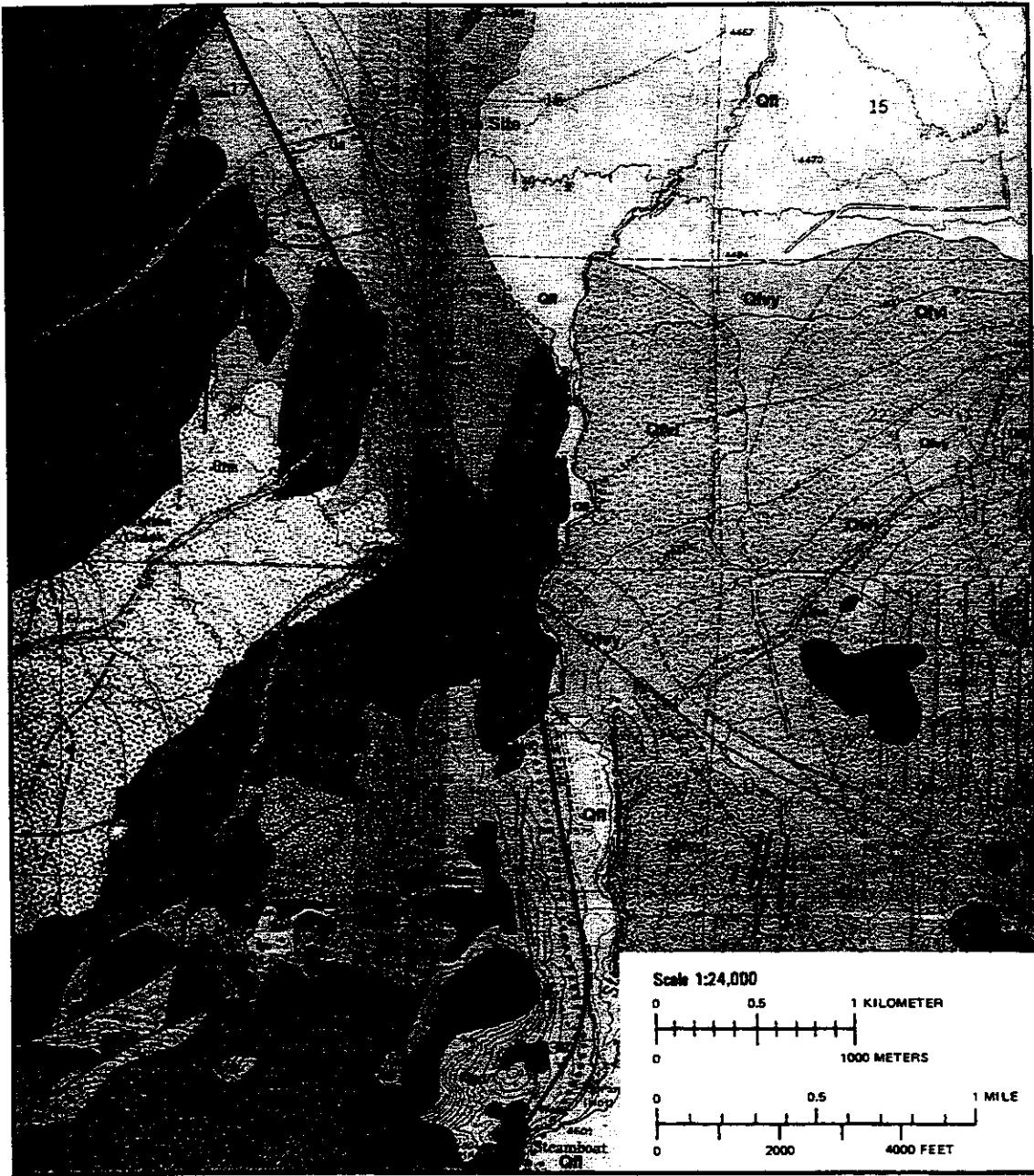


Fig. 1.2 MT. Rose NE Quadrangle Geologic Map

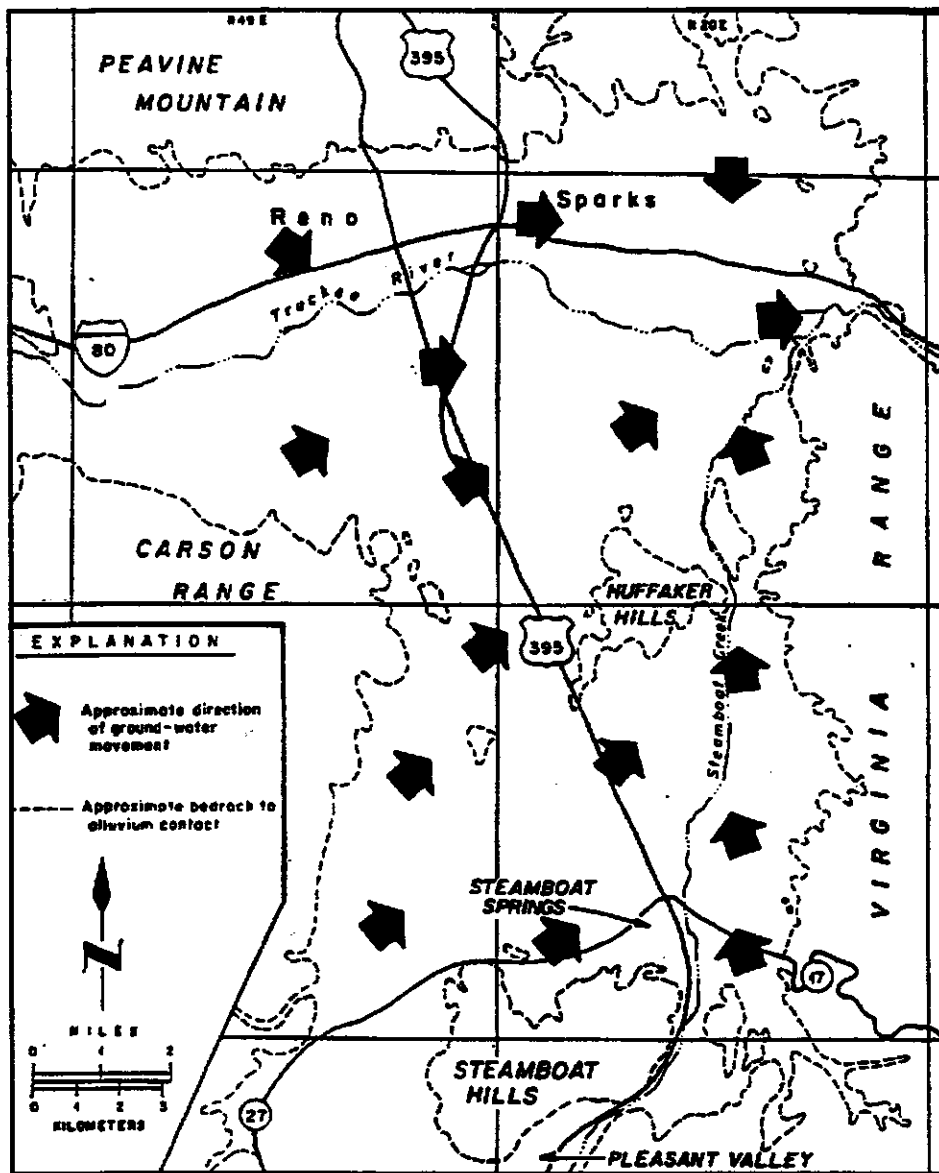


Fig. 1.3 General Direction of groundwater movement in the Truckee Meadows (Gates and Watters, 1992)

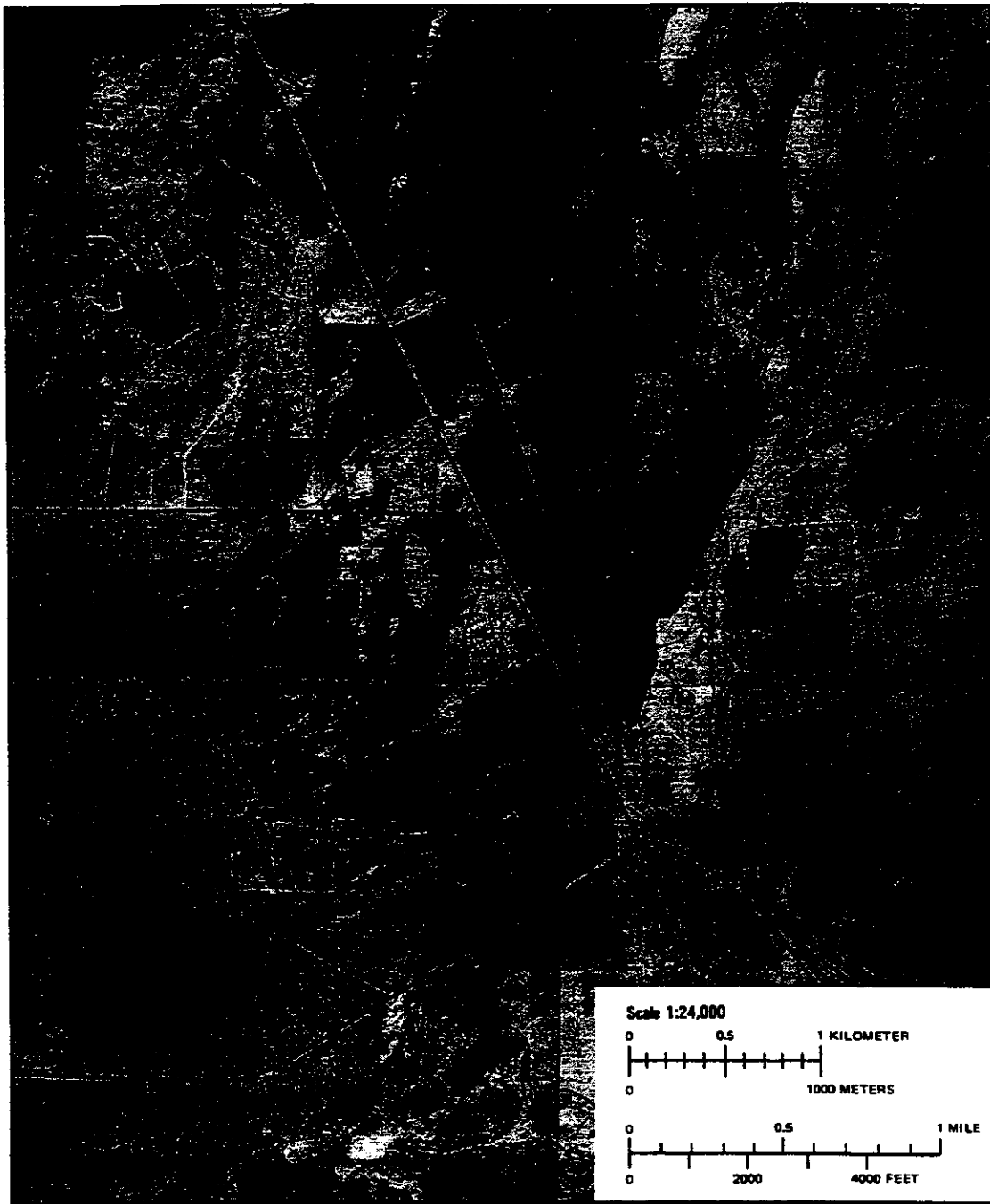


Fig. 1.4 SCS Washoe County South Part, Part of Sheets 27 and 28

Chapter 2

General Field and Laboratory Work

2.1. Proposed Approach

It was proposed that the need for, and the implementation of, a coupled procedure for the evaluation of the soil properties (i.e., the change in void ratio, hydraulic conductivity, strength, and stress-strain behavior with consolidation and, therefore, time) and the selection of an analysis scheme for the assessment of changes in flow conditions associated with highway fill construction be assessed. It was hypothesized that the field and laboratory tests and soil property evaluation would need to be tailored to the analytical scheme to provide for a more accurate determination of the response. This would mean that certain modifications might need to be made to traditional field and laboratory testing procedures. Likewise, it was felt that the two-dimensional analysis incorporate changing (spatial and time varying) property values that account for staged construction conditions. It was proposed that the degree to which field and laboratory analysis schemes affect each other and need to be coupled should best be determined via a typical field application.

A study area across a segment of the planned US 395 Extension was offered by the Nevada Department of Transportation (NDOT) as a field test case. Based on boring logs and cone penetration data for the general area, a transverse section at station 557+00 near the Zolezzi Lane crossing was chosen. See Fig. 2.1. At this location the water level is within one to two feet of the ground surface, the controlling aquifer is shallow, and samples, cone penetration testing, and installation of pneumatic piezometers to a shallow depth (< 25 ft.) would likely suffice. In consultation with NDOT, it was judged that three holes, each with three to four piezometers at different depths, and four other holes with one piezometer each would likely provide sufficient information on the flow regime. NDOT would provide Standard Penetration Test (SPT) data and Shelby tube (or other) samples from the three more heavily instrumented holes. In addition, slug type permeability tests would be undertaken adjacent to one of the holes containing three to four piezometers. The slug tests and piezometer installation would be undertaken in consultation with University of Nevada, Reno personnel. University personnel would provide ongoing readings from the piezometers using the NDOT pneumatic readout system. Such readings would encompass a time span from one-half year before to one year after construction.

More advanced laboratory testing would be carried out using GDS volume controllers in conjunction with the CKC Soil Equipment Company triaxial test

system on the University of Nevada, Reno campus. Such stress path controlled stress-strain-strength and permeability tests would be tied back to field and standard laboratory test results where possible.

2.2. Pre Construction Field Work

2.2.1. Installing Piezometers

Starting on October 11, 1993, the geotechnical field crew from NDOT in conjunction with University of Nevada, Reno personnel were on site to install fifteen piezometers in eight different locations along a 690 ft. wide cross section north of Zolezzi lane (see Fig. 2.1 and 2.2). These piezometers were installed according to the manufacture's recommendations. The typical installation of a piezometer consisted of the following steps (see Fig 2.3):

- Boring a hole to a depth 1.5 ft. below the required depth of the piezometer;
- Filling the bottom of the borehole with coarse clean sand to a height of four inches;
- Deairing the piezometer by putting it in a cloth bag filled with sand under water;
- Placing the piezometer in the hole and then filling the hole with coarse sand until the height of the sand layer is two feet total from the bottom of the hole;

- Sealing the hole by placing bentonite chips to a height of two feet above the top of the sand;
- Backfilling the remainder of hole with soil to the ground surface.

The piezometers installed were pneumatic piezometers, Model No. 514177, supplied by the Slope Indicator Company. Twin pneumatic tubes run from the piezometer to a terminal at the surface. Readings are obtained with a pneumatic indicator. The piezometer contains a flexible diaphragm with external water pressure acting on one side of the diaphragm and applied gas pressure acting on the other. When a reading is required, a pneumatic indicator is connected to the tubing. Compressed nitrogen gas from the indicator flows down the input tube to increase gas pressure on the diaphragm. When the gas pressure exceeds the water pressure, the diaphragm is forced away from the vent tube, allowing excess gas to escape via the vent tube. When the returned flow of gas is detected at the surface, the gas supply is shut off. Gas pressure in the piezometer decreases until water pressure forces the diaphragm to its original closed position, preventing further escape of gas through the vent tube. At this point, gas pressure equals water pressure, and a reading can be obtained from the pressure gauge on the indicator. All the piezometers were calibrated and a chart of calibration was provided with each of them.

The fifteen piezometers , in eight locations, were numbered according to the hole location (number 1 to 8) and depth (letters A to D). See Figures 2.1 and 2.2 and Table 2.1 for plan and vertical views and the numbering scheme. Eleven of the piezometers (Pz3 through Pz6) were installed so that they would be beneath the roadway embankment after construction. Three of these were toward the east fill slope edge (Pz3), seven are in the middle, and one (Pz6) is toward the west fill slope edge (the upstream end of the groundwater flow regime). The seven in the middle were placed three in one hole and a single in another hole at the same location (Pz4) and two and one in another two holes 110 ft. west (Pz5). Two out of the thirteen piezometers (Pz1 and Pz2) were installed to the east side of the embankment and the other two (Pz7 and Pz8) were installed to the west side. One of the piezometers (Pz4D) was installed in the controlling artesian layer at a depth of 21 ft. below the ground surface.

During the installation process, continuous and "undisturbed" samples were alternately obtained from different locations and at different depths. The "undisturbed" samples were taken through an 8 inch diameter hollow stem auger using Shelby tubes that were sealed at the site with wax, capped and then transported to the University in a padded rack. At the University, they were stored vertically in the moist room. Representative soil samples obtained as part of SPT testing were logged by NDOT personnel and a copy of the boring log is included

as Appendix No. 1. Table 2.2 provides the depths and locations of the samples obtained. Continuous samples were taken in 5 ft. long 4 inch diameter plastic tubes and stored vertically along with the Shelby tube samples in the moist room on the University campus. While such samples are continuous and can be viewed through their clear plastic wall, expansion in the oversize tube precludes that they are undisturbed.

After the installation of the fifteen piezometers, a trench approximately four feet deep was excavated to carry all the pneumatic tubes from the piezometers to monitoring stations. There were three different monitoring stations, two of them were located at the east edge of the fill (at Pz3) and the other was located at the west side of the fill (between Pz7 and Pz8). Each monitoring station consisted of steel casing with a steel cover which was kept locked unless readings were being taken.

2.2.2. Standard Penetration Testing

Standard Penetration Tests (SPT) were performed in three borings (Pz3 through Pz5) at different depths in order to estimate relative density and soil strength characteristics from the recorded blow counts and to obtain disturbed but representative samples of the soil for water content, grain size, index tests, and soil classification. Additional samples were obtained and logged using a 2.8 inch

diameter “California” sampler . Table 2.3 provides locations and depths where SPT tests were performed.

Please note that a Mobile drill rig with a hammer with a 60% energy ratio was used . Unfortunately the water level in the hole was not routinely adjusted to match the higher external water level and some loosening of the soil is likely to have occurred at the bottom of the hole due to upward flow. However as will be mentioned later in this Chapter, the two holes B1 & B2, investigated by NDOT, were done using a rotary mud hole advancement.

2.2.3. Well Installation

In order to assess the in-place hydraulic conductivity of the soils, two wells for slug tests were installed at the east edge of the embankment near the location of Pz3. The two wells are five feet apart and five feet away from Pz3. A typical cross section for the two wells as well as a plan view for the location is shown in Figure 2.4. Note that the three piezometers at this location (Pz3 A, B and C) are in three separate holes. The casing for the two wells is made of polyvinyl chloride (PVC) and has an inner diameter of 2 inches (outer diameter of 2 ½ -inches). The casing was installed in the 9 1/4 inch diameter holes resulting from the use of the 8 inch auger. While the slotted length was the same for both wells, the different lengths and sand filter yielded effective lengths of 48 and 24 inches respectively.

Both wells have the same effective depth which is 11 ft. from the original ground surface.

2.2.4. Cone Penetration Test

On December 22, 1993, Tonto Environmental Drilling from Sacramento, California, arrived on site to perform piezo cone penetration tests in four locations. These locations are Pz3, Pz4, Pz5 and Pz6. Tip resistance, sleeve friction, friction ratio, pore pressure ratio and other relevant parameters were recorded continuously with depth. Plots of the readings appear as Figs. 2.6a to 2.6d. (Note the superposition of piezometers in these logs.) In addition to this, dissipation of porewater pressure was recorded with time at different depths as an aid in assessing the hydraulic conductivity. All the recorded data were sent to the Sacramento office for interpretation. A copy of the interpreted logs is included as Appendix No. 2. Note that Roberston and Campenella (1984) correlations were employed in these interpretations.

2.2.5. Monitoring the Piezometric Surface

Soon after the installation of the piezometers, readings were taken to monitor the piezometric surface. A pneumatic pressure indicator by Slope

Indicator, Model 5141 (Serial No. 136) was provided by NDOT for this purpose. A University of Nevada, Reno graduate student was trained by NDOT personnel in obtaining the readings. Readings for the fifteen piezometers were scheduled to be taken every week for the full time of the project to assess the difference in piezometric surface before and after the construction of the fill in order to assess the effect of fill construction on the piezometric surface. Piezometric readings were also taken the day after SPT tests and the day of cone testing. It should be noted that the same person, using the same order and procedure in readings, was employed in order to reduce the possibility of operator effects.

2.2.6. In Place Hydraulic Conductivity

Soon after the installation of the two wells, a slug test (falling head test) was performed in both of the wells. A typical slug test consisted of the following steps:

- Extending the stand-pipe by a known length with an O-ring coupled section in order to be higher than the original ground surface;
- Measuring the distance between the top of the stand-pipe and the existing piezometric water level in the hole;
- Filling the stand-pipe with water to its top, and then;

- Monitoring the drop of water in the stand-pipe with time. (Monitoring was done using a water level indicator.)

Data were recorded and a sample of these data is included as Appendix No.

3.

2.3. During Construction

Three months before the construction of the fill, irrigation water, located on the west edge of the fill near Pz6 (see the irrigation channel in Fig. 2.2) was completely shut down. This is the water channel shown in Fig. 1.2 and 1.4. After a month, a concrete lined channel was used to divert the irrigation water until the construction of the fill was completed.

During the construction of the fill, readings of the piezometers were taken every week to provide a continuous record of the piezometric surface (especially to catch any excess porewater pressure that might develop as a result of fill loading). According to the piezometric data, there were both horizontal and vertical hydraulic gradients across the site, indicating flow of water was taking place. It was only possible to calculate average gradients since piezometers were finite distances apart. Further, there were no stand-pipes installed at the ground surface in the locations of the piezometers to monitor a drop of the ground water table surface and, therefore, any change from a confined to an unconfined flow situation. Accordingly, a crew from the University of Nevada, Reno installed

eight stand-pipes on April 15, 1994, of one inch diameter, to depths of three to five feet measured from the ground surface. Soon after this installation was complete, water level readings were taken in the stand-pipes. However, within three weeks, these stand-pipes were covered by the roadway embankment, and it was no longer possible to continue monitoring the position of the water surface.

In the mean time, slug tests were routinely performed on both wells (Nos. 1 and 2) until it was realized that another well far enough from the first two was needed in order to allow separate evaluations of vertical and horizontal hydraulic conductivities. Based on this realization, a third well was installed on June 10, 1994. This well was located approximately fifteen feet north of well No. 2 along the east edge of the fill. It was installed by hand augering to a depth of 9'-2" with an effective depth at eight feet and an effective length of 28 inches. A typical cross section for the well is shown in Fig. 2.5. Four weeks after the installation was completed, a construction access road was constructed over this well. This access road was not in the original plans. Readings from this well were unavailable after this date.

Backfill material, different from what was used for the majority of the roadway embankment, was employed adjacent to the Zolezzi lane overpass structure. (See p160 of the "Soils and Foundation Workshop Manual" (1993) for approach embankment details.) Samples of both fill materials were obtained for

material property characterization for computer modeling of the stress state change brought about by fill construction.

2.4. Laboratory Work

A typical geotechnical investigation was undertaken in proximity to the Zolezzi site by NDOT in early 1993. NDOT logged soil and groundwater level, using a rotary mud, in two holes (B1 and B2 of Fig. 2.1) 230 ft. apart and 70 ft. deep. B1 and B2 are 320 ft. and 180 ft. away from Pz4 respectively. The boring logs are shown in Figs. 2.7a and 2.7b along with the percent fines, water content and occasional Atterberg limits established from laboratory evaluation of representative (split spoon) samples obtained during SPT testing. (Note the blow counts given on the left side of the soil column). It is the upper 20 ft. of brown to gray-brown silty sand resting on the silty gravel artesian layer that constitutes the flow regime of interest in the current study.

While description of this soil is the same as noted in the logs for Pz1 through Pz8 of Appendix No. 1, the stratified nature of the soil as indicated in the Soil Survey (see Table 1.3) suggested that a more detailed laboratory inspection of a continuous soil sample taken during piezometer installation was in order. This was further warranted by differences between the CPT and SPT logs. (Compare

Appendix 2 entries to those of Appendix 1 and Figs. 2.7a and 2.7b over a depth of 21 ft.)

While relatively small scale stratification may not be important in relation to stability and deformational behavior, it is likely to have a controlling effect upon groundwater flow (i.e. cause anisotropic permeability). Therefore, a continuous clear tube sample from Pz4 for the depth of 8 to 21 ft. was logged. A complete description is provided as Appendix No. 4

2.4.1. Standard Geotechnical Tests

A number of standard geotechnical tests were performed both in the field and on laboratory samples. These tests were the in-place field density test, specific gravity, sieve analysis, Atterberg limit and standard consolidation tests. Such information was used for soil classification and characterization, density evaluation, and correlations for various soil properties.

2.4.2. Field Density

The unit weight of the soil is a significant parameter in the input data for the FEDAM model (stress strain behavior model). Field density tests were performed to determine the in-place dry unit weight and moisture content of the unsaturated

soil at ground surface at the site. The sand cone test (ASTM D1556) was employed for this purpose. This test was performed immediately below the grass cover at a depth of approximately one foot from the ground surface at two locations, Pz3 and Pz5. Table 2.4 provides the results of these two tests and indicates the potential variation in the unit weight and the moisture content.

Unit weights of the saturated soil below the water table can be assessed knowing the specific gravity and water content values of the soil. Such values are reported subsequently.

2.4.3. Specific Gravity and Water Content

The specific gravity of the soil solids is generally used in the calculation of the density state of a soil. Test method ASTM D854 (fine material) was employed relative to the samples from the test site. This test was performed on twenty samples obtained from Pz2, Pz3, well 1, well 2, Pz4, Pz5, Pz7 and Pz8 locations at different depths. Table 2.5 provides the results from these tests (and those from NDOT's B1 and B2) along with the moisture content results (w) and calculated values of void ratio ($e = wG_s$, where saturation is 100%) and dry unit weight ($\gamma_d = \frac{G_s \gamma_w}{1 + w}$) of the soil at the specified locations and depths. Such densities were

used as a guide in the preparation of any reconstituted laboratory samples. The corresponding unit weight (γ) is $g = \gamma_d (1+w)$.

2.4.4. Particle Size Analysis

Particle size analysis is the most common of all the basic soil property tests. It is used qualitatively along with other tests to estimate strength, stiffness, permeability, and other engineering properties. This test is divided into two parts, mechanical analysis and hydrometer analysis. The mechanical (or sieve) analysis is performed for particle sizes greater than the No. 200 sieve, whereas the hydrometer analysis is typically performed for particle sizes less than the No. 200 sieve. The mechanical analysis (ASTM D422) was performed on various samples. The location and depths of the samples assessed is indicated in Table 2.5 (i.e. those with a data entry in the minus No. 200 column). Figures 2.8a through 2.8n are the plots of the grain size distribution for these samples. Corresponding values of the mean particle size (D_{50}) and uniformity coefficient ($C_u = D_{60}/D_{10}$) are indicated in the figures.

2.4.5. Atterberg Limits

As noted in the SCS information (Table 1.3) and the NDOT boring logs for B1 and B2 (Fig 2.7) the material to 20 ft. depth is basically nonplastic (NP) to a PI of 5. Manual “feel” of all samples noted in Table 2.5 confirmed this. Basically only one sample of a higher (>40%) and more plastic fines content was singled out for special consideration. The minus No. 40 fraction of this material yielded a plastic limit (PL) of 27 and a liquid limit (LL) of 33 and, therefore, a PI of only 6. This was the most plastic of all the samples encountered.

2.4.6. Maximum and Minimum Dry Unit Weight and Void Ratio

Maximum and minimum dry unit weights ($\gamma_{d_{\min}}$, $\gamma_{d_{\max}}$) of these dirty sands were desired in order to establish minimum and maximum void ratios, i.e.

$$e = \frac{G_s \gamma_w}{\gamma_d} - 1$$

where e_{\max} is obtained based on $\gamma_{d_{\min}}$ and e_{\min} based on $\gamma_{d_{\max}}$.

In turn, the field void ratio can then be used to establish relative density, D_r , as

$$D_r = \frac{e_{\max} - e}{e_{\max} - e_{\min}}$$

where e is the field void ratio as reported, for instance, in Table 2.5.

To simplify matters, e_{\max} and e_{\min} were established from $\gamma_{d_{\min}}$ and $\gamma_{d_{\max}}$ from bulk samples prepared at two fines contents, 23% and 38%. Note that the D_{50} and uniformity coefficient of different samples were pretty much the same ($D_{50} \cong 0.2$ mm, $C_u \cong 10$).

The maximum dry unit weight was taken as the modified AASHTO (ASTM D1557) test value using the $\frac{1}{30}$ cu.ft. mold, while the minimum dry unit weight was established by spooning the material loose into the $\frac{1}{30}$ cu.ft. mold (ASTM D4254). Values for the two fines contents are reported in Table 2.6 along with maximum and minimum void ratios calculated using $G_s = 2.65$ (an average value).

2.4.7. Consolidation Test

Two standard consolidation test (ASTM D2435) were performed in order to assess the overconsolidation ratio and preconsolidation pressure (and, therefore, the compressibility of the soil). From time rate readings, permeability might also be indirectly assessed. A sample located at Pz3 at a depth of 7 ft. was tested. A second sample at Pz2 at a depth of approximately 10 ft. was also tested. Table 2.7 provides the results of these tests. As shown in the consolidation plot (Fig 2.9), the preconsolidation pressure is about 60 to 65 kPa (1250-1300 psf). The effective overburden pressure in the field at this depth is 650 psf (based upon a total unit

weight of 120 lb/ft³ and a piezometric head of three feet), thus giving an overconsolidation ratio (OCR) of approximately 2.

2.5. Summary

The foregoing data will be used in later discussion. No specific conclusions are made here.

Table 2.1 Piezometer Locations

Piezometer No.	Piezometer Tip Elevation	Depth Relative to Ground Surface	Distance from Pz1 (in ft)
Pz1	4479.0	9.0	0.0
Pz2	4481.0	8.0	100.0
Pz3A	4482.2	7.8	199.0
Pz3B	4477.3	12.7	204.0
Pz3C	4472.6	17.4	209.0
Pz4A	4484.5	7.0	296.0
Pz4B	4479.5	12.0	296.0
Pz4C	4474.5	17.0	296.0
Pz4D	4470.5	21.0	296.0
Pz5A	4488.7	5.3	406.0
Pz5B	4484.0	10.0	406.0
Pz5C	4476.2	17.8	406.0
Pz6	4478.1	17.4	478.0
Pz7	4487.2	9.8	590.0
Pz8	4488.5	9.5	690.0

Table 2.2 Soil Sample Locations

Location	Depth Relative to Ground Surface (ft)		Type of Sample
	from	to	
Pz1	1.5	3.5	Clear Tube Sample
	7.0	9.0	Clear Tube Sample
Pz2	0.0	4.0	Two Clear Tube Samples
	5.0	9.8	Clear Tube Sample
Pz3	2.0	4.0	Shelby Tube
	6.6	8.6	Shelby Tube
	11.6	13.6	Shelby Tube
	16.6	18.6	Shelby Tube
Pz4	4.0	6.0	Shelby Tube
	9.0	11.0	Clear Tube Sample *
	14.0	16.0	Clear Tube Sample *
	20.0	22.0	Clear ubeSample *
Pz5	2.0	4.0	Shelby Tube
	7.0	9.0	Shelby Tube
	12.0	16.0	Two Shelby Tubes
Pz6	N/A		
Pz7	0.0	2.0	Clear Tube Sample
	8.4	9.5	Clear Sample
Pz8	0.0	1.0	Clear Sample
	3.5	5.5	Clear Sample

* Logged, See Appendix No. 4

Table 2.3 Standard Penetration Testing Locations

Location	Depth Relative to Ground Surface (ft)		No. of Blows per Six inches (Blows per foot)
	from	to	
Pz3	4.0	5.5	1-3-5 (8)
	8.5	10.0	2-6-6 (12)
	13.5	15.0	2-4-7 (11)
Pz4	6.0	7.5	1-2-4 (6)
	11.0	12.5	5-7-5 (12)
	18.0	19.5	5-6-11 (12) *
Pz5	4.0	5.5	1-2-4 (6)
	9.0	10.5	2-5-6 (11)
	16.0	17.5	6-6-13 (19) *

* Pebble in lower part of sampler

Table 2.4 Field Density Results

Location	Depth (ft)	Moisture Content w (%)	Moist Unit Weight γ (pcf)	Dry Unit Weight γ_{dry} (pcf)
Pz3	1.0	26.9	95	74.6
Pz5	1.5	16.6	105	90.2

Table 2.5 Summary of The Soil Properties For Different Samples

Location	Depth		W %	Gs	e	γ_a pcf	γ pcf	- #200 %
	from	to						
Pz 2	7'-6"		33.2	2.65	0.874	88.2	117.5	20.3
	9'-6"		24.6	2.65	0.647	100.4	125.1	20.3
	9'-11"		21.2	2.65	0.559	106.1	128.6	20.3
	10'-6"		25.1	2.63	0.661	98.9	123.7	29.9
Pz 3	1'-6"	2'-6"	15.9	2.67	0.424	117.1	135.7	21.7
	8'-6"		18.4	2.70	0.496	112.5	133.2	19.4
	9'-6"		16.1	2.70	0.435	117.3	136.3	20.3
	10'-2"		18.4	2.69	0.495	112.3	132.9	29.8
	13'-0"		12.1	2.69	0.325	126.7	142.0	
Well 1	4'-6"	5'-0"	28.6	2.61	0.746	93.3	119.9	44.3
Well 2	2'-0"			2.63				9.0
	4'-0"			2.68				22.1
	9'-6"		24.6	2.68	0.647	101.7	126.7	28.7
	9'-11"		21.2	2.68	0.559	107.4	130.2	28.7
	12'-8"			2.61				33.6
Pz 4	7'-0"	7'-6"	22.7	2.60	0.592	102.0	125.2	
	11'-0"	12'-6"	22.4	2.66	0.595	104.0	127.2	20.2
	14'-6"		20.8	2.71	0.562	108.0	130.5	27.0
	17'-6"		22.7	2.73	0.619	105.3	129.2	36.8
	21'-0"	22'-0"	24.8	2.64	0.655	99.6	124.2	34.8
Pz 5	4'-0"	4'-6"	24.4	2.65	0.646	100.5	124.9	33.5
	8'-6"		22.1	2.65	0.585	104.3	127.4	33.5
	9'-0"	10'-6"	26.1	2.65	0.691	97.8	123.3	33.5
Pz 7	3'-5"	4'-0"	23.5	2.65	0.621	101.9	125.8	33.5
	8'-2"	8'-8"	47.2	2.65	1.249	73.5	108.1	62.6
	9'-0"	9'-6"	31.9	2.61	0.832	88.9	117.3	32.4
	9'-6"	10'-0"	29.6	2.64	0.782	92.4	119.8	52.1
Pz 8	9'-9"			2.65				27.5
B1	3'-7"		21.0	2.68	0.563	107.0	129.5	37.0
	8'-6"							24.0
	11'-7"		25.0	2.68	0.670	100.0	125.0	42.0
	18'-8"		20.1	2.68	0.539	109.0	130.5	29.0
B2	4'-8"							46.0
	8'-9"							32.0
	13'-6"							31.0
	18'-9"							46.0

Table 2.6 Maximum and Minimum Dry Unit Weight and Void Ratios

% Fines	γ_{dmax} <i>pcf</i>	γ_{dmin} <i>pcf</i>	e_{min}^*	e_{max}^*
23	123.8	77.7	0.319	1.193
38	77.7	75.4	0.336	1.128

* Based on $G_s = 2.65$

Table 2.7 Consolidation Test Results

Load (<i>kpa</i>)	Voids Ratio (<i>e</i>)	Coefficient of Consolidation (C_v) (<i>cm²/min</i>)
25	0.6360	0.07296
50	0.6350	0.05296
100	0.6335	0.0619
200	0.6320	0.22187
400	0.6302	0.08245
800	0.6280	0.3291
1600	0.6261	0.18183

$w = 23.8\%$, $G_s = 2.68$, $e_o = 0.637$

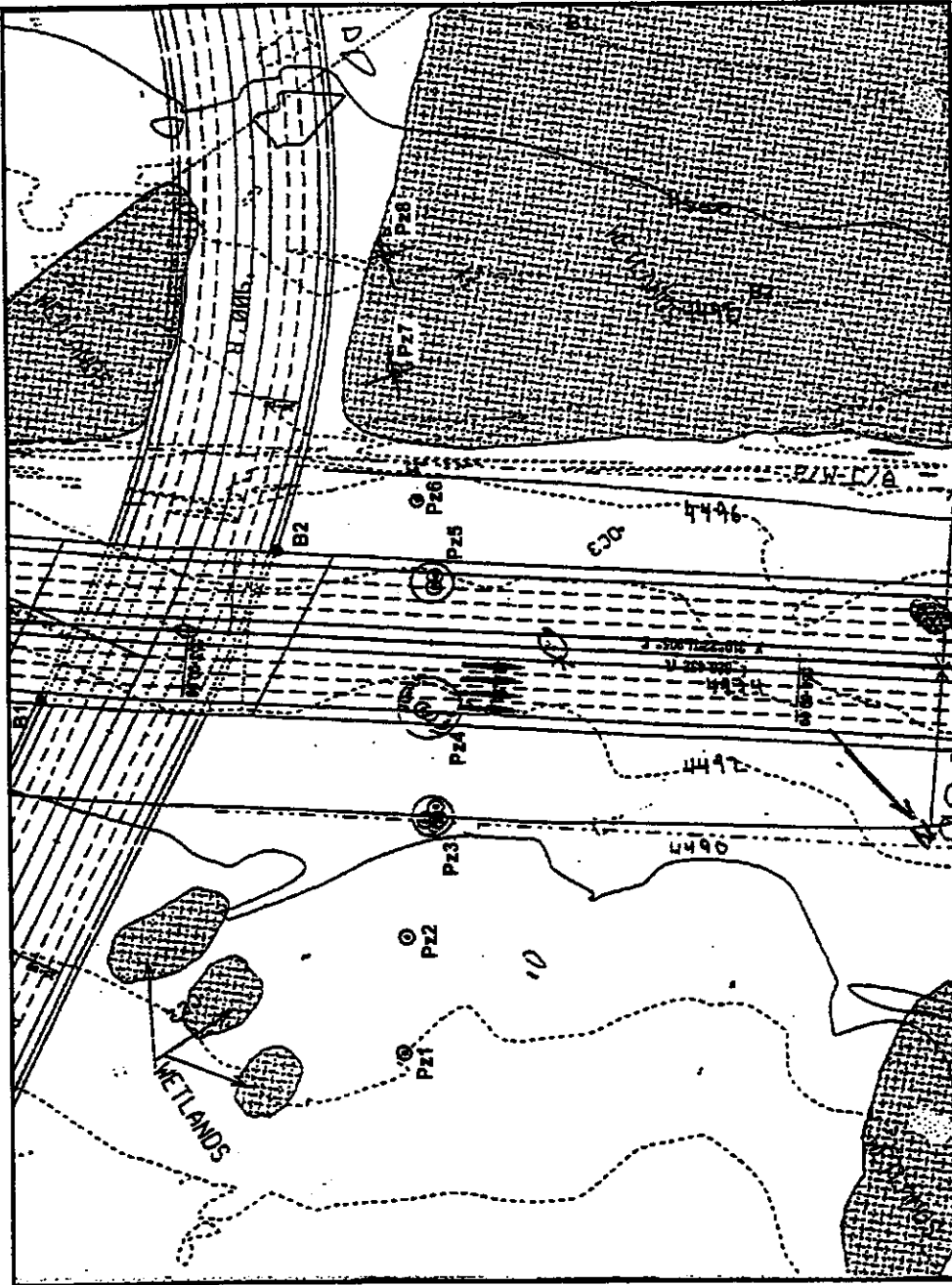


Fig. 2.1 Zolezzi Lane Map from NDOT Plans

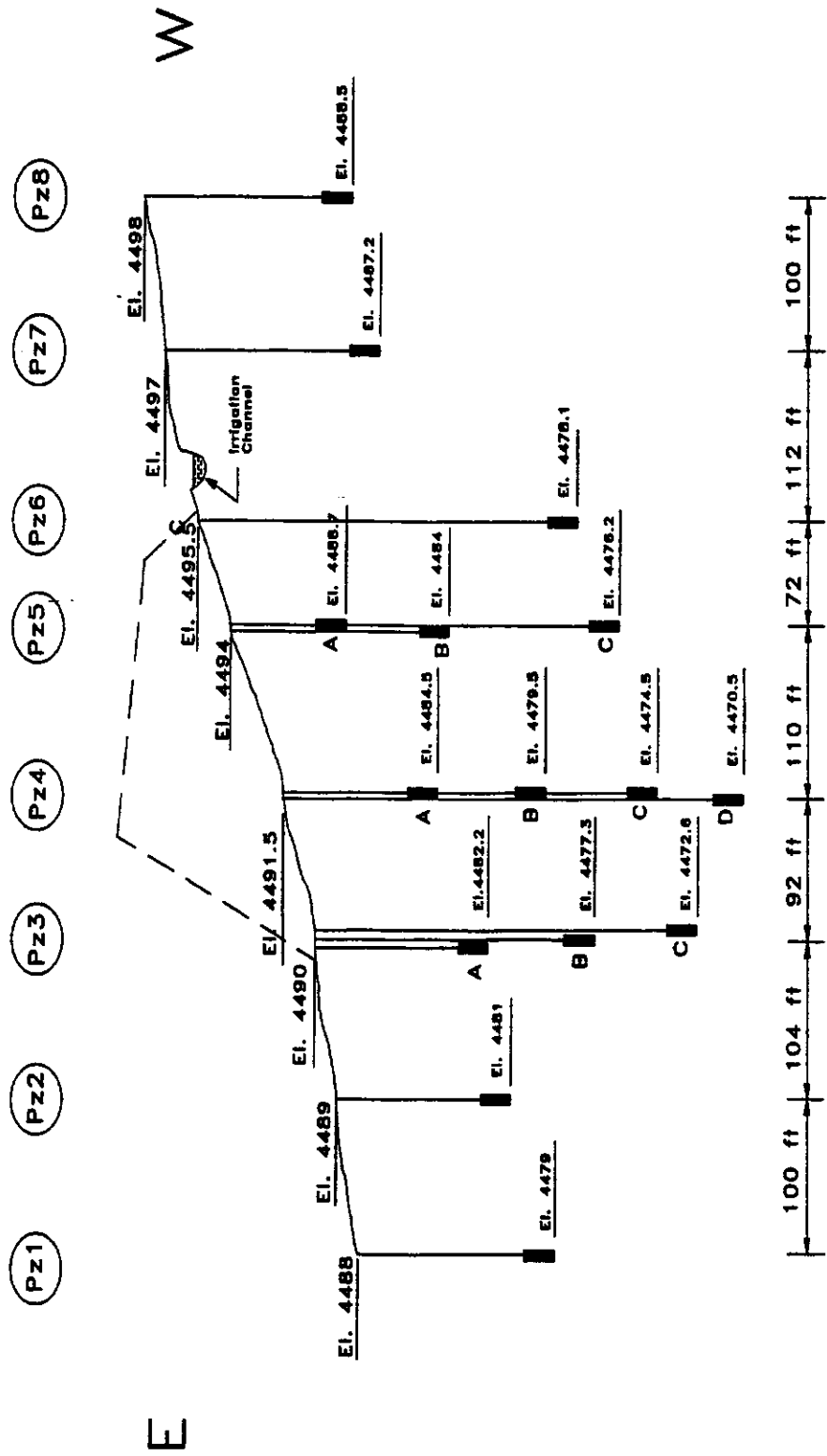


Fig. 2.2 Vertical Cross Section showing the Piezometer Depths

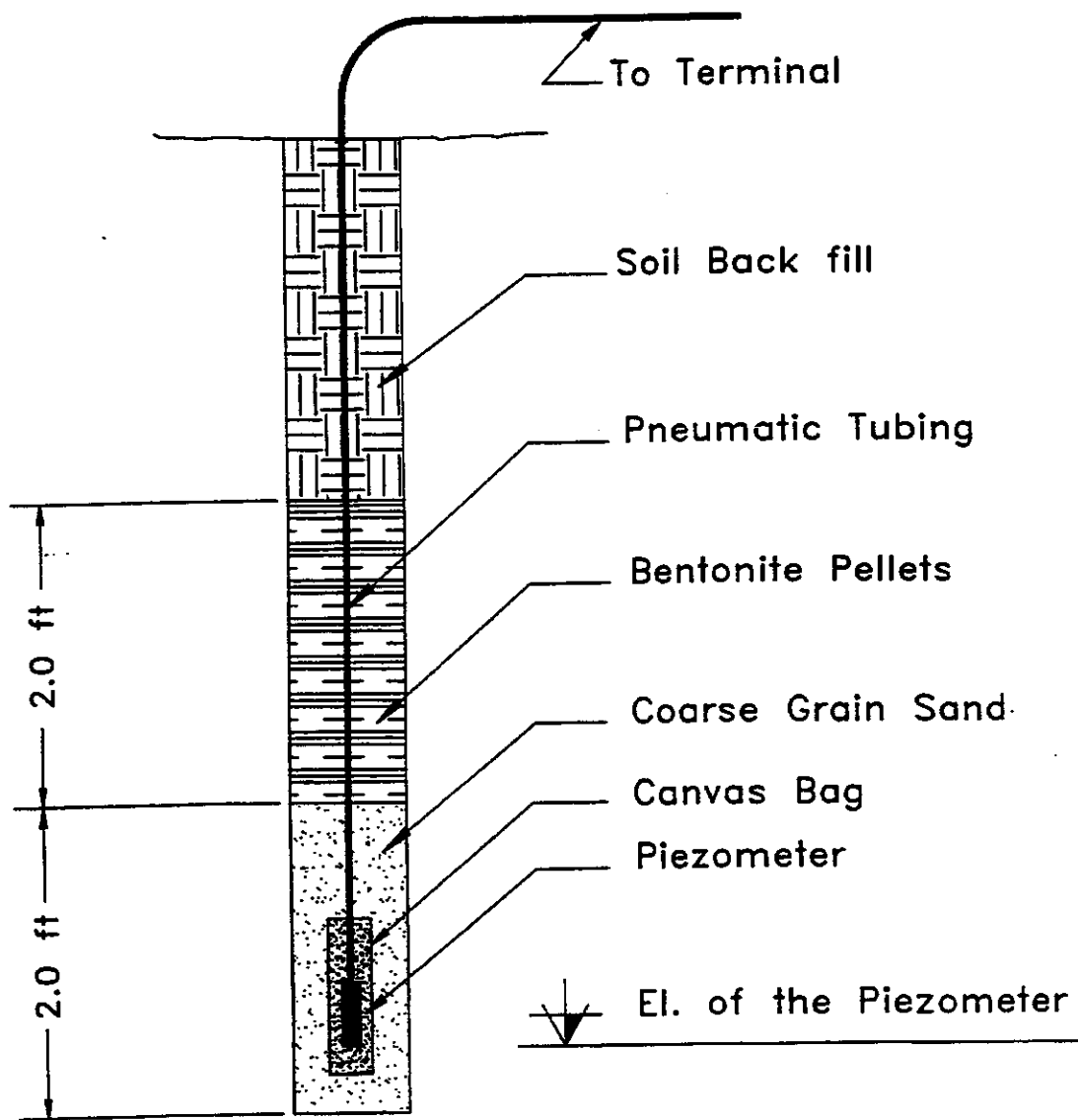
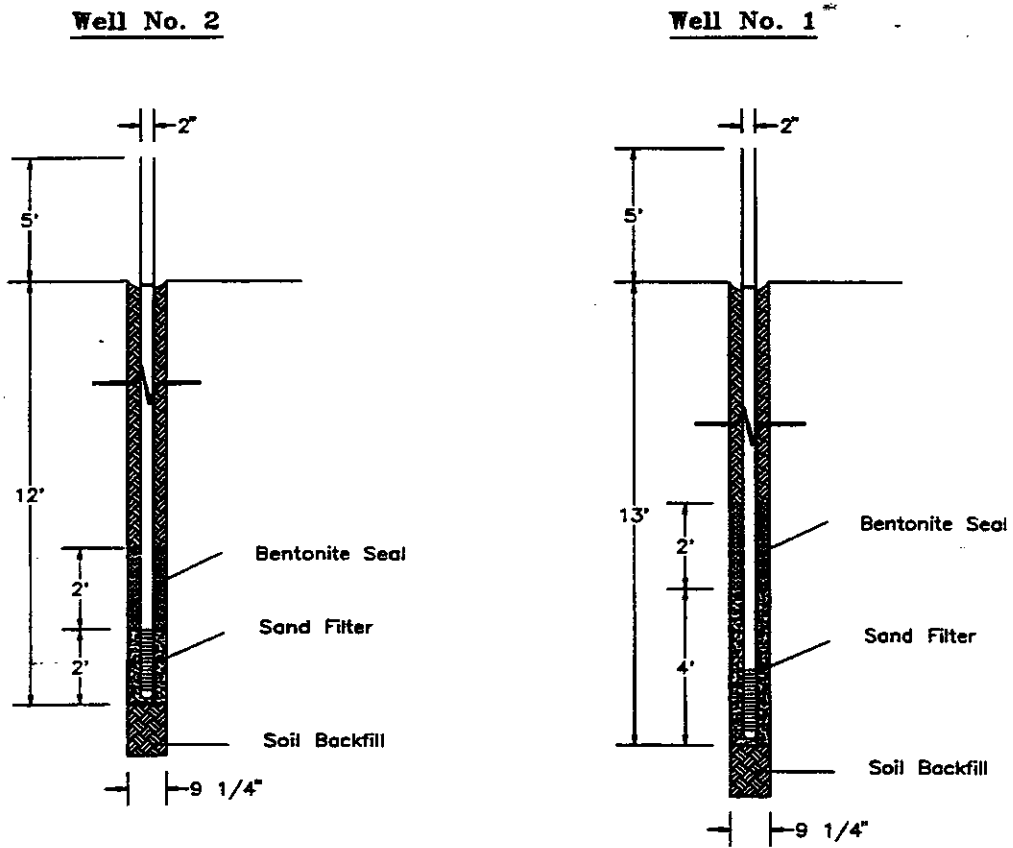
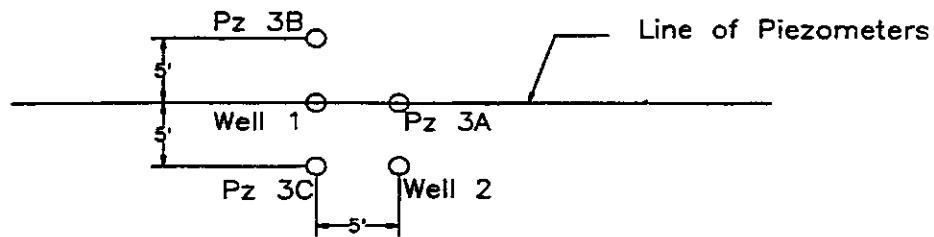


Fig. 2.3 Piezometer Installed in The Borehole

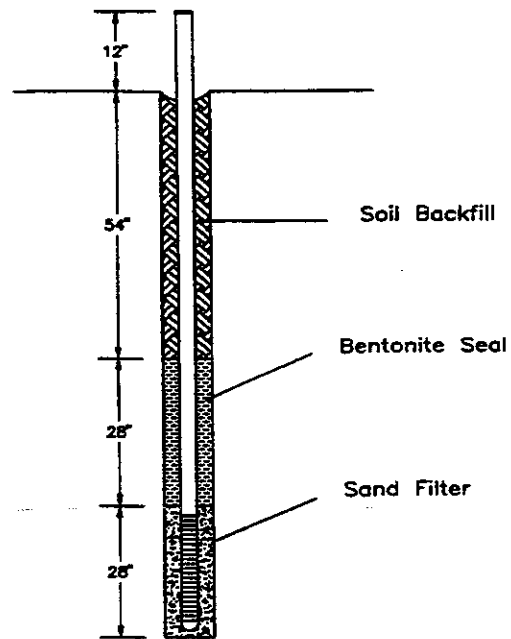


Cross Section of the Two Wells

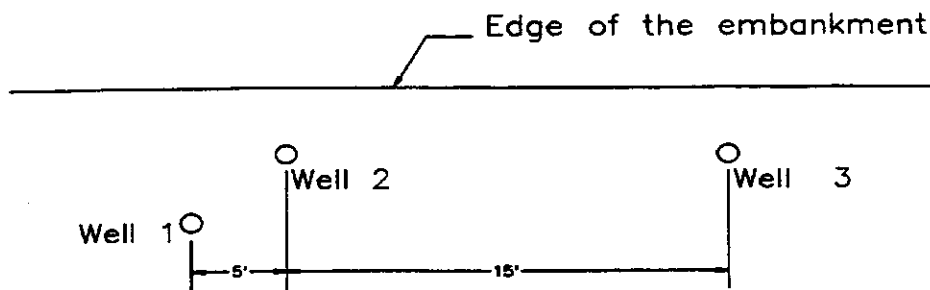


Plan View

Fig. 2.4 Location and Profile for Wells 1 and 2

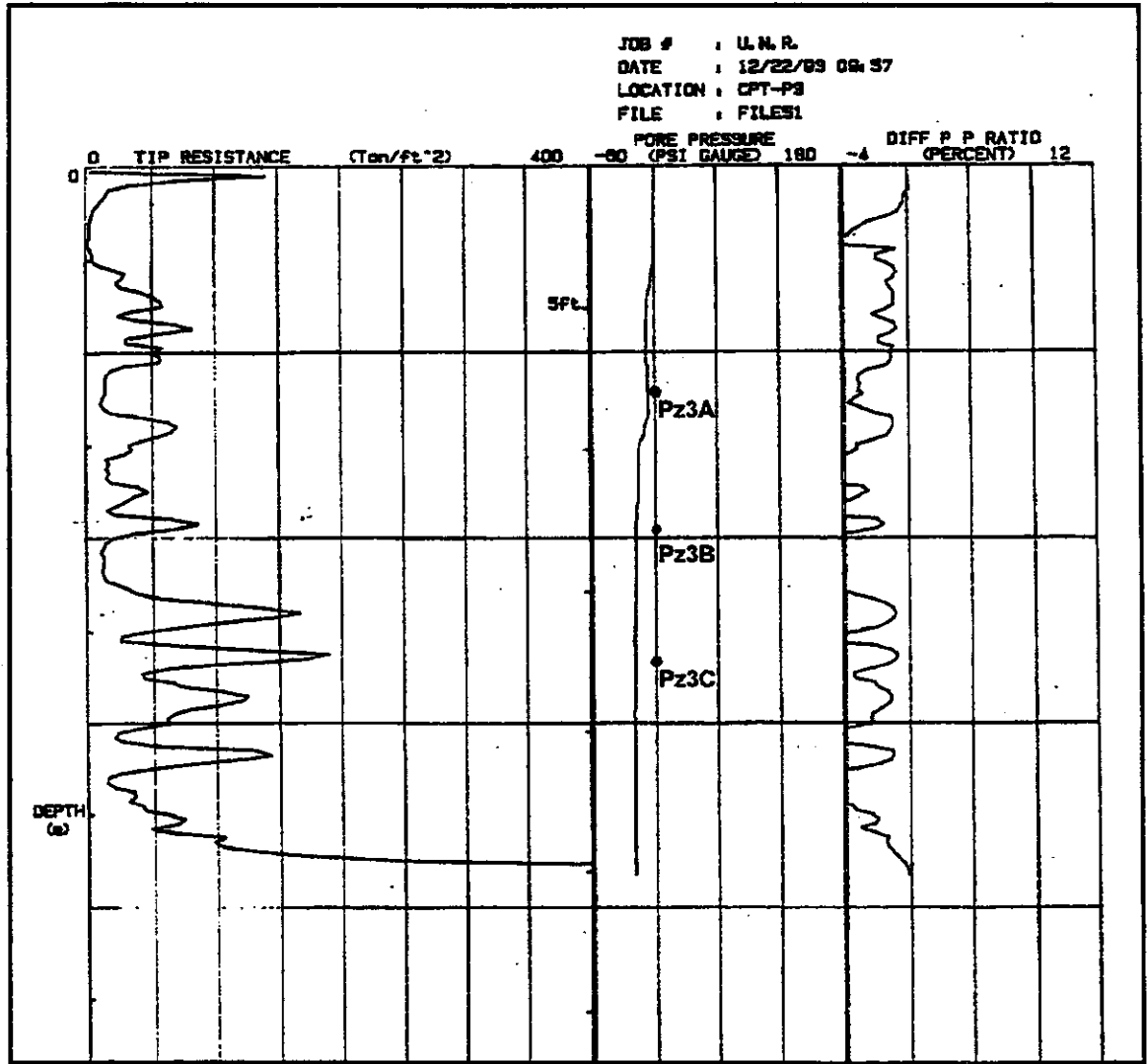


Cross section for well 3



Plan view

Fig. 2.5 **Location and Profile for Well 3**



Note: Piezometers Pz3A, Pz3, and Pz3C have been superposed for reference

Fig 2.6a Piezo Cone Plots for Pz3

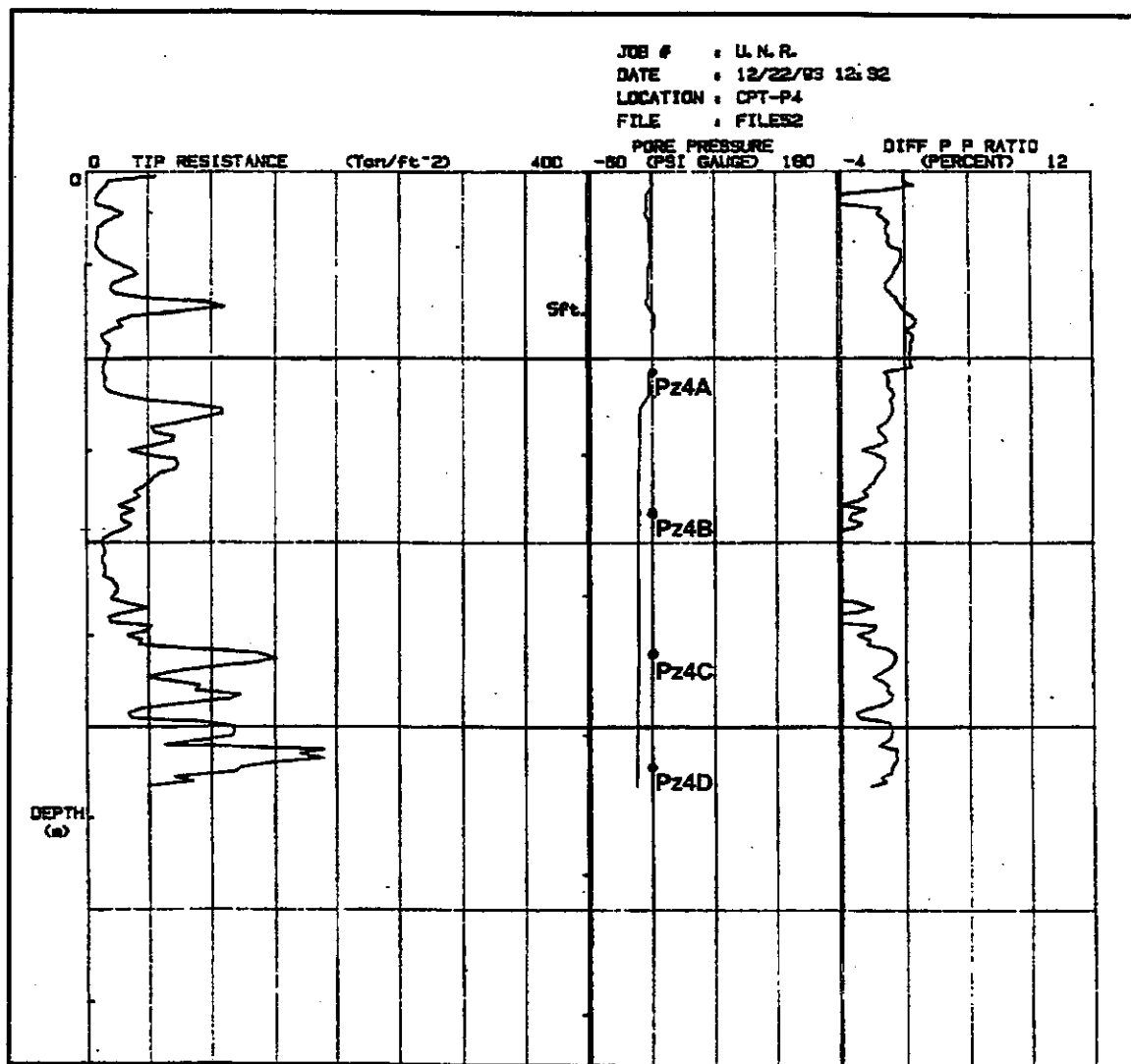


Fig 2.6b Piezo Cone Plots for Pz4

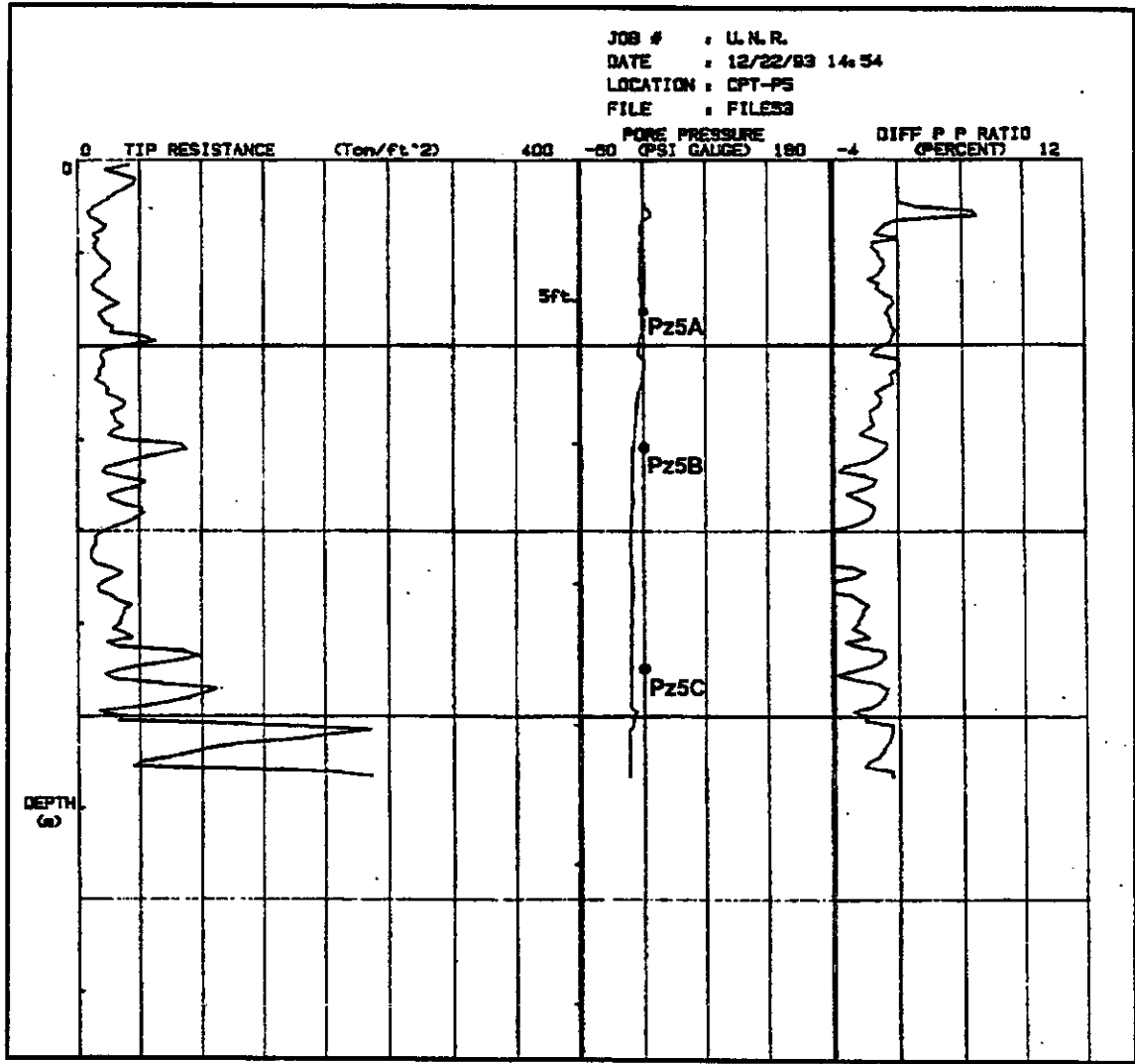


Fig 2.6c Piezo Cone Plots for Pz5

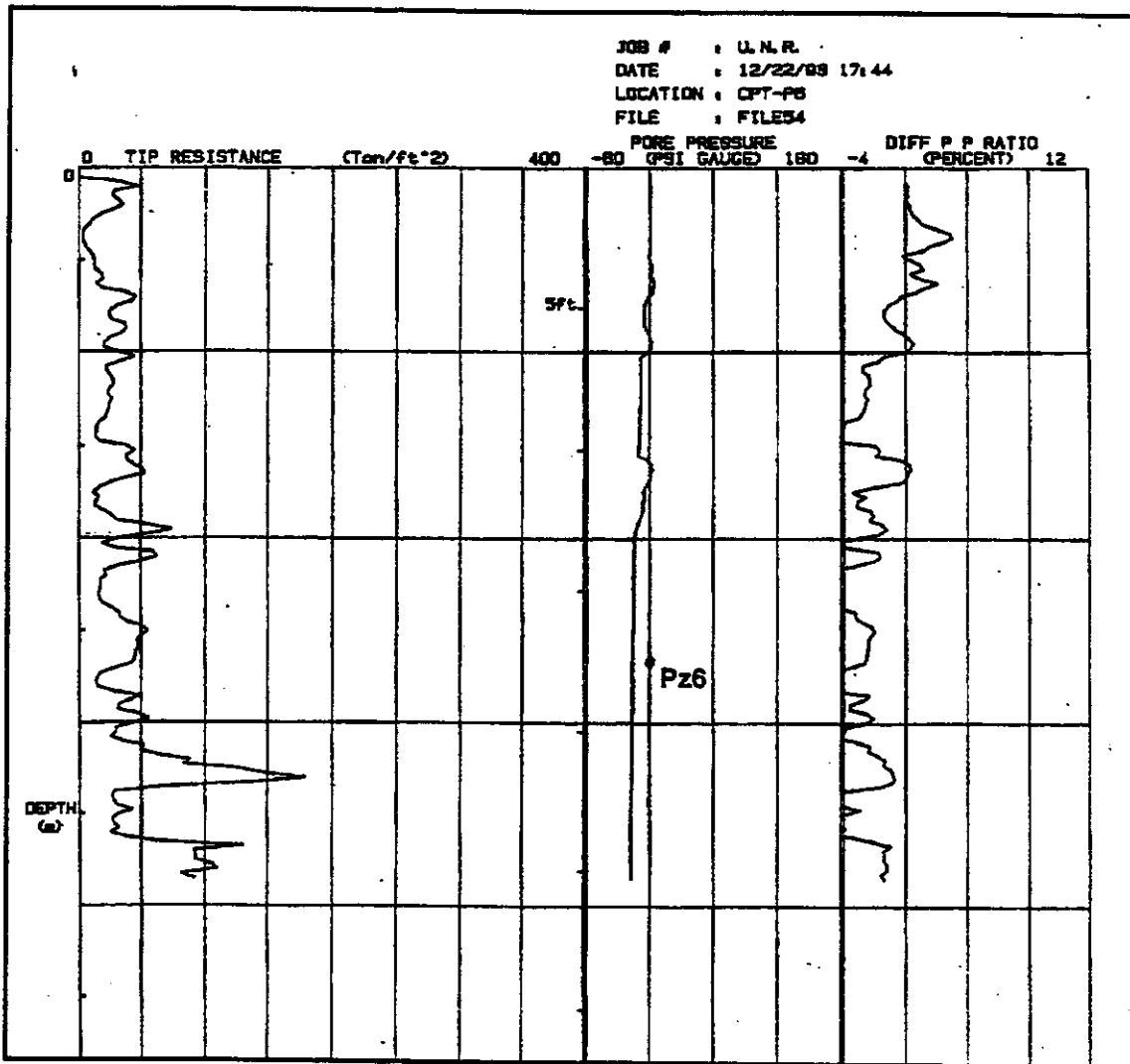


Fig 2.6d Piezo Cone Plots for Pz6

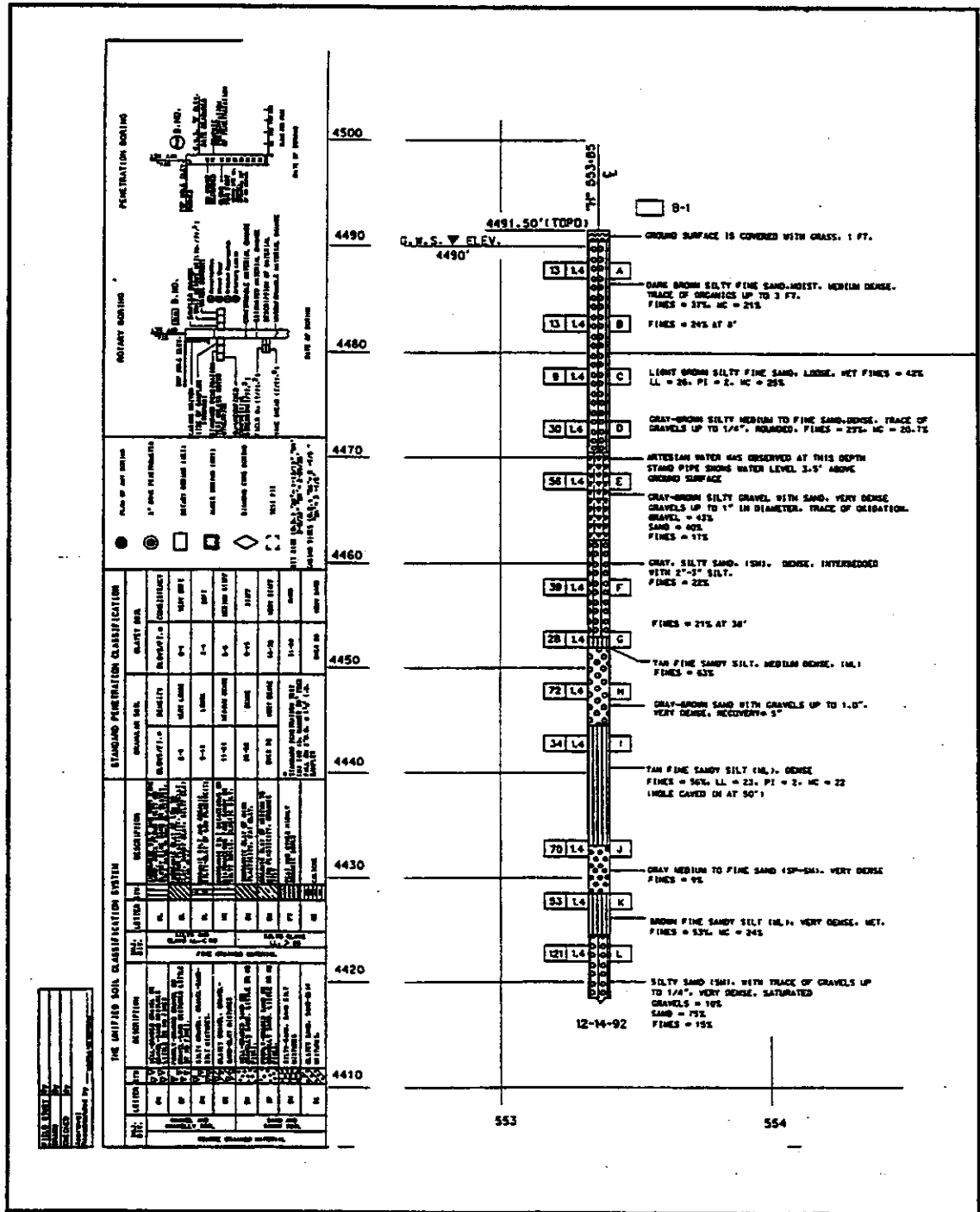


Fig. 2.7a NDOT B1

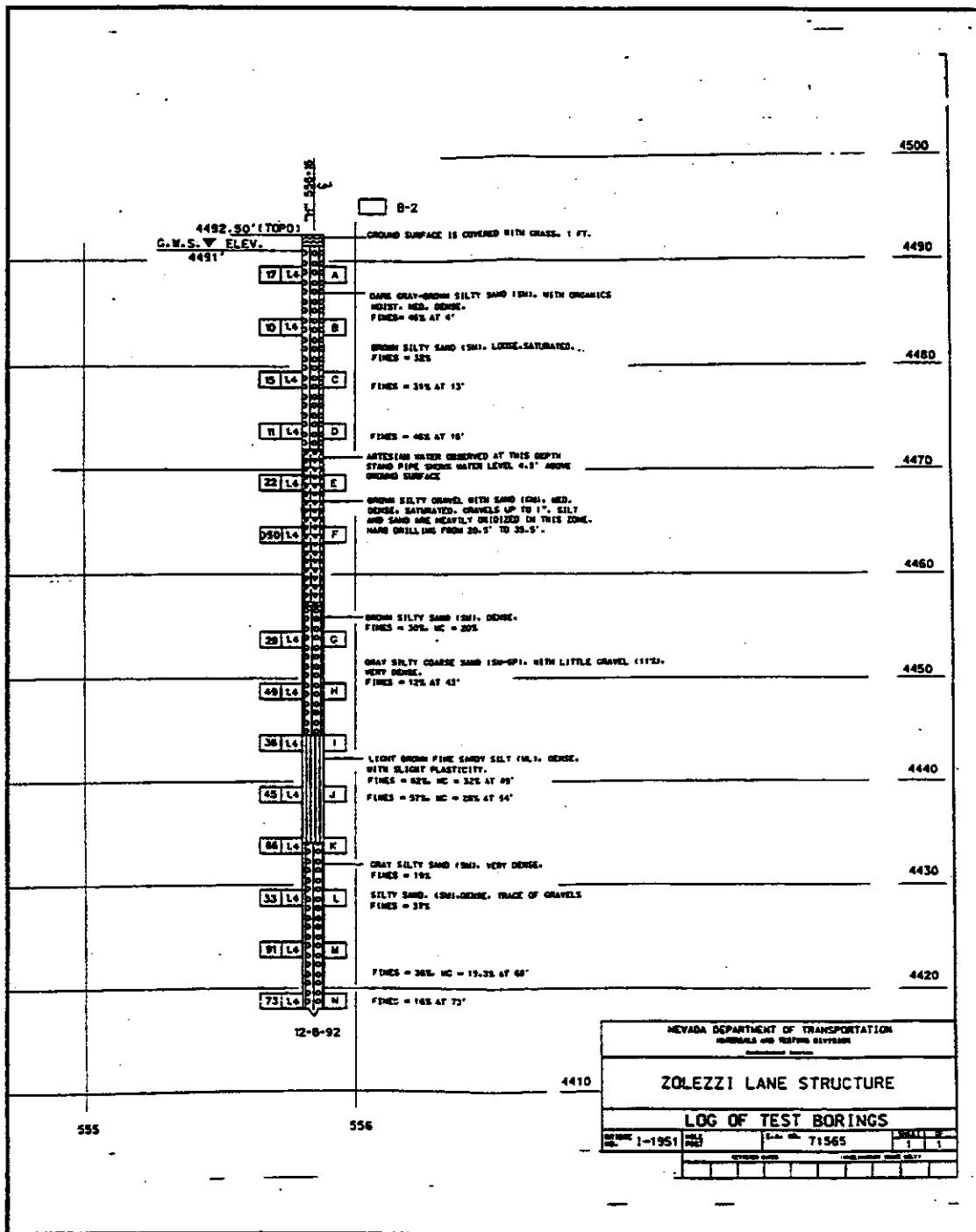


Fig. 2.7b NDOT B2

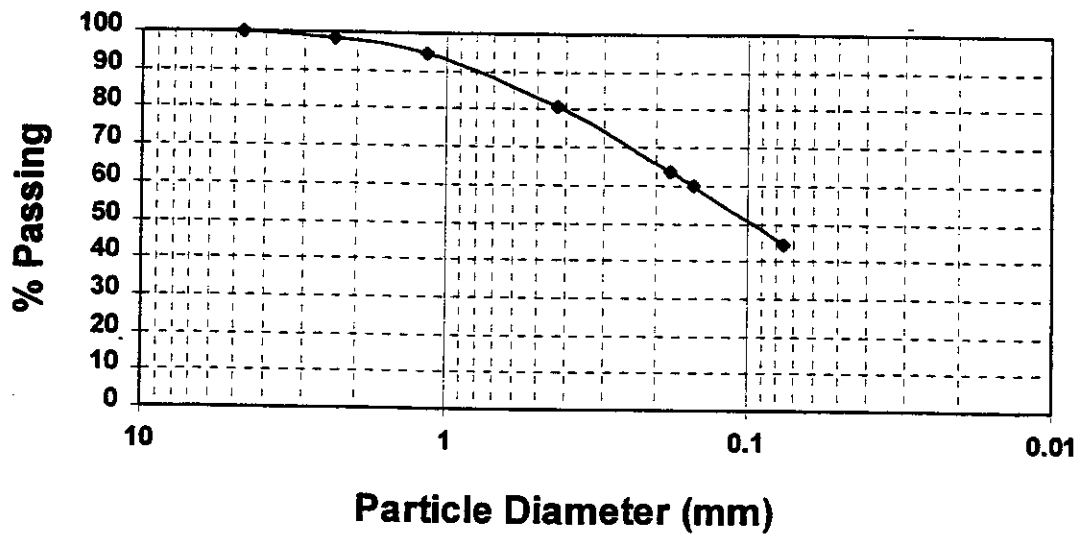


Fig 2.8a Grain Size Curve For well 1 ($D=5$ ft), $D_{50}=0.10$ mm, $C_u=14$

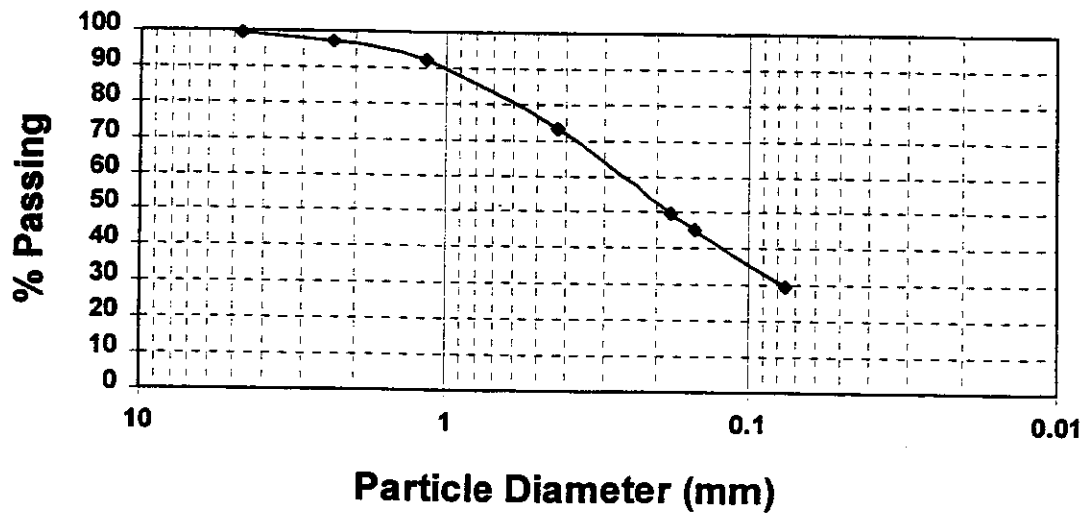


Fig 2.8b Grain Size Curve For Pz3 ($D=10$ ft), $D_{50}=0.19$ mm, $C_u=10$

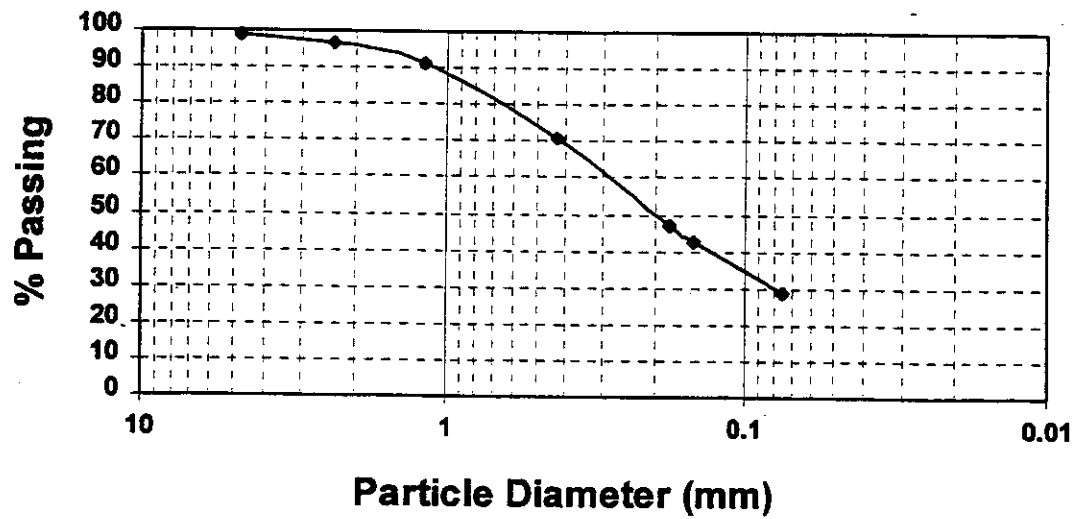


Fig 2.8c Grain Size Curve For Well2 (D=10 ft), $D_{50}=0.20$ mm, $C_u=13$

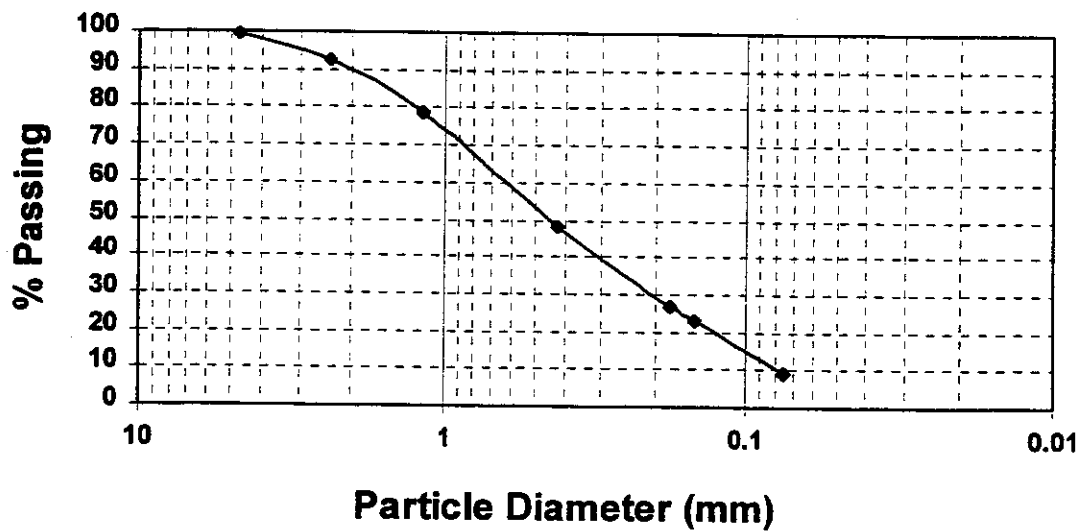


Fig 2.8d Grain Size Curve For Well2 (D=2 ft), $D_{50}=0.43$ mm, $C_u=8$

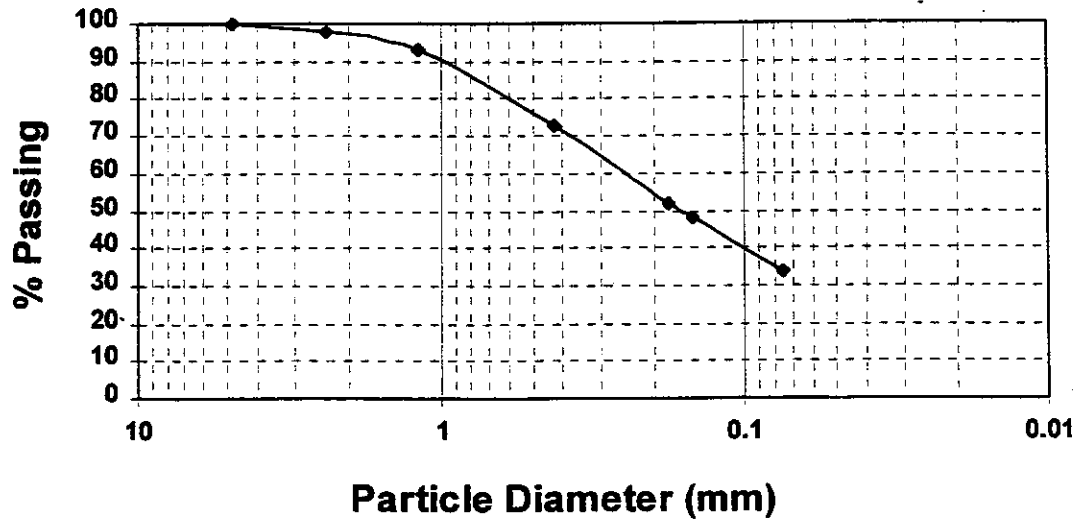


Fig 2.8e Grain Size Curve For Well2 ($D=12.75$ ft), $D_{50}=0.16$ mm, $C_u=11$

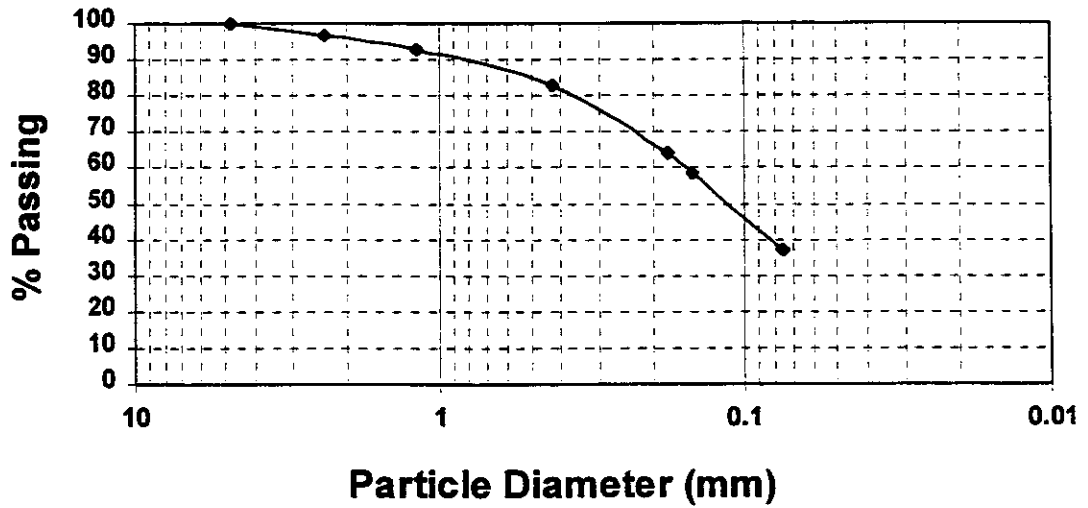


Fig 2.8f Grain Size Curve For Pz4 ($D=17.5$ ft), $D_{50}=0.11$ mm, $C_u=6$

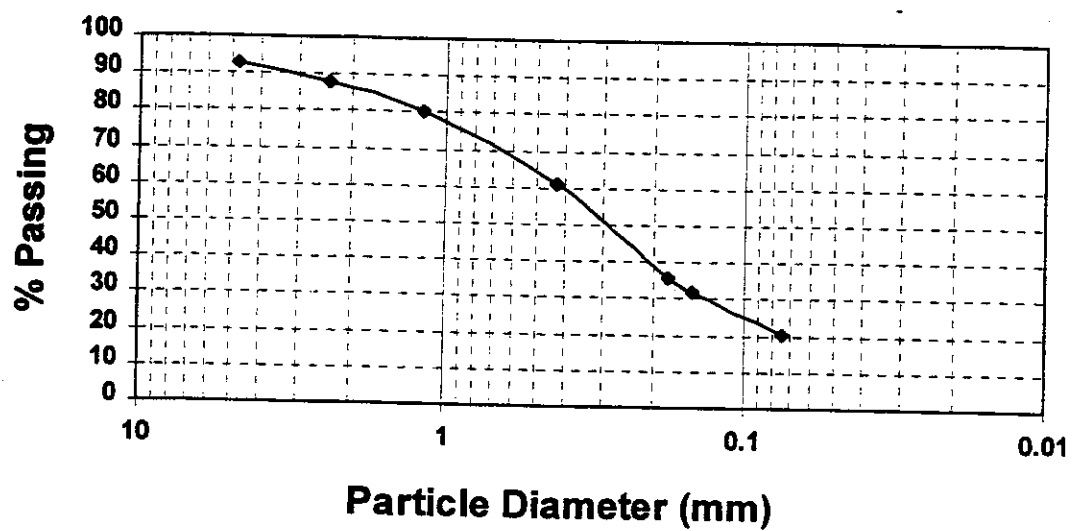


Fig 2.8g Grain Size Curve For Pz4 (D=12 ft), $D_{50}=0.28$ mm, $C_u=11$

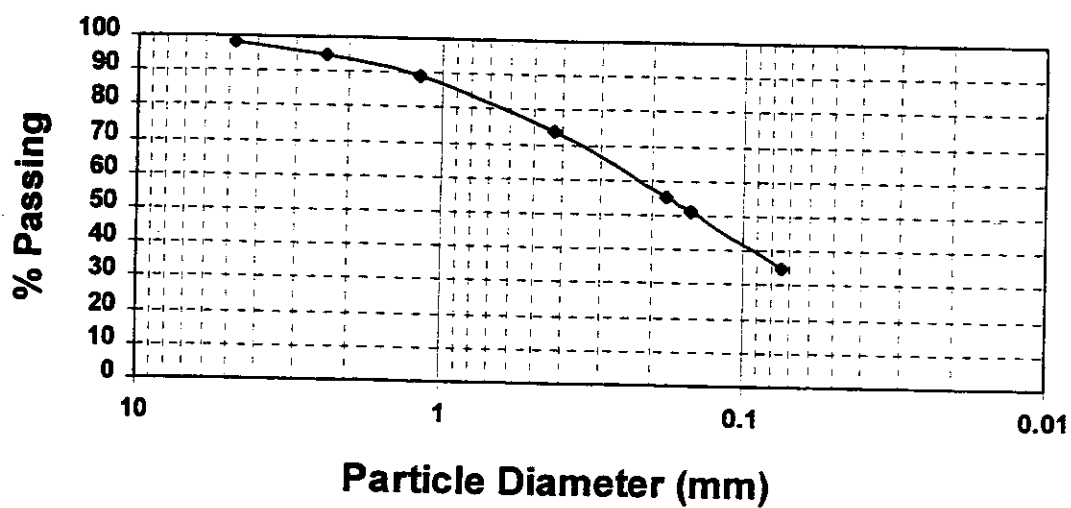


Fig 2.8h Grain Size Curve For Pz4 (D=21.5 ft), $D_{50}=0.13$ mm, $C_u=10$

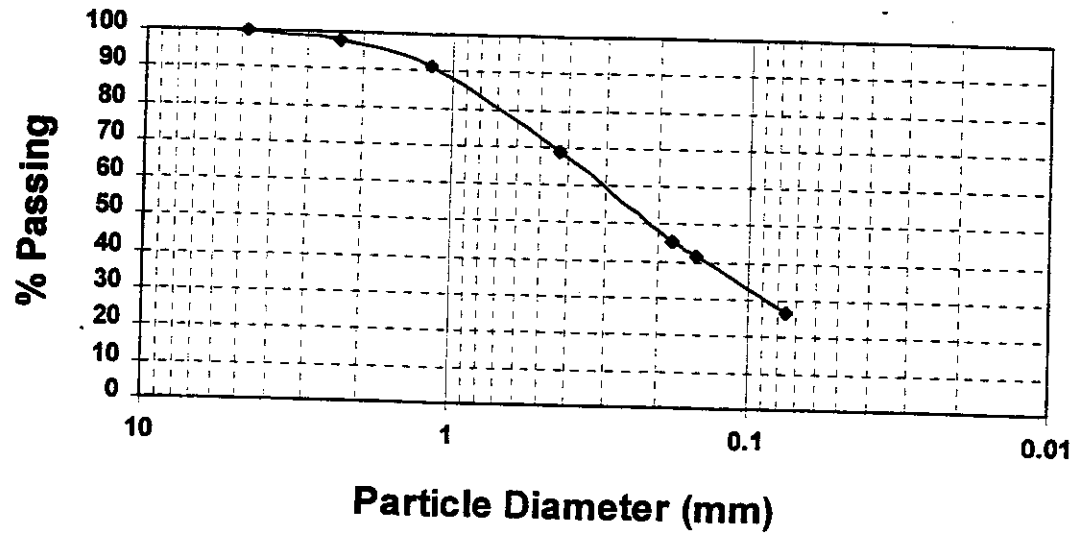


Fig 2.8i Grain Size Curve For Pz4 ($D=14.5$ ft), $D_{50}=0.20$ mm, $C_u=10$

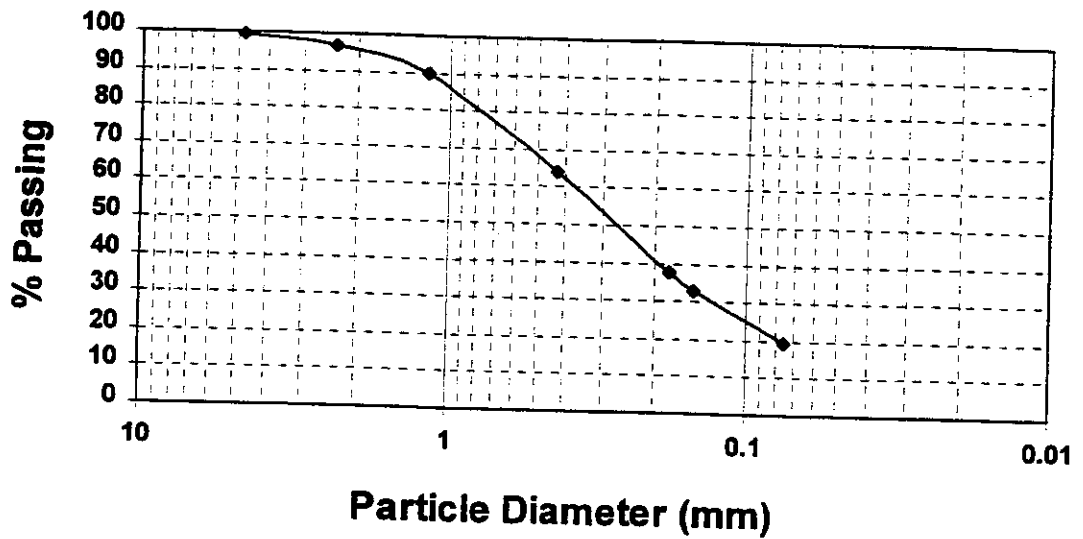


Fig 2.8j Grain Size Curve For Pz3 ($D=8.5$ ft), $D_{50}=0.26$ mm, $C_u=7$

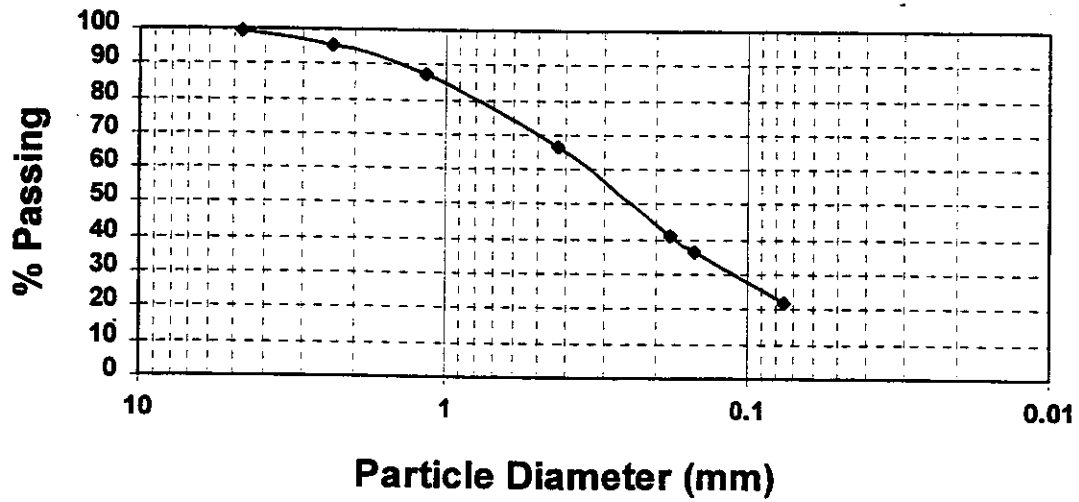


Fig 2.8k Grain Size Curve For Well 2 ($D=4$ ft), $D_{50}=0.23$ mm, $C_u=10$

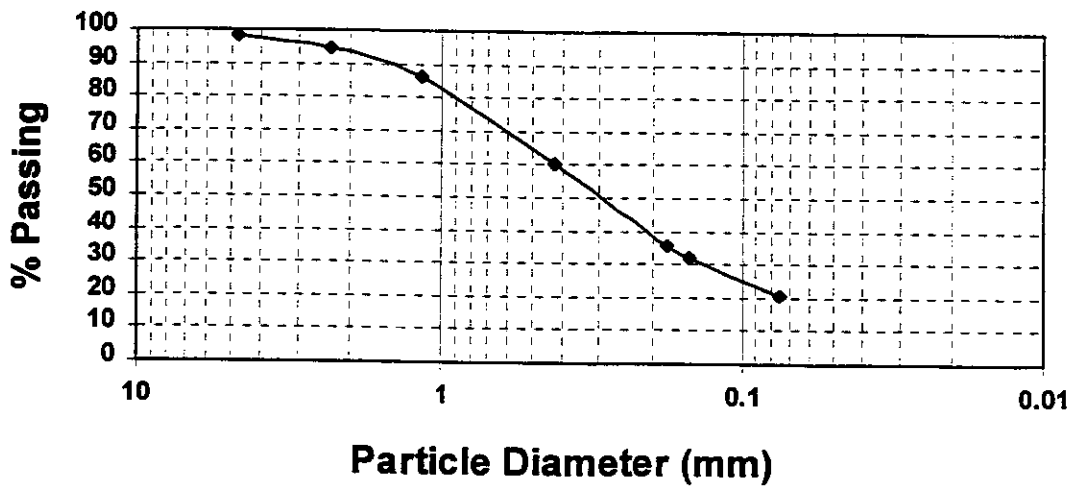


Fig 2.8l Grain Size Curve For Pz3 ($D=9.5$ ft), $D_{50}=0.30$ mm, $C_u=12$

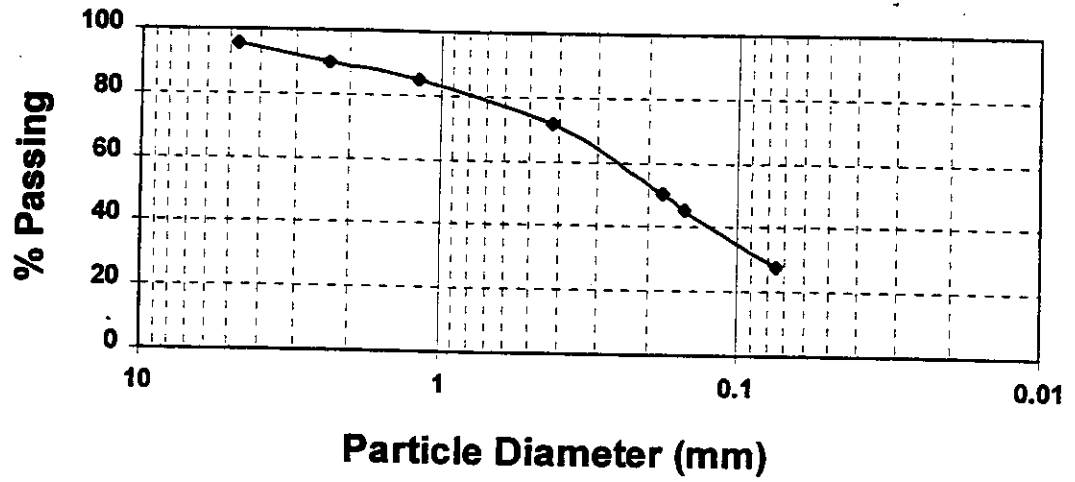


Fig 2.8m Grain Size Curve For Pz7 (D=9.75 ft), $D_{50}=0.18$ mm, $C_u=8$

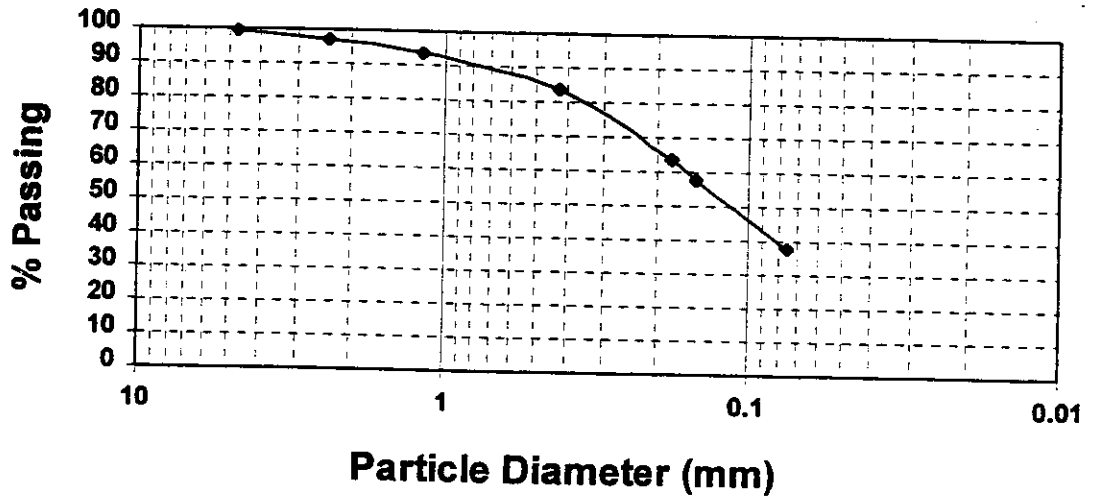


Fig 2.8n Grain Size Curve For Pz2 (D=8.5 ft), $D_{50}=0.12$ mm, $C_u=6$

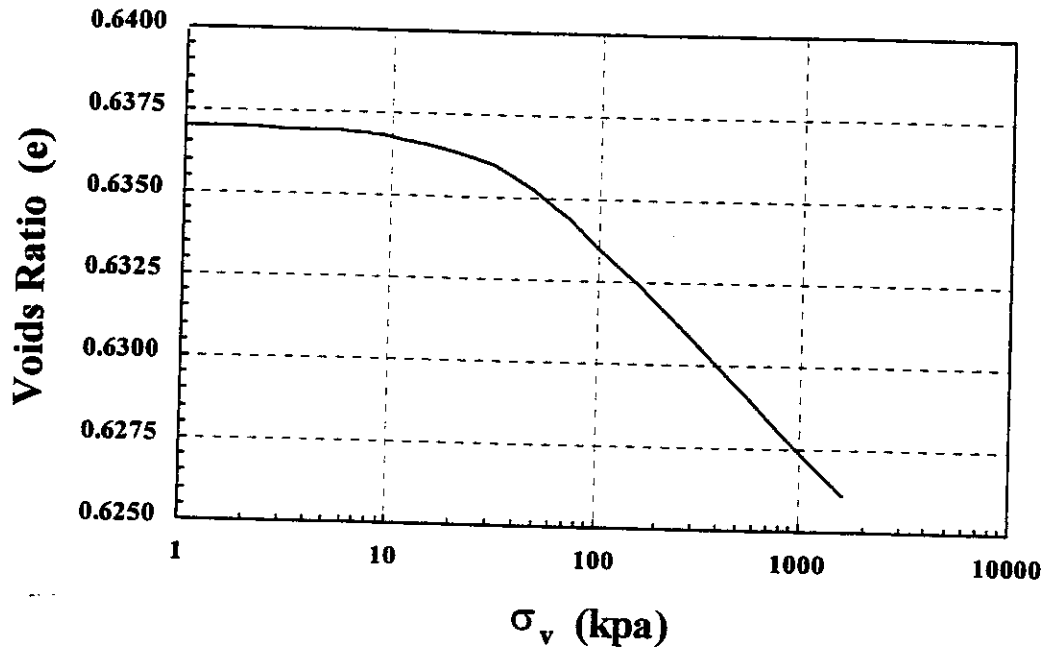


Fig 2.9 **Standard Consolidation Data Curve**

Chapter 3

Laboratory Triaxial Hydraulic Conductivity Tests

3.1. Hydraulic Conductivity

Hydraulic conductivity is defined as the coefficient of proportionality relating the rate at which water can move through a permeable medium. This property depends on the grain size, density, and the kinematic viscosity of the water. Also, particle and void orientation and soil stratification (structure) have a significant influence on the ratio between the horizontal and the vertical permeability. Different test procedures were used to determine the permeability of the soils in both directions. Laboratory tests were performed on undisturbed Shelby samples obtained during the installation of the piezometers. The proposed testing program was to use the CKC Soil Equipment triaxial system (stress path computer controlled system) along with the GDS system volume controllers in order to be able to assess the permeability under different stress conditions.

3.2. Sample Preparation

Samples for vertical hydraulic conductivity testing were prepared in a flexible wall permeameter so that the corresponding stress state could be

controlled. A triaxial chamber was used for this purpose. Fig. 3.1 shows a sketch of the chamber and specimen for vertical versus horizontal permeability assessment. The diameter of the samples used was approximately 2.8 inches which is the diameter of the extruded Shelby tube samples. The trimmed height of the samples was approximately 6.5 inches (from 2 to 2.5 times the sample diameter) in order to minimize the end friction effect from the sample cap and base as the result of an applied deviator stress. The preparation of the samples consisted of the following steps:

1. Boiling the porous stones in water for about 15 minutes;
2. Cutting a length of Shelby tube (with sample) of approximately 7 inches using an electrical saw;
3. Removing the burr, resulting from the saw cut, using a grinder;
4. Stretching a latex membrane taught against the sides of a combination membrane and O-ring stretcher by means of a vacuum;
5. Extruding the sample horizontally with a lab extruder into the membrane in the membrane/O-ring stretcher;
6. Trimming the ends of the sample;
7. Measuring the height and the diameter of the sample to 0.001 inch using a pi tape and calipers, and calculating the volume of the sample knowing the micrometered double thickness of the membrane;

8. Putting two wetted filter papers, one on the top and the other on the bottom of the sample, between the cap/base and the sample in order to prevent clogging of the porous stones;
9. Carefully placing the sample in the chamber between the cap and base and affixing the membrane to the cap and base with O-rings;
10. Filling the chamber with water until above the sample; affixing the piston and tightening the piston screw to hold the sample;
11. Placing in the triaxial chamber under the load head and putting the sample under pressure for consolidation.

In addition to the stratified undisturbed Shelby tube specimens, reconstituted samples of two fines content and density state combinations (20 and 35% fines both at $e \cong 0.60$ and $\gamma_d = 103.4 \text{ lb/ft}^3$) were also tested.

3.3. Saturation

Undisturbed soil samples of sufficient fines content that are obtained from below the groundwater table will develop capillary tension that hold them together but may, upon release of confining pressure, release gases that were in solution in the pore fluid of the soil specimen. These soils will require re-saturation prior to testing since soil hydraulic conductivity decreases with a decrease in the degree of saturation. Other reasons to saturate a test specimen are to simulate the static

water pressure applied previously to the sample in the field, to obtain accurate volume change measurements of the test specimen (volume change is based on water flowing into or out of the test specimen), and to perform K_0 consolidation with the CKC triaxial system.

A "Back Pressure Saturation" procedure has been developed over the years to saturate specimens prior to testing. This involves increasing the sample porewater pressure (back pressure) and the cell pressure simultaneously in increments. The soil specimen should undergo no volume change during the back pressure saturation process other than that caused by the small effective stresses imposed upon the sample during saturation. The effective stress is the difference between the back and the cell pressures employed and should be sufficiently lower than the effective consolidation stress that is to be applied to the specimen after saturation so as to have no effect upon the test.

The method used to check the degree of saturation of a specimen involves increasing the cell pressure by a small amount under undrained conditions and observing the increase in porewater pressure. A parameter known as the B-value is calculated which is the ratio of porewater pressure increase to the cell pressure increment applied. The theory behind the B-value and the derivation of its equation is given in Skempton (1954), i.e.

$$B = \frac{\Delta u_b}{\Delta \sigma_3} = \frac{1}{1 + \frac{nC_f}{C_s}}$$

where

Δu_b = the increase in pore fluid pressure (air and water) due to the increase in cell pressure

$\Delta \sigma_3$ = the increase in cell pressure

n = the initial porosity of test specimen

C_f = the compressibility of the fluid (water with dissolved air) in the voids

C_s = the compressibility of the soil skeleton structure

A typical B-value indicating 100% saturation will be 1.0. (However, for conditions not typical of the Zolezzi lane site involving stiff, overconsolidated, or cemented soils, and dense sand at a high confining pressure the compressibility of the soil skeleton can approach 10^{-2} kPa resulting in a low B-value at 100% saturation.) For this research program, the back and cell pressures were raised together by 30 kPa increments (keeping the effective stress at 30 kPa) over a period of three to five days until the B-value approached a value of one.

3.4. Stress Application

Two different drained finite element model stress paths were duplicated in the lab in order to try to capture the likely change in the hydraulic conductivity of the near surface soil between the fill and the artesian layer. One of the stress paths reflects the change in stress of an element beneath the centerline of the embankment, while the other corresponds to that of an element beneath the edge (toe) of the fill. Each of these two elements experience different stress changes. The first experiences an increase in the vertical stress under presumed conditions of no-lateral strain (a K_0 consolidation stress change), while the other experiences a presumed increase in the vertical stress without an increase in the horizontal stresses. The first element was modeled in the lab in the CKC computer controlled system using the drained K_0 consolidation routine over the stress range indicated from the FEDAM finite element model. The second element was modeled by increasing the deviatoric stress with time (under drained conditions) while keeping the confining pressure constant. This second stress path if carried to failure, is the same as that of the standard drained triaxial test.

According to the proposed coupled laboratory testing and numerical analysis program, modeling of the second element (i.e. the standard drained triaxial) was to be performed first. Such data would then be used as input in the FEDAM program to assess stress state changes and strains occurring in the first

element (to confirm that K_0 conditions result). Based on the coefficient of consolidation, C_v , obtained from the standard consolidation test and the corresponding backcalculated value of permeability of the soil, the rate of loading used to yield drained conditions during deviatoric stress application was chosen to be 1 kPa/min. Trial samples were used to ensure that the soil did not develop an excess porewater pressure for this chosen rate of loading.

Samples for the second element were to be isotropically consolidated to different confining pressures (depending on the depth at which the samples were taken) as in standard triaxial test. A permeability test was then performed before the start of shear loading. Thereafter, each specimen was to be loaded in increments of 20 kPa deviator stress over 20 minutes; and this value of pressure held constant for an hour, during which time a permeability test would then be performed at each stage of deviatoric stress increase. Permeability testing would then be halted when the deviatoric pressure reached 120 (or 140) kPa, after which, the test specimen would then be subjected to a strain controlled shear test to evaluate its drained strength. The intent was to assess changes in permeability during shear loading, of an approximately modified standard drained test, thus yielding a variation in permeability over this assumed stress path (for element 2 below the edge of the fill) while yielding the drained strength for use in the FEADAM analysis.

3.5. Equipment

3.5.1. Stress Path

A computer controlled CKC stress path system (Li et al, 1988) was used to apply the stresses to the test specimen. For this automated triaxial testing system, nine channels are employed: five channels are used to monitor the output signals from the five sensors with which the system is equipped. One channel monitors the drainage condition, two are used to monitor electro pneumatic (e/p) valve drive signals, and the other one is used for a zero reference to minimize the zero shift of the grounded system. The five converters are configured to high resolution controllers to control the axial load and the lateral pressure, respectively. The signal conditioner accommodates the five sensors.

The microcomputer with disk drives and high resolution graphics serves as the "brain" of the whole system. It receives and stores the real time data in its memory and issues control signals to regulate the testing process accordingly. Since the system is capable of performing different types of loading, a predefined stress path is introduced to the microcomputer, and thus applied to the sample.

3.5.2. Hydraulic Conductivity

To serve the purpose of measuring the hydraulic conductivity of a saturated sample under back pressure, a closed loop system capable of accurately measuring the volume of water moving into or out of the sample should be used. Two separate systems were used for this purpose, the GDS system volume controllers and a permeability board.

3.5.2.1. GDS

The GDS system (Bishop and Wesley, 1975) volume controllers employ the “flow pump” method of permeability testing which basically entails applying a specified flow rate, either into or out of the base of the test specimen while a constant back pressure is maintained at the top of the test specimen. The resulting hydraulic gradient imposed upon the test specimen is calculated to achieve the target flow rate. The advantages of using the flow pump method of permeability testing are these:

- The reliance on measuring the flow rate into and out of the sample is avoided.
- Permeability results can be obtained much more rapidly and at much smaller gradients than in conventional test procedures.

- The head difference across a test specimen can be measured for the zero flow condition and used as a reference for measuring head differences induced upon the test specimen by externally applied flow rates.
- The head difference caused by the externally imposed flow rate can be recorded with time.
- The transient response of the system that precedes the development of a steady state condition can be used to evaluate permeability; such is not the case with constant head and falling head test methods.

3.5.2.2. Permeability Board

The permeability board supplied by AMI consists of three regulators, two reservoirs, and four clear tubes. Fig. 3.2 shows a sketch of the permeability board used in performing the hydraulic conductivity tests. The three regulators are to regulate the cell pressure, the headwater pressure, and the tailwater pressure. Each of the two reservoirs and two out of the four tubes are connected to the headwater regulator, while the others are connected to the tailwater regulator. During the process of measuring the hydraulic conductivity, the water path from the triaxial cell drainage lines was switched from the CKC system to the permeability board. A gradient was applied to the sample by introducing a difference in pressures between the head and the tail of the specimen. The concept used is that of falling

headwater - rising tailwater which makes the gradient change with time. The volume of water going into and out of the test specimen is calculated from readings taken from the clear tubes.

3.6. Horizontal Hydraulic Conductivity

Given that natural samples may be layered or, in the case of the present samples, are likely to vary in fines content in relatively indistinguishable units vertically, differences in horizontal and vertical permeability are to be expected. If one has a composite system of horizontal units of varying permeability as indicated in Fig. 3.3, then the vertical flow rate through a soil column (or triaxial specimen) will be

$$q = \frac{\Delta h}{\frac{H_1}{k_1} + \frac{H_2}{k_2} + \dots + \frac{H_N}{k_N}} A$$

In this equation, H_1, H_2, \dots, H_N and k_1, k_2, \dots, k_N are the heights and permeabilities, respectively, of the various units, A is the cross sectional area of the column (or triaxial test specimen) and Δh is the water level or head difference across the sample (top versus bottom). However, if

$$q = kiA$$

where i , the hydraulic gradient, is $i = \frac{\Delta h}{L}$ (and $L = \sum H_i$) and we assess k_{av} as

$$k_{av} = \frac{q}{iA} = \left(\frac{\Delta h}{\frac{H_1}{k_1} + \frac{H_2}{k_2} + \dots + \frac{H_N}{k_N}} \right) A \bigg/ \left(\frac{\Delta h}{L} \right) A$$

then

$$k_{av} = \frac{L}{\frac{H_1}{k_1} + \frac{H_2}{k_2} + \dots + \frac{H_N}{k_N}}$$

or

$$k_{av} = \frac{1}{\frac{H_1}{L} \frac{1}{k_1} + \frac{H_2}{L} \frac{1}{k_2} + \dots + \frac{H_N}{L} \frac{1}{k_N}}$$

In this instance, k_{av} is dramatically affected by the presence of any unit (say j) of very low permeability (k_j). For instance, if $k_j = 10^{-6}$ cm/sec and all other units are 10^{-4} cm/sec and all thicknesses are the same ($H_i = L/N$) then

$$k_{av} = \frac{N}{\frac{1}{k_1} + \frac{1}{k_2} + \dots + \frac{1}{k_j} + \dots + \frac{1}{k_N}}$$

Let's say $N = 11$, then

$$k_{av} = \frac{11}{10 \frac{1}{10^{-4}} + \frac{1}{10^{-6}}} = \frac{11}{10^5 + 10^6} = \frac{11}{10^6(1.1)} = 1 \times 10^{-5} \frac{\text{cm}}{\text{sec}} = 10^{-5} \text{ cm/sec}$$

By contrast, if flow is horizontal through a rectangular column of width B

$$q = (k_1 H_1 + k_2 H_2 + \dots + k_N) i B \quad \text{where } A = BL$$

and if k_{av} is assessed as

$$k_{av} = \frac{q}{iA} = \frac{\sum k_i H_i iB}{iBL}$$

$$k_{av} = \frac{\sum k_i H_i}{L} = \frac{\sum k_i H_i}{\sum H_i}$$

then for the same example (all H_i are L/N , $N = 11$, $k_j = 10^{-6}$ cm/sec and all other units are 10^{-4} cm/sec)

$$k_{av} = \frac{10^{-6} + 10(10^{-4})}{11} = 0.91 \times 10^{-4} \cong 10^{-4} \text{ cm/sec}$$

Therefore, the assessed permeability (k_{av}) is 10 times less in the vertical (for flow in series through the various units) than in the horizontal direction (for flow in parallel through the various units) due to the presence of a unit of one hundred fold less permeability of less than 1/10 the height. Note that the horizontal permeability is basically that of the more permeable material.

For the above reason, it was felt that the horizontal (as well as the vertical) permeabilities should be determined in the lab, since it would be the change in horizontal flow that is of greatest concern relative to the field problem, i.e. the effect of fill construction on (essentially horizontal) groundwater flow conditions.

3.7. Horizontal Hydraulic Conductivity Tests

Lab tests were conducted on undisturbed samples to assess the hydraulic conductivity in the horizontal direction (i.e. in the direction of the stratified

lenses). The idea was to let water flow from the center of the specimen to its outer radius where it could be collected and measured. A special cap and base were designed for this purpose, and the samples were tested in the triaxial chamber. There was a porous stone of 0.5 in. diameter in the middle of the cap and the base had an outer channel for collecting the water see Fig 3.1b. Special steps involved in preparing samples for horizontal permeability testing were as follows:

1. Samples were trimmed to the required length (about 6 in.).
2. A hole of 0.5 in. in diameter was drilled in the middle of the specimen along its length.
3. This hole was then filled with coarse sand.
4. A filter paper was wrapped around the sample. Note that this filter paper was slit in order not to provide any restraint during stress path testing.
5. A layer of coarse sand was placed between the filter paper and the membrane for the purpose of collecting water and delivering it to the outer channel of the base.
6. A thin layer of Navajo Red Wheel clay was used as a sealer at the ends of the specimen between the sample cap and the base.

These samples were placed under backpressure for 4 to 5 days prior to testing to ensure their saturation. Despite of the fact that the B-value check is not completely valid (due to the presence of the sand column), a routine check was

made prior to testing. During the hydraulic conductivity testing, a small hydraulic gradient was applied from the center (sand column) so that water would flow outward across the sample (i.e. radial flow). Readings for the volume of water going into and coming out of the specimen were taken with time, from which the hydraulic conductivity in the horizontal direction was calculated. The equation used for this calculation was:

$$k_{hz} = \frac{a_{in} * a_{out}}{a_{in} + a_{out}} \frac{1}{2\pi Lt} \ln\left(\frac{h_1}{h_2}\right) \ln\left(\frac{R}{r_o}\right)$$

where

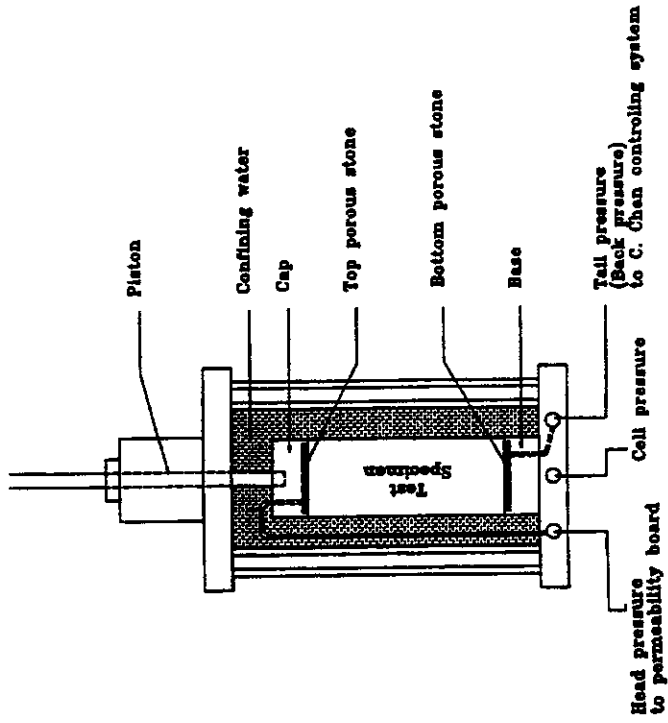
- a_{in} is a calibration factor for water going into the sample (cc/cm)
- a_{out} is a calibration factor for water coming out of the sample (cc/cm)
- L is the height of the sample (cm)
- t is the time (sec)
- h_1 is the head applied in the center of the specimen (cm)
- h_2 is the head applied at the edge of the specimen (cm)
- R is the outer radius of the specimen (cm)
- r_o is the radius of the hole (cm)

A mathematical proof of the above equation, as well as a sample of the readings and the calculations, is provided in Appendix 5.

3.8. Summary

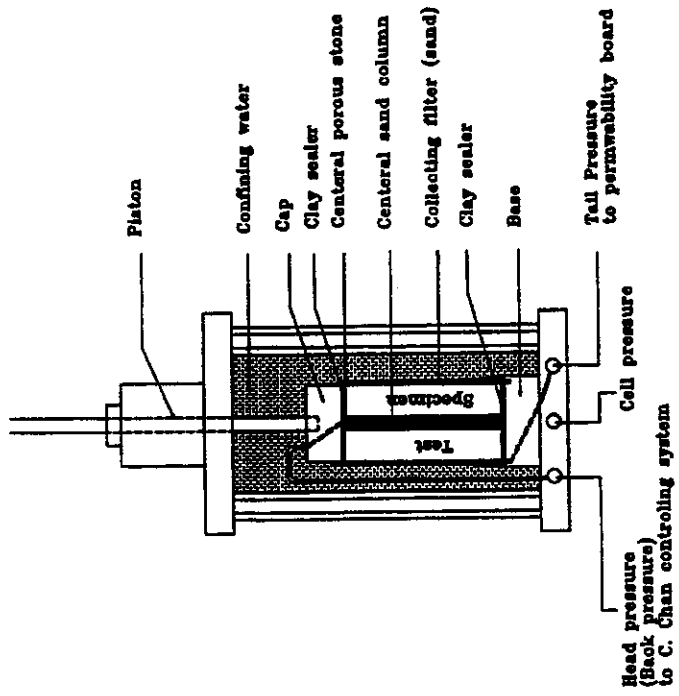
Results of laboratory horizontal and vertical permeability tests for isotropic stresses and element 1 and 2 stress paths are presented and discussed later.

Vertical Permeability Testing



a.

Horizontal Permeability Testing



b.

Fig. 3.1 Triaxial Test Set-up for a) Vertical and b) Horizontal Permeability Assessments

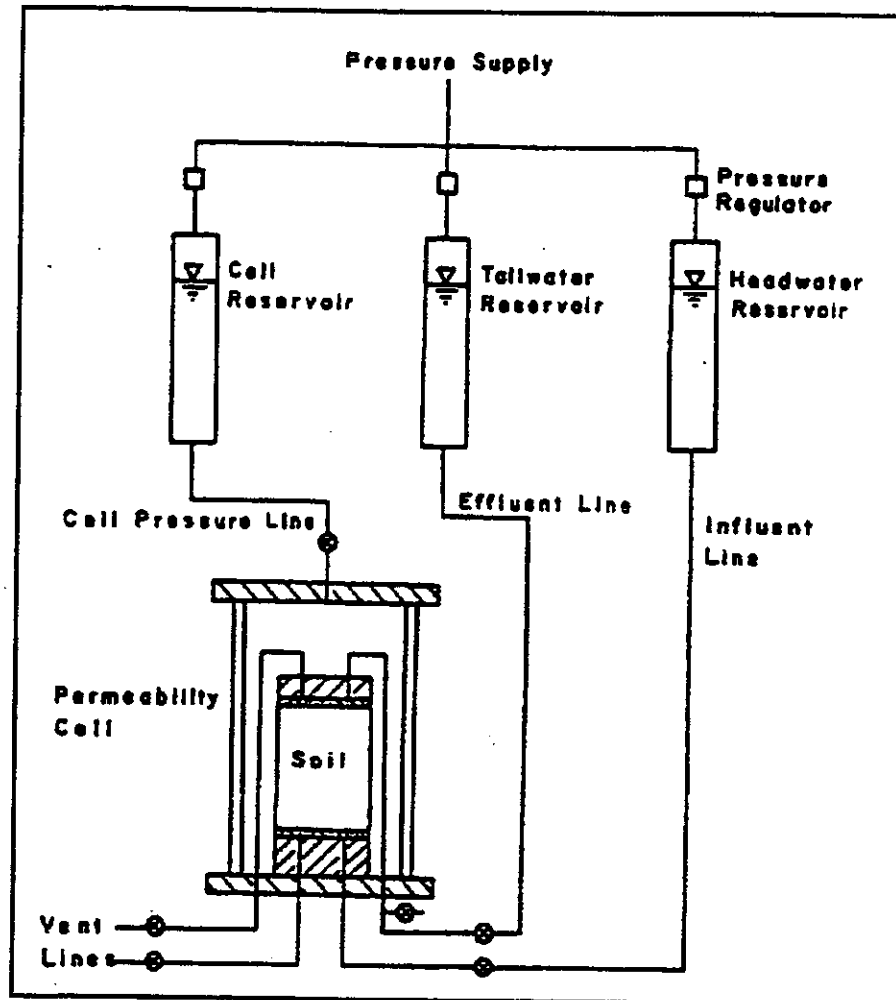


Fig. 3.2 A Schematic Sketch Permeability Board

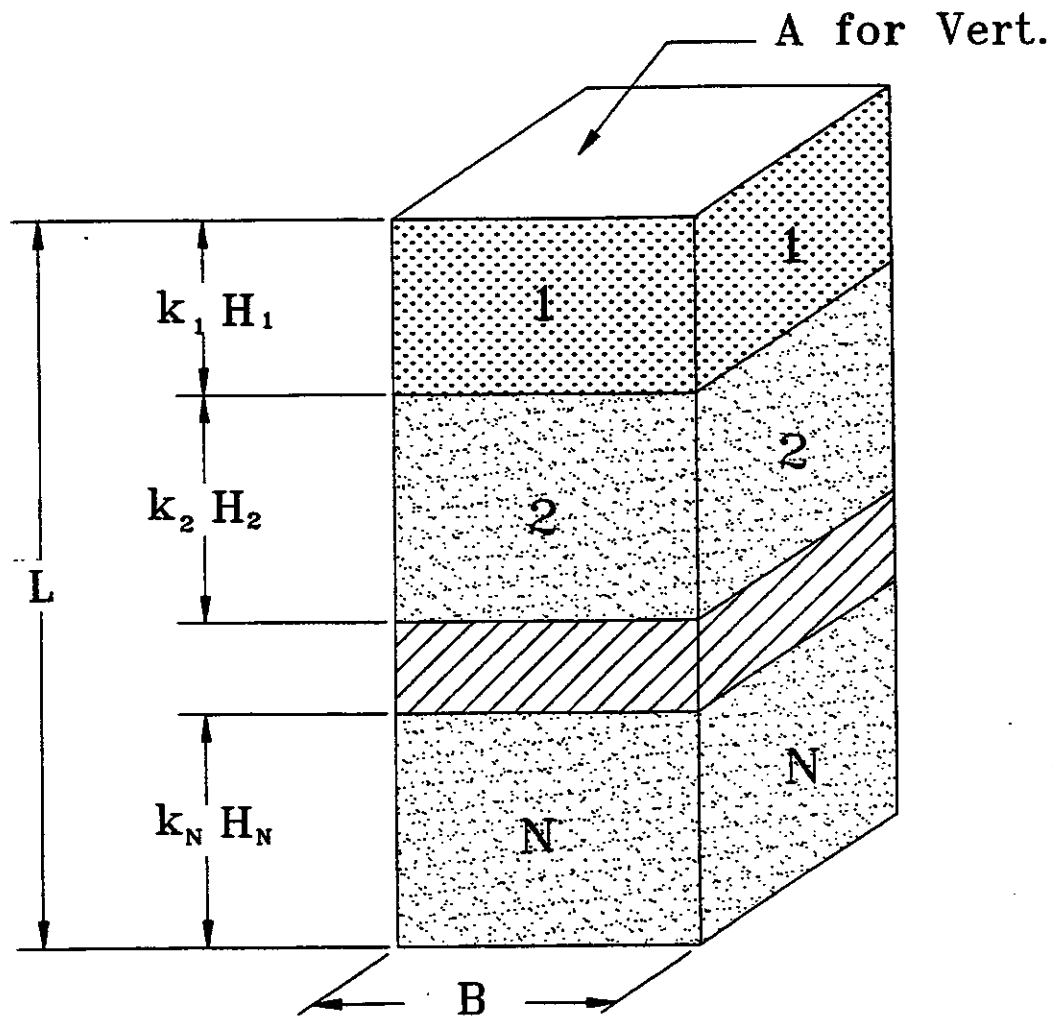


Fig. 3.3 Permeability in Layered Soils

Chapter 4

Field Hydraulic Conductivity Tests

4.1. Field Tests

Given the previously mentioned slug tests performed in wells 1-3 at Pz3 (see Chapter 2) and the resulting several orders of magnitude difference in permeabilities from lab (and field CPT) versus slug test results, the desire to obtain additional field test (i.e. a bailing test) and lab test (i.e. reconstituted instead of just undisturbed sample) permeabilities grew. This chapter is devoted to a discussion of the field tests: the CPT dissipations, the slug test and, separately, the bailing test which was added to the program and was undertaken east of the already constructed highway fill at Pz2 location.

4.2. CPT Dissipations

In conjunction with the CPT logs obtained 12/22/93, dissipations of the negative porewater pressures included during advancement of the cone were obtained at 3.9, 6.6, 9, 11.5, and 16.6 ft. depths at Pz3 location. Fig 4.1 shows the recorded dissipation (negative porewater pressure versus time) at the 11.5 ft. depth. A value t_{50} of 310 seconds or 5.2 minutes yields a permeability (k) of 4×10^{-7}

cm/sec average (or 3.3×10^{-8} to 2×10^{-6} cm/sec range) from Fig 4.2 for this one dissipation. Similar evaluations were made for the four other dissipations. Table 4.1 and Fig 4.3 show the results of these evaluations.

4.3. Slug Test

The slug test is a falling head test performed in the field to determine the largely horizontal hydraulic conductivity of the soil region in which the screen of the well is embedded. This test is performed by applying a hydraulic head (above the static water table) in the well and, then, monitoring the decrease in head with time. Wells 1 and 2 were used for this purpose. As it was described earlier (Chapter 2), Well 1 had a screen length of 4 ft. and an effective depth of 10 ft., while Well 2 had a screen length of 2 ft. with the same effective depth (10 ft.) as Well 1. Note that the screen length is the height of the permeable sand around the slotted portion of the PVC tube and not the height of the slotted portion of the PVC. Wells 1 and 2 are located near Pz3 and 7 ft. apart from each other (see Fig 2.4). They both have the same inner and outer diameters. The difference in the screen lengths for the two wells was employed in order to try and separate the horizontal and the vertical hydraulic conductivity. Well 3 was added (see Fig 2.5) when it was thought that the proximity of Well 2 had an effect on Well 1's

response, and vice versa. Unfortunately, Well 3 was covered by a construction road soon after its installation and, therefore, did not provide any data.

Different methods were adopted to assess the field permeability from the recorded slug test data. Equations from p 7.1-104 of DM-7 (1986) which is reproduced as Fig 4.4 were used in these assessments. The well is best characterized by the figure entitled "piezometer" for which both the middle (isotropic) and right hand (anisotropic) panel equations at the bottom of the page apply. Appendix 6 provides an example of the use of Well 1 and 2 data to separate the horizontal and the vertical permeabilities. Please note, however, that values of "m" in such calculations varied from one day's readings to the next (and at times, were negative) so that attempts to separate field horizontal and vertical permeabilities were abandoned. Therefore, the isotropic permeability was adopted.

An additional attempt using lab determined horizontal and vertical permeabilities that differed as a function of the percent fines, in conjunction with the change in the soil (as characterized by the CPT logs) over the 2 versus the 4 ft. screen lengths of the two wells, and layered permeability equations (see Chapter 3) to establish the equivalent field determined isotropic permeability likewise proved fruitless.

4.4. Bailing Test

A shallow well (Well 4) was installed above the artesian layer near Pz2 as shown in Fig 4.5. The well was constructed Feb. 1995 using the NDOT drill rig, boring to the desired depth with an 8-inch hollow stem auger (that yielded a 9 ¼ inch hole), placing 5 inch diameter slotted PVC pipe into the hole, on top of a 2 ft. length of hole plug at the bottom, and placing a sand pack in the annular space between the casing and the boring to the ground surface. The length of the sand pack and pipe was 10 ft.. The original intent was to use the well to perform a pumping test to evaluate the gross lateral hydraulic conductivity of the soils overlying the artesian layer. A pump test planning program and design (Walton, 1987) were performed to estimate the response of the aquifer to the pump test. The results of the planning and design program indicated that even with very low pumping rates, 1-gallon per minute, the well would be essentially pumped dry before there would be enough of a response in the planned observation wells to provide any reasonable data. Therefore, it was decided to change from a pumping to a recovery (bailing) test for the purpose of evaluating the overall lateral hydraulic conductivity of the near surface soils.

Prior to performing the recovery test, the well was developed and then allowed to equilibrate. Developing the well consisted of manually swabbing and bailing the well numerous times until no further decrease in water turbidity was

noted. The recovery test was performed by bailing all of the water out of the well casing and timing the rise of water inside the casing as water flowed out of the soils and back into the well. The lateral hydraulic conductivity was calculated utilizing a method which is detailed in Boast and Kirkham (1971). In general, this method is a solution to the Laplace equation with boundary conditions defined for radial flow of water into an auger hole from an unconfined aquifer taking into consideration the geometry of the well and aquifer. Evaluation of the hydraulic conductivity utilizing this method involves calculating the rate of rise of water in the well casing from the start of the test to $\frac{1}{4}$ full and selecting the appropriate shape factor out of a table provided in the reference.

4.5. Summary

In addition to the slug test and CPT dissipations, a bailing test was added to the tests performed in situ. The results of these and the lab test permeabilities are presented in Chapter 8.

Table 4.1 Permeability Value resulting from CPT Dissipations

Depth (ft)	t ₅₀ (min)	Hydraulic Conductivity		
		L. Limit (cm/sec)	Average (cm/sec)	U. Limit (cm/sec)
3.90	12.86	1.0 x 10 ⁻⁸	1.0 x 10 ⁻⁷	6.0 x 10 ⁻⁷
6.59	9.86	1.7 x 10 ⁻⁸	1.7 x 10 ⁻⁷	8.0 x 10 ⁻⁷
9.00	4.86	3.5 x 10 ⁻⁸	4.0 x 10 ⁻⁷	1.5 x 10 ⁻⁶
11.50	3.44	5.0 x 10 ⁻⁸	5.5 x 10 ⁻⁷	2.3 x 10 ⁻⁶
16.56	2.57	7.0 x 10 ⁻⁸	7.0 x 10 ⁻⁷	3.0 x 10 ⁻⁶

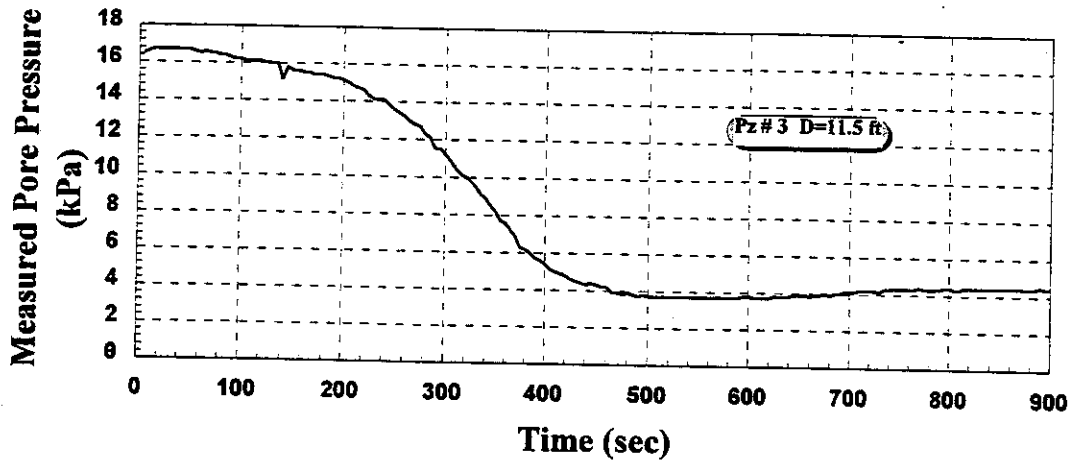


Fig 4.1 Cone Dissipation Plot

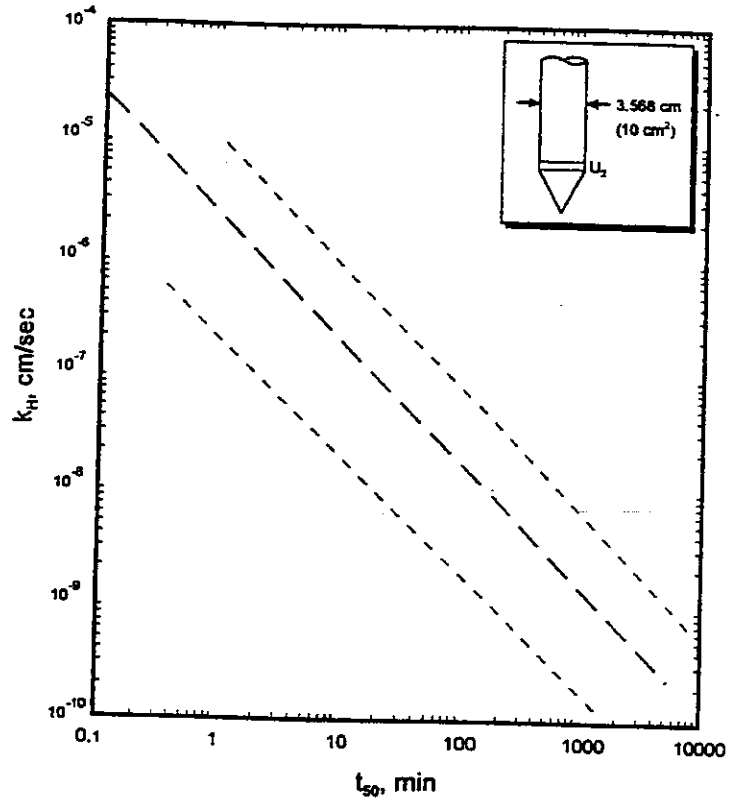


Fig 4.2 Average Values of Laboratory Derived Horizontal Coefficient of Permeability (k_H) and CPTU t_{50} for U_2 Pore Pressure Location (ConeTec Investigations Ltd., 1990).

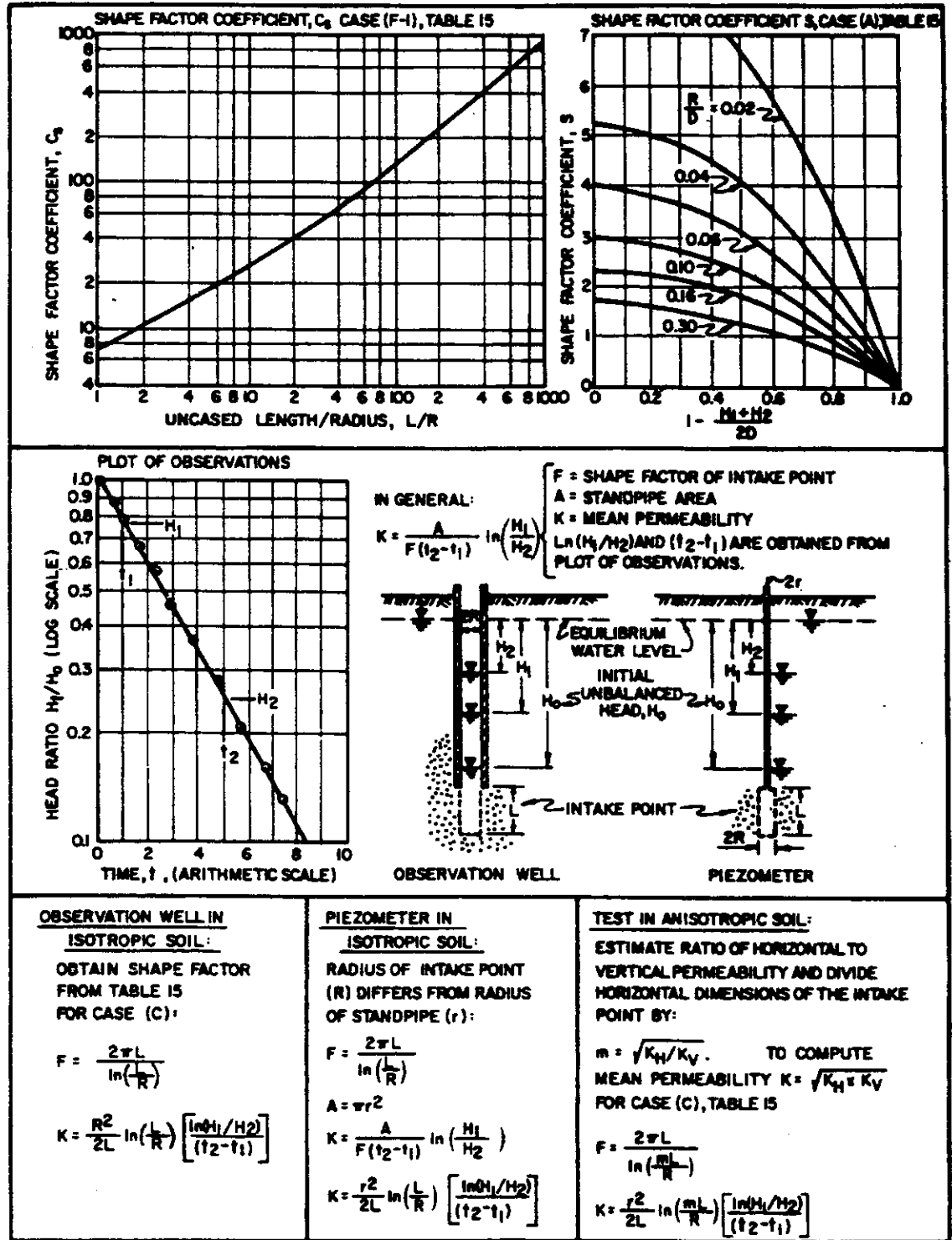


Fig 4.3 Analysis of Permeability by Variable Head Test (DM-7).

Chapter 5

Analytical Modeling

5.1. Stress Modeling

FEADAM84 is a readily available incremental finite element program for two dimensional, plane strain analysis of earth and rockfill dams and embankments. It calculates the stresses, strains, and displacements due to incremental embankment construction and/or load application. The nonlinear and stress path dependent stress-strain and volumetric model was developed by Duncan, Byrne, Wong and Mabry (1980), but modified by Seed and Duncan (1984).

A successive-increment procedure is used for approximating nonlinear stress and stress path dependent behavior of soil, in which progressive (construction) loading is divided into a number of small increments, and the soil behavior is assumed to be linear within each increment. The modulus values used to model each soil element are re-evaluated each increment in accordance with a) the stress in the element, and b) the previous stress history of the element.

The nonlinear, stress-level and stress-path-dependent soil behavior characterization used in FEADAM84 is a modified version of the hyperbolic

stress-strain, strength, and volumetric strain model proposed by Duncan et al. (1980) used in the earlier program FEADAM. The original 1980 model assumes that stress-strain curves for soils at a different confining stress ($\bar{\sigma}_3$) can be approximated as hyperbolas. The hyperbola can be represented by an equation of the form,

$$(\sigma_1 - \sigma_3) = \frac{\varepsilon}{\frac{1}{E_i} + \frac{\varepsilon}{(\sigma_1 - \sigma_3)_{ult}}}$$

where,

ε = axial strain

$(\sigma_1 - \sigma_3)$ = deviatoric stress

E_i = the initial tangent modulus

$(\sigma_1 - \sigma_3)_{ult}$ = the asymptotic value of the deviatoric stress

The 1980 model suffers from two serious problems concerning unloading-reloading which, coupled with the fact that modeling unloading-reloading behavior is not absolutely vital in many finite element geotechnical applications resulted in deletion of the unloading-reloading modulus from the program FEADAM in 1982. Instead, primary loading moduli were used for all elements regardless of stress

level. FEADAM84 incorporates an improved model for unloading-reloading moduli in order to overcome the earlier problems.

For each load increment, FEADAM84 will provide the following:

1. Nodal point forces
2. Incremental and total nodal displacements
3. The modulus values used in the computation, and
4. The stresses, strains, and stress levels of each element.

It is important to mention that FEADAM84 is mainly used for stress computation in the elements during construction phases. If the stress level for a certain element is 1.0, that means that this element has reached failure. If we have a continuous set of elements that are failing in a given construction phase, then a failure surface is being generated and a failure mechanism is indicated.

5.1.1. The Model

The scope in the use of this model was to calculate the stress change in the elements beneath the fill-embankment, both under centerline and beneath the edge, due to fill loading. Time dependent consolidation of the soil above the artesian layer in response to these undrained stress changes would in turn cause a change in the soil's permeability and this would, in turn affect the groundwater flow regime.

To undertake the embankment loading assessment, it was first necessary to evaluate the original stresses in the elements before the start of fill construction.

The soil profile employed for the site is shown in Fig. 5.1. Note that the upper soil (soil 1) is the silty sand (SM) layer of greatest concern. It sits atop the artesian layer (soil 2). Initial vertical effective stresses were calculated by spreadsheet based on assumed level ground conditions for two separate cases of groundwater flow pore pressures. In one instance, static water conditions with the groundwater table at 4 ft. depth was assumed as shown in Fig 5.2. (Note the 4 ft. water level jump at the artesian interface) In another, steady-state upward flow was assumed with the piezometric water level one foot below ground surface and 4 ft. higher than this in the artesian layer. A saturated unit weight of 125 lb/ft^3 was used. Horizontal effective stresses were evaluated as K_0 times the vertical. After an initial comparison for K_0 values of 0.3, 0.4 and 0.5, the value of 0.5 for an $\text{OCR}=2$ was used thereafter.

The typical cross section of the fill embankment was obtained from the engineering plans provided by NDOT (sheets No. 7, 28, and 31). The cross section under study is located at station 557+00. The embankment cross section is trapezoidal: 32 ft. average height, 148 ft. wide at the top, and 279 ft. wide at the bottom with 2:1 side slope. See Fig. 5.3a.

A preliminary study was undertaken to ascertain any limitations associated with the proposed finite element mesh. One limitation of the program is the maximum number of nodes (550) that can be used in any FEADAM84 model. Accordingly, the mesh is restricted by the number of elements that can be employed. Accordingly, a cross section area 290 ft. east by 292 ft. west (from the edges of the fill) with an average depth of 75 ft. was employed.

Data provided by the CPT logs shows a vertical and lateral variation in the soil above the artesian layer. It is the change in the permeability of the soil over this depth that is of fundamental concern in the present research. Accordingly, a large number of elements was used to accurately model the conditions in this soil. Since our model is limited by the total number of nodes used, large elements were employed below the gravel artesian layer, while fairly small elements were used in modeling the soils above it

5.1.2. Initial Stresses

For the initial stress analysis, an average soil classification for all the soil above the artesian layer was employed. The soils below the artesian layer were classified based on information from the two boring logs (B1 and B2) provided by NDOT (Figs. 2.7a and 2.7b). Soils in the entire subsurface model are one of four types (see Fig 5.2):

1. Dark gray brown medium dense silty sand (SM)
2. Brown medium dense silty gravel with sand, the artesian layer (GM)
3. Brown dense silty sand (SM)
4. Light brown dense fine sandy silt (ML)

The input values for different parameters required by the FEADAM84 were chosen based on values recommended by Duncan et al (1984) and separately Byrne et al, 1987) for these four different soil types. Table 5.1 provides the required parameters and the recommended values that were adopted.

Based on the results obtained from the consolidation test, the overconsolidation ratio for the soils above the artesian layer was taken to be 2. Therefore, the drained bulk modulus number (K_b) was increased by a factor of three (Duncan) over the values given for normally consolidated soil.

The finite element mesh of Fig 5.3b was constructed for the specified area of interest. The mesh contains 324 elements and 385 nodes. Nodes at the bottom were given a fixed-fixed boundary condition in both directions (i.e. there is minor influence of the fill loading on the soils beneath them). Nodes along the vertical edges were given fixed boundary conditions in the horizontal direction. The first lift is the bottom soil (dense SM) and is modeled by elements 1 to 54. The second lift represents a second soil type (dense ML) and is modeled by elements from 55 to 108. The third is taken to be the same soil as lift one (dense SM) and is

modeled by elements 109 to 162. The fourth lift represents the artesian layer (medium dense GM) and is modeled by elements 162 to 216. The fifth and the sixth lifts represent the soil above the artesian layer (medium dense SM) and are modeled by elements 216 to 324.

The initial stress conditions for the various elements for the two different groundwater conditions and $K_0=0.5$ are given as Appendix No. 7.

5.1.3. Embankment Loading Model

The embankment material is an altered igneous rockfill imported from an aggregate pit on the eastern side of the valley. Samples obtained during construction were taken to be analyzed. However, due to the large sizes of rock employed, no specific laboratory tests were performed. Duncan provides the anticipated range of values for the hyperbolic finite element parameters for different types of soils. Since the rockfill can be characterized visually as a GW soil, Duncan's recommended values for this soil type were employed for the rockfill in the model. A sensitivity study was undertaken to artesian changes due to the assigned values of the required parameters for the FEADAM84 model to identify the more influential parameters affecting stresses in the elements of greatest interest. Elements of special interest are elements 290 and 307, which are at the edge of the fill, and elements 298 and 299, which are beneath the center of

the fill. Table 5.2 shows the results of this study.

Based on the sensitivity study, it was concluded that the only influential rockfill parameter is its unit weight (γ). The value used for this parameter was chosen based on engineering judgment associated with typical values reported for rockfill unit weight. Average values after Duncan were assigned to the rest of the parameters. Table 5.1 shows the rockfill parameters used in the embankment model.

A finite element mesh of 60 elements and 56 nodes (see Fig 5.3) was used to model the embankment. All nodes along the outer surface were given free boundary conditions. Our interest was primarily in the stresses after the completion of the fill. The fill embankment was assumed to be constructed in four lifts each of an average height of 8.0 ft.

5.1.4. Results

The results pertaining to the elements of greater interest indicated there was an increase in the horizontal and the vertical stresses in the centerline elements, while there was an increase in the vertical stress without any significant change in the horizontal stress in the edge elements. Lab test samples were stress path consolidated to general stress states indicated from finite element results (i.e. the

initial state and then to the final state) prior to the assessment of hydraulic conductivity.

5.2. Seepage Modeling

SEEP (V2.84, Wong 1983) is a readily available finite element computer program that can be used to solve a two-dimensional or axisymmetric steady state confined or unconfined groundwater flow problem. SEEP was used to model the flow conditions in the field. Input data required by SEEP consists of three main parts:

1. The finite element mesh
2. The hydraulic conductivities in two directions, and the angle between them
3. The boundary conditions.

Output data provided by SEEP are the

1. Nodal point hydraulic heads
2. Nodal flow rates
3. Quantity of seepage flowing into and out of the model.

The boundary conditions used for the model were the hydraulic heads obtained from piezometer readings. While such readings fluctuated over the year, a set of readings taken within an hour of elapsed time on a given day were used to

represent a single steady state condition.. Therefore, we were able to use SEEP for flow modeling of this nature.

5.2.1. The Model

The purpose in using this model was to predict the change in flow conditions prior to and after fill construction. Boundary conditions and layering were assessed from the soil borings and the CPT-logs. The input that were obtained from laboratory and field testing were the hydraulic conductivities in two perpendicular directions. Initial values had to be employed in order to perform the modeling. A value for the horizontal hydraulic conductivity was obtained from the bailing test described in Chapter 4. This value represents an average over the total depth of the well (10 ft.). This value was used in the model as an initial value for the horizontal hydraulic conductivity. A ratio between the horizontal and the vertical hydraulic conductivity was assumed. The intent was to then calibrate the model in order to be able to predict correctly. Calibration of the model would be performed by comparing the output hydraulic heads for the internal nodes versus the observed hydraulic heads at the same points. Most of the nodes used in the finite element mesh, particularly the outer nodes, were points where the piezometers are located. The hydraulic head is known at these points. By means

of comparing the hydraulic heads, we should be able to adjust the ratio between the horizontal and the vertical hydraulic conductivity.

5.2.2. Summary

Results of the finite element and seepage modeling are discussed in a later chapter.

Table 5.1 Parameters and Values Used in the FEADAM Model

Parameters for Drained Behavior

Required Parameter	Soil (1)	Soil (2)	Soil (3)	Soil (4)	Rockfill
Unit weight (γ) (kips/ft ³)	0.125	0.130	0.135	0.130	0.125
Modulus number (K)	880.00	450.00	200.00	120.00	540.00
Elastic unloading modulus number (K_{ur})	0.00	0.00	0.00	0.00	0.00
Modulus exponent (n)	0.50	0.25	0.40	0.45	0.43
Failure ratio (R_f)	0.70	0.70	0.70	0.70	0.64
Bulk modulus number (K_b)	500.00	350.00	50.00	110.00	135.00
Bulk modulus exponent (m)	0.25	0.00	0.20	0.20	0.20
Cohesion (c) (kips/ft ²)	0.00	0.00	0.00	0.00	0.00
Friction angle (ϕ)	41.00	34.00	33.00	30.00	42.00
$\Delta\phi$ (degrees per log cycle)	4.00	6.00	3.00	6.00	9.00
Earth pressure coefficient at rest (K_0)	0.5000	0.4408	0.4553	0.5000	0.3309

Parameters for Undrained Behavior

Required Parameter	Soil
Unit weight (γ) (kips/ft ³)	0.125
Modulus number (K)*	3000.00
Elastic unloading modulus number (K_{ur})	0.00
Modulus exponent (n)	0.50
Failure ratio (R_f)	0.70
Bulk modulus number (K_b)*	350000.00
Bulk modulus exponent (m)	0.25
Cohesion (c) (kips/ft ²)	5.00
Friction angle (ϕ)	0.00
$\Delta\phi$ (degrees per log cycle)	0.00
Earth pressure coefficient at rest (K_0)	0.5000

Table 5.2 Results of the Sensitivity Study

Required Parameter	% Change in Value	% Change in Stress of Middle Element	% Change in Stress of Edge Element
Unit weight (γ) (<i>kips/ft³</i>)	+27	+22	+16
Modulus number (K)	+76	+0.1	-2
Modulus exponent (n)	+18.6	+0.1	+0.1
Failure ratio (R_f)	+21.8	+0.4	+0.4
Bulk modulus number (K_b)	-248	-0.1	+3
Bulk modulus exponent (m)	-100	-0.1	+1
Friction angle (ϕ)	-40	-0.2	+1
$\Delta\phi$ (degrees per log cycle)	-70	-0.2	+0.5

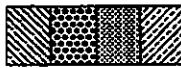
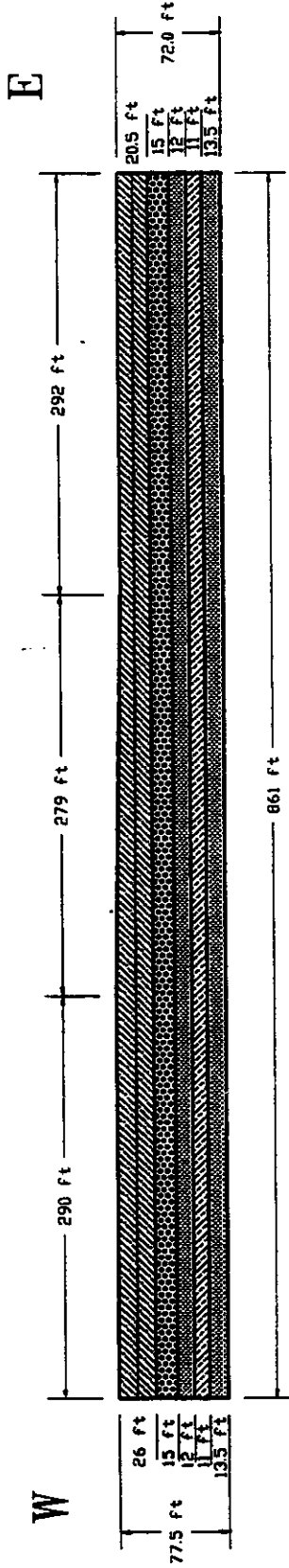
Where

% Change = (new value - original value)/(original value) * 100

Positive sign (+) = increase in vertical stress response value

Negative sign (-) = decrease in vertical stress response value

Initial FEADAM Model



- Soil (1), Dark gray brown silty sand (SM), Medium dense
- Soil (2), Artesian layer, brown silty gravel with sand (GM), Medium dense
- Soil (3), Brown silty sand (SM), Dense
- Soil (4), Light brown fine sandy silt (ML), Dense

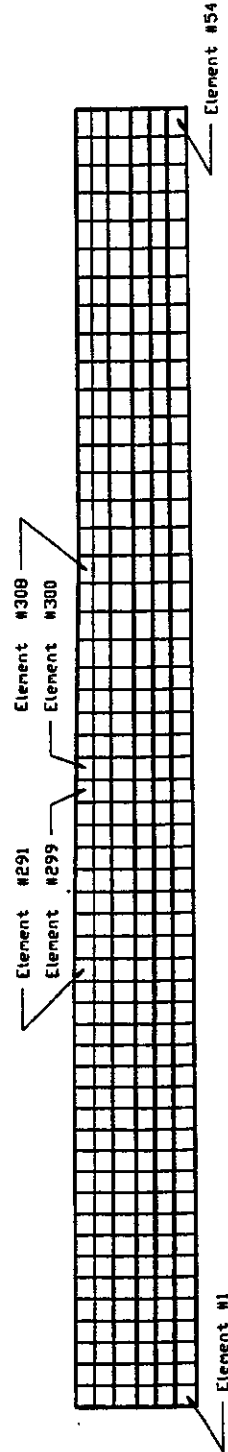


Fig. 5.1 Subsurface and Its Finite Element Mesh

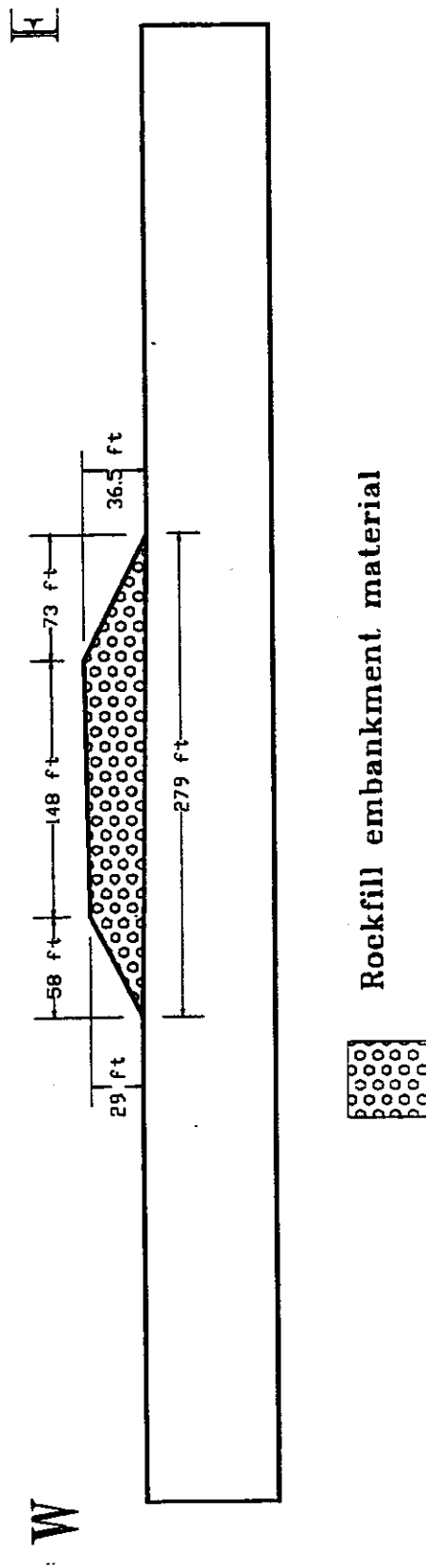


Fig. 5.2a Embankment Cross Section

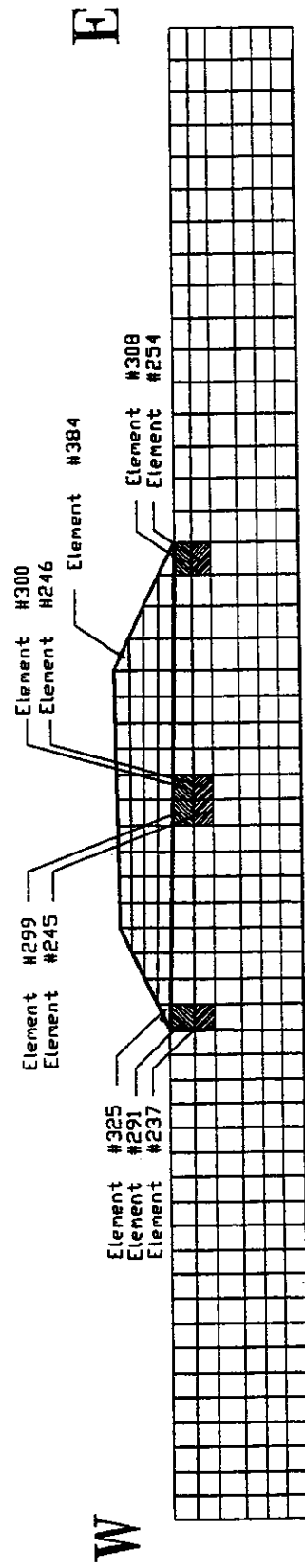


Fig. 5.2b Finite Element Mesh with Embankment

Chapter 6

Piezometric Readings and their Implications

6.1. Preview

This Chapter contains discussion relative to the piezometric readings and immediate conclusions drawn from studying them. Following that there is consideration in Chapter 7 of field CPT/SPT evaluation of in situ properties versus standard lab test results. A discussion of the evaluation of permeability, both field and lab, then ensues in Chapter 8. Comments relative to the use of the SEEP model are given followed by a discussion of the predicted stress-state, deformation and porewater pressure generation (and dissipation) response as assessed using finite element analysis (FEADAM) and stress-path triaxial tests in Chapter 9. Overall conclusions and recommendations are then presented in Chapter 10.

6.2. Piezometric Readings and their Implication

As shown in Fig 2.3, the piezometer layout was intended to reflect changes that would occur beneath and downstream of the highway fill constructed in a north-south direction. Piezometer locations Pz1 and Pz2 are located to the east of the fill, while Pzs 3,4,5 and 6 ended up beneath the constructed fill. Piezometers

Pz 7 and 8 are upstream of the fill and unless a back-up of the subsurface water (largely snow melt) flowing from the Carson range via the artesian layer (at a depth of 21 ft. depth) were to occur, they were meant to reflect unchanged upstream conditions. It was anticipated that this alluvial deposit would experience consolidation due to the imposed fill load and that flow in the subsurface soil immediately beneath the fill (0 to 21 ft.) would be restricted or altered thus leading to a change in piezometer readings both beneath the fill and on the downstream side (the east side of the fill). It was expected that a coupled field-lab-analytical model test program would be necessary to evaluate and predict such changes. This feeling was enhanced or promoted by study of the soil/geologic descriptions and characterizations (see Chapter 1) and the CPT logs that indicated the presence of cohesive material (material characterized with undrained strength rather than a friction angle and relative density).

Figures 6.1 through 6.15 show the individual records of piezometric water levels (level of water in the piezometer relative to ground surface) over the time span between 10/2/93 and 8/25/95. The reader will note there is a gap from February to April of 1995 when the pneumatic readout box was sent to the Slope Indicator Co. for repair and recalibration. These readings span a period seven months prior to, to one year beyond construction of the fill. Such readings were meant to provide a baseline (i.e. Pz4D in the artesian layer and Pz7 and Pz8

upstream) with which to compare fill induced changes in other piezometers (all other piezometers). However, if one compares Pz1 (one of the piezometers where a change was expected) with Pz4D (the control piezometer in the artesian layer), the reader will notice that they parallel each other almost identically. Since Pz1 represents the lowest water level of all those at the site and Pz4D the highest, and Pz1 has not changed with respect to the control (Pz4D), the effect of fill construction on all other piezometers can, therefore, be made by considering the shift of the piezometer's readings within the band established by Pz1 and Pz4D.

There is a consistent difference of approximately 6 ft between Pz1 and Pz4D readings. Note that readings were stopped (one month prematurely) of two complete cycles of seasonal groundwater table fluctuations. It was felt that all needed information had been obtained by them. Over that time period, the water level in Pz1 and Pz4D fluctuated 6 to 7 ft. due to seasonal effects.

If the reader compares the readings of Pz7 and Pz8 (west or upstream of the fill) and Pz2 (all at 8 to 10 ft depth) in Fig 6.16, Pz3A and Pz4A (both at approximately 7 ft depth beneath the fill) in Fig 6.17, Pz3A, Pz3B and Pz3C (at different depths near the toe of the fill) in Fig 6.18, Pz4A, Pz4B and Pz4C (at different depths under the west shoulder of the fill) in Fig 6.19, Pz5A, Pz5B and Pz5C (at different depths under the east shoulder of the fill) in Fig 6.20, and Pz3C, Pz4C, Pz5C and Pz6 (all at approximately 17 ft depth from toe to toe of the fill) in

Fig 6.21, all with the heavier or highlighted Pz1 and Pz4D span or baseline values, you will notice that there was very little deviation from the Pz1/Pz4D pattern. Individual piezometer recordings that start off near the bottom of this span, remained there while those in the middle or near the top, remained there. Therefore, with the exception of very minor deviations as will be noted subsequently, nothing happened outside the normal seasonal fluctuation as characterized by Pz4D in the artesian layer.

Therefore, there was no effect, (except for these minor deviations that the authors will highlight subsequently) that fill construction had on the records. There were no changes brought about by the fill construction and all previous and subsequent discussion of a coupled field-lab-analytical analysis program to show the authors' capability to predict changes are of lesser significance by comparison. Therefore, if the reader is content to know that at a medium dense cohesionless site (silty-sandy, there was no clay) with a shallow controlling artesian layer (at approximately 20 ft.) similar response should be expected, the reader should go to Chapter 10 to review the report's conclusions. If some conclusions regarding additional work presented in this chapter warrant interest, the reader can return to that part of the present chapter.

The basic conclusion noted above was conveyed to NDOT personnel verbally midyear 1996. However, the authors' desire to discover something

beyond this, and the difficulties that ensued (particularly in getting a better handle on the evaluation of permeability) has delayed submission of the current report until now (5/1/97). In the ensuing chapters, the authors intend to discuss discrepancies between CPT/SPT and lab evaluation of soil properties, the wide range in assessed permeabilities, difficulties with finite element modeling and triaxial test capabilities and limitations. The lessons learned should explain or permit other investigators to avoid similar difficulties if the need arises to undertake a similar effort relative to a cohesive site.

It should be pointed out that while piezometer readings are typically meant to portray consolidation or stability response of a soft clay deposit, similar instrumentation may be warranted at another cohesionless site if evidence is needed to portray that nothing happened so that lawsuits from landowners claiming something has gone awry are not falsely awarded.

6.3. Small Changes

To a lesser scale, there is evidence in the piezometer readings that something (in fact the opposite of what was expected) happened. Pz3A (Fig 6.17, 6.18), Pz4A (Fig 6.17, 6.19), Pz4B (Fig 6.19), Pz4C (Fig 6.19, 6.21), Pz5A and Pz5B (Fig 6.20) all show a small negative porewater pressure and piezometer water level change over the first half of the construction period. (Note that the coarse sand packing around Pz5A actually desaturated as indicated by the horizontal line that develops.) If the reader consults Fig 6.22 showing the layout

of the piezometers, note that the affected piezometers reflect an area under the fill where the material tried to dilate. The short period over which this change persisted reflects an undrained or partially drained pore pressure build-up, followed by quick dissipation. Normally, piezometer readings in clay show an undrained rise or jump (Δh_p) as large as the fill surcharge ($\gamma_{fill} H_{fill}$) divided by the unit weight of water (i.e. $\Delta h_p = \gamma_{fill} H_{fill} / \gamma_w$). See, for instance, the records of Fig 6.23 corresponding to a the lateral and vertical positive pore pressure variation relative to a smaller 21 ft. high fill. The approximate 2 ft. or 6 kPa negative porewater pressure change at the Zollezi lane site reflects an undrained dilative tendency attributable to cohesionless material. Most of the following discussion on finite element model (FEADAM) results and stress-path triaxial test results are focused on the authors' ability to generate or model such behavior. The negative pore pressure change reflects a temporary restraint of dilative volume change followed by the volume increase as the negative pore pressure dissipates. Therefore, contrary to the expected rise in pore pressure and, with its dissipation, a volume decrease with time, the encountered pore pressure decrease signals a subsequent volume increase. Such volume increase, if anything, would yield a slight increase in permeability (rather than its decrease with consolidation that was expected).

As discussed in the next chapter, one might well have anticipated such negative porewater pressures due to fill construction (in areas where high shear stresses develop) from the negative piezo cone record that was generated.

Before leaving the piezometer readings, note in Fig 6.16 the water level difference, Δh , at any given time from Pz8 to Pz7 to Pz2 to Pz1 that indicates the overall hydraulic gradient i ($i = \frac{\Delta h}{L}$, L is the horizontal distance between piezometers) reflecting west to east flow in this silty sand layer. All of the piezometers mentioned are at about 8 to 10 ft. depth. The same holds true from Pz4A to 3A (both at about 7.5 ft. depth) and Pz6 to Pz5C to Pz4C to Pz3C (all between 10 and 13 ft.) in Fig 6.21. By contrast, there is very little water level difference and hydraulic gradient vertically from Pz3C to Pz3B to Pz3A in Fig 6.18 or from Pz4C to Pz4B to Pz4A in Fig 6.19.

6.4. Summary

Based on the study of the observed piezometer readings, there was no change in the ground water flow conditions during or after fill construction at the Zolezzi site. If anything there was a small pore pressure drop indicating a dilative response and a possible increase in permeability in the silty-sand layer sandwiched between the fill and artesian layer. This is contrary to the anticipated consolidation and decrease in permeability of a more cohesive fine grained soil that was expected. Succeeding chapters (7 - 9) deal with the attempts to explain / predict the observed phenomenon.

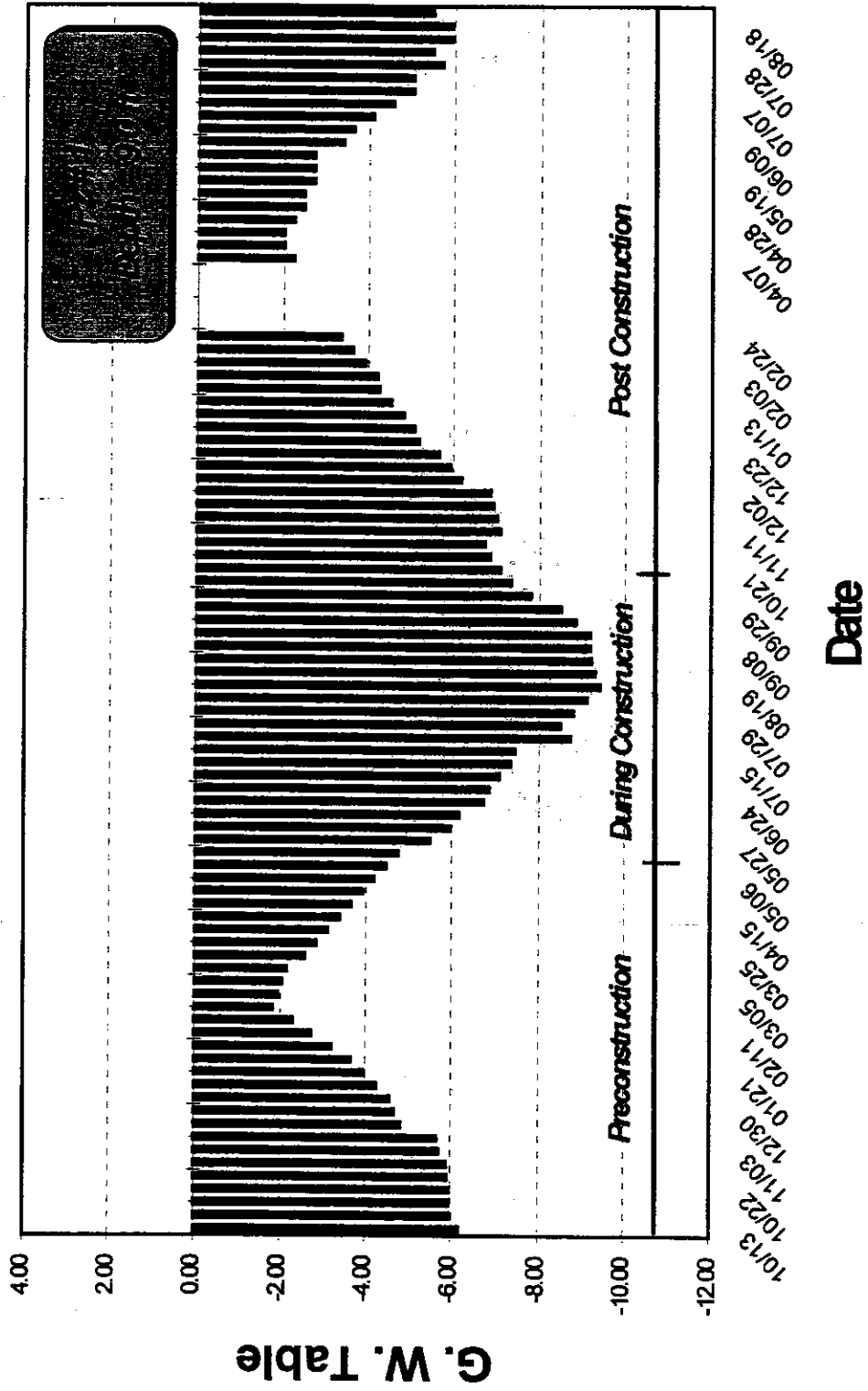


Fig. 6.1 Pz1 Readings

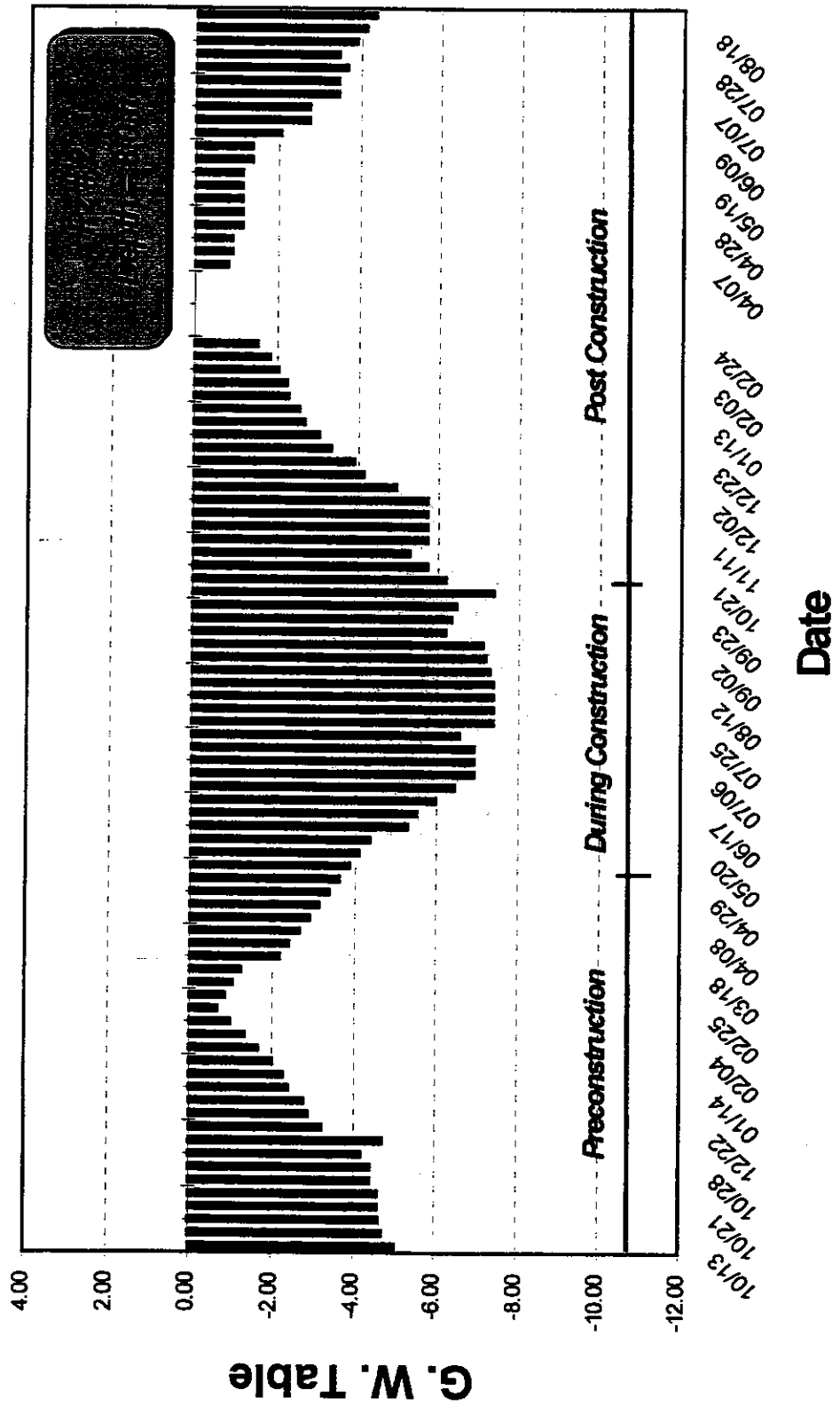


Fig. 6.2 Pz2 Readings

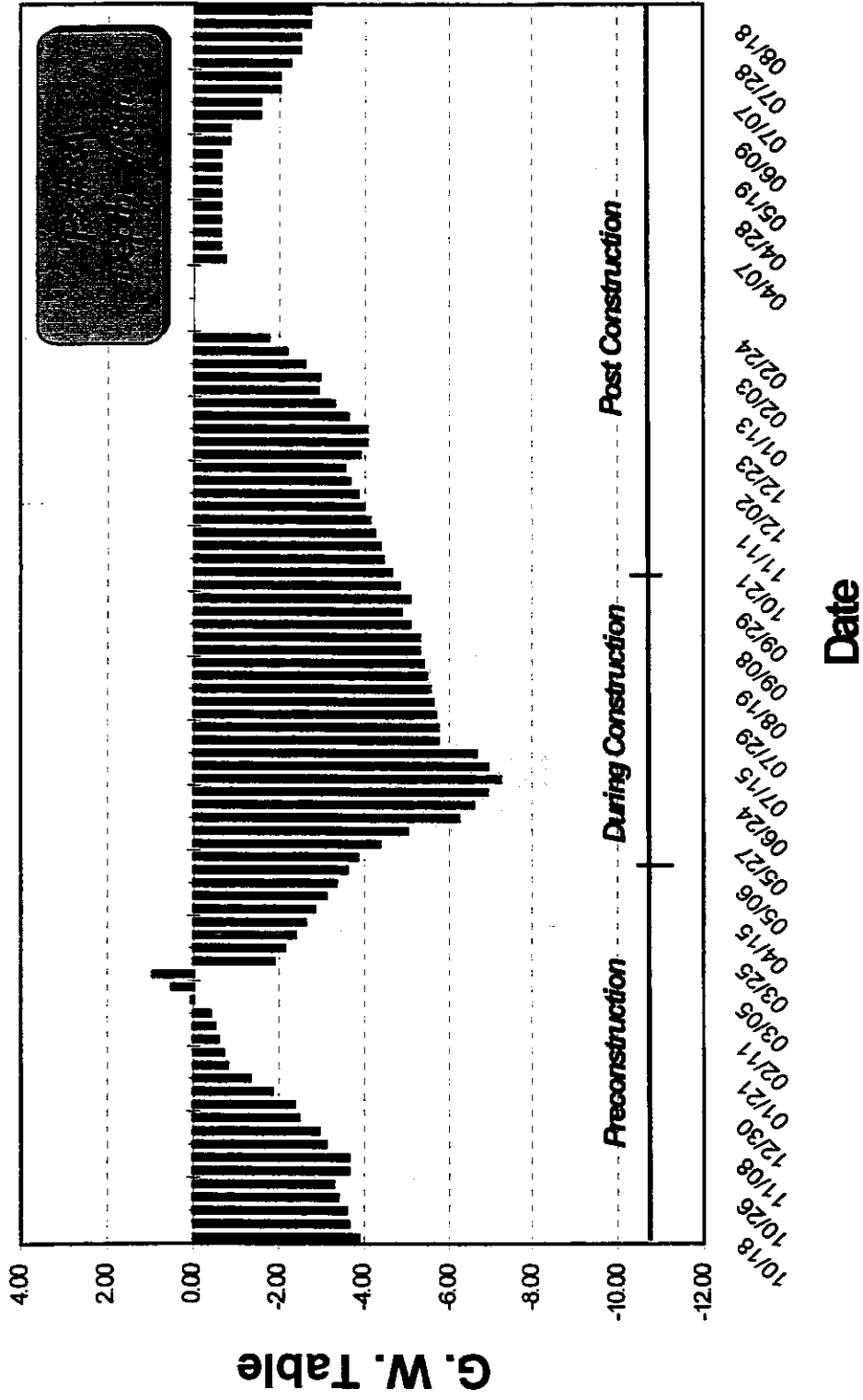


Fig. 6.3 Pz3A Readings

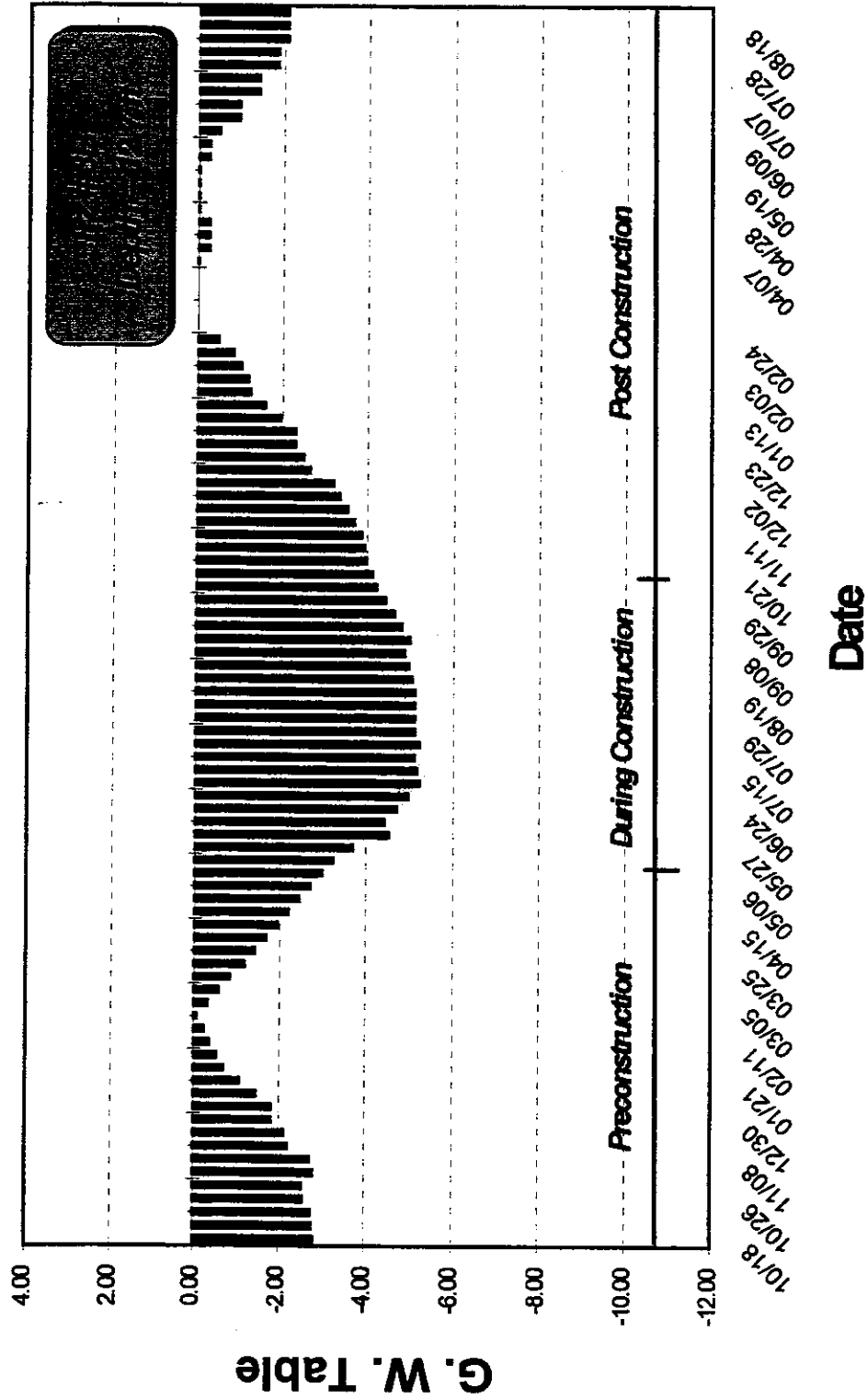


Fig. 6.4 Pz3B Readings

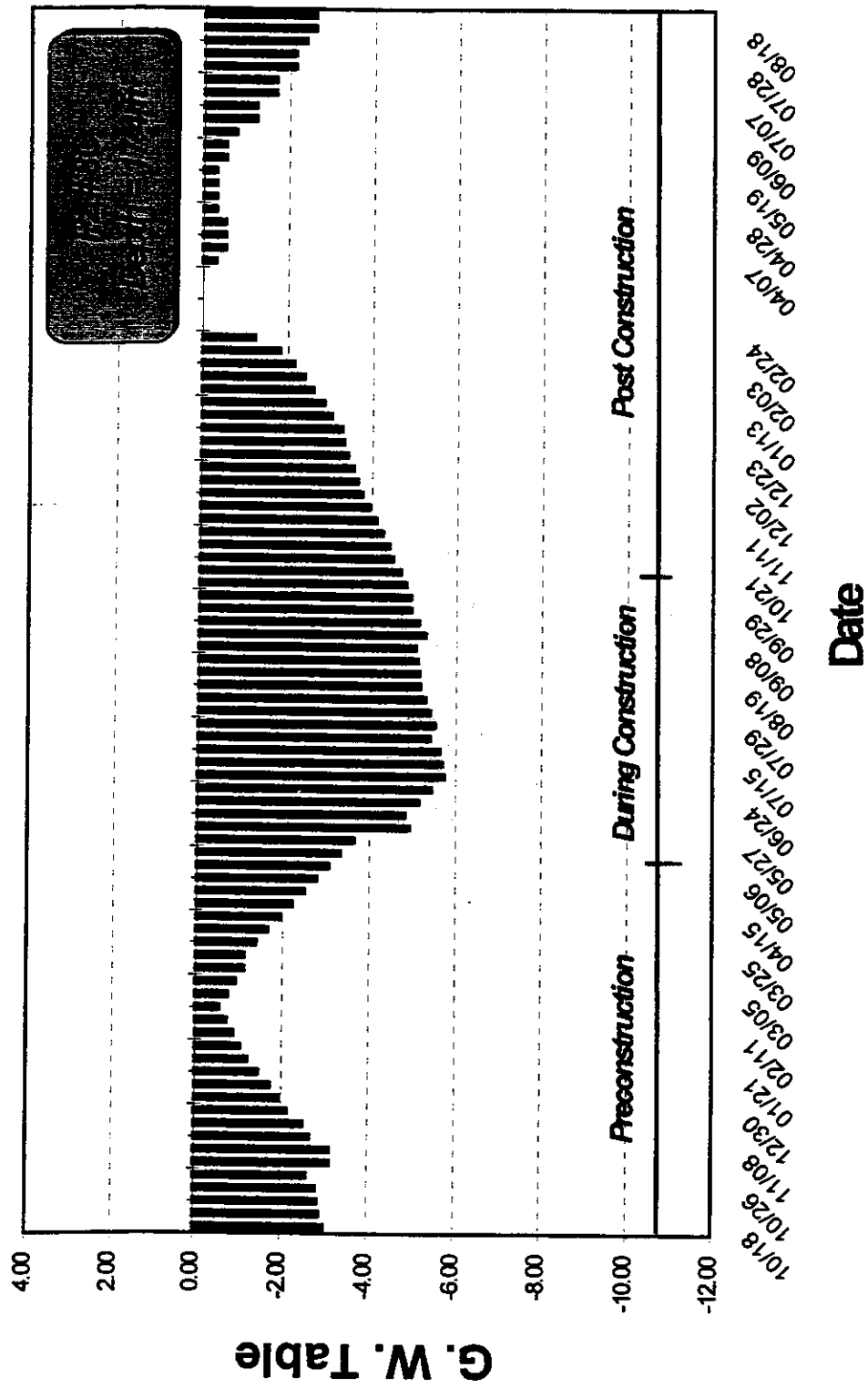


Fig. 6.5 Pz3C Readings

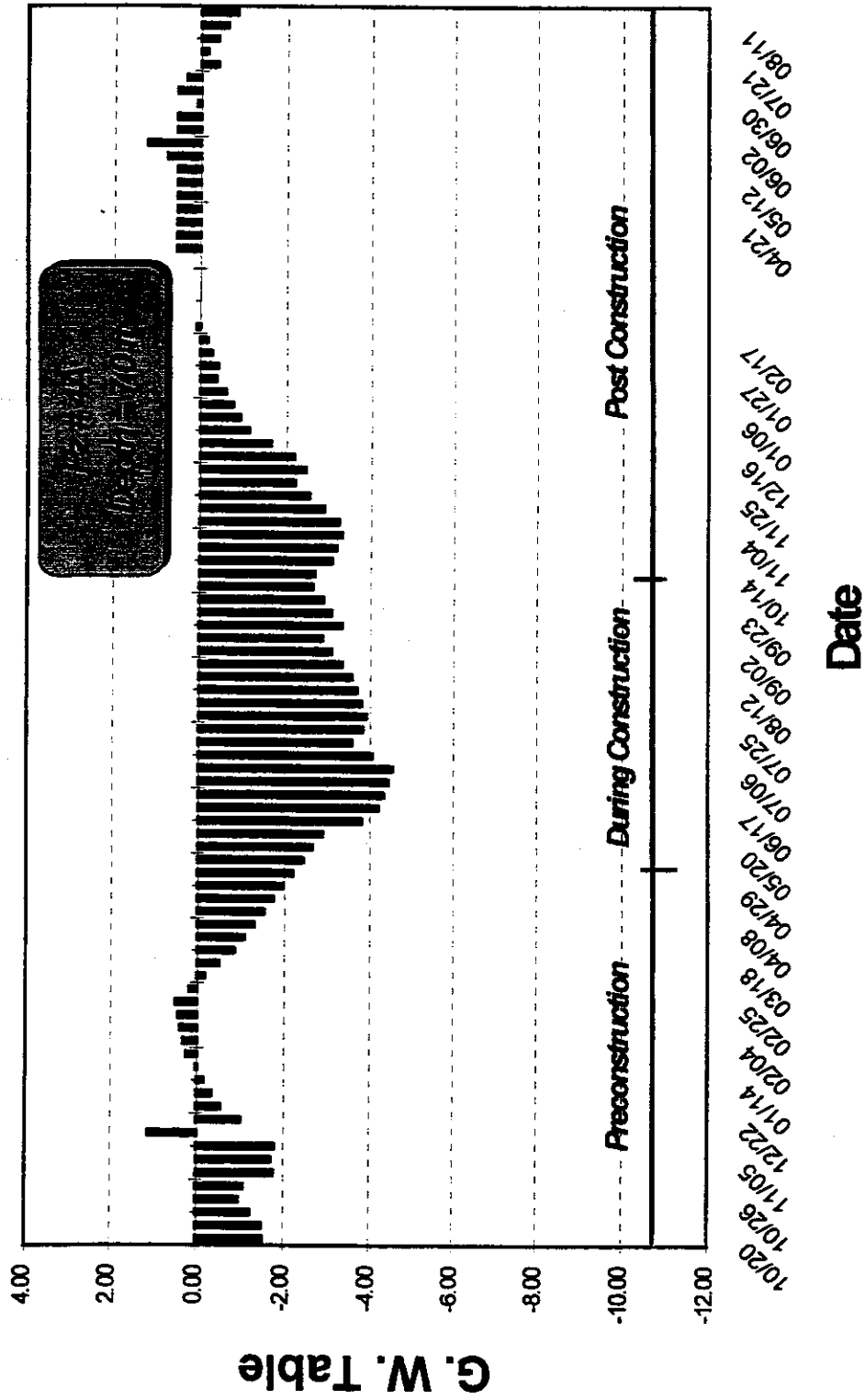


Fig. 6.6 Pz4A Readings

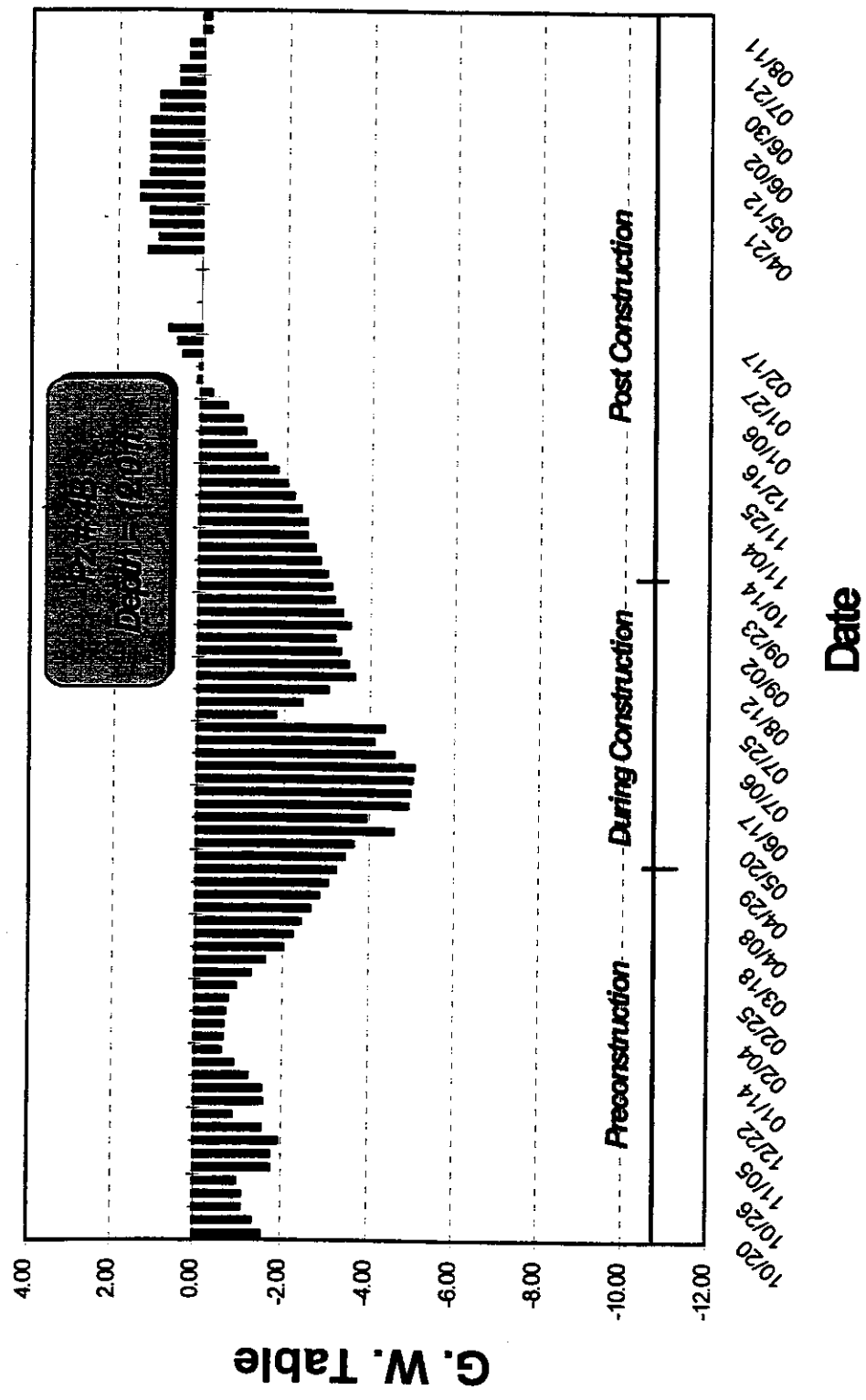


Fig. 6.7 Pz4B Readings

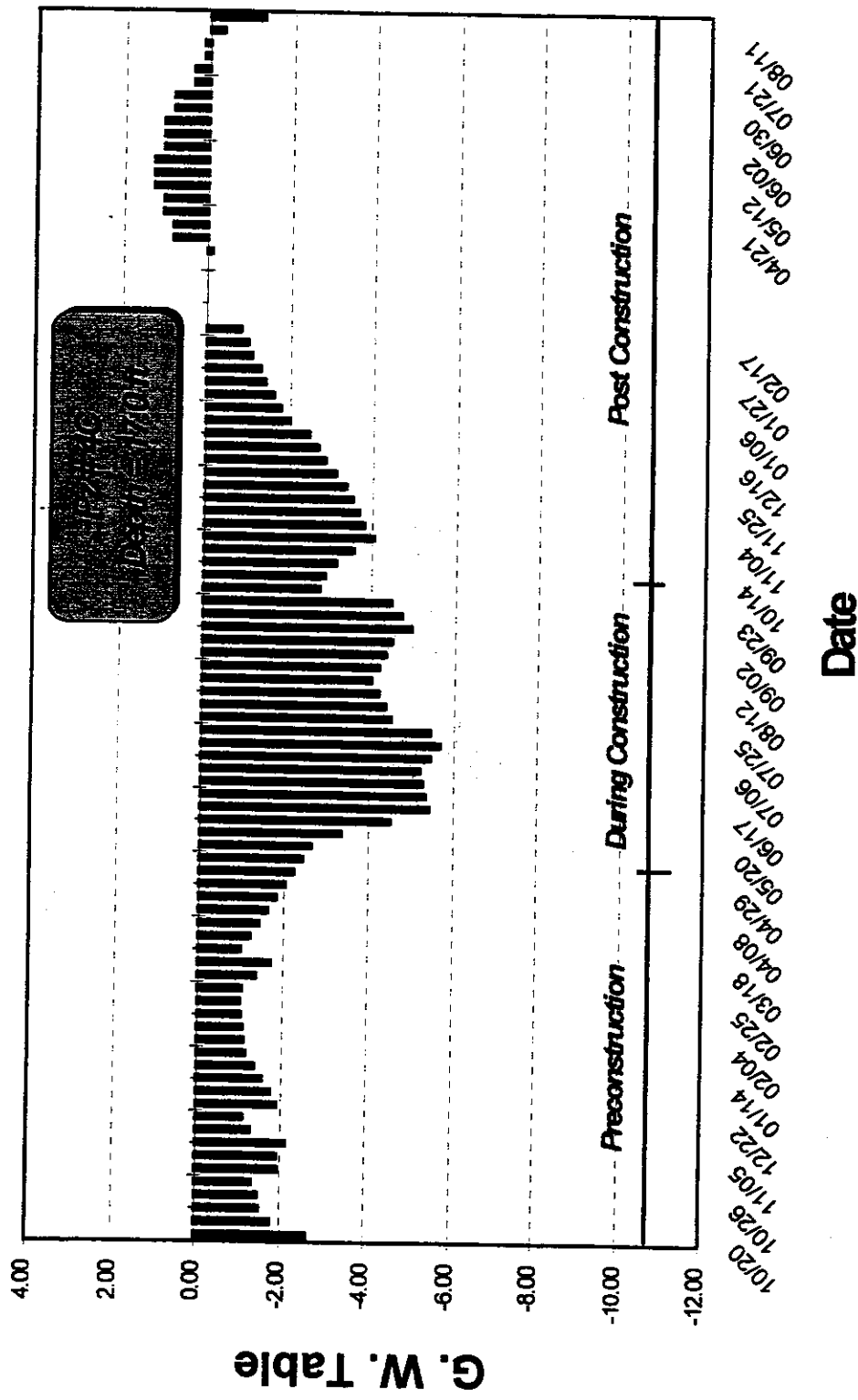


Fig. 6.8 Pz4C Readings

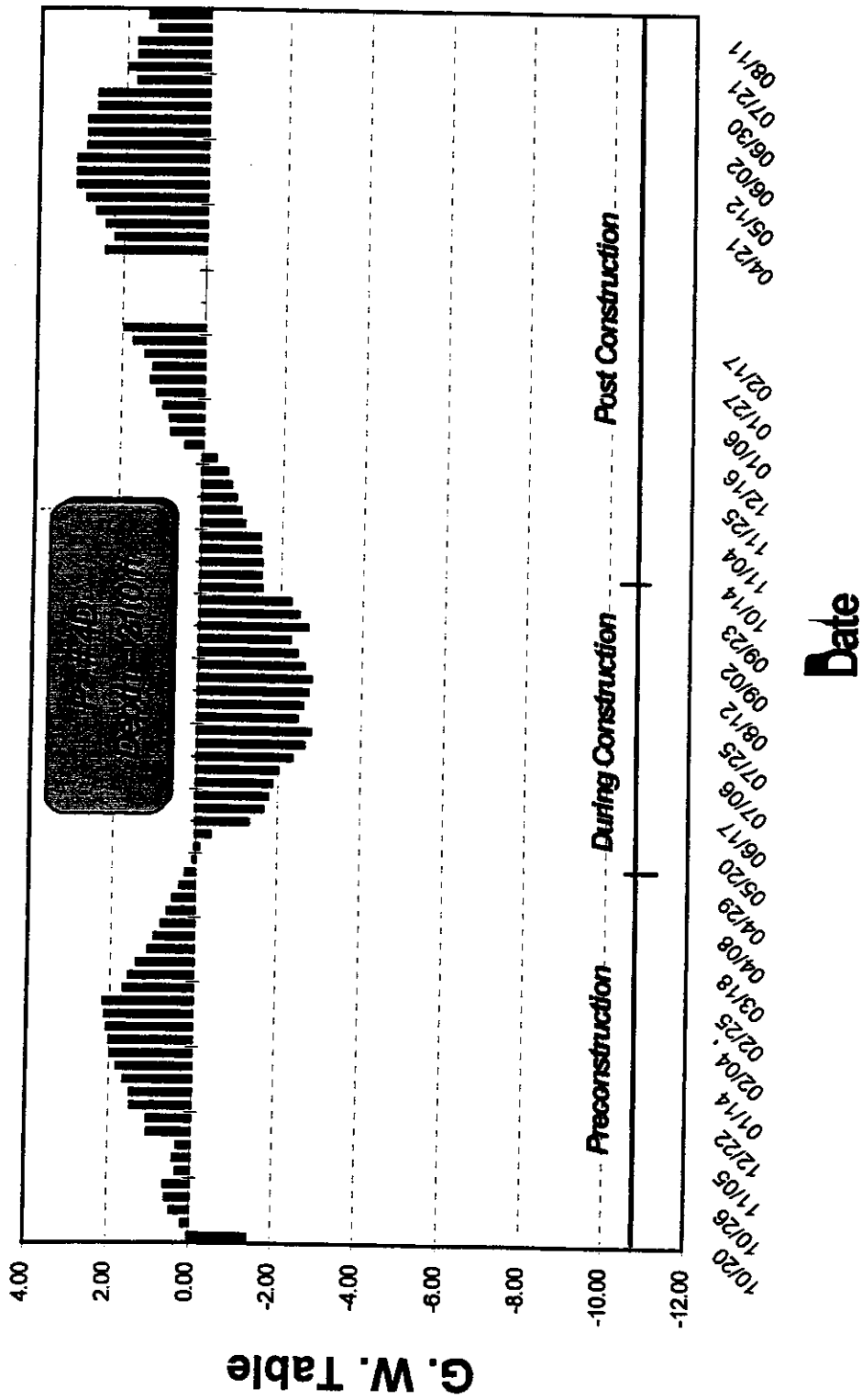


Fig. 6.9 Pz4D Readings

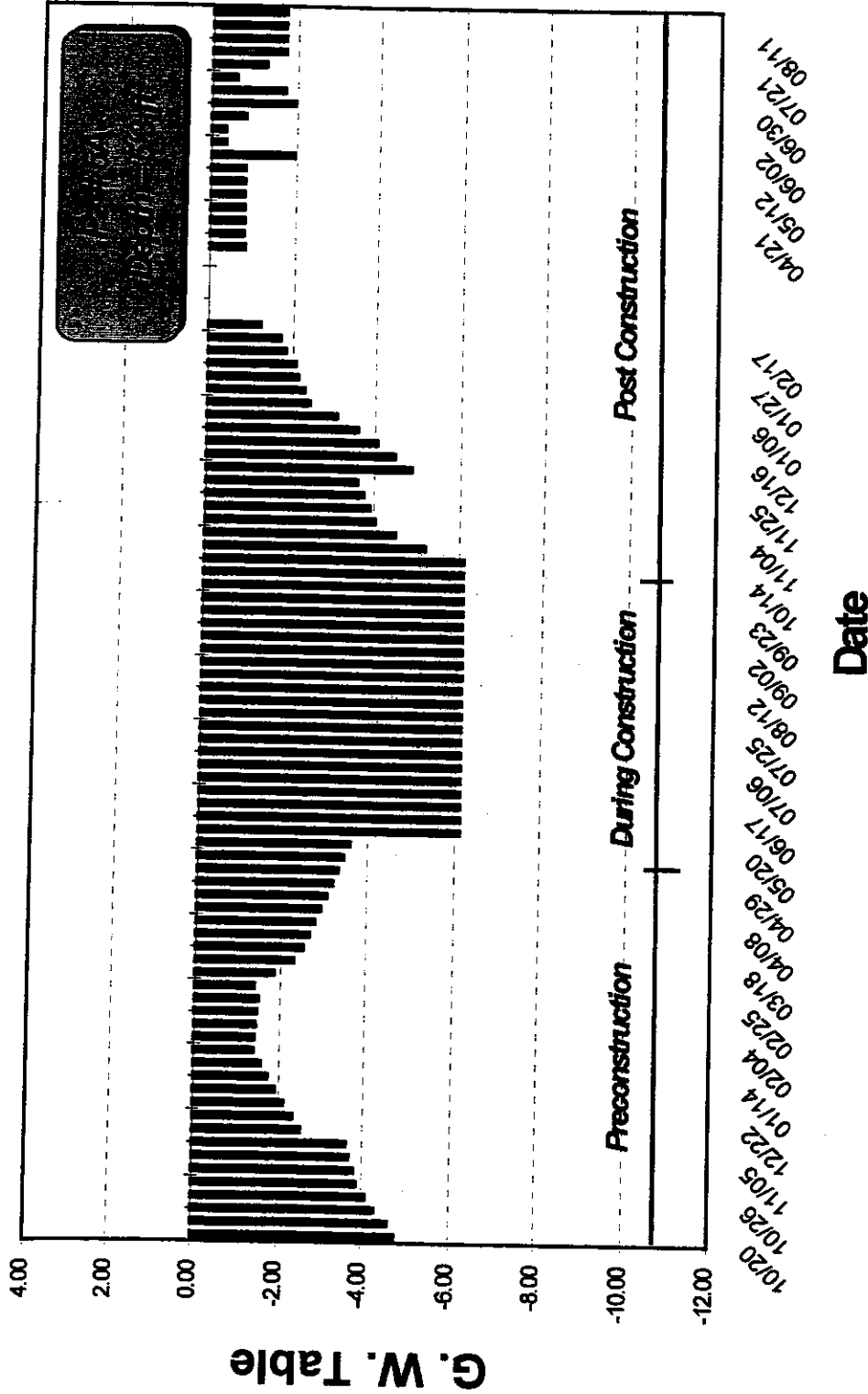


Fig. 6.10 Pz5A Readings

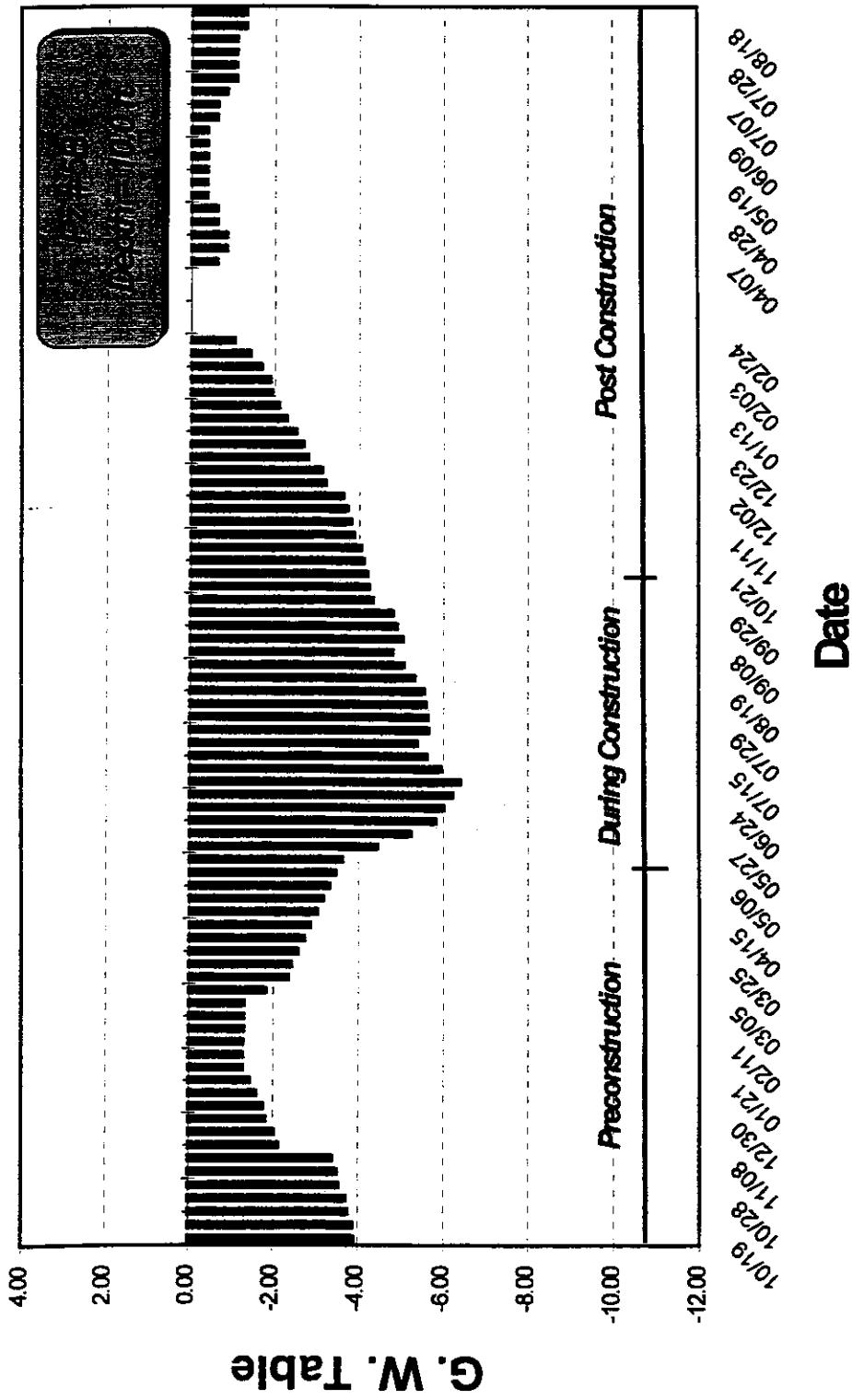


Fig. 6.11 Pz5B Readings

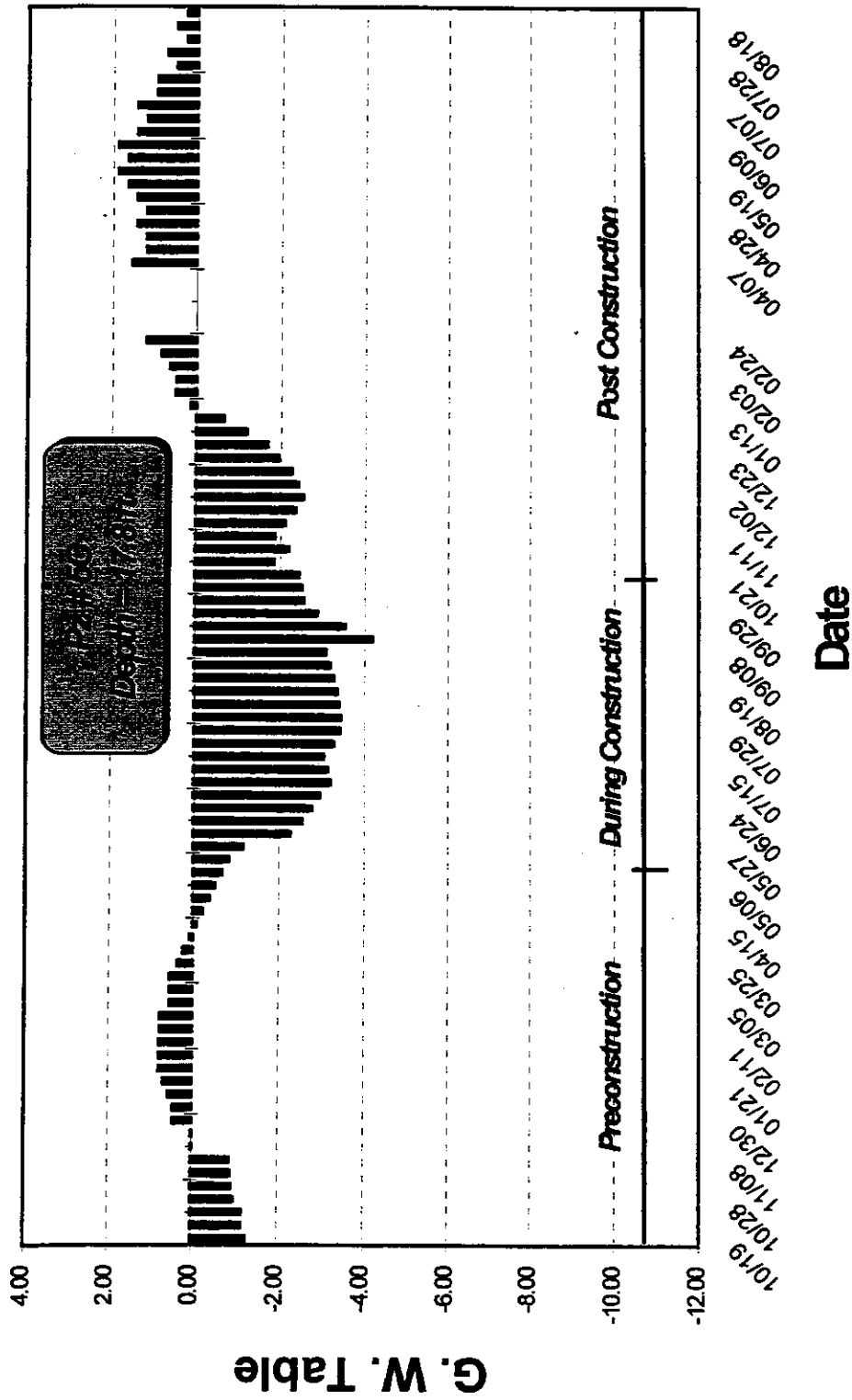


Fig. 6.12 Pz5C Readings

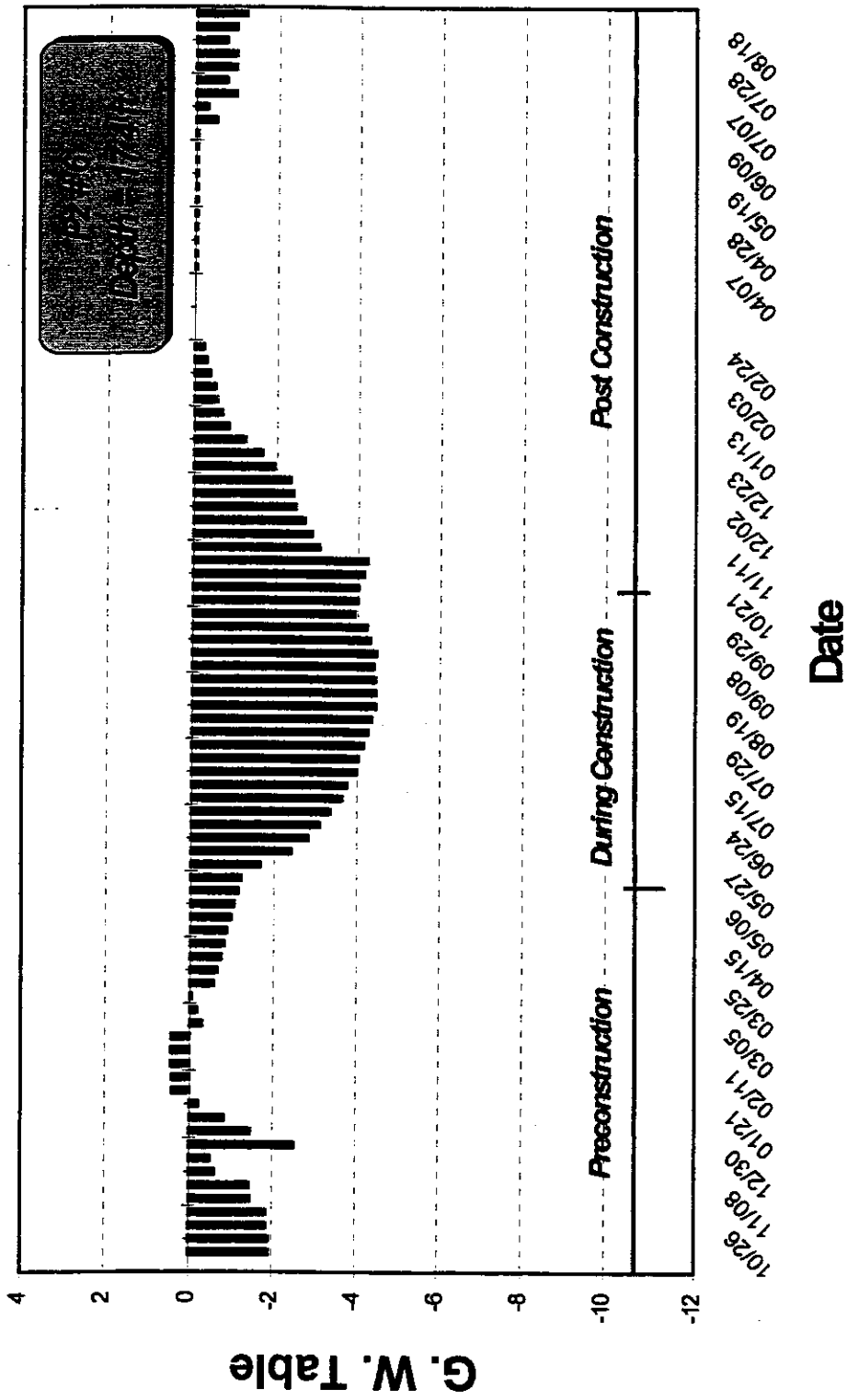


Fig. 6.13 Pz6 Readings

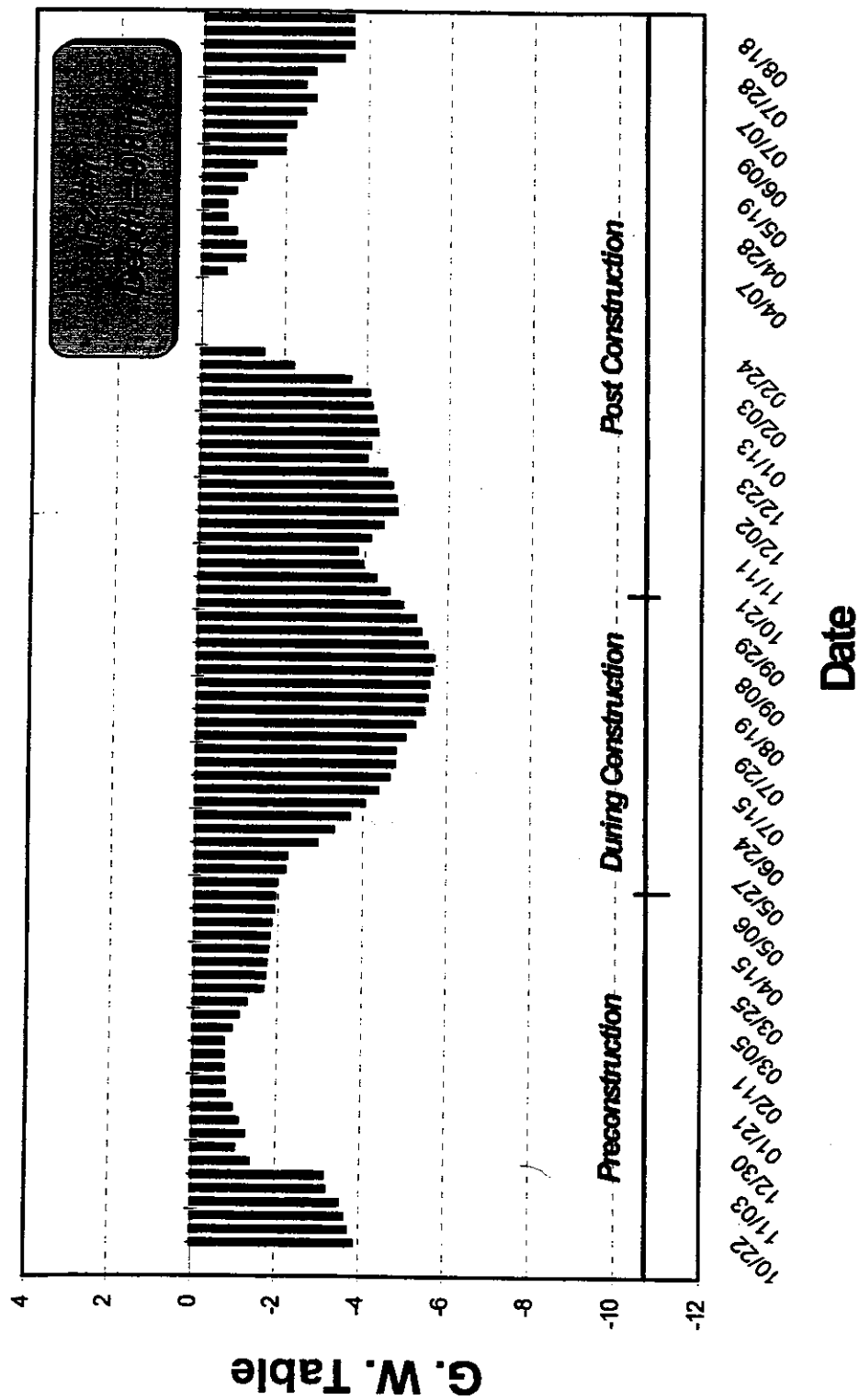


Fig. 6.14 Pz7 Readings

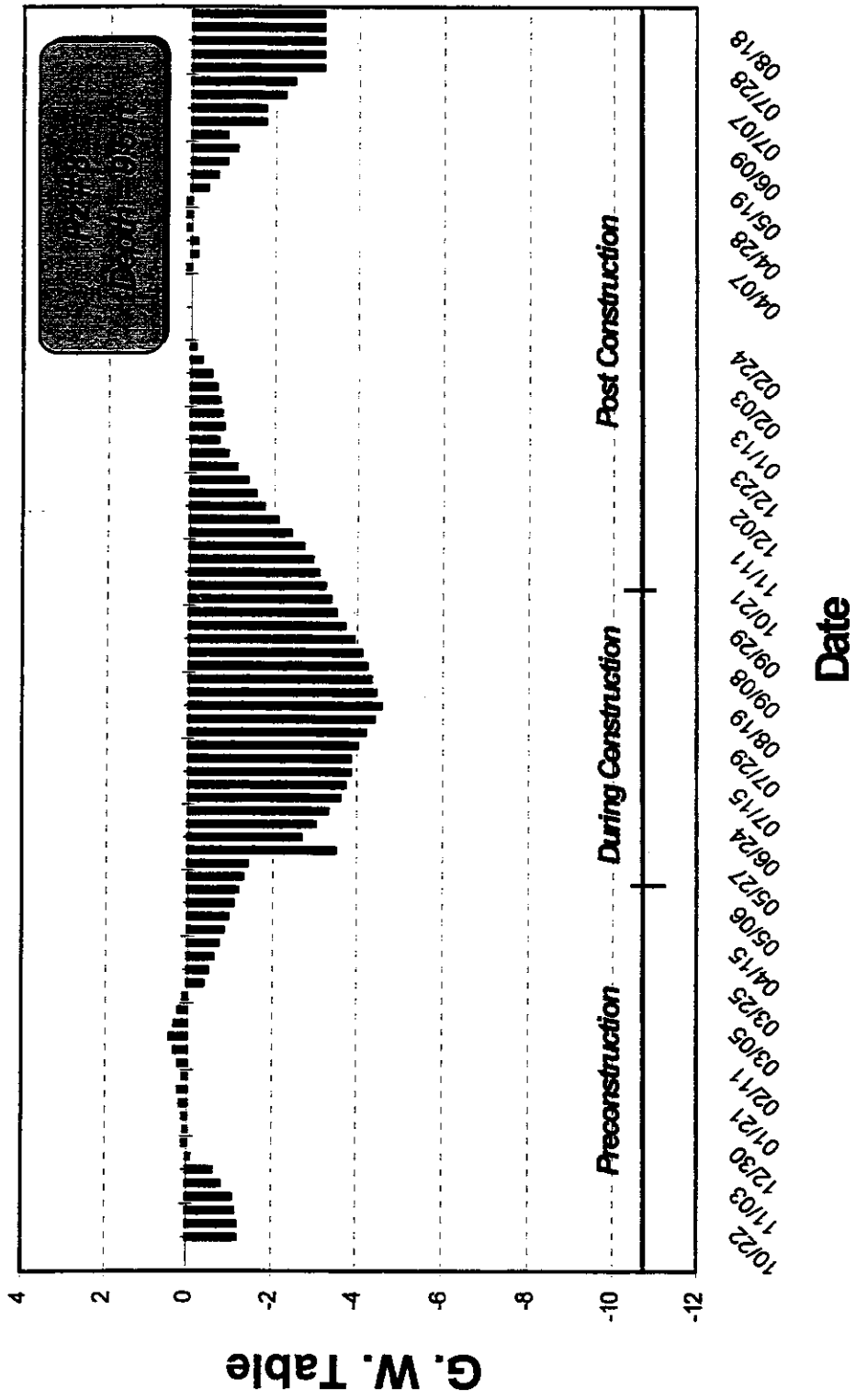


Fig. 6.15 Pz8 Readings

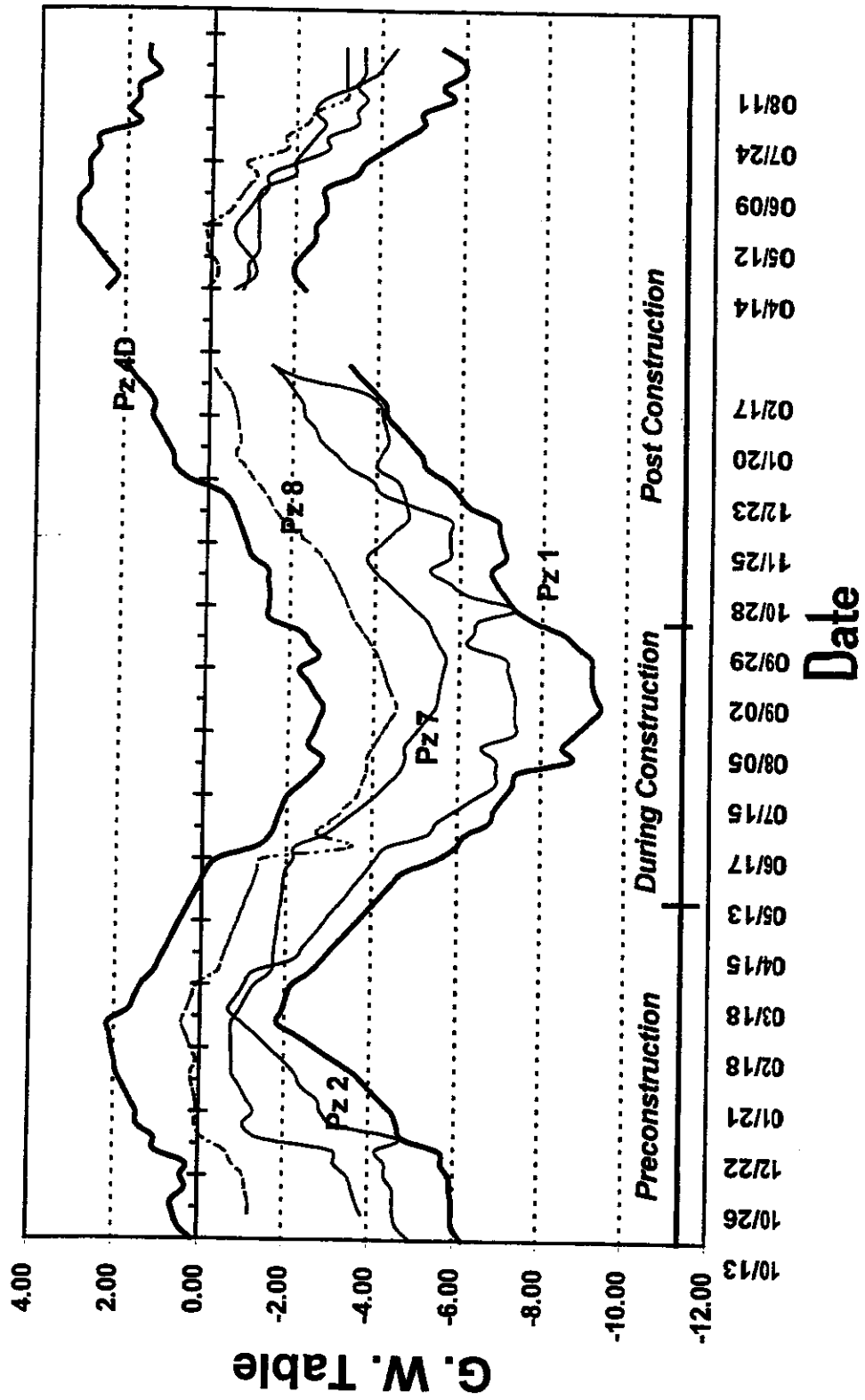


Fig. 6.16 Pz2, Pz7 and Pz8 Reading Profiles

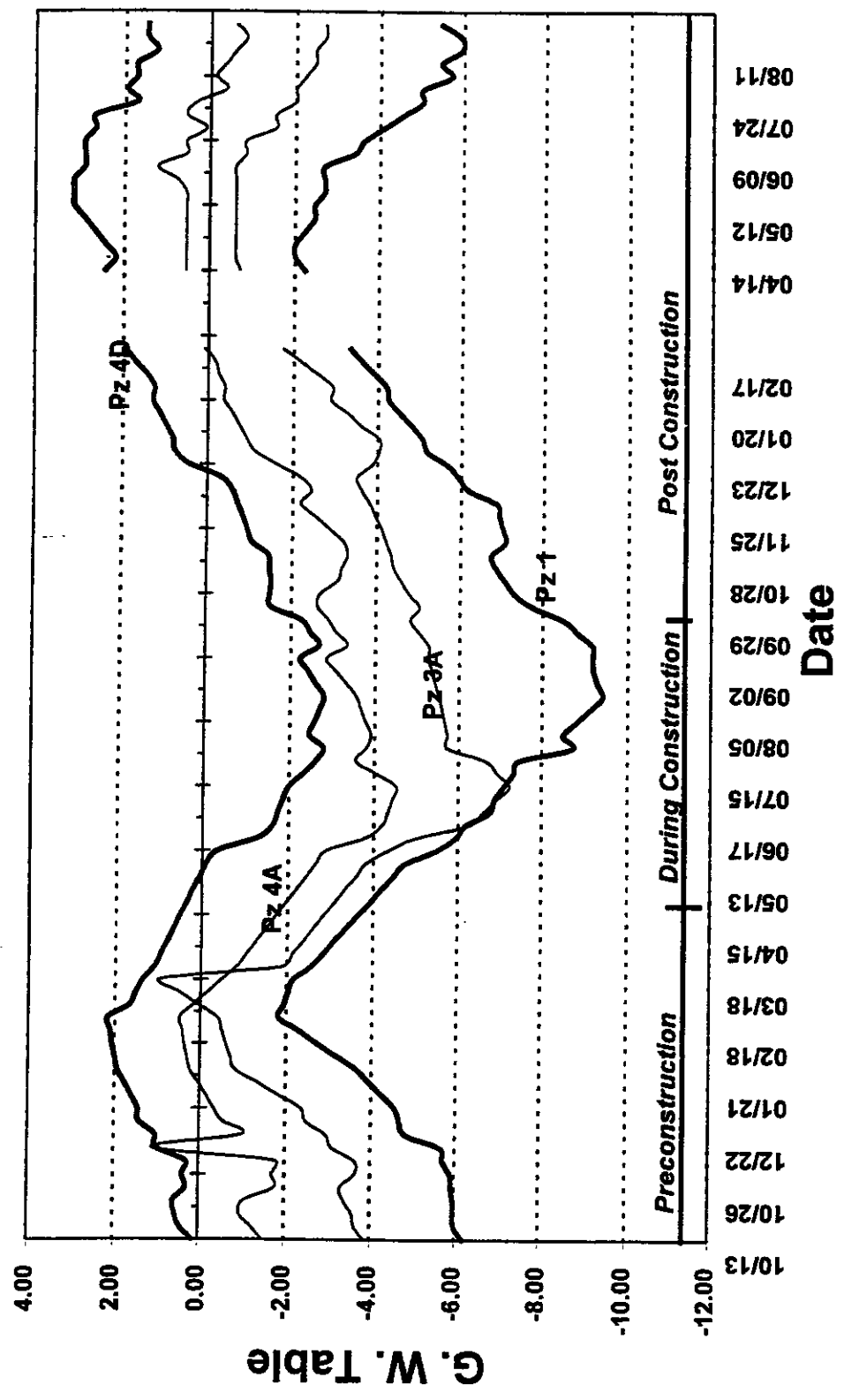


Fig. 6.17 Pz3A and Pz4A Reading Profiles

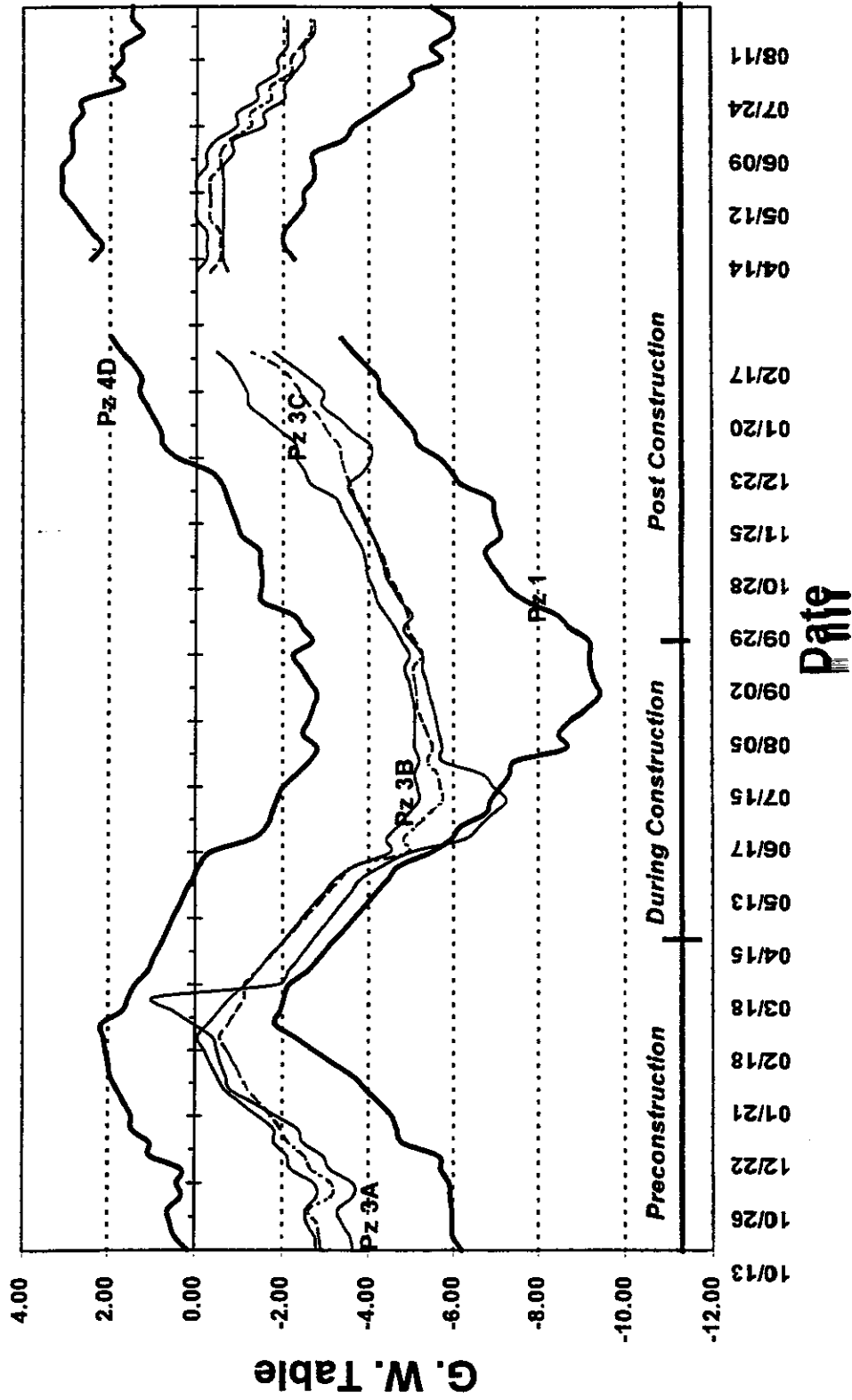


Fig. 6.18 Pz3A, Pz3B and Pz3C Reading Profiles

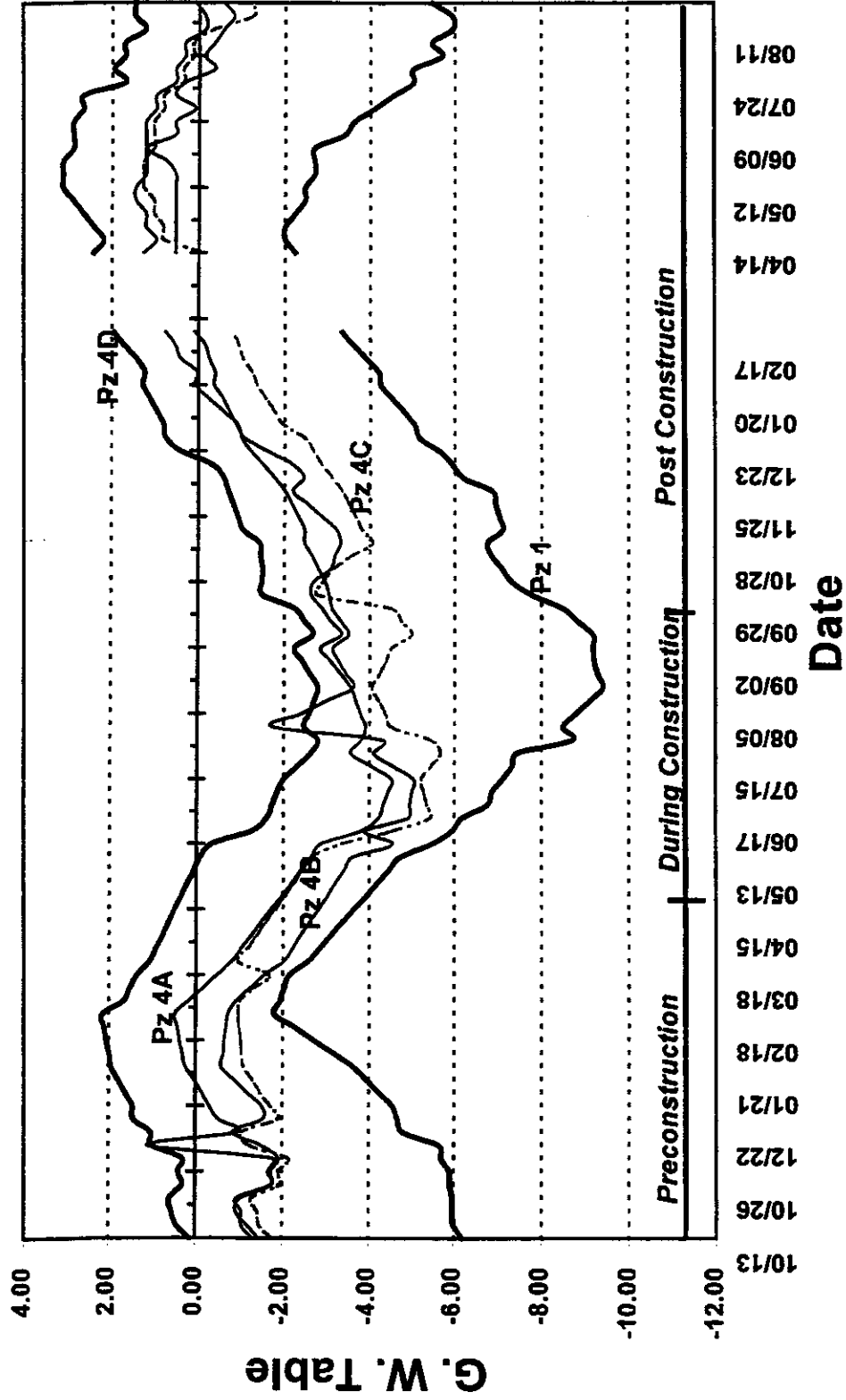


Fig. 6.19 Pz 4A, Pz4B and Pz4C Reading Profiles

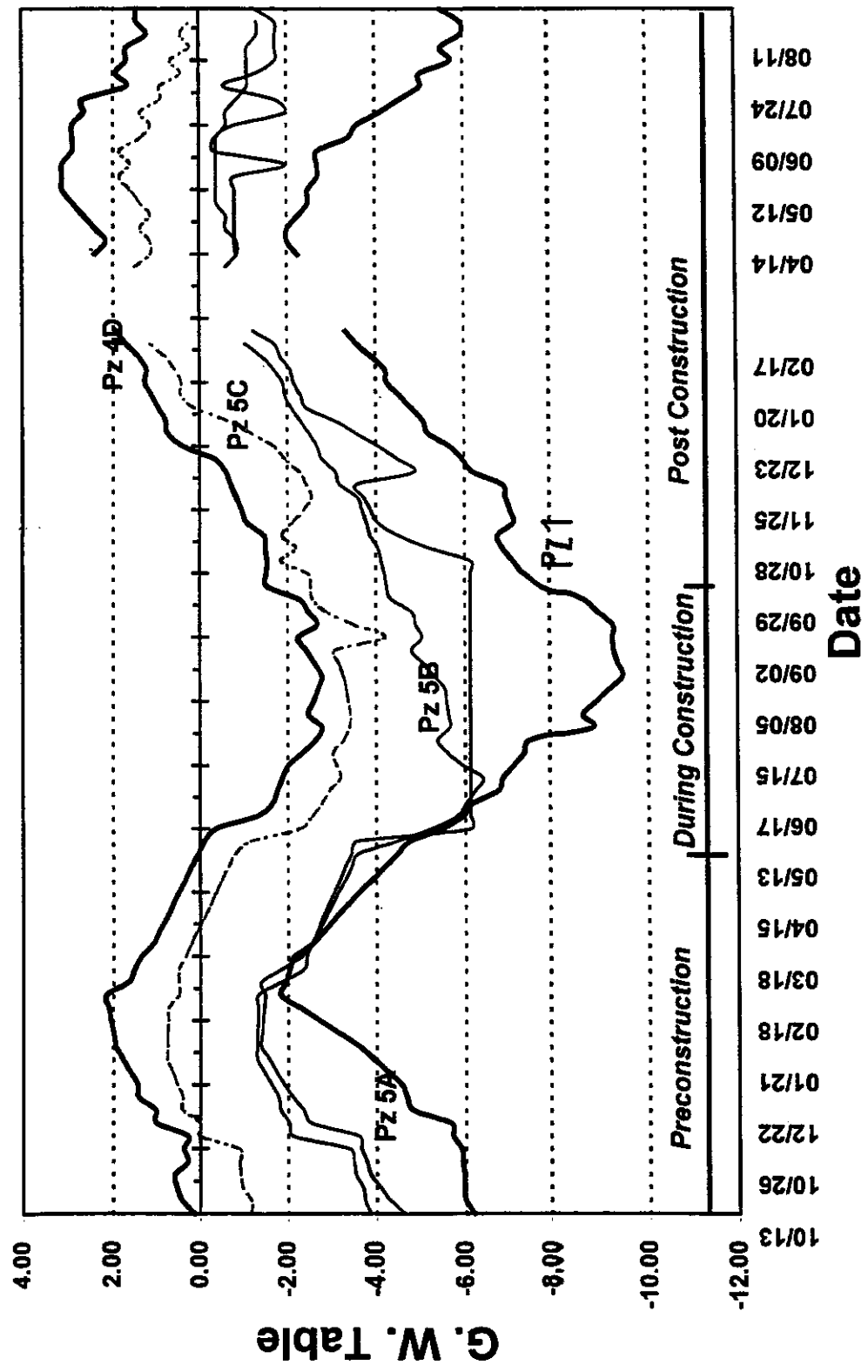


Fig. 6.20 Pz5A, Pz5B and Pz5C Reading Profiles

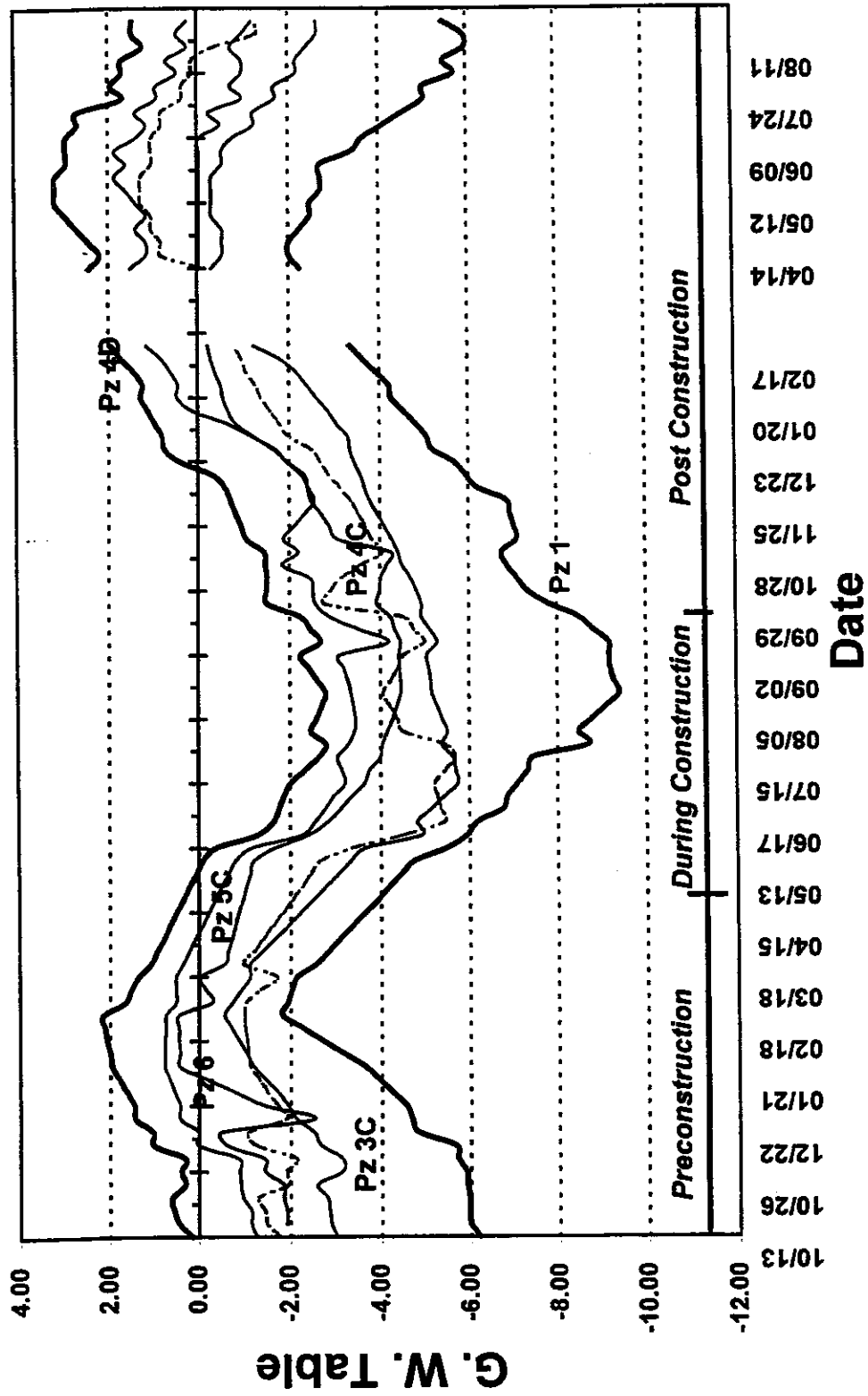


Fig. 6.21 Pz3C, Pz4C, Pz5C and Pz6 Reading Profiles

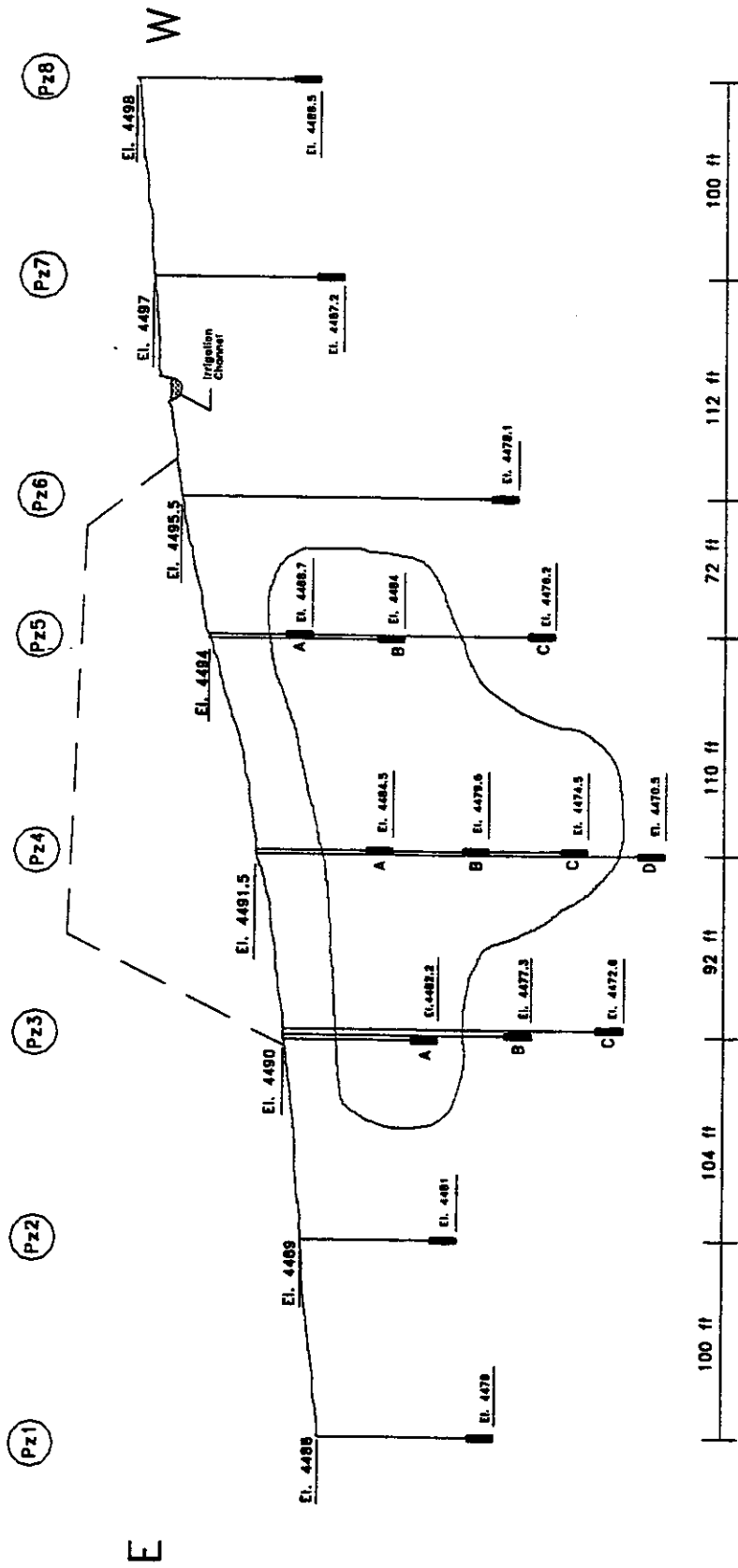


Fig. 6.22 Zone of Fill Induced Negative Porewater Pressures

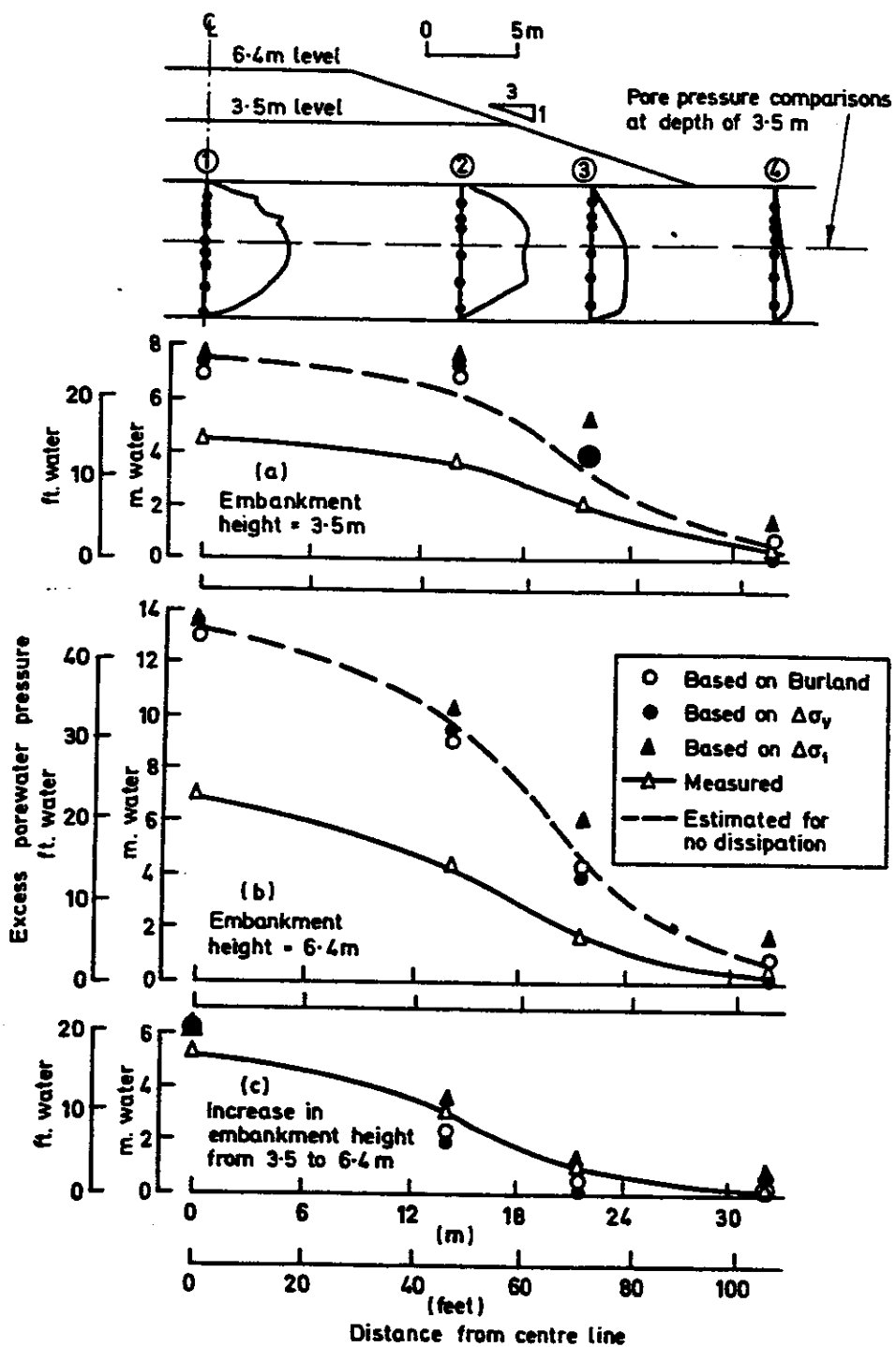


Fig. 6.23 Lateral Distribution of Excess porewater Pressure-Tickton

Chapter 7

Comparison of Lab and Field Evaluation of In Situ Strength and Density

7.1. Overview

Part of the present study was devoted to a comparison of laboratory triaxial and field SPT/CPT strength evaluations. Such comparison is important in terms of developing faith in strength and perhaps stress-strain parameters evaluated from field or lab and used as input for analytical models. If little faith is generated, then such parameters need to be established from personal or reported experience from field cases where model parameters have been back calculated (i.e. calibrated). Note that recommended FEADAM parameter values were employed in the initial finite element analysis used to plan the stress path triaxial testing program. Based on the discussion that follows, no overriding justification was found for using strength obtained from field data or stress-strain parameters obtained in the lab to repeat or iterate on the FEADAM results. (In the end, the strength the obtained from standard triaxial tests on undisturbed and reconstituted samples and recommended stress-strain parameters were employed exclusively.)

7.2. Comparison for Samples 1-4

Consider first a comparison of field SPT/CPT interpretations specific to the location and lab results associated with triaxial test samples 1- 4. This initial comparison should highlight differences that can then be expanded upon before a more general evaluation is made. Samples 1 and 2 are Shelby tube samples taken during augering to install Pz3. They are from 6 and 8 ft. depths respectively, and represent samples of silty sand of approximately 20 to 30% fines (see the soil logs of Appendices A and B, and Tables 2.2, 2.3 and 2.5). Samples 3 and 4 are undisturbed Shelby tube samples of material with 30 to 40% fines at Pz3 and Pz5 locations, both obtained 3 ft. below the ground surface.

Table 7.1 represents a sample by sample comparison of CPT/SPT interpretations and lab test results. Evaluation of relative density (D_r) and friction angle (ϕ) from SPT blow counts (N) and evaluation of the equivalent N from the CPT tip resistance (Q_c) will be discussed subsequently. For the present, note that this is considerable disagreement as to soil type (CPT versus SPT/ lab) and D_r and ϕ values (lab>CPT>SPT). Realize of course that SPT split spoon and Shelby tube samples can't be obtained in the same hole at the same depth. Likewise the CPT test was undertaken in its own hole no more than 5 ft. away. Therefore, values from SPT and CPT tests closest to or encompassing the Shelby tube lab sample depth are used.

7.3. CPT

Note that different from the SPT and lab test procedures, where a sample is available for inspection, the CPT test relies solely upon readings from the tip and sleeve sensors to classify the soil. Such blind dependence results in the dilemma that the CPT treated all or some part of the depth in the immediate vicinity of each sample as fine grained silt-clay soil. For such material, the Roberston and Campanella (1983) program provides an interpretation of the material's undrained strength, S_u , rather than an interpretation of the material's drained friction angle, ϕ , and its relative density, D_r . However, all this indicates that it treats the material as cohesive (i.e. plastic) rather than nonplastic (or cohesionless). However, all samples are cohesionless materials even though samples 3 and 4 contain fines that approach or in thin partings/seams exceed 35% fines. Certainly the piezometer readings (Chapter 6) which showed no porewater pressure increase as the result of construction (or a short lived decrease due to the dilatant response of cohesionless material) and the negative (i.e. dilatant) porewater pressure response of the CPT's own piezo tip record (Fig 2.6) are indicative of the cohesionless behavior of such material. This is confirmed, of course, by the sieve and Atterberg limits analysis performed on the samples. As noted in Chapter 2, a particularly "clayey" part of one sample yield a plasticity index (PI) of only 6. Therefore, while the CPT gives

a continuous averaged record that “appears” to be very accurate, it was fooled at this site into providing misleading data.

Alternatively, one might argue that according to the AASHTO soil classification system, at 35% fines we have silt-clay soils and certainly different partings/seams of this material are present at the site and this is what is reflected in the output. But this begs the question as how we should characterize the material as a whole for analytical purposes. Certainly we would not model the whole soil on the basis of these thin partings/seams as cohesive (i.e. plastic) for stability and settlement analysis. In that sense the SPT (N) or the lab test sample response represents an average of the overall or larger scale material that would be preferred for stability and settlement analysis. On the other hand, the CPT’s continuous jump from cohesionless to cohesive material values as output (see logs in Appendix 2) is indicative of the variable nature of the material. This has implications relative to permeability testing and the effect of such impervious partings/seams on the lab assessed vertical permeability.

Note that the negative (i.e. the dilatant) piezo cone pore pressure readings should be used to warn the CPT interpretation program that the material is cohesionless (i.e. sufficiently pervious to allow enough water movement to yield this negative porewater pressure record) so the program classifies the soil and evaluates the data accordingly. This would be a decided improvement in the CPT

test data interpretation. Of course, most cones in use are not piezo cones and, therefore, they would not benefit from such programming distinction.

The fact that there are undrained negative pore pressures during cone advancement (see Fig 2.6) would indicate that ϕ values calculated based on tip resistance assuming drained conditions are in error. In the absence of such generated negative pore pressure, tip resistance would be less, and so would ϕ . Of course, such negative pore pressures should likewise be present in the SPT blow count response of the sand. While one might apply the Peck, Hanson and Thornburn (1974) correction for negative pore pressures, such correction is only applied to N values in excess of 15, not the lower values found here. As indicated by the piezo tip results, negative values occur even for recorded (or CPT equivalent) N values less than 15.

Note also that the conversion of the cone's tip resistance to a blow count N relies on the soil's D_{50} as shown by the Roberston and Campanella curve of Fig 7.1. Tip resistance in tsf is divided by a value varying from 4 for sand to silty sand, to 3 for silty sand to sandy silt, to 2.5 for sandy silt to clayey silt, to 1 for clay, to give equivalent blow counts. Therefore, if the soil's characterization as assessed from tip resistance and friction ratio is in error, so is the inferred D_{50} value and this conversion number. One should note that for "clay", the cone program yields an undrained strength (c or S_u) that is less than the tip resistance

divided by 9 (based on cone or pile tip capacity (Q_c) equal to $9c$ or $9S_u$). The S_u obtained from the cone program is the equivalent blow count divided by 15 (for S_u in tsf) which is the commonly cited Terzaghi and Peck relationship between S_u and N . (Therefore $S_u = N/15 = (Q_c/1)/15$ not $Q_c/9$). For other cohesive material, i.e. silty clay to clay, clayey silt to silty clay and sandy silt to clayey silt, a value of one is also used to establish S_u from the Q_c .

7.4. SPT

The SPT values at the site suffer from the fact that water levels in the auger were not equalized with those outside the hole. On the other hand, there was partial compensation offered by the negative pore pressure (as indicated by the CPT piezo tip log) that likely developed during driving the split spoon sampler even in this lower blow count material. Evaluation of ϕ and D_r based on blow count, N , will be discussed later.

7.5. Lab Triaxial Test Strength

By contrast, the lab test strengths (ϕ) are potentially higher or lower than true field values due to any densification of loose samples or loosening of dense samples that occurs to the samples during Shelby tube insertion and subsequent

transfer of the sample from cut sections of the tube to the triaxial cell. While the capillary tension in such finer grained cohesionless material is sufficient to keep the samples from falling apart*, the fact that such materials are more permeable than clay make such samples susceptible to densification or loosening during undisturbed sampling and handling. Consider the painstaking evaluation of void ratio changes and their affect on the undrained residual strength of samples from the Van Norman Dam (Castro et al, 1992). Realize that the void ratio (e) and dry unit weight (γ_d) values given in Table 2.5 were calculated ($e = wG_s$; $\gamma_d = G_s\gamma_w/(1+e)$) based on the assumption that with application of the forming pressure in the triaxial test, saturated conditions are virtually reestablished and the table values are applicable at that time.

During Shelby tube insertion, the sample will densify (or dilate) when sheared or subject to a stress state greater than can be supported by a confining pressure that is the negative of the maximum saturated capillary tension that can develop in this material, i.e.

$$u_o = \frac{4T_o}{d_{eff}} = \frac{4T_o}{\frac{1}{5}D_{10}} = \frac{20T_o}{D_{10}}; \quad T_o = 0.075 \text{ g/cm (surface tension)}$$

For the typical D_{10} value of 0.03 mm(0.003 cm) for this silty sand, u_o equals -50 kPa. Alternatively, Seed and Lee (1967) consider that sand desaturates because

*For example, recall the stability of the 120 ft. vertical face of the Helm's pit in similar alluvial material adjacent to I-80 immediately after the January flood of 1997. Such temporary stability was due to capillary tension.

water cavitates in sand at -100 kPa. As an attempt to get around this, one may resort to using reconstituted samples prepared to the desired density. Such samples lose structure or reinforcement afforded by any bedded nature of the in situ material. Strangely enough, reconstituted samples with the absence of such strength enhancing structure, yielded a drained frictional angle (ϕ) basically the same as the ϕ values from the undisturbed samples. Hence, loosening (due to dilatant behavior during sampling) of the undisturbed samples may have compensated for the added strength of such material associated with structure.

Figure 7.2 provides the correlation between the drained or effective stress friction angle, ϕ , and void ratio, e , for all lab tests carried to failure. The curve of Fig 7.2 is superimposed in Fig 7.3 on curves reported in Lambe and Whitman (1969) for general comparison with other cohesionless materials. (This alluvial material fits the trend of other fluvial, i.e. river deposits.) Figure 7.2 includes data from tests on samples 2-4 mentioned previously (sample 1 was not failed), as well as samples 5 and 6 from Pz2 at 10.5 ft. depth, sample 12 from Pz2 at 10 ft. depth and reconstituted samples 7 and 8. Table 7.2 contains data regarding sample location, void ratio (e), percent fines (upper half, lower half of sample and average in select cases), consolidation pressure employed and comments on details of the test. For instance, samples 3 and 8 were tested undrained and the pore pressure recorded was used to establish the effective stress at failure and the effective stress

friction angle. Fig 7.4 shows the pore pressure curves for these tests. Note that even for an $e = 0.746$ sample 3 exhibited a negative pore pressure recovery near the end of the test. Sample 8, by comparison yielded a very large negative porewater pressure (150 kPa) such that the effective confining pressure at peak deviator stress, σ_d , was $\bar{\sigma}_3 = 30 - (-150) = 180$ kPa.

Samples 2 and 4 were subject to staged deviatoric stress increases (to 140 kPa for sample 2 and to 120 kPa for sample 4) with permeability measured after each 20 kPa deviatoric stress increment before being sheared to failure. Samples 5 and 9 were K_0 consolidated, then sample 5 was sheared to failure. (Sample 9, like 10, was a horizontal permeability test sample with a central coarse sand core as shown in Fig 3.1b and therefore was, purposely, not failed.) Samples 7 and 8 were the reconstituted samples ($e = 0.560$) meant to reflect an estimated average void ratio at Pz3A at a depth of 7.8 ft. (between $e = 0.637$ at 7 ft. corresponding to the standard consolidation test sample and $e = 0.496$ of sample 2 at 8 ft. depth). Due to operator error, sample 1 was not failed, while sample 11's failure was not recorded via the computer. Sample 12 is that one used for the stress path test to be described in Chapter 9.

Figure 7.5 is a plot of all the failed drained test stress-strain curves. The vertical axis represents stress level, SL, i.e. the deviator stress divided by the peak or failing value. Figure 7.6 presents the associated volume change curves for all

isotropically consolidated drained tests, including that for sample 1 which was not failed. Note that all such drained volume change curves, with the exception of sample 2, exhibit a dilatant tendency. Sample 2 was loaded to a deviatoric stress of $\sigma_d = 140$ kPa and, different than other such stage loaded samples, was unloaded before being reloaded all the way to failure. Therefore, its volume change curve is not representative (i.e. the unloading affected the subsequent reload volume change response). Note that the greater dilatancy associated with the position (and upward slope) of the volume change curves corresponds to the greater recorded ϕ (sample 6 with $\phi = 40.5^\circ$, sample 4 with $\phi = 42.5^\circ$ and sample 7 with $\phi = 43.6^\circ$). Note sample 1, though not brought to failure, would have been expected to yield a lower ϕ because of its more compressive (less dilatant) volume change curve. At the time the sample 1 test was stopped for permeability determination it had a mobilized friction of $\phi_m = 31.8^\circ$.

Note the range in drained strain ϵ_1 at 50 percent stress level (SL = 0.5), $\epsilon_1(50)$, from the curves of Fig 7.5 is nicely predicted by the accompanying Fig 7.7 given that $C_u = 10$ and $e = 0.50$ to 0.65 in the associated tests. Fig 7.7 was derived from data by Norris (1977) on isotropically consolidated tests on reconstituted samples of 18 different natural sands.

An interesting and important finding from the drained tests is the responses of samples 5 and 6 which were taken from the same Shelby tube with a common

trimmed end at 10.5 ft. depth (Pz2). Sample 5 was K_0 consolidated so its consolidation response along with that of sample 9 (from Pz2 at 9.5 ft.) could be compared with that of a traditional consolidation test (from Pz3 at 7 ft., directly between samples 1 and 2). As shown in Fig 7.8, the volume change curve during subsequent shear of the K_0 consolidated sample 5 overlies that of the standard test as described below. In fact, if one can run the standard test, i.e. isotropically consolidate the sample from a forming pressure (in this case 30 kPa) to the required constant confining pressure (here 80 kPa) of the standard test and then shear from zero deviatoric stress (σ_d), the test will pass through or satisfy a K_0 condition at a certain σ_d (120 kPa in this case) where the volume change during isotropic consolidation added to the volume change during shear become equal to the sum of the axial strain during isotropic consolidation and shear (i.e. $\epsilon_{v\text{total}} = \epsilon_{1\text{total}}$ such that $\epsilon_{3\text{total}} = 0$). Note that in the test on sample 6, $\epsilon_v = 0.6\%$, $\epsilon_1 = 0.3\%$ was recorded in isotropic consolidation and during drained shear, $\epsilon_v = 0.3\%$ and $\epsilon_1 = 0.3\%$ occurred up to a value of $\sigma_d = 120$ kPa at which point $\epsilon_{v\text{total}} = 0.6\% + 0.3\% = 0.9\%$ matched $\epsilon_{1\text{total}} = 0.3\% + 0.6\%$ and the K_0 condition was achieved ($\epsilon_v = \epsilon_1 = 0.9\%$, $\epsilon_3 = 0$). This agrees with the $\epsilon_v = 0.9\%$, $\epsilon_1 = 0.9\%$ in K_0 consolidation ($\epsilon_3 = 0$) of sample 5 from the all around forming pressure of 30 kPa to a pressure of $\bar{\sigma}_3 = 77$ (approximately 80 kPa) at which point $\sigma_{d0} = 120$ kPa or $\bar{\sigma}_1 = 77 + 120 = 197$ kPa ($K_0 = \bar{\sigma}_3/\bar{\sigma}_1 = 77/197 = 0.39$). Superposing

the subsequent volume change curve obtained in drained shear of test 5 on that from sample 6 (the isotropically consolidated sample) at $\varepsilon_v = 0.9\% - 0.6\% = 0.3\%$, $\varepsilon_1 = 0.9\% - 0.3\% = 0.6\%$ and $\sigma_d = 120$ kPa at $\varepsilon_1 = 0.6\%$, basically the same volume change response results. Both tests yielded virtually the same ϕ of $40.6^\circ \pm 0.1^\circ$ as indicated in Table 7.2.

While Fig 7.4 presents the porewater pressure curves of undrained tests on samples 3 (undisturbed) and 8 (reconstituted), the corresponding stress level (i.e. normalized deviator stress, σ_d/σ_{df}) versus axial strain curves are shown in Fig 7.9. Note that the considerable difference of the two curves. (Sample 8's slow gain in resistance for $SL > 0.1$ is due the slow increase in negative porewater pressures as indicated in Fig 7.4.) What is interesting is that both tests were sheared undrained after isotropically consolidating the samples. Sample 3 was isotropically consolidated from 30 kPa to a test pressure of 60 kPa representing the mean effective stress of a sample at a preconsolidation pressure (P'_p) of 100 kPa (i.e. $1/3(1+2K_o)100$ kPa, $K_o = 0.4$) corresponding to an overconsolidation ratio $OCR = 2$ (i.e. $P'_p = OCR \bar{\sigma}_{v0} = 2(50) = 100$ kPa) of a sample at 10 ft. depth. At the same time, 60 kPa is more than 1.5 times the P'_p of the sample from its location (Pz3 at 3 ft.) thus satisfying SHANSEP conditions (Ladd and Foote, 1974) in an attempt to overcome sample disturbance. The 60 kPa also approaches the minor principle effective stress of a sample at 10 ft. depth under centerline of the fill. By contrast,

the reconstituted sample 8 was isotropically consolidated from its forming pressure of 30 kPa to 65 kPa and then rebounded to 30 kPa. The rebounded consolidation pressure of 30 kPa represents the mean effective stress of a sample at 10 ft. depth at an OCR of 2 (i.e. $1/3(1+2K_o)50$, $K_o = 0.4$ for OCR = 2).

While sample 8 was tested undrained after consolidation to the pressure of 30 kPa and sample 3 to a pressure of 60 kPa the undrained strength ($S_u = 1/2 \sigma_{df}$) of sample 8 was 260 kPa and that of sample 3 was only 55 kPa. Such difference is due to the high void ratio ($e = 0.746$), low drained ϕ ($= 33.4^\circ$) and more compressive volume change tendency of sample 3 than 8 ($e = 0.560$, $\phi = 39.6^\circ$, and large negative porewater pressure at failure). Nevertheless these undrained strengths were used as an estimate for later undrained FEADAM stress analysis.

These undrained strength values (55 to 260 kPa) nicely bracket the great majority of undrained strengths reported by the CPT where it interpreted a good part of the profile as "cohesive" material. Therefore, while the CPT misinterpreted the material it gives undrained strength values that may be realistic (even though for a cohesionless material).

In fact, if one compares the drained and undrained effective stress paths of the reconstituted samples 7 and 8 (both of the same void ratio, $e = 0.560$), see Fig 7.10, one will notice the much greater undrained strength that results because of the large negative porewater pressure at failure in the undrained test. The deviator

stress at failure in the undrained test is five times that in the drained test, even though the drained test ϕ was larger ($\phi = 43.6^\circ$ versus 39.6°). Note, however, that most of sample 8's resistance derives from movement along the failure envelope (i.e. the ESP at a slightly decreasing ϕ above and to the right of the top of sample 7's ESP).

The undrained effective stress path (ESP) for sample 3 is superposed in Fig 7.10 for reference. Note that more important than the friction angle ϕ (33.4° for sample 3 versus 39.6° to 43.6° for samples 7 and 8) is the volume change tendency during shear (compressive and dilative) and the resultant undrained porewater pressure change (positive as in sample 3 or negative as in 8 of Fig 7.4) on the consequent undrained ESP (e.g. sample 3 versus sample 8), the effective confining pressure at failure ($\bar{\sigma}_{3f} = 45$ kPa in sample 3 versus 180 in sample 8), the undrained strength ($S_u = 1$ ksf in sample 3 versus 5 ksf in sample 8) and the resulting strains / displacements at mobilized stress levels. With dissipation of the undrained porewater pressure and the switch to drained (i.e. fully consolidated) conditions (e.g. sample 7's ESP), additional strains / displacements may be large (going, for the most part, horizontally from a point along sample 8's ESP to one on sample 7's ESP) or small (going from the ESP of sample 3 to that of 7, since most of the strain has already occurred along the ESP of sample 3). More on this in Chapter 9.

7.6. Broader Comparison

While Table 7.1 reflects a comparison of SPT, CPT and lab strengths at 4 specific sample locations, the authors thought to make a broader comparison. Table 7.3 provides an evaluation of relative density (D_r) and the friction angle (ϕ) of the silty sand (SM) material at Pz3, Pz4 and Pz5 stations as established from two SPT blow count correlations: Peck, Hanson and Thornburn (1974) and DM-7 (1982). The DM-7 charts employed are reproduced as Figs 7.11 and 7.12 while the Ph&T charts appear as Fig 7.13. Both correlations depend upon the effective overburden pressure ($\bar{\sigma}_{v0}$) at the depth the blow count (N) is obtained. This was calculated assuming a total unit weight (γ) of 120 lbs/ft³ for the material and using the piezometer readings taken the day following the SPT sampling. Note that the Peck, Hanson and Thornburn procedure yields a correction factor (C_N) that when multiplied by N yields a corrected blow count (N_1) corresponding to an effective overburden pressure of 1 tsf. This N_1 value can also be used to assess liquefaction potential.

From such evaluation the deposit would appear to be loose over its upper portion (to, say, 8 ft. depth), and medium dense from that level to the artesian layer at 21 ft. depth. However, this is based upon blow counts obtained where water level inside the hollow stem auger was not maintained level with the external water level. Water level differences of 1 to 5 ft. at shallow depth, 5 to 10 ft. at

middle depth, and 12 to 17 ft. at the greater depth that likely occurred would have resulted in upward flow at the bottom of the hole and, therefore, loosened the material during the blow count determination. Therefore, there is the likelihood that the values of blow count and, thus, the relative density and the friction angle should be higher than those indicated in Table 7.2. By contrast the DM-7 evaluation requires that the uncorrected blow count is used with knowledge of overburden pressure to get relative density (Fig 7.11) and with D_r and soil classification to get ϕ (Fig 7.12). For the current work, a range in ϕ for the established D_r over the zone distinguished as SM is established. One should note that the SPT values used in Table 7.1 are part of the present Table (7.3).

One will note the CPT logs (see Appendix 2) indicate the presence of considerable amounts of clay, silty clay and clayey silt as opposed to just silty sand as per visual inspection of the split spoon samples from SPT testing at these Pz3, Pz4 and Pz5 locations. Table 7.4 compares N , D_r and ϕ values derived from SPT blow counts and CPT correlations over depths where the CPT log indicates the presence of sand, silty sand or sandy silt. While the middle and lower depth blow counts and relative densities are somewhat similar, the CPT correlations indicate considerably higher values at the shallow depth. At all depths the friction angles from CPT correlations are much higher than those from SPT blow count correlations.

One drawback of the CPT test is its inability to ascertain the presence of gravel or pebbles as noted in the logs for SPT and Shelby tube samples at Pz1, Pz2 and Pz5 locations (see Appendix 1). Secondly, one needs to assume the depth to groundwater. However, as judged from separate runs of the data for 0 and 10 ft. water depths, this doesn't have a significant effect on the CPT correlation results.

Lastly, given that void ratios were assessed very simply (see Table 2.5) from lab determined water contents ($e = \frac{wG_s}{S}$, but $S = 1$ at the time of sampling for all samples taken below the water table), it was decided to establish maximum and minimum void ratios and compute relative densities, and to see the associated effect on ϕ values assessed using DM-7 Fig 7.12. Given the range in $\gamma_{d_{max}}$, $\gamma_{d_{min}}$, e_{max} and e_{min} reported in Table 2.6 for 23 and 38% fines, average values of $e_{max} = 1.16$ and $e_{min} = 0.328$ for $D_r = 0\%$ and $D_r = 100\%$ are shown as end points for the superposed line representing the silty sand (SM) of the upper layer. (Note that these correspond to slightly adjusted values of $\gamma_{d_{max}}$ and $\gamma_{d_{min}}$ for the chart's assumed value of $G_s = 2.68$.) The associated superposed material line falls out of range (below the ML line at $D_r = 0\%$ and above the SW line at $D_r = 100\%$) for the zone applicable to an SM soil. Given this line, a range in D_r and ϕ as assessed for the comparable range in e (see Table 2.5) at Pz3, Pz4 and Pz5 locations are as indicated below.

Pz3	Pz4	Pz5
$e = 0.49$ to 0.42	$e = 0.65$ to 0.59	$e = 0.69$ to 0.59
$D_r = 80$ to 89%	$D_r = 61$ to 69%	$D_r = 56$ to 69%
$\phi = 37^\circ$ to 39°	$\phi = 33.5^\circ$ to 34.5°	$\phi = 32.5^\circ$ to 34.5°

These values can be compared with those in Table 7.3. As can be seen the ϕ and D_r as assessed from actual lab assessed e and D_r values are higher for Pz3 and within the range from blow counts at Pz4 and Pz5 locations.

Of course the above takes ϕ for the given lab e and D_r values based on the assumption that strength ϕ varies as indicated in Fig 7.12. By contrast the ϕ versus e relationship of Fig 7.2 (and in Fig 7.3) as established from tests on actual samples is shown superposed on Fig 7.12. Note the much higher strength values from actual lab testing.

In the same regard, Table 7.5 compares relative densities from CPT, SPT correlations with values based on lab assessed e 's at these same Pz locations. As can be judged, SPT values are more conservative. (CPT values, as indicated at Pz4 location, are not always conservative). Therefore, using the same strength correlation (Fig 7.12) ϕ 's based on lab assessed e 's will be higher. Furthermore, this strength relationship is in turn conservative as compared to actual lab assessed ϕ 's (see the superposed ϕ versus e line) in the case of this deposit.

Normally, sand strength is obtained by correlation from soundings (CPT) or penetrations (SPT). Alternatively, if it is tested in the lab it is common to run a drained triaxial test on a reconstituted sample isotropically consolidated under a confining pressure of say 100 kPa (1 tsf) and to take the secant drained friction angle so obtained to apply at all low to moderate values of overburden pressure. Seldom is the method of sample preparation (hence, sample fabric), anisotropic consolidation or curvature of the Mohr-Coulomb envelope considered in routine work. At most, the variation in the friction angle with void ratio, e , or relative density, D_r , is investigated (Fig 7.2). Certainly, a DOT materials' lab is not likely to undertake static undrained tests with the intent of assessing the residual strength in the event of liquefaction or undertake cyclic triaxial tests. Usually the length (mileage) of a project and the need to quickly assess average or conservative strengths of different soil units over varying subsurface conditions takes precedence over sophistication.

The task here, however, was to consider what tests might be necessary as part of an uncoupled or coupled field-lab-analytical assessment of potential changes in groundwater flow conditions resulting from embankment construction. Accordingly, since the undisturbed Shelby tube soil samples contained sufficient fines for capillary tension to keep them intact, it was possible to run tests on the extruded samples. Such tests on undisturbed samples taken to a pressure in excess

of field values (SHANSEP approach) yielded values consistent with the reconstituted test results.

While the lab triaxial tests described have only been discussed relative to strengths they have provided, further discussion of their use relative to field stress-strain-strength-pore pressure generation will be highlighted when we discuss their use in conjunction with finite element analysis.

7.7. Other Lab Data

Note that the two undisturbed K_0 consolidated triaxial tests (samples 5 and 9) yielded consolidation curves similar to that obtained in the conventional consolidation test (Fig 2.9). Fig 7.14 superposes the conventional test curve with its vertical axis converted to volumetric strain, on top of the K_0 consolidated triaxial curves. Of course, the triaxial test curves start at a zero strain at the all-around forming pressure of 30 kPa. Nevertheless, when Casagrande's technique is applied to each curve to establish the respective preconsolidation pressure, values of 102 kPa (sample 5) and 92 kPa (sample 9) are obtained. In conjunction with their in situ vertical stresses of 40.5 and 45.3 kPa, respectively, this gives overconsolidation ratios of 2.1 and 2, respectively. By contrast, the much stiffer standard test consolidation curve also yields a preconsolidation pressure of 60 to 65 kPa and a similar $OCR = 63/31.3 = 2$. Samples 5 and 9 are from 10.5 and 9.5

ft. depths from Pz2 station, while sample 10 is from 7 ft. depth at Pz3 location (between samples 1 and 2).

Note that the straight line C_c slopes of these lab curves at the higher pressure range are 0.0404 (sample 5), 0.0575 (sample 9) and 0.00631 (1-D) while their initial void ratios are 0.661, 0.577 and 0.637, respectively. Therefore, the much stiffer standard test curve response is due to conditions other than its void ratio. As we will see later, this sample gives a back calculated permeability that is the lowest of any obtained primarily because of this stiffness.

For comparison, the isotropic consolidation response of samples 6, 7 and 8 are shown in Fig 7.15. Samples 7 and 8 are the two reconstituted samples having initial void ratios of 0.560, while sample 6 (like 5) is from Pz2 at 10.5 ft. depth and a void ratio of 0.585. The response of samples 7 and 8 reflects normal consolidation behavior for consolidation to 65 kPa pressure before subsequent rebound to 30 kPa (followed by shear loading to failure).

One last item is the attempted correlation of water content of samples obtained below water level and, therefore, void ratio with the percent fines. Fig 7.16 shows the data from Table 2.5 for samples where both water content and percent fines were established. Note that there is a trend. Therefore, one should expect a relationship between (saturated) water content or void ratio and percent fines present. This is indicative of the effect that changes in the material have

upon the density achieved as the result of alluvial deposition. Superposed on this plot are the maximum and minimum void ratios and a liquid limit value.

7.8. Summary

CPT and SPT correlations yielded strengths that were less than lab determined values on undisturbed and reconstituted samples (Fig 7.2). The lab determined values are deemed to be the more appropriate in light of the agreement between the drained and undrained ϕ values, and the negative porewater pressures in the undrained tests and the associated negative pore pressures recorded in the field (i.e. the CPT piezo cone records and select Pz readings during fill construction). Certainly the soil above the artesian layer is cohesionless (SM) in character and behavior. The fact that the CPT interpolations indicated plastic or cohesive fine-grained material strongly suggests that CPT work must be confirmed against SPT or other field work where samples can be obtained. Note that some of the most useful data collected was that from water content samples taken from split spoon samples from below the water table. In conjunction with lab determined e_{\max} ($\gamma_{d_{\min}}$) and e_{\min} ($\gamma_{d_{\max}}$) values, they provide a much greater confidence as to the likely field density state (D_r) and the explanation of observed

behavior (i.e. the generation of negative pore pressures due to the undrained shear of dilatant medium to dense sands during fill loading).

Table 7.1 Comparison of CPT, SPT and Lab Test Strengths for Samples 1-4

Sample No.	Location	SPT	CPT			Lab	
			Depth	Soil Type	Equiv. N		S_u or D_r / ϕ
1	Pz3	Depth 4 - 5.5 ft. SM N = 8 D_r = 35 to 37 % ϕ = 30.5 to 31.5°	4.9 ft.	Sandy silt to clayey silt	18	3.1 tsf	Sample Depth 6 ft. SM e (NA) D_r (NA) ϕ (NA)
			5.7 ft.	SM to ML	16	60 - 70 % / 42 - 44°	
			6.6 ft.	SM to ML	14	50 - 60 % / 42 - 44°	
2	Pz3	Depth 8.5 - 10 ft. SM N = 12 D_r = 45 - 50 % ϕ = 32 to 33.5°	7.4 ft.	SM to ML	11	50 - 60 % / 40 - 42°	Depth 8 ft. e = 0.496 D_r = 80 % ϕ = 46.5°
			8.2 ft.	Sandy silt to clayey silt	6	0.9 tsf	
			9.0 ft.	SM to ML	10	40 - 50 % / 38 - 40°	
3	Pz3	Depth 3 - 5.5 ft. SM N = 8 D_r = 35 to 37 % ϕ = 30.5 to 31.5°	2.5	Clay	3	0.2 tsf	Depth 3 ft. SM e = 0.746 D_r = 50 % ϕ = 33.4°
			3.3	Clay	3	0.2 tsf	
4	Pz5	Depth 4 - 5.5 ft. SM N = 6 D_r = 25 - 30 % ϕ = 29 - 30°	2.5	Sandy silt to clayey silt	6	1.0 tsf	Depth 3 ft. SM e = 0.642 D_r = 63 % ϕ = 42.5°
			3.3	Clayey silt to silty clay	7	0.9 tsf	

Table 7.2 Data from Triaxial Tests for Strength

Sample No.	Location / Depth	Void Ratio (e)	Percent Fines	Consolidation Pressure (kPa)	ϕ (°)	Comments D (drained) U (undrained)
1	Pz3 at 6 ft.	--	20	45	--	Sheared (D) in 20 kPa stages to 100 kPa. Vertical permeability evaluated at each stage. Not failed.
2	Pz3 at 8 ft.	0.496	19	60	46.5	Sheared (D) in 20 kPa stages to 140 kPa. Vertical permeability evaluated at each stage. Unloaded to $\sigma_d = 0$, then sheared (D) to failure.
3	Pz3 at 3 ft.	0.746	32	60	33.4	Sheared to failure (U).
4	Pz5 at 3 ft.	0.642	31/65 (48 av)	65	42.5	Sheared (D) in 20 kPa stages to 120 kPa. Vertical permeability evaluated at each stage. Then sheared (D) to failure from $\sigma_d = 120$ kPa.
5	Pz2 at 10.5 ft.	0.661	32/29 (30 av)	77	40.5	Vertical permeability evaluated at 30 kPa forming pressure. K_o consolidated to $\sigma_3 = 77$ kPa. Vertical permeability evaluated, then sheared (D) to failure.

Table 7.2 Data from Triaxial Tests for Strength (Cont'd)

Sample No.	Location / Depth	Void Ratio (e)	Percent Fines	Consolidation Pressure (kPa)	ϕ (°)	Comments D (drained) U (undrained)
6	Pz2 at 10.5 ft.	0.585	65/26 (45 av)	80	40.7	Vertical permeability evaluated at 30 kPa forming pressure. Anisotropically consolidated to $\sigma_3 = 80 / \sigma_d = 20$. Vertical permeability evaluated, then sheared (D) to failure.
7	Reconstituted	0.56	20	30/65/30	43.6	Isotropic permeability assessed vertically at 30 kPa forming pressure, at 65 kPa isotropic consolidation pressure and at 30 kPa rebounded consolidation pressure. Then sheared (D) to failure.
8	Reconstituted	0.56	20	30/65/30	39.6	Isotropic permeability assessed vertically at 30 kPa forming pressure, at 65 kPa isotropic consolidation pressure and at 30 kPa rebounded consolidation pressure. Then sheared (U) to failure.

Table 7.2 Data from Triaxial Tests for Strength (Cont'd)

Sample No.	Location / Depth	Void Ratio (e)	Percent Fines	Consolidation Pressure (kPa)	ϕ (°)	Comments D (drained) U (undrained)
9	Pz2 at 9.5 ft.	0.577	36/56 (46 av)	59	--	Horizontal permeability evaluated at 30 kPa forming pressure. K_o consolidated to $\sigma_3 = 59$ kPa and horizontal permeability evaluated. Sample not failed.
10	Pz2 at 9.5 ft.	0.524	26/27 (26 av)	30	--	Horizontal permeability evaluated at 30 kPa forming pressure, then house air failed and sample collapsed.
11	Reconstituted	0.605	37	30	--	Isotropic permeability assessed vertically at 30 kPa forming pressure. Data during (U) shear failure mistakenly not recorded.
12	Pz2 at 10 ft.	0.654	36	70	41.6°	Stress path test described in Chapter 9.
1-D	Pz3 at 7 ft.	0.637				Standard consolidation test sample used for comparison with K_o consolidation phases of samples 5 and 9

Table 7.3 Correlations From SPT Blow Counts

Piez. No.	Depth (ft.)	N	σ_{v0} (psf)	PH&T				DM-7		
				C_N	N_1	D_r (%)	ϕ (°)	D_r (%)	ϕ (°)**	γ_d (pcf)
Pz3	4 - 5.5	8	538	1.5	12	37	30.5	35	30.5 - 31.5	95 - 108
	8.5 - 10	12	828	1.3	16	45	32	50	32 - 33.5	97 - 112
	13.5 - 15	11	1022	1.2	13	40	31	50	32 - 33.5	97 - 112
Pz4	6 - 7.5	6	497	1.5	9	30	29.5	25	29 - 30	92 - 106
	11 - 12.5	12	785	1.3	16	45	32	50	32 - 33.5	97 - 112
	18 - 19	12	1219	1.17	14	42	31.5	50	32 - 33.5	97 - 112
	19 - 19.5	22	1219	1.17	26	60	35	65 *	33.5 - 36	100 - 115
Pz5	4 - 5.5	6	567	1.45	9	30	29.5	25	29 - 30	92 - 106
	9 - 10.5	11	826	1.3	14	42	31.5	50	32 - 33.5	97 - 112
	16 - 17	12	1042	1.2	19	55	34	55	32.5 - 34	98 - 113
	17 - 17.5	26	1042	1.2	31	67	36.5	70 *	34 - 36.5	100 - 116

* Used right side axis of Fig 7.11 for sand with fine to medium gravel

** Lower limit of SM; range in Fig 7.12 would be less if ML limit used

Table 7.4 Comparison of SPT and CPT, D_r and ϕ

Range of Depth (ft.)	SPT			CPT ***		
	N (N_1)	D_r (%)	ϕ (°)	Equivalent N*	D_r ** (%)	ϕ (°)**
4 - 7.5	6 - 8 (9 - 12)	25 - 37	29 - 31.5	7 - 22	50 - 80	40 - 46
8.5 - 15	11 - 12 (13 - 16)	40 - 50	31 - 33.5	5 - 21	40 - 80	38 - 44
16 - 19.5	12 - 26 (14 - 31)	65 - 70	32 - 36.5	11 - 33	50 - 80	40 - 44

* All blow counts, i.e. cohesionless and silt-clay

** Only for soil considered cohesionless

*** Only for Pz3, 4, 5 not 6

Table 7.5 Comparison of Range in D_r from CPT, SPT and Lab Void Ratio

Piezometer No.	Depth (ft.)	CPT *	SPT	Lab Void Ratios
Pz3	1.5 to 10.2	40 to 70 %	35 to 50 %	80 to 89 %
Pz4	7 to 22	50 to 90 %	25 to 65 %	61 to 69 %
Pz5	3.5 to 10.5	50 to 70 %	25 to 70 %	56 to 69 %

* Only from cohesionless materials

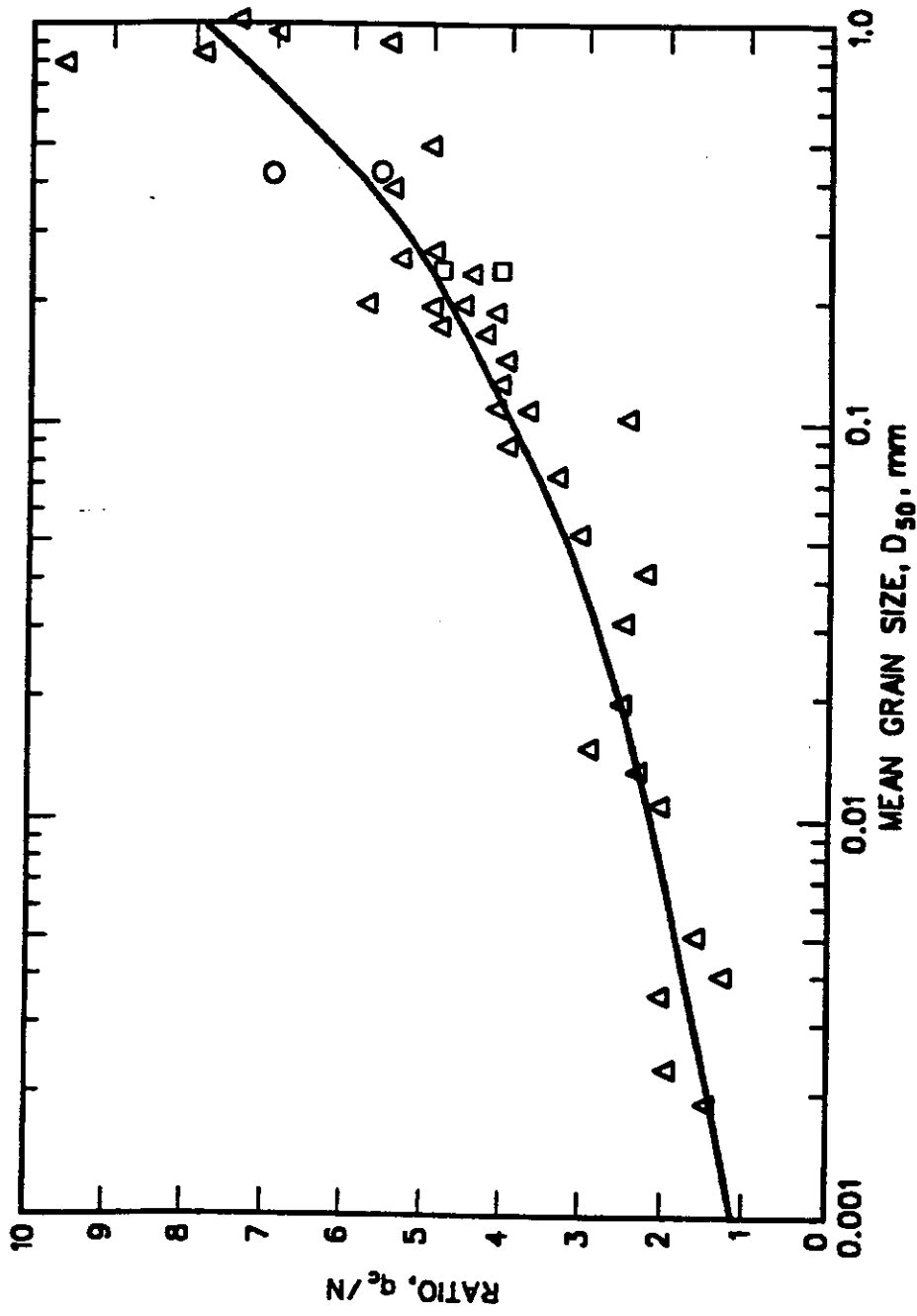


Fig. 7.1 Correlation Between Grain Size and Ratio of Cone Bearing and Standard Penetration Test Resistance (after Robertson and Campanella, 1983).

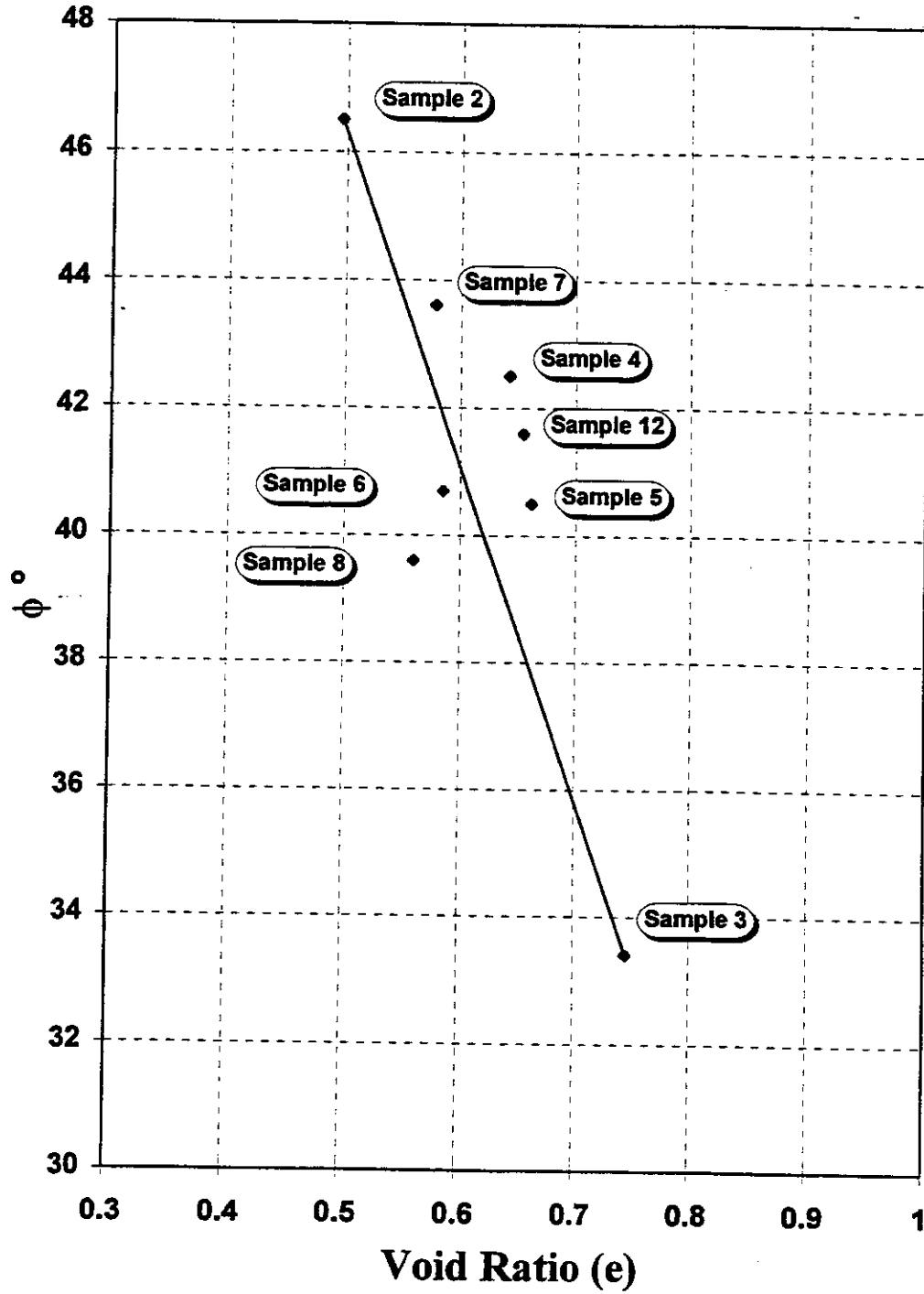


Fig 7.2 Correlation Between Drained or Effective Stress Friction Angle from Standard Triaxial Tests and Void Ratio.

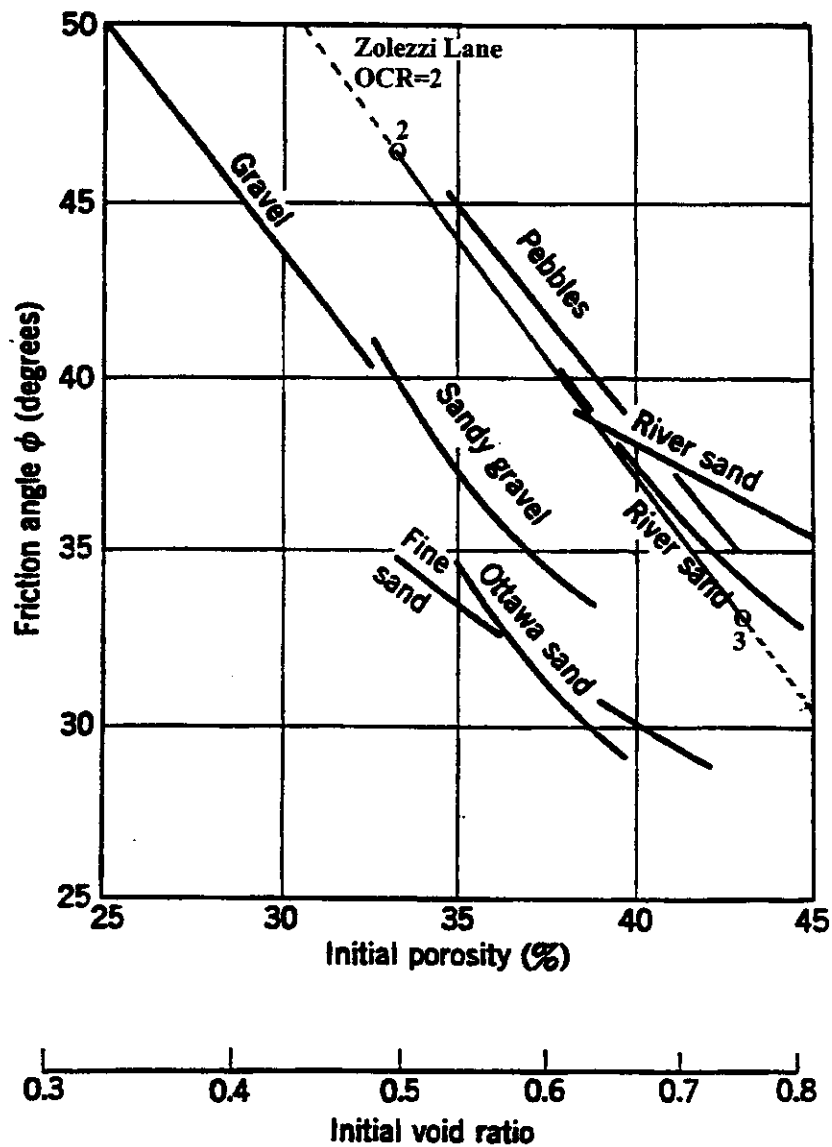


Fig 7.3 Friction Angle Versus Void Ratio for Several Granular Soils from Lambe and Whitman (1969) with Superposed Fig. 7.2 Results.

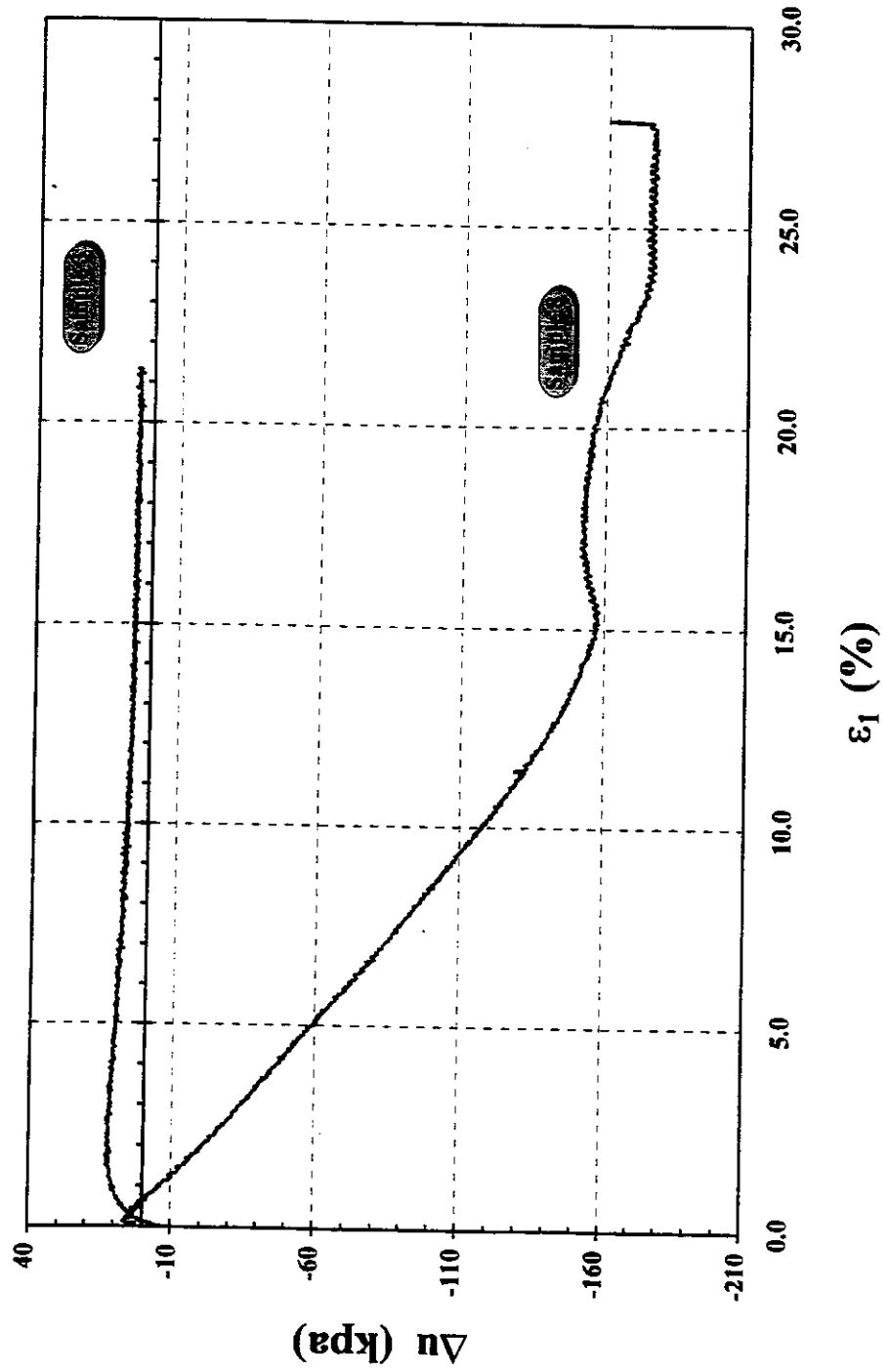


Fig 7.4 Pore Pressure Curves for Undrained Tests

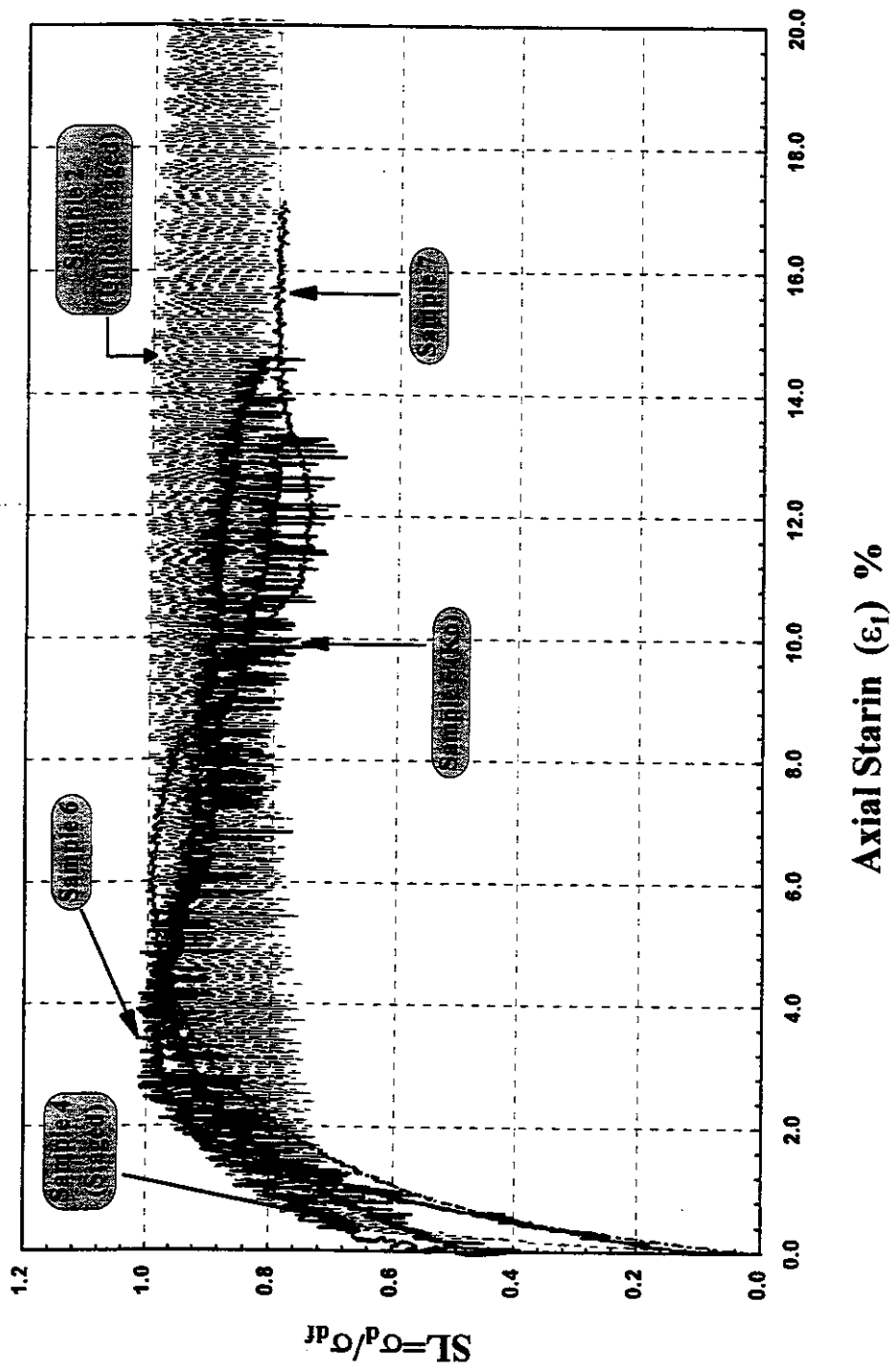


Fig. 7.5 Normalized Stress Versus Strain Curves.

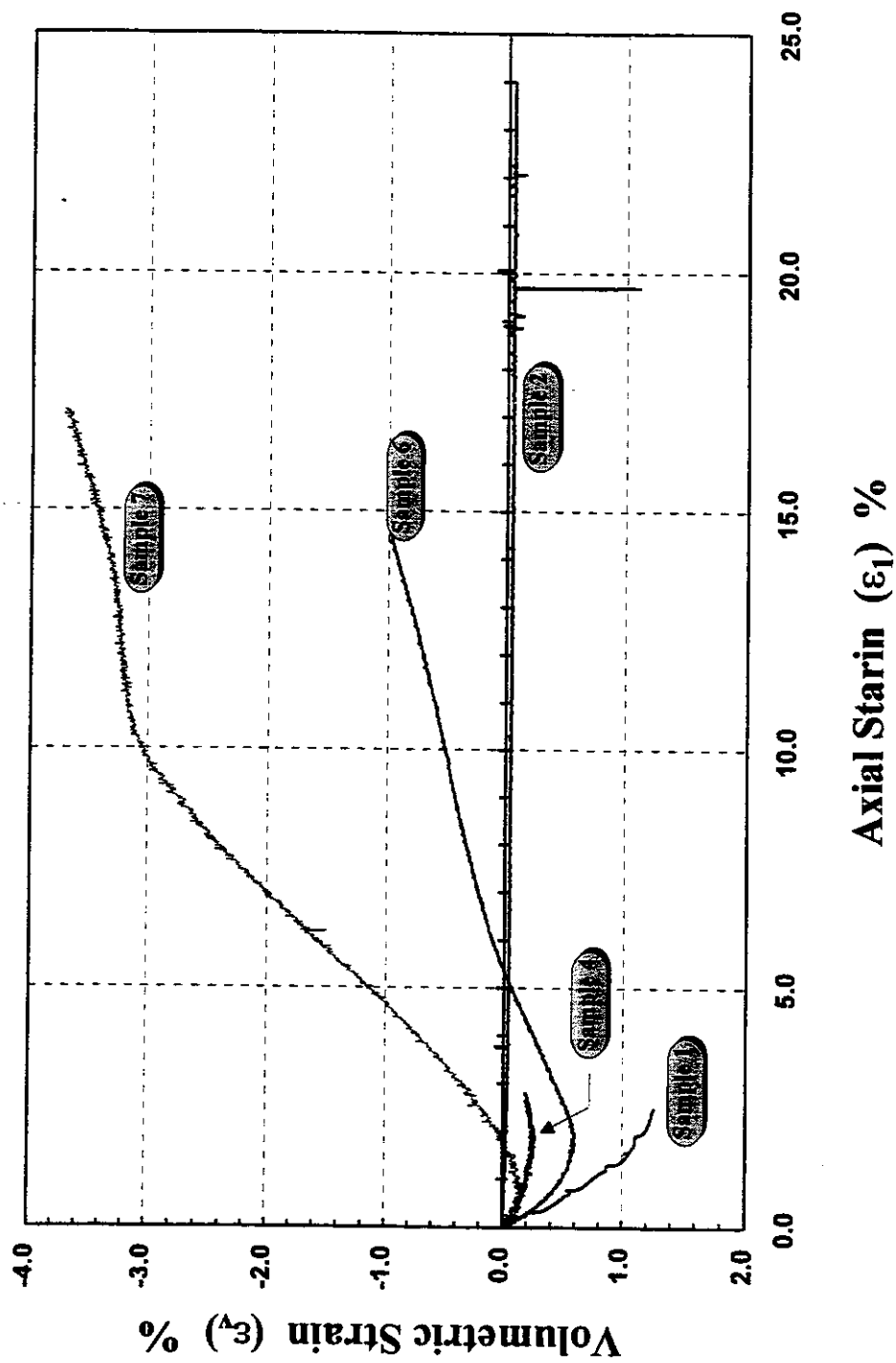


Fig. 7.6 Drained Volume Change Curves.

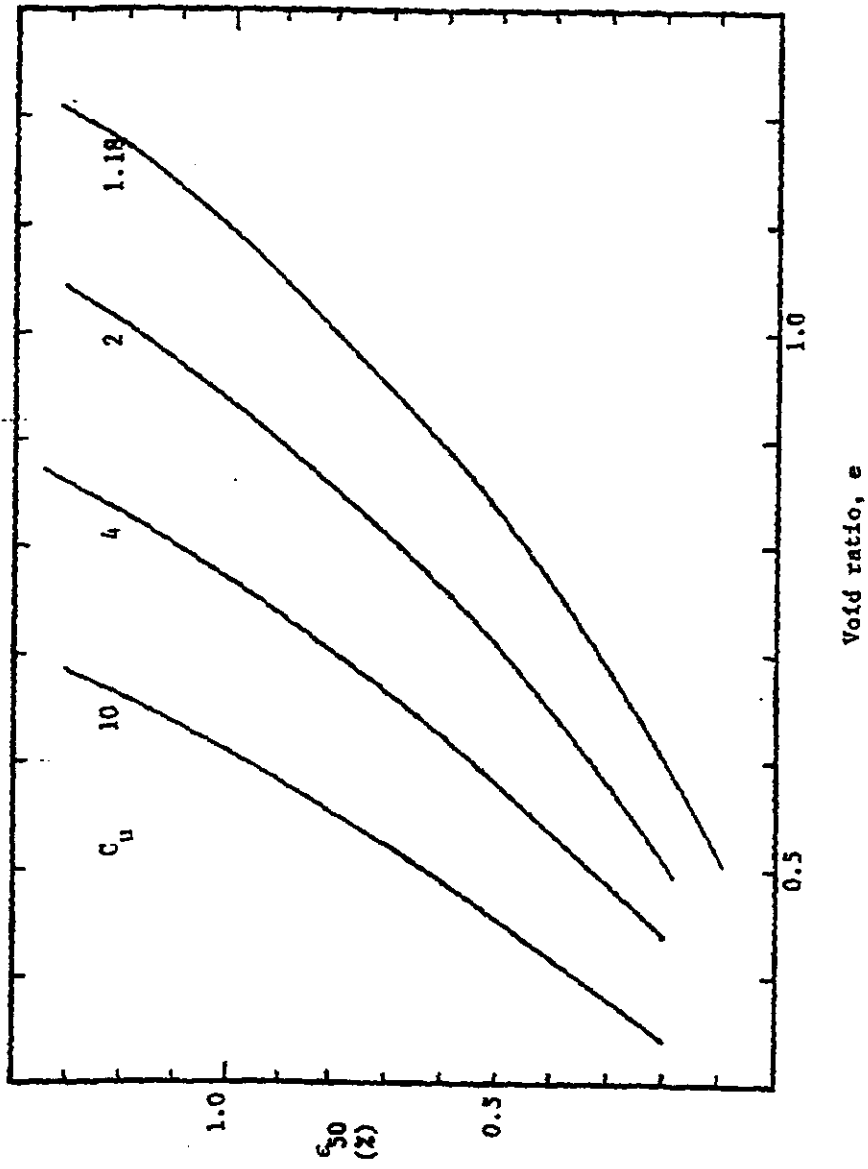


Fig. 7.7 Estimation of ϵ_{50} as a Function of e and C_u .

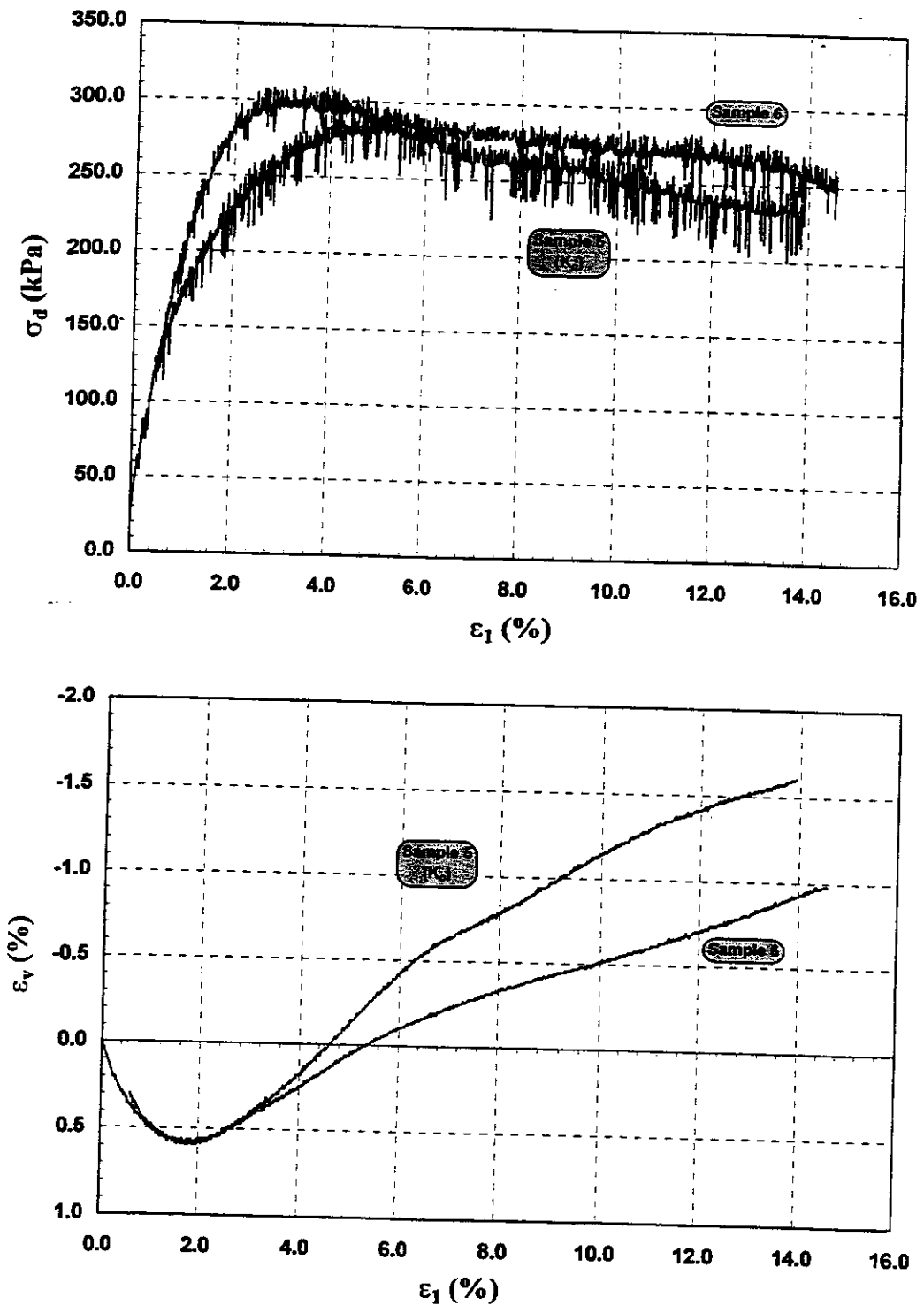


Fig. 7.8 Comparison of Standard Test and K_0 Consolidated Test Shear Response.

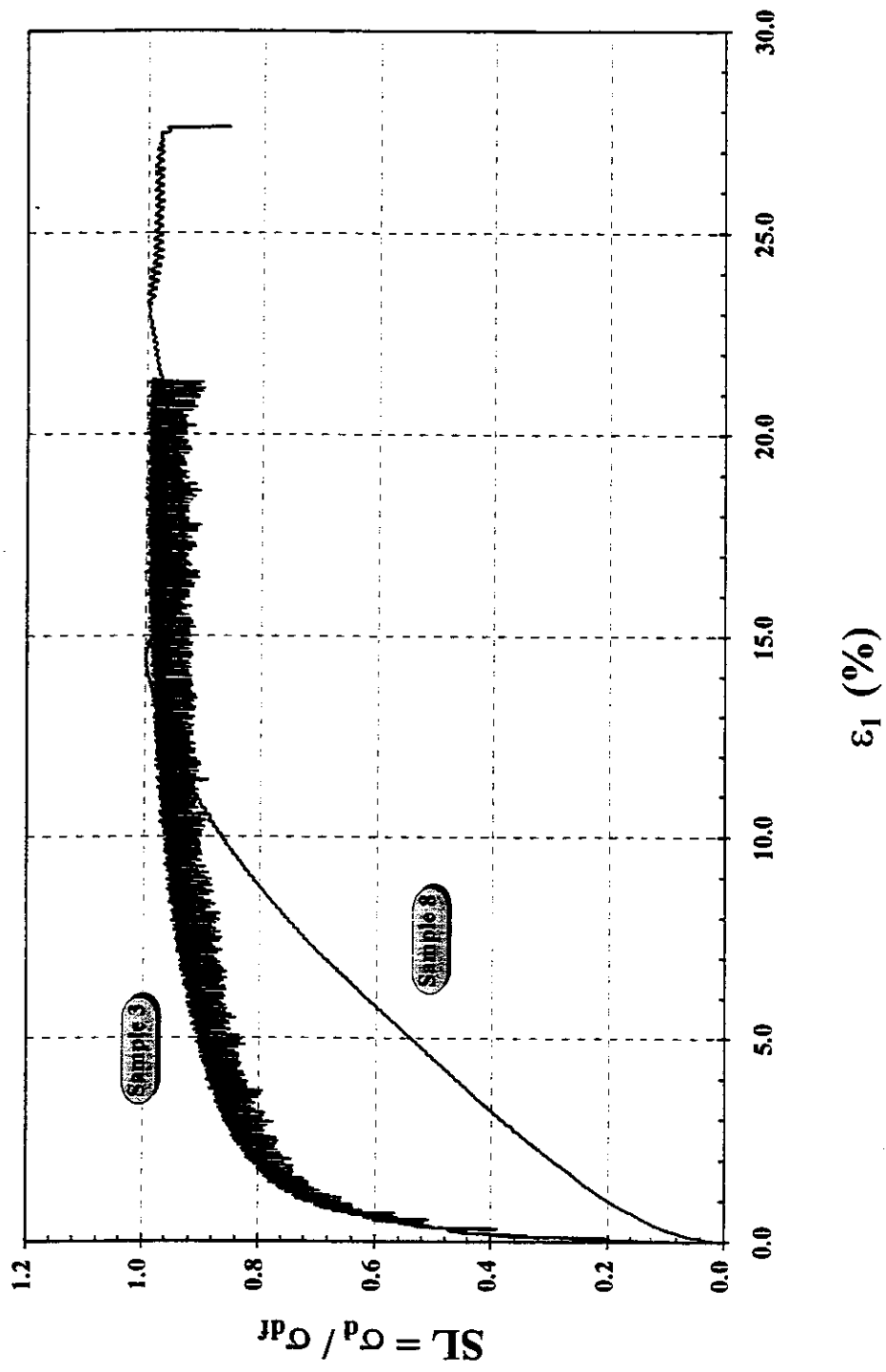


Fig. 7.9 Undrained Test Stress-Strain Curves.

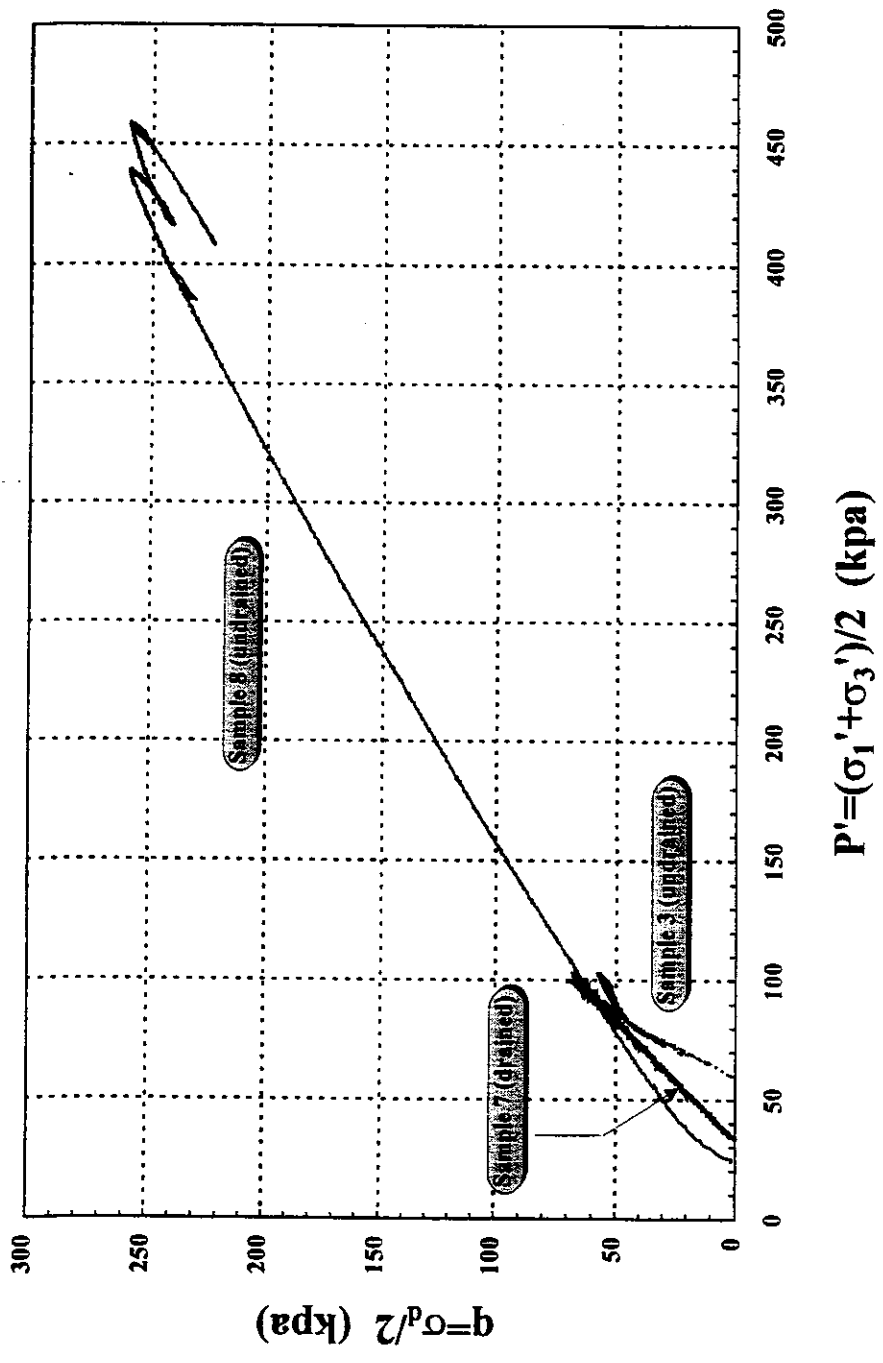


Fig. 7.10 Drained and Undrained Effective Stress Paths for the Reconstituted Samples 7 and 8.

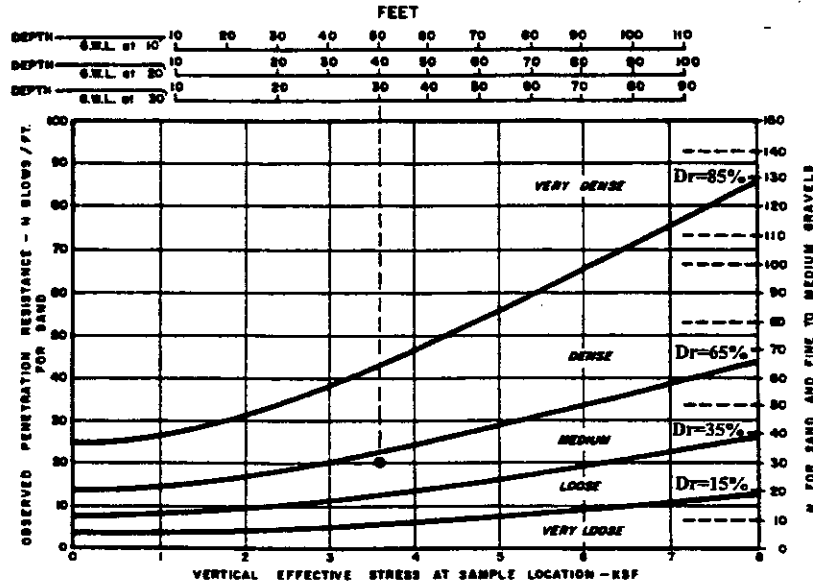


Fig. 7.11 Estimated Compactness of Sand From Standard Penetration Test (DM-7).

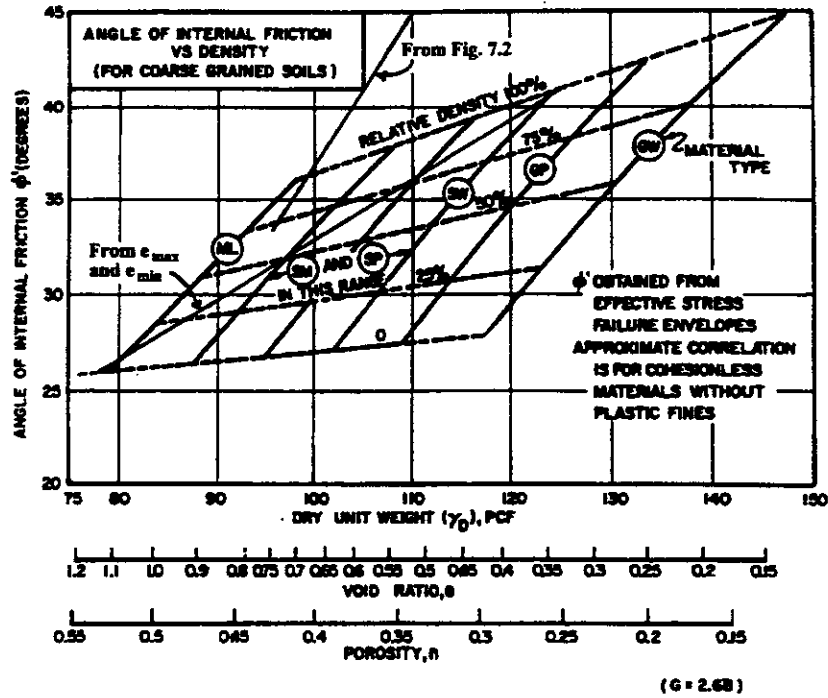


Fig. 7.12 Correlations of Strength Characteristics for Granular Soils (DM-7).

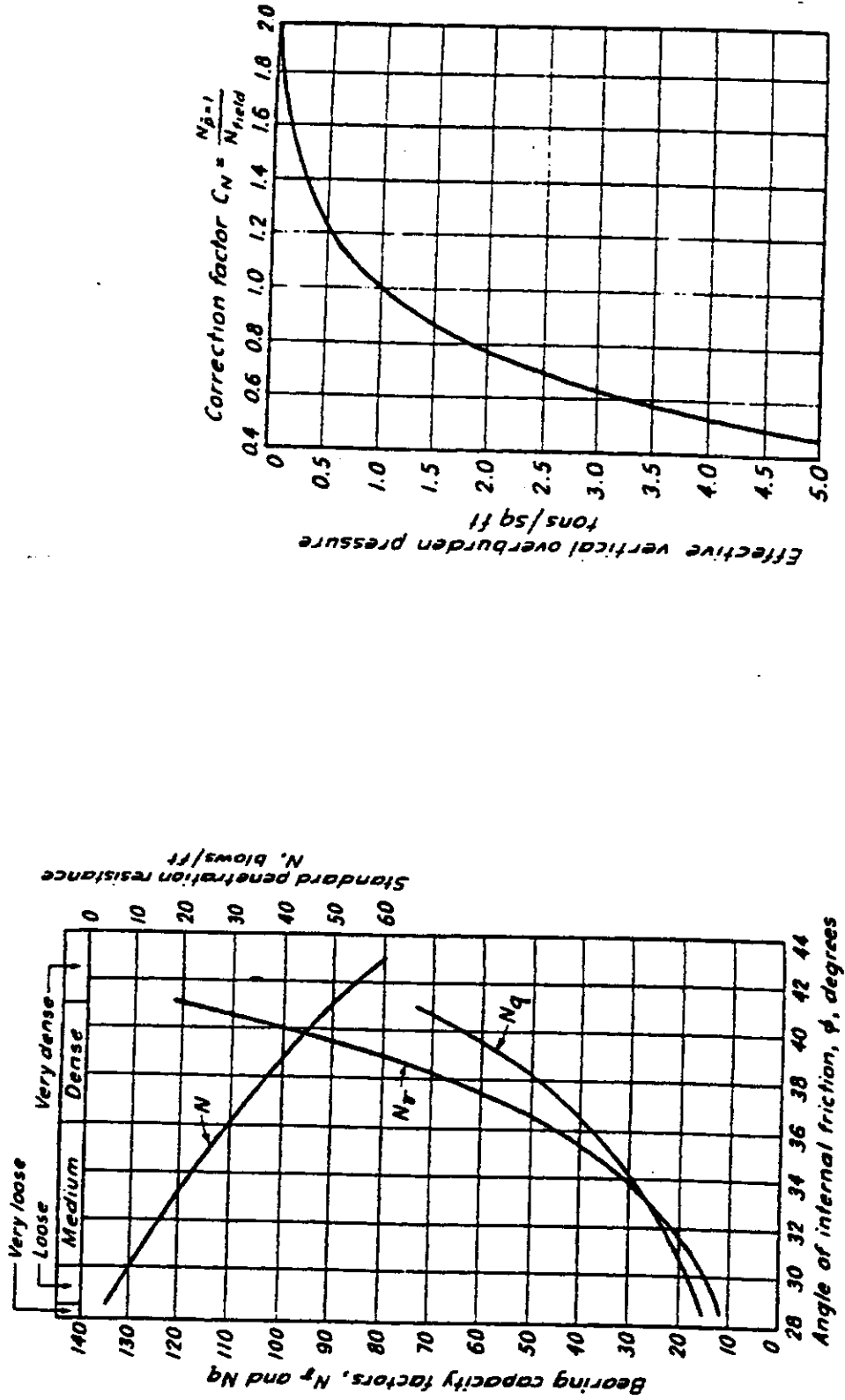


Fig. 7.13 Correlations of N Values with Sand Parameters (PH&T).

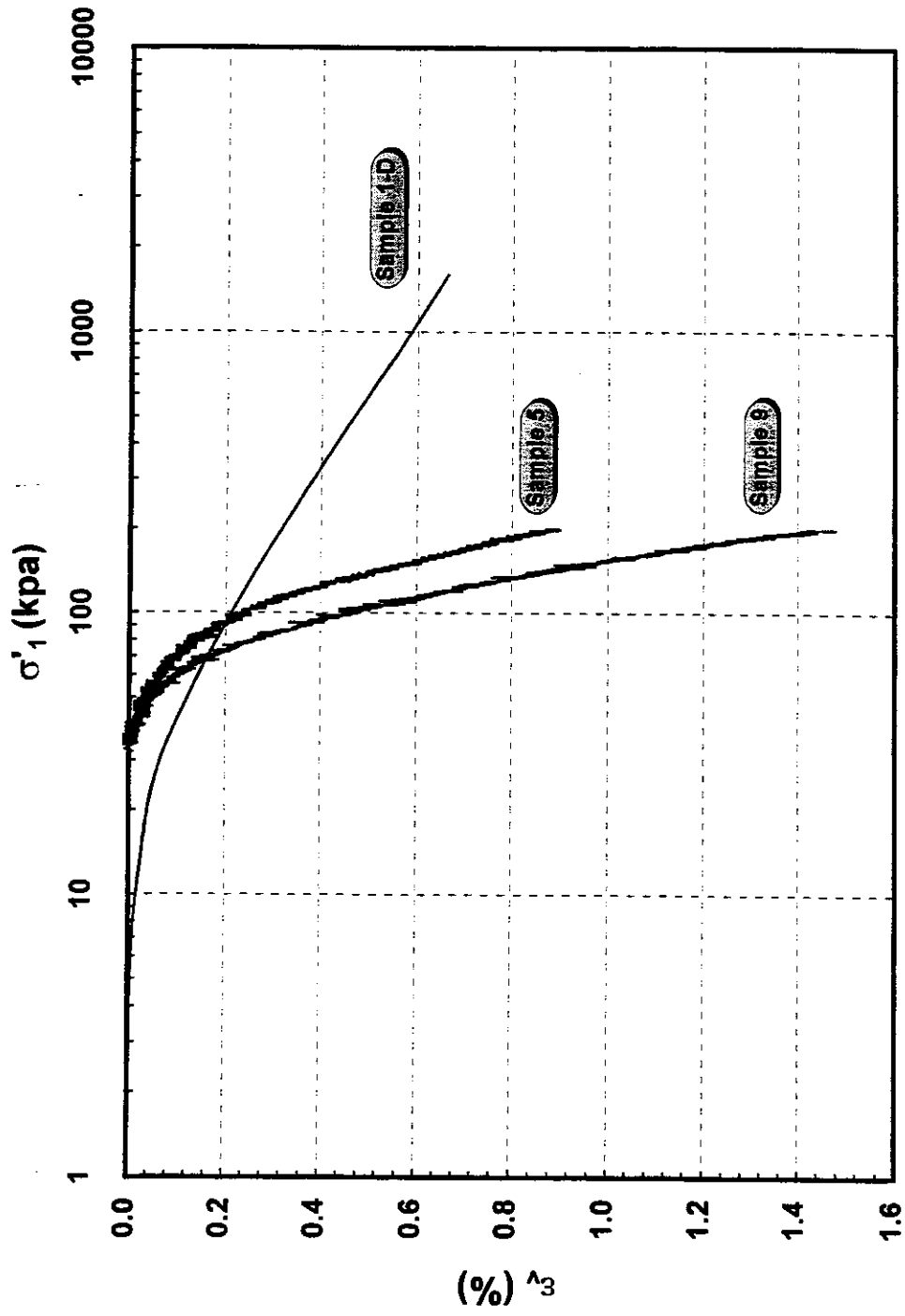


Fig. 7.14 Standard One - Dimensional and K_0 Consolidation Curves.

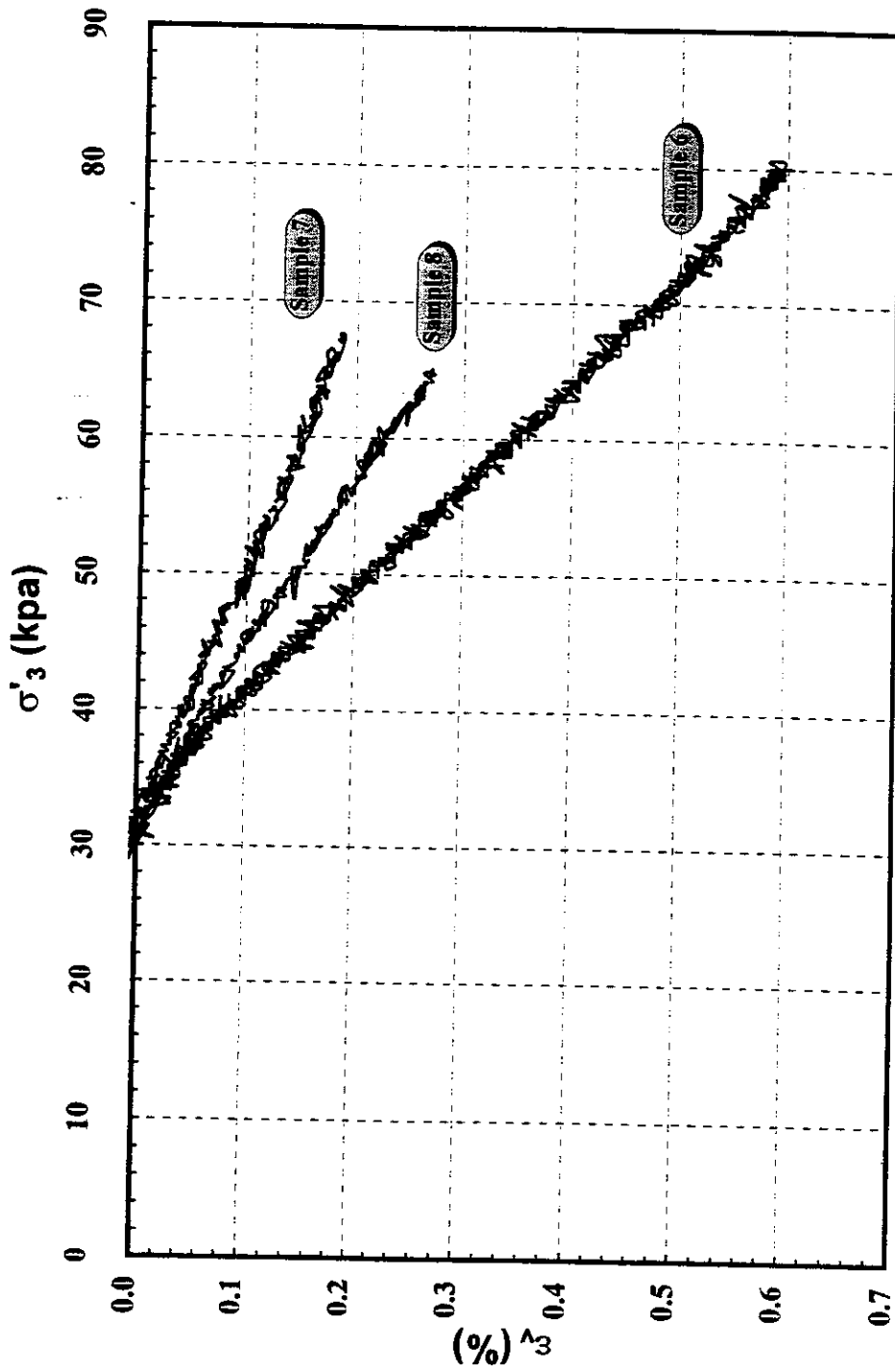


Fig. 7.15 Isotropic Consolidation Curves.

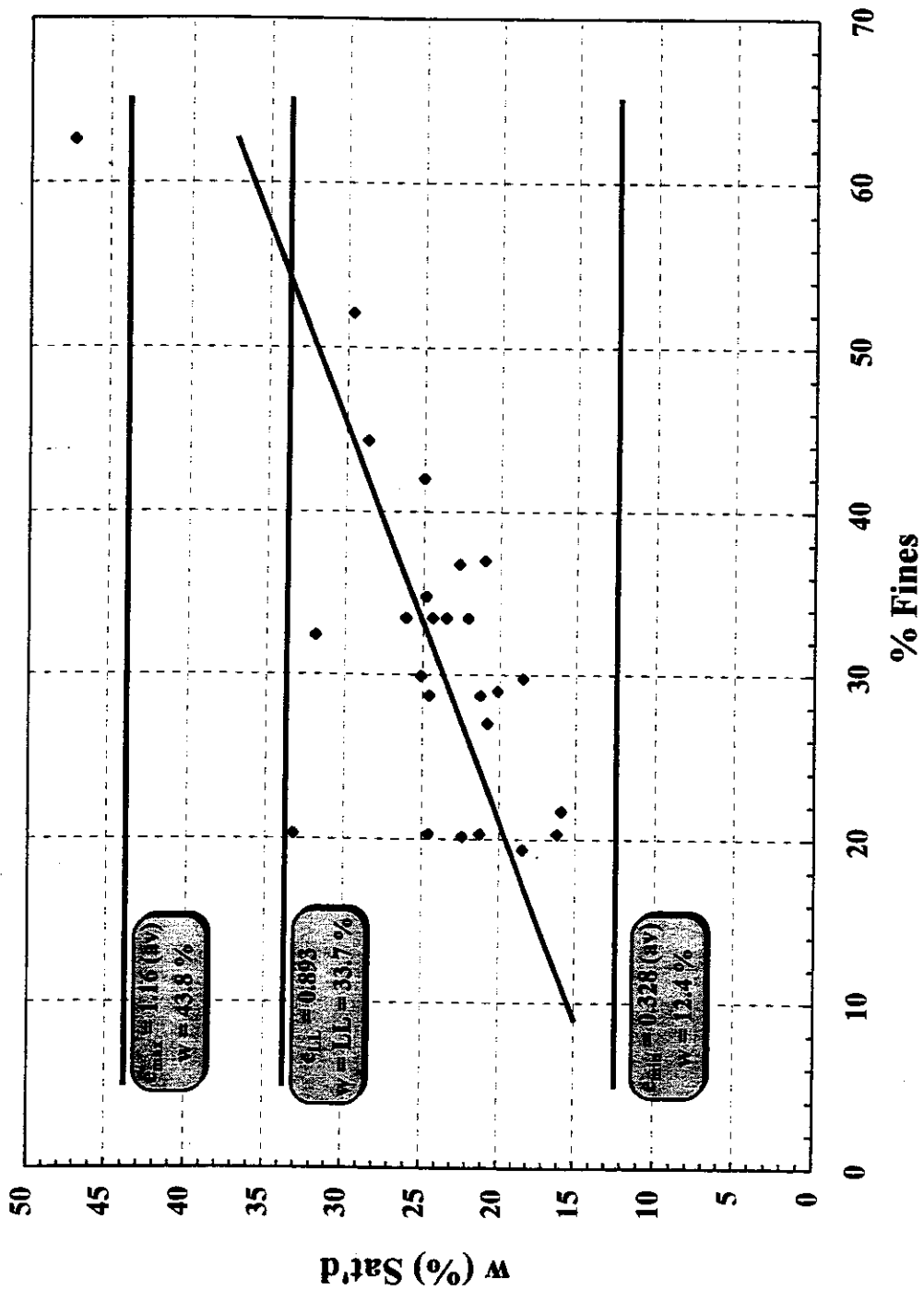


Fig. 7.16 Correlation Between Standard Water Content or Void Ratio and Percent Fines.

Chapter 8

Lab and Field Permeability Test Results

8.1. Overview

As discussed in Chapters 2 and 3, lab triaxial permeability tests (using GDS controllers across a specimen maintained at a particular stress state), CPT cone dissipations, and slug and bailing field tests were all performed in order to assess hydraulic conductivities. In addition, permeability was backcalculated from the standard consolidation test.

8.2. Lab Tests

In total, eight vertical triaxial and two horizontal triaxial test permeabilities were assessed. The vertical triaxial permeabilities were obtained under isotropic stresses, under different levels of deviatoric stress (staged σ_d loading), and for a condition of K_0 consolidation. However, after learning that there were differences in orders of magnitude in permeability from one sample to the next due to variability in the material, and only variation within a single order of magnitude as a function of stress state (isotropic consolidation, K_0 consolidation, staged σ_d loading), stress state dependency became a minor issue.

While the authors tried to account for material variability through consideration of differences in void ratio, fines content and uniformity coefficient, such attempts didn't provide any logical relationship. Table 8.1 provides a summary of order of magnitude permeabilities by sample, sample location and sample properties (e , fines and C_u) for triaxial test samples 1 - 11. Note that no permeability was assessed for sample 3 (an undrained test) or sample 12 (the stress path test). Samples 7, 8 (both at 20 % fines) and 11 (at 38 % fines) are the reconstituted samples whose permeability will be discussed in a separate section. Samples 9 and 10 are the undisturbed samples tested under horizontal flow conditions (Fig 3.1b). sample 12 is the stress path test sample whose permeability was not assessed. Also included is the standard consolidation test sample where permeability was back calculated from time rate of consolidation (C_v) readings.

Permeabilities are separated as vertical and horizontal. Field test results are also listed in Table 8.1 for the sake of comparison. Note that field bailing and slug tests are listed as providing horizontal permeability and the CPT dissipations as mixed. The field values reflect different effective lengths (2 and 4 ft. for the wells used in the slug tests and 10 ft. for the bailing test). Discussion of the field tests follows in the next section.

Most discouraging were the results from triaxial test samples 5, 6, 9, and 10 which were from 9.5 ft. and 10.5 ft. depth at Pz2 location, i.e. two with a common

trimmed end at 9.5 ft. (one above, one below 9.5 ft.) and the other two with a common end at 10.5 ft. They show some variation in void ratio and fines content (even percent fines in the upper versus the lower half of the same sample) but there are two orders of magnitude difference in permeability. What is worse, one might even expect such difference by direction due to layering (horizontal greater than vertical), but not that difference in the same direction (10^{-5} versus 10^{-7} cm/sec horizontally) and certainly not with the sample with the lower percent fines (though it does have a lower void ratio) yielding the lower permeability (by two orders of magnitude).

There is no clear pattern to the undisturbed lab test sample values. To add further insult, the one standard consolidation test (sample 1-D) yielded the lowest permeability (10^{-9} cm/sec). Given the dependency of permeability ($k = C_v \frac{a_v}{1 + e_o} \gamma_w$) upon the coefficient of consolidation (C_v) and the compressibility ($a_v = \frac{C_c}{2.3\bar{\sigma}}$), the low value of k obtained was most affected by C_c . But the one order of magnitude difference in C_c of the consolidation curves of samples 5 and 6 versus sample 1-D (the standard consolidation test) would not account for the three to four orders of magnitude difference in vertical permeability between 5 and 6 versus 1-D. Therefore a second standard consolidation test on an undisturbed sample from a 9.5 ft. depth at Pz2 was undertaken. This sample was obtained from

a separate NDOT sampling operation on 9/11/96, one year after the completion of piezometer readings. It has been held for just such an emergency. See Appendix 10 for the boring log. Note that SPT blow counts were obtained (with equalized water levels) immediately above and below the Shelby tube sample. Such N values agree very well with N values at Pz3 location (unequal water levels) prior to construction of the fill.

8.3. Field Tests

The difficulty in assessing a meaningful in situ permeability at the Zolezzi Lane site relates to the level of facies changes that occur laterally and the structuring that occurs vertically in this alluvial deposit. Cone penetration dissipation reflect in situ permeability as assessed very locally around the piezocone tip and using the Roberston and Campenella (1984) correlations yielded a lower estimate of permeability (10^{-7} cm/sec). Part of this phenomena is likely the distortion and smearing of the very thin horizontal seams/partings due to cone insertion and the consequent restriction in flow this might have caused.

Most faith should be placed in the bailing and slug tests because they reflect the response of a larger volume of material. Even so, there is variability over the larger volume as shown for instance in Fig 8.1 which is an attempt to delineate differences based on the CPT logs which used sensor readings to reflect switches

from cohesionless to "silt-clay" soils. While such soil classifications were not born out in the lab, they still reflect a variation of the (same) material that may be worth characterizing. As shown, the two and the four foot effective lengths of the slug test wells have a center (10 ft. depth) in the same material but the longer effective length has ends in the more permeable material (cohesionless versus the shaded finer grained soil according to the CPT logs). Even so, the permeability of the shorter length section in supposedly finer grained material was greater, not less than that of the other.

The authors fully recognized that bedding can play a significant role in permeability results. Usually horizontal permeability is much less affected by the presence of relatively thin impervious partings than vertical permeability as discussed in Chapter 3. Some attempt was made to account for this by assessing differences in percent fines of the upper and lower halves of the triaxial test specimens. However, what the authors did not expect was the presence and random orientation of root holes or micropores in samples at 10 ft. depth. Such open root holes/micropores were only noticed upon oven or air drying the failed or discarded lab test samples. While the soil survey indicated the presence of such micropores, the authors had assumed that they would be restricted to the upper organic mat, or at most to the 5 ft. depth of the soil survey report, but not to 10 ft. and possibly greater depth.

Table 7.2 Data from Triaxial Tests for Strength

Sample No.	Location / Depth	Void Ratio (e)	Percent Fines	Consolidation Pressure (kPa)	ϕ (°)	Comments D (drained) U (undrained)
1	Pz3 at 6 ft.	--	20	45	--	Sheared (D) in 20 kPa stages to 100 kPa. Vertical permeability evaluated at each stage. Not failed.
2	Pz3 at 8 ft.	0.496	19	60	46.5	Sheared (D) in 20 kPa stages to 140 kPa. Vertical permeability evaluated at each stage. Unloaded to $\sigma_d = 0$, then sheared (D) to failure.
3	Pz3 at 3 ft.	0.746	32	60	33.4	Sheared to failure (U).
4	Pz5 at 3 ft.	0.642	31/65 (48 av)	65	42.5	Sheared (D) in 20 kPa stages to 120 kPa. Vertical permeability evaluated at each stage. Then sheared (D) to failure from $\sigma_d = 120$ kPa.
5	Pz2 at 10.5 ft.	0.661	32/29 (30 av)	77	40.5	Vertical permeability evaluated at 30 kPa forming pressure. K_o consolidated to $\sigma_3 = 77$ kPa. Vertical permeability evaluated, then sheared (D) to failure.

Table 7.2 Data from Triaxial Tests for Strength (Cont'd)

Sample No.	Location / Depth	Void Ratio (e)	Percent Fines	Consolidation Pressure (kPa)	ϕ (°)	Comments D (drained) U (undrained)
6	Pz2 at 10.5 ft.	0.585	65/26 (45 av)	80	40.7	Vertical permeability evaluated at 30 kPa forming pressure. Anisotropically consolidated to $\sigma_3 = 80 / \sigma_d = 20$. Vertical permeability evaluated, then sheared (D) to failure.
7	Reconstituted	0.56	20	30/65/30	43.6	Isotropic permeability assessed vertically at 30 kPa forming pressure, at 65 kPa isotropic consolidation pressure and at 30 kPa rebounded consolidation pressure. Then sheared (D) to failure.
8	Reconstituted	0.56	20	30/65/30	39.6	Isotropic permeability assessed vertically at 30 kPa forming pressure, at 65 kPa isotropic consolidation pressure and at 30 kPa rebounded consolidation pressure. Then sheared (U) to failure.

Table 7.2 Data from Triaxial Tests for Strength (Cont'd)

Sample No.	Location / Depth	Void Ratio (e)	Percent Fines	Consolidation Pressure (kPa)	ϕ (°)	Comments D (drained) U (undrained)
9	Pz2 at 9.5 ft.	0.577	36/56 (46 av)	59	--	Horizontal permeability evaluated at 30 kPa forming pressure. K_o consolidated to $\sigma_3 = 59$ kPa and horizontal permeability evaluated. Sample not failed.
10	Pz2 at 9.5 ft.	0.524	26/27 (26 av)	30	--	Horizontal permeability evaluated at 30 kPa forming pressure, then house air failed and sample collapsed.
11	Reconstituted	0.605	37	30	--	Isotropic permeability assessed vertically at 30 kPa forming pressure. Data during (U) shear failure mistakenly not recorded.
12	Pz2 at 10 ft.	0.654	36	70	41.6°	Stress path test described in Chapter 9.
1-D	Pz3 at 7 ft.	0.637				Standard consolidation test sample used for comparison with K_o consolidation phases of samples 5 and 9

Table 7.3 Correlations From SPT Blow Counts

Piez. No.	Depth (ft.)	N	σ_{v0} (psf)	PH&T				DM-7		
				C_N	N_1	D_r (%)	ϕ (°)	D_r (%)	ϕ (°)**	γ_d (pcf)
Pz3	4 - 5.5	8	538	1.5	12	37	30.5	35	30.5 - 31.5	95 - 108
	8.5 - 10	12	828	1.3	16	45	32	50	32 - 33.5	97 - 112
	13.5 - 15	11	1022	1.2	13	40	31	50	32 - 33.5	97 - 112
Pz4	6 - 7.5	6	497	1.5	9	30	29.5	25	29 - 30	92 - 106
	11 - 12.5	12	785	1.3	16	45	32	50	32 - 33.5	97 - 112
	18 - 19	12	1219	1.17	14	42	31.5	50	32 - 33.5	97 - 112
	19 - 19.5	22	1219	1.17	26	60	35	65 *	33.5 - 36	100 - 115
Pz5	4 - 5.5	6	567	1.45	9	30	29.5	25	29 - 30	92 - 106
	9 - 10.5	11	826	1.3	14	42	31.5	50	32 - 33.5	97 - 112
	16 - 17	12	1042	1.2	19	55	34	55	32.5 - 34	98 - 113
	17 - 17.5	26	1042	1.2	31	67	36.5	70 *	34 - 36.5	100 - 116

* Used right side axis of Fig 7.11 for sand with fine to medium gravel

** Lower limit of SM; range in Fig 7.12 would be less if ML limit used

Table 7.4 Comparison of SPT and CPT, D_r and ϕ

Range of Depth (ft.)	SPT			CPT ***		
	N (N_1)	D_r (%)	ϕ (°)	Equivalent N*	D_r ** (%)	ϕ (°)**
4 - 7.5	6 - 8 (9 - 12)	25 - 37	29 - 31.5	7 - 22	50 - 80	40 - 46
8.5 - 15	11 - 12 (13 - 16)	40 - 50	31 - 33.5	5 - 21	40 - 80	38 - 44
16 - 19.5	12 - 26 (14 - 31)	65 - 70	32 - 36.5	11 - 33	50 - 80	40 - 44

* All blow counts, i.e. cohesionless and silt-clay

** Only for soil considered cohesionless

*** Only for Pz3, 4, 5 not 6

Table 7.5 Comparison of Range in D_r from CPT, SPT and Lab Void Ratio

Piezometer No.	Depth (ft.)	CPT *	SPT	Lab Void Ratios
Pz3	1.5 to 10.2	40 to 70 %	35 to 50 %	80 to 89 %
Pz4	7 to 22	50 to 90 %	25 to 65 %	61 to 69 %
Pz5	3.5 to 10.5	50 to 70 %	25 to 70 %	56 to 69 %

* Only from cohesionless materials

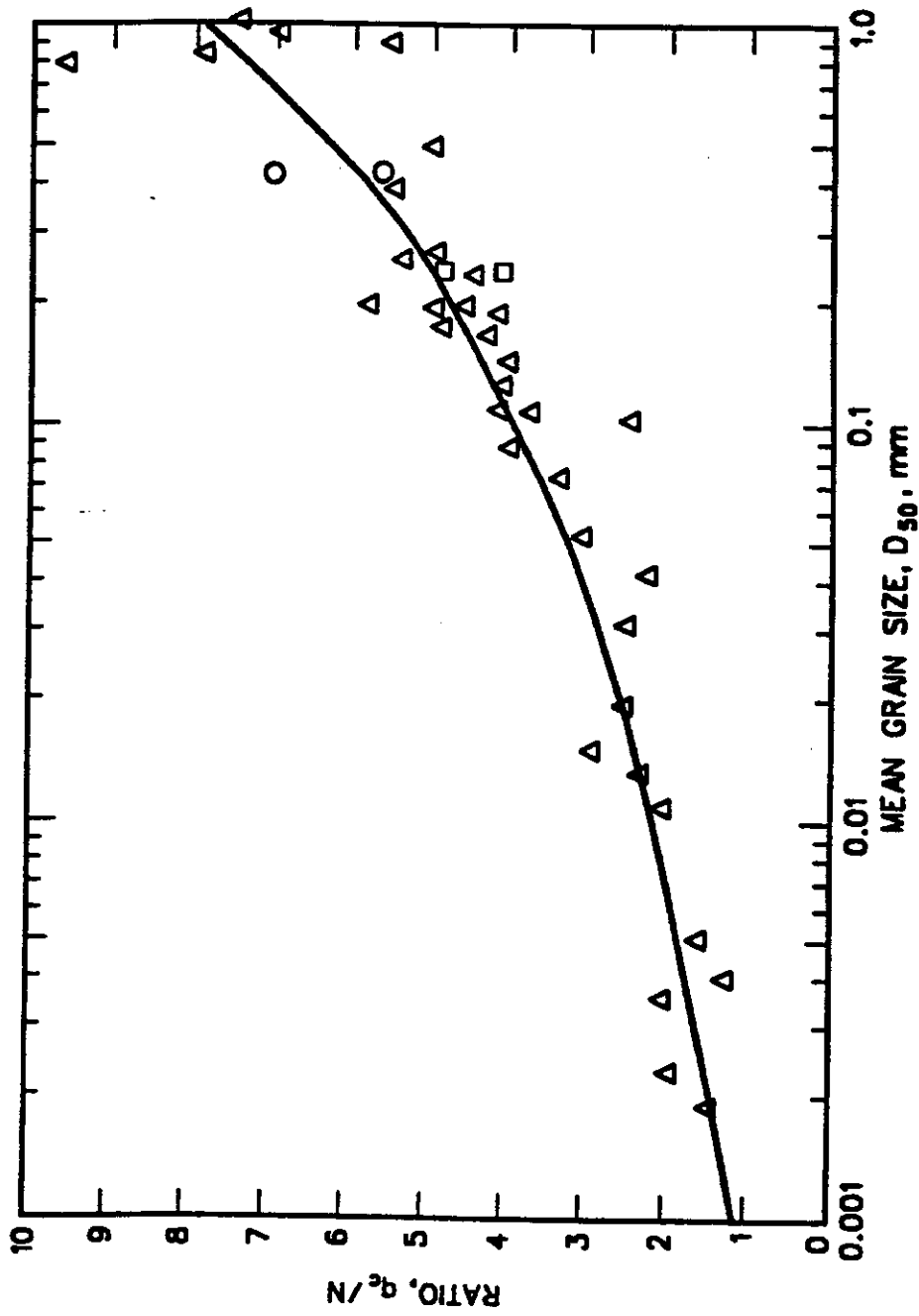


Fig. 7.1 Correlation Between Grain Size and Ratio of Cone Bearing and Standard Penetration Test Resistance (after Robertson and Campanella, 1983).

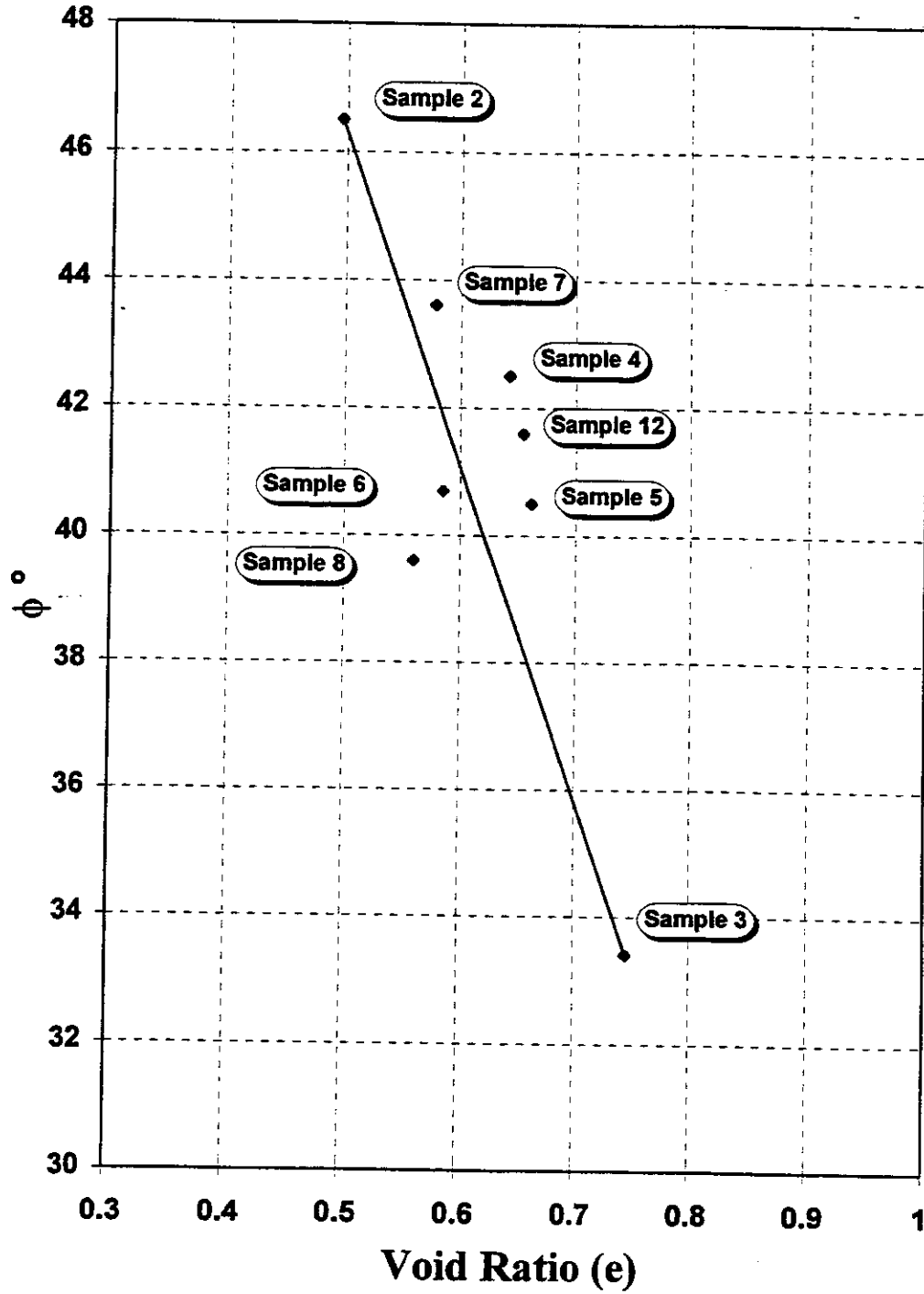


Fig 7.2 Correlation Between Drained or Effective Stress Friction Angle from Standard Triaxial Tests and Void Ratio.

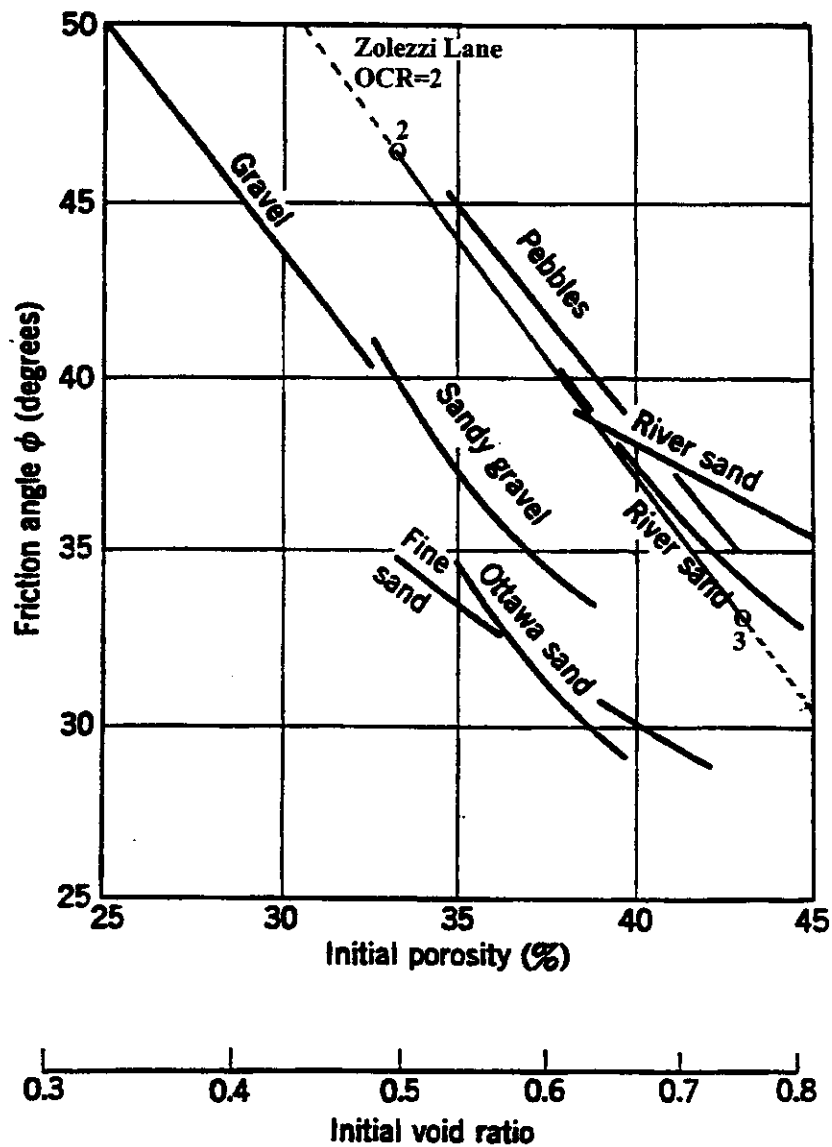


Fig 7.3 Friction Angle Versus Void Ratio for Several Granular Soils from Lambe and Whitman (1969) with Superposed Fig. 7.2 Results.

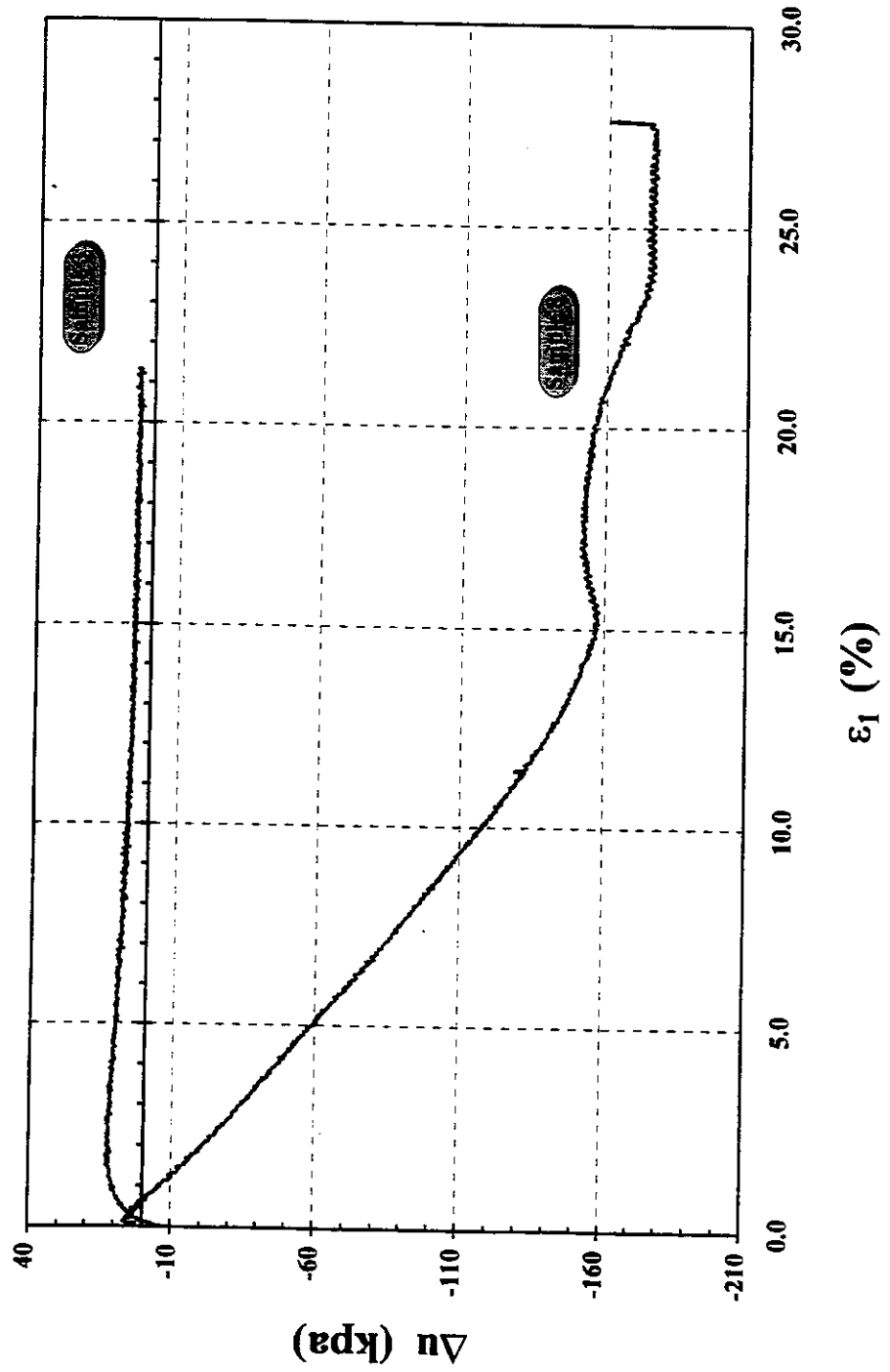


Fig 7.4 Pore Pressure Curves for Undrained Tests

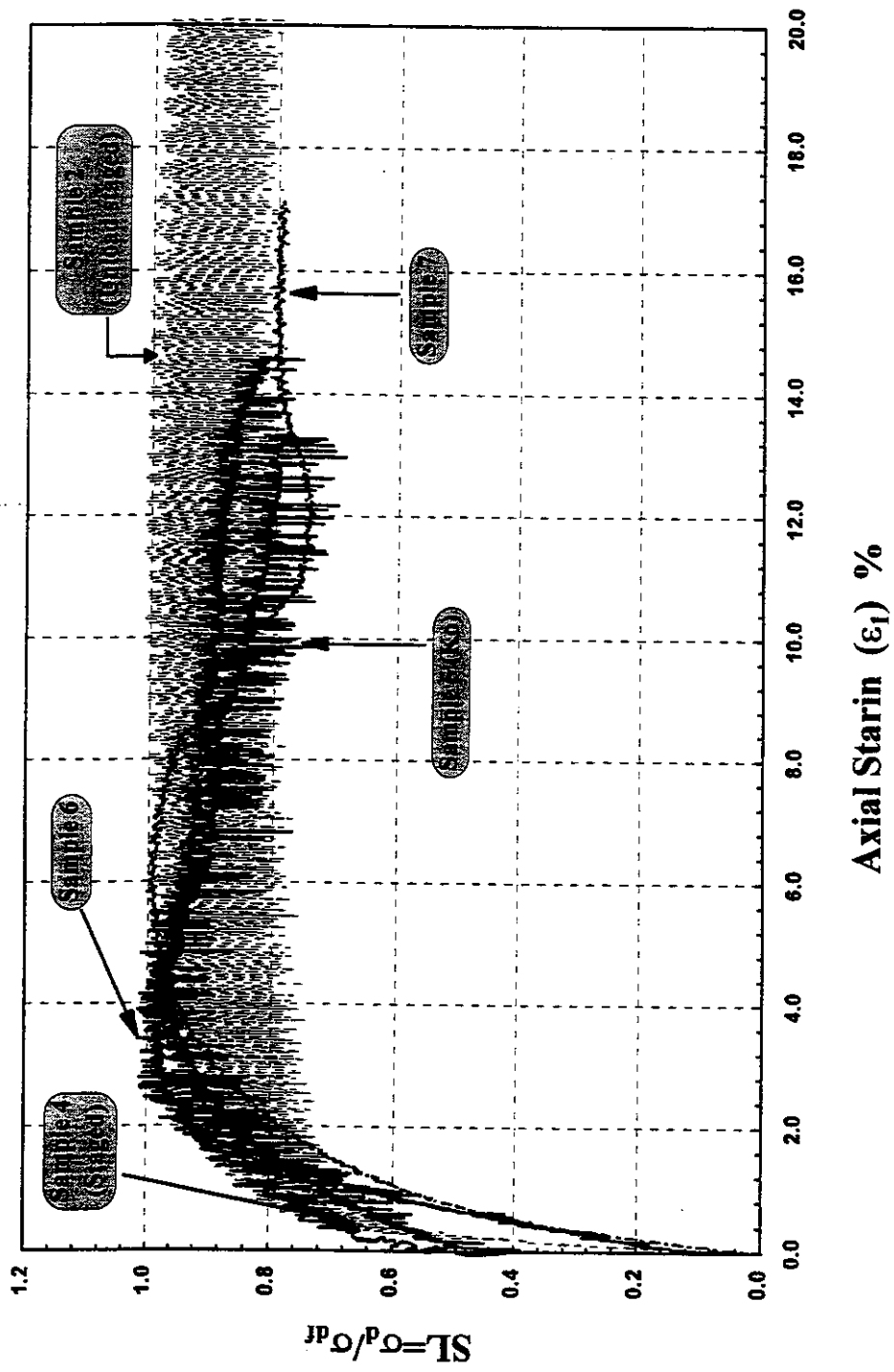


Fig. 7.5 Normalized Stress Versus Strain Curves.

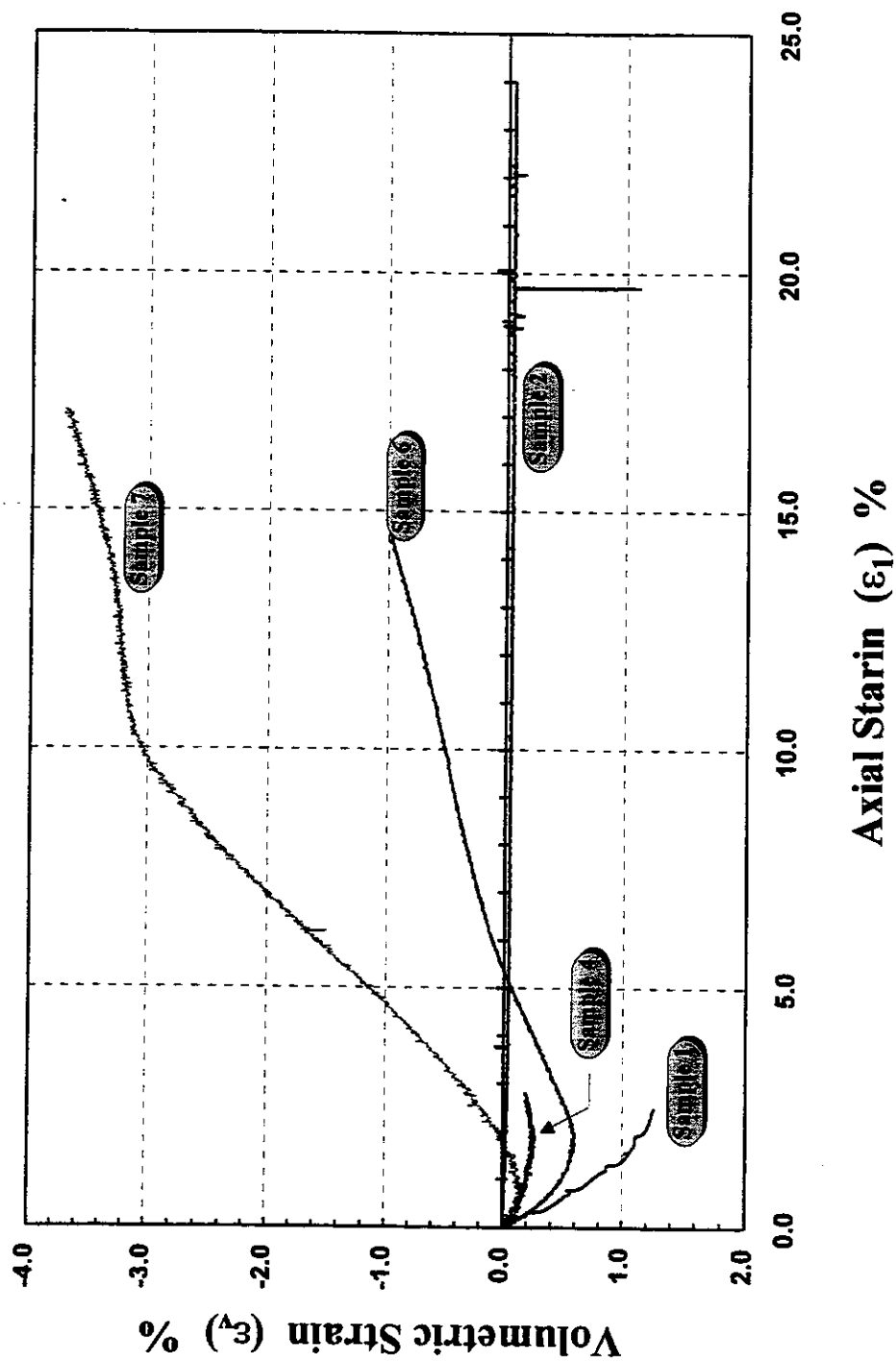


Fig. 7.6 Drained Volume Change Curves.

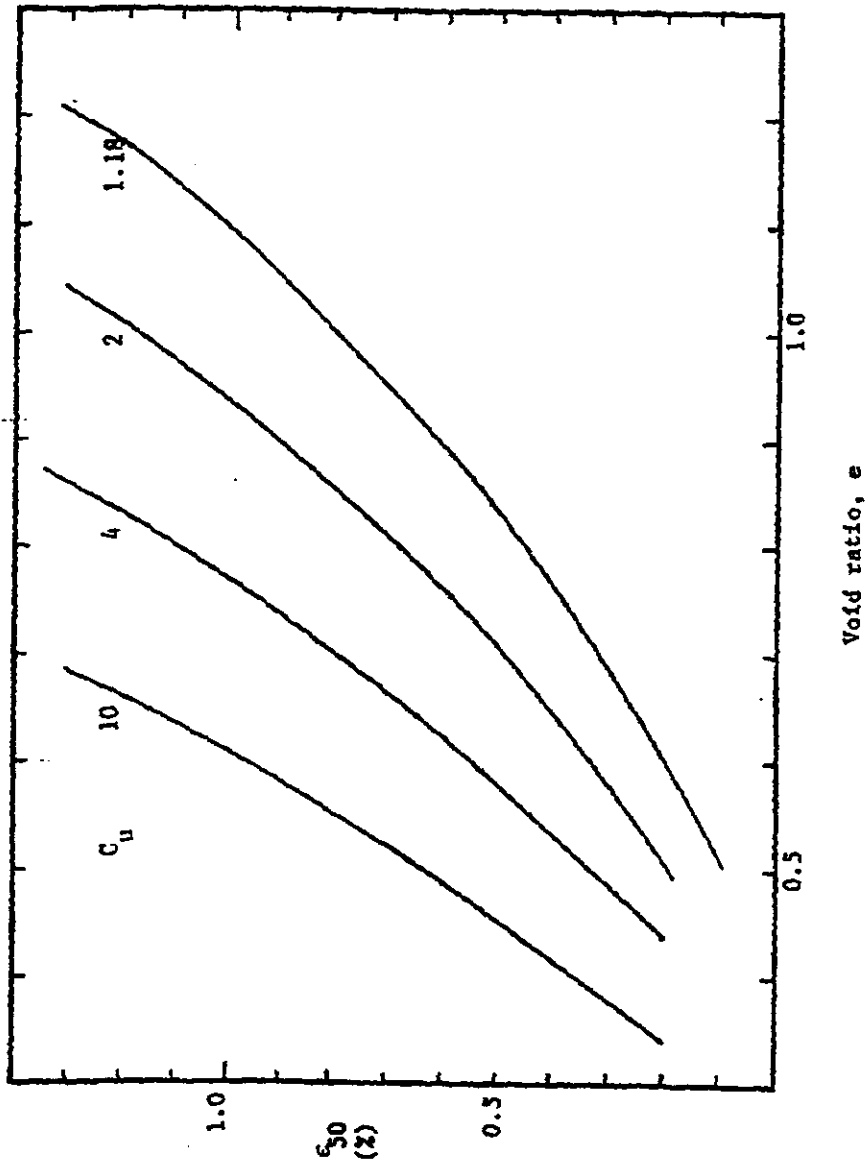


Fig. 7.7 Estimation of ϵ_{50} as a Function of e and C_u .

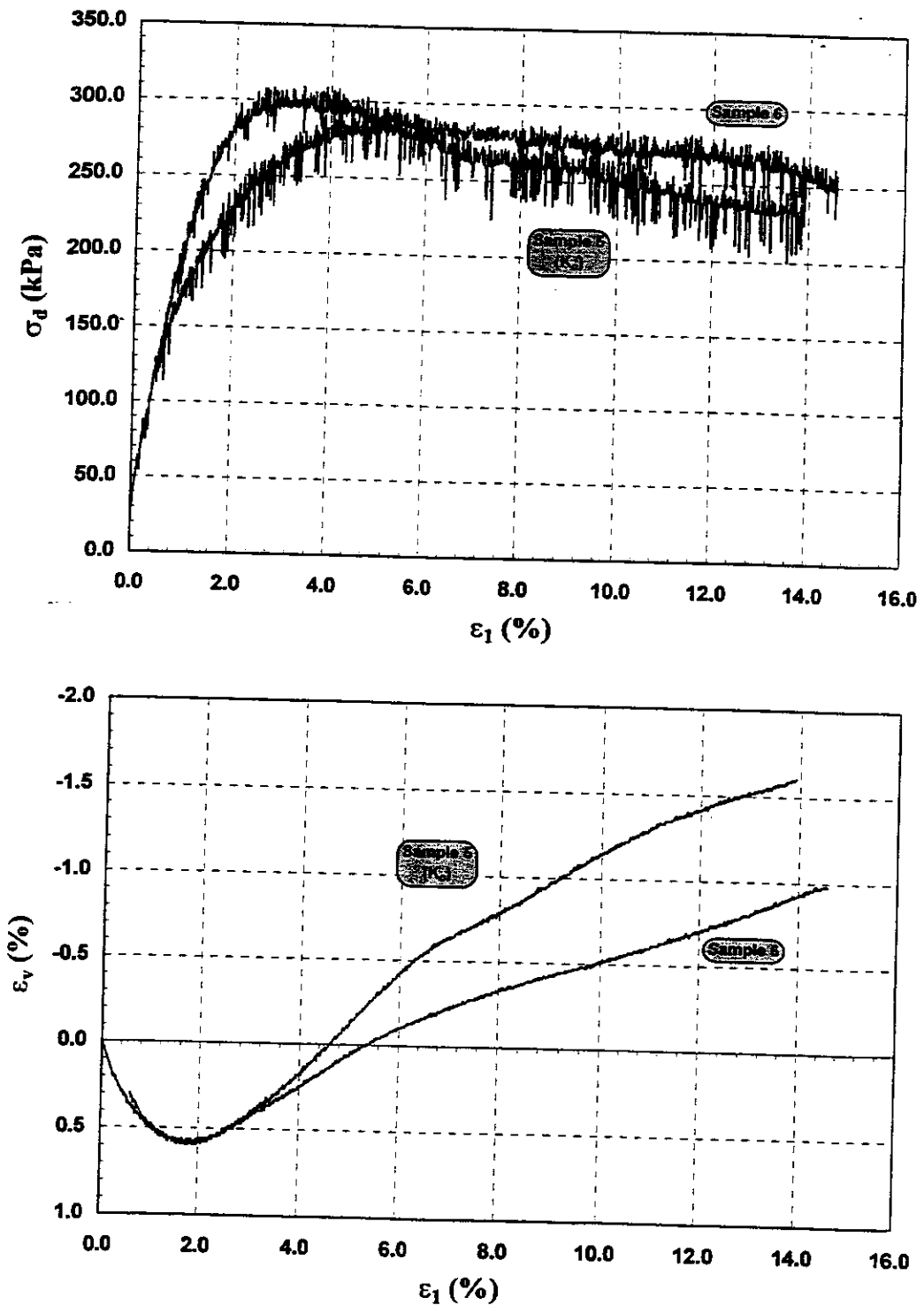


Fig. 7.8 Comparison of Standard Test and K_0 Consolidated Test Shear Response.

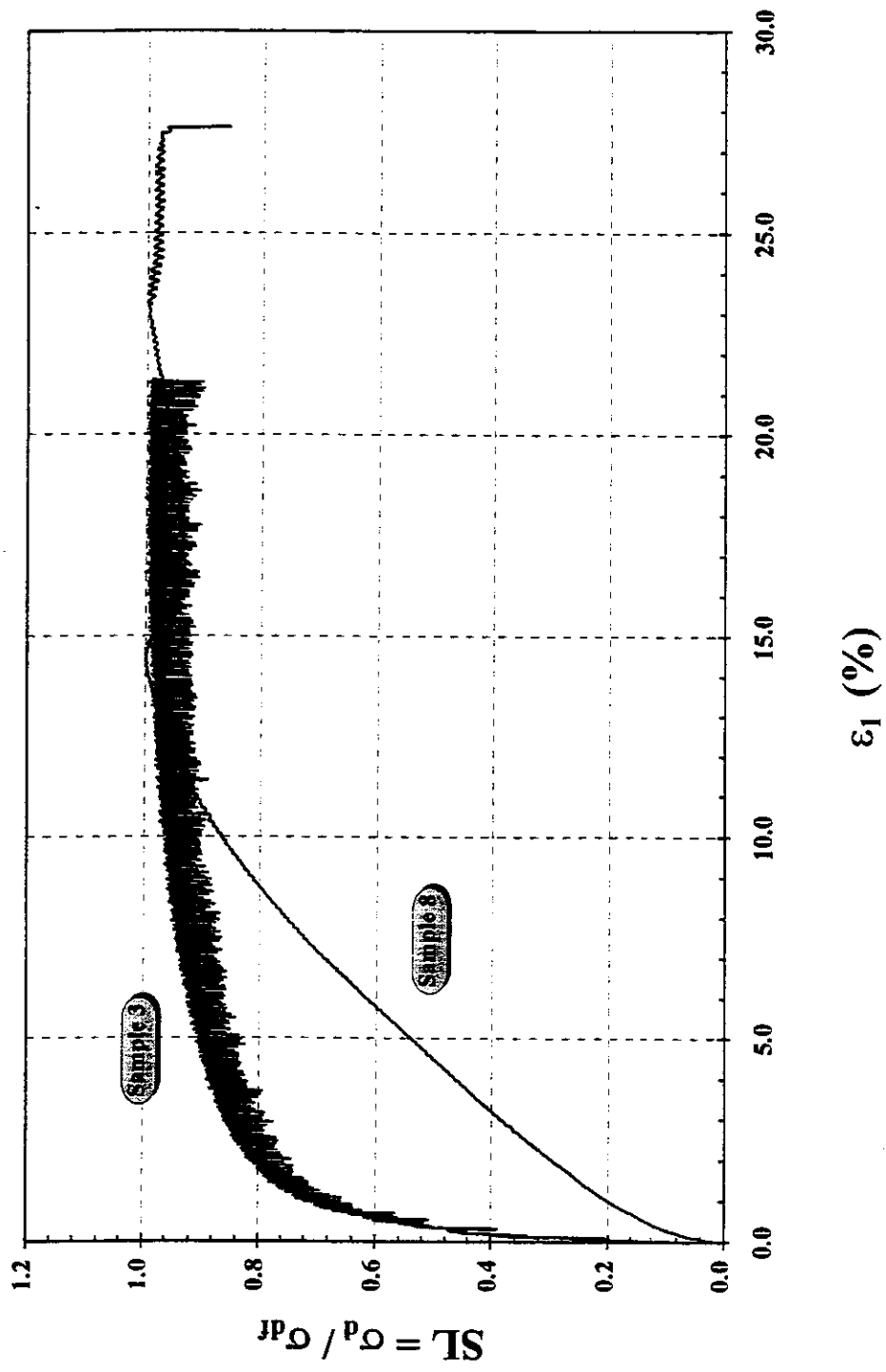


Fig. 7.9 Undrained Test Stress-Strain Curves.

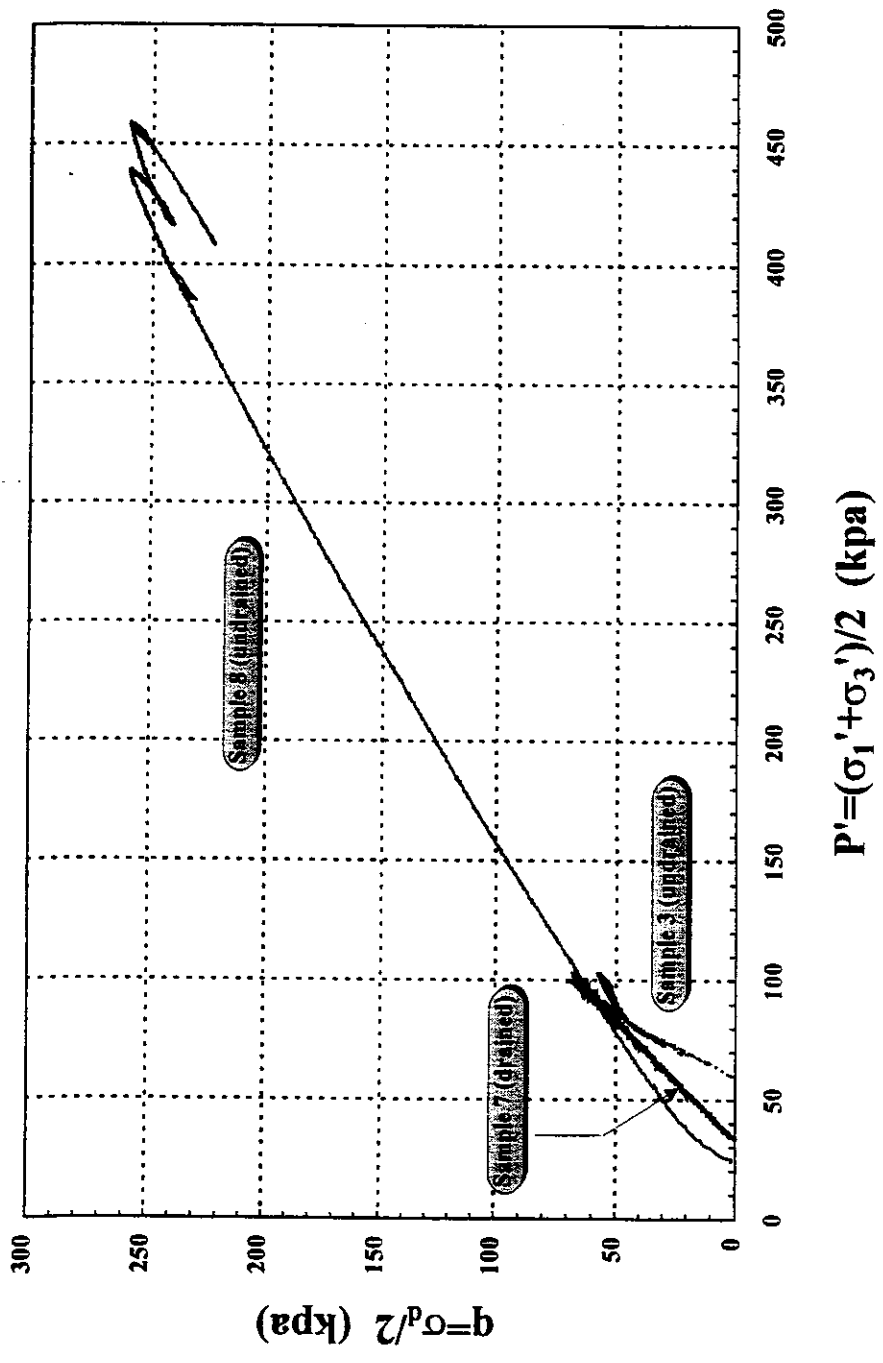


Fig. 7.10 Drained and Undrained Effective Stress Paths for the Reconstituted Samples 7 and 8.

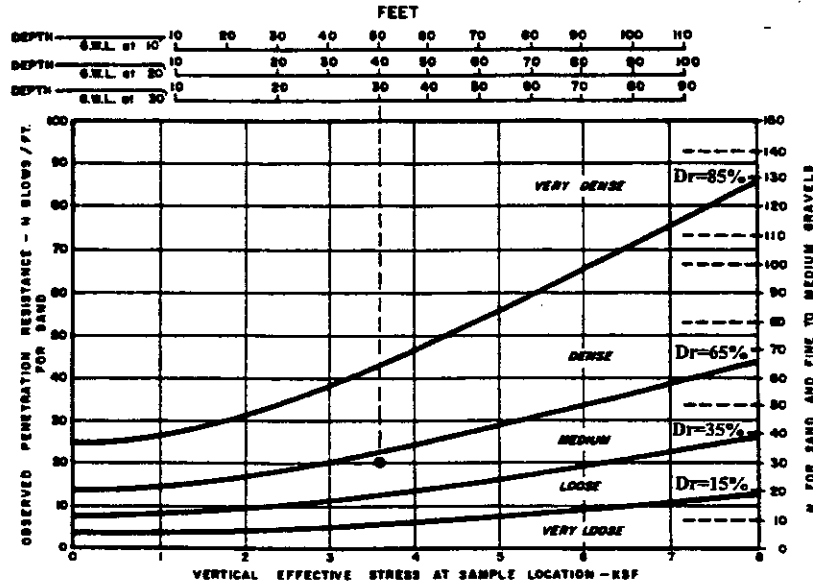


Fig. 7.11 Estimated Compactness of Sand From Standard Penetration Test (DM-7).

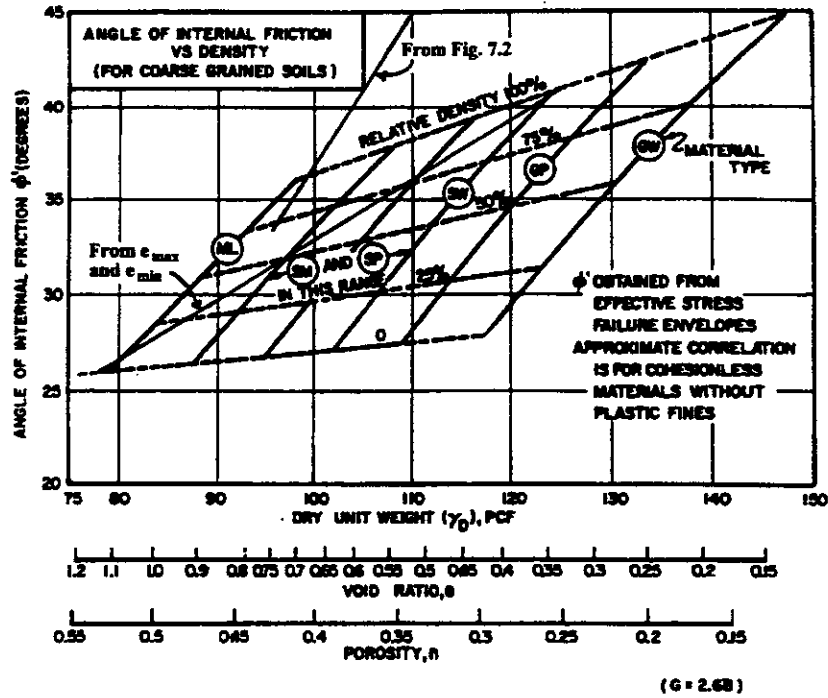


Fig. 7.12 Correlations of Strength Characteristics for Granular Soils (DM-7).

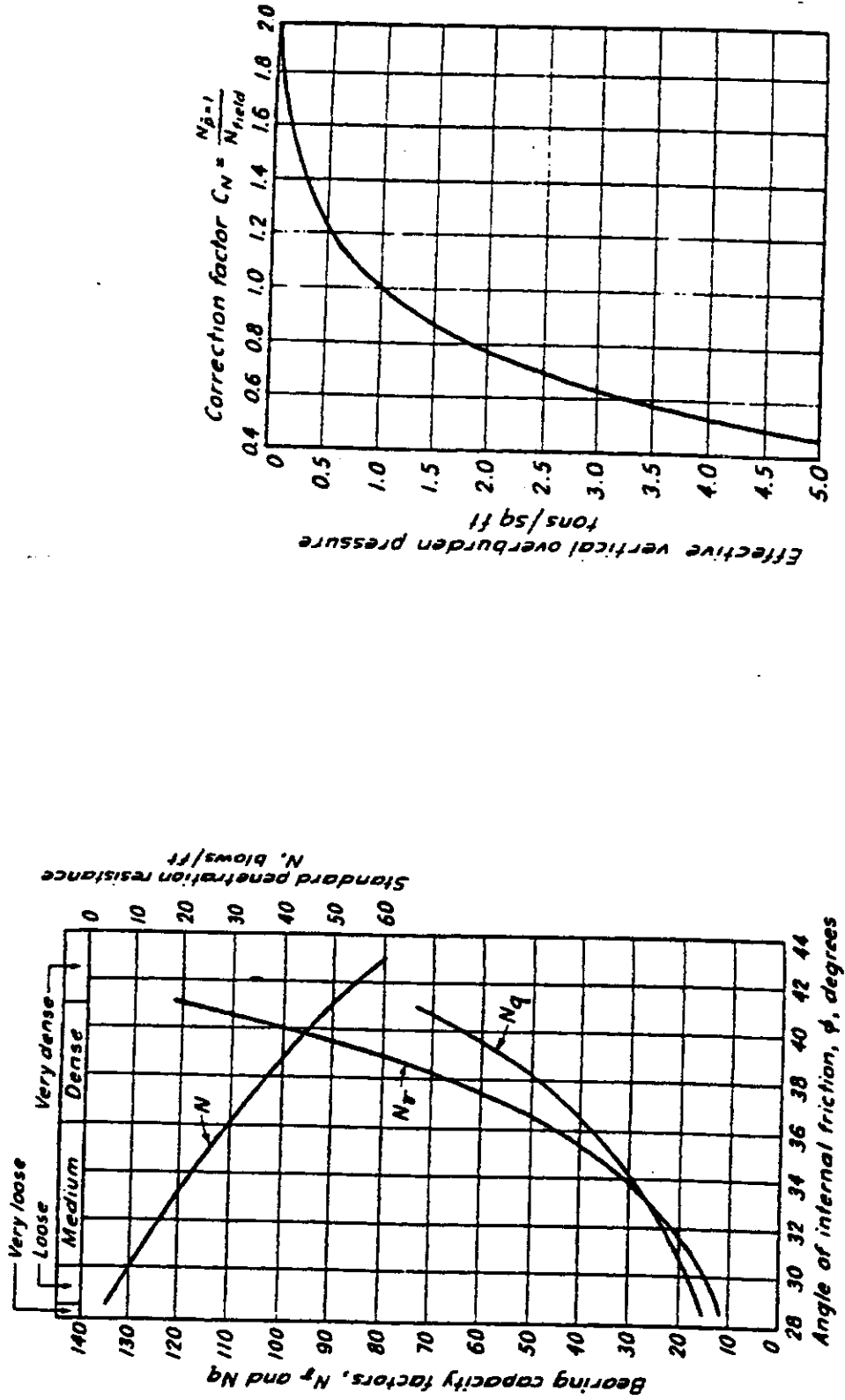


Fig. 7.13 Correlations of N Values with Sand Parameters (PH&T).

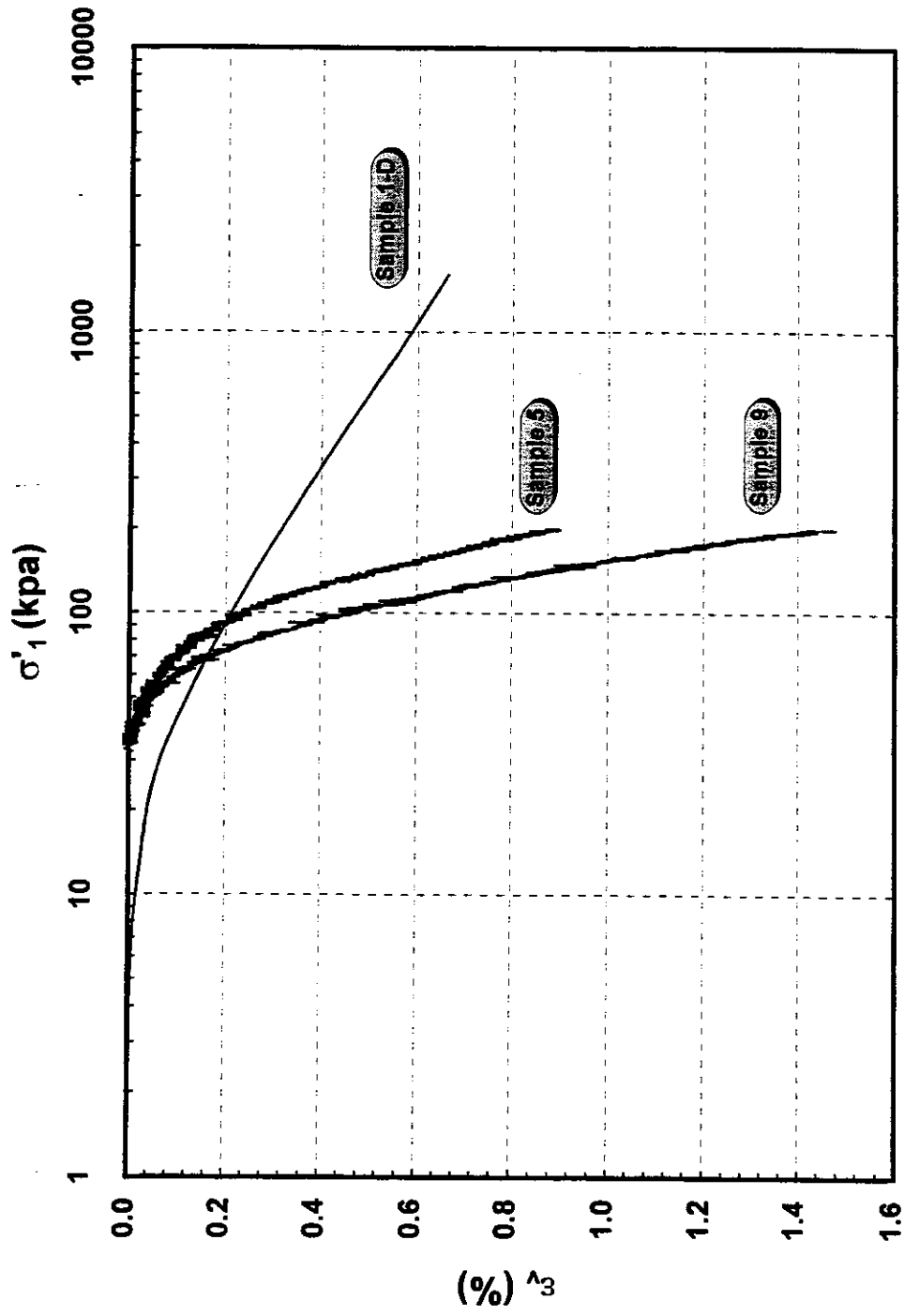


Fig. 7.14 Standard One - Dimensional and K_0 Consolidation Curves.

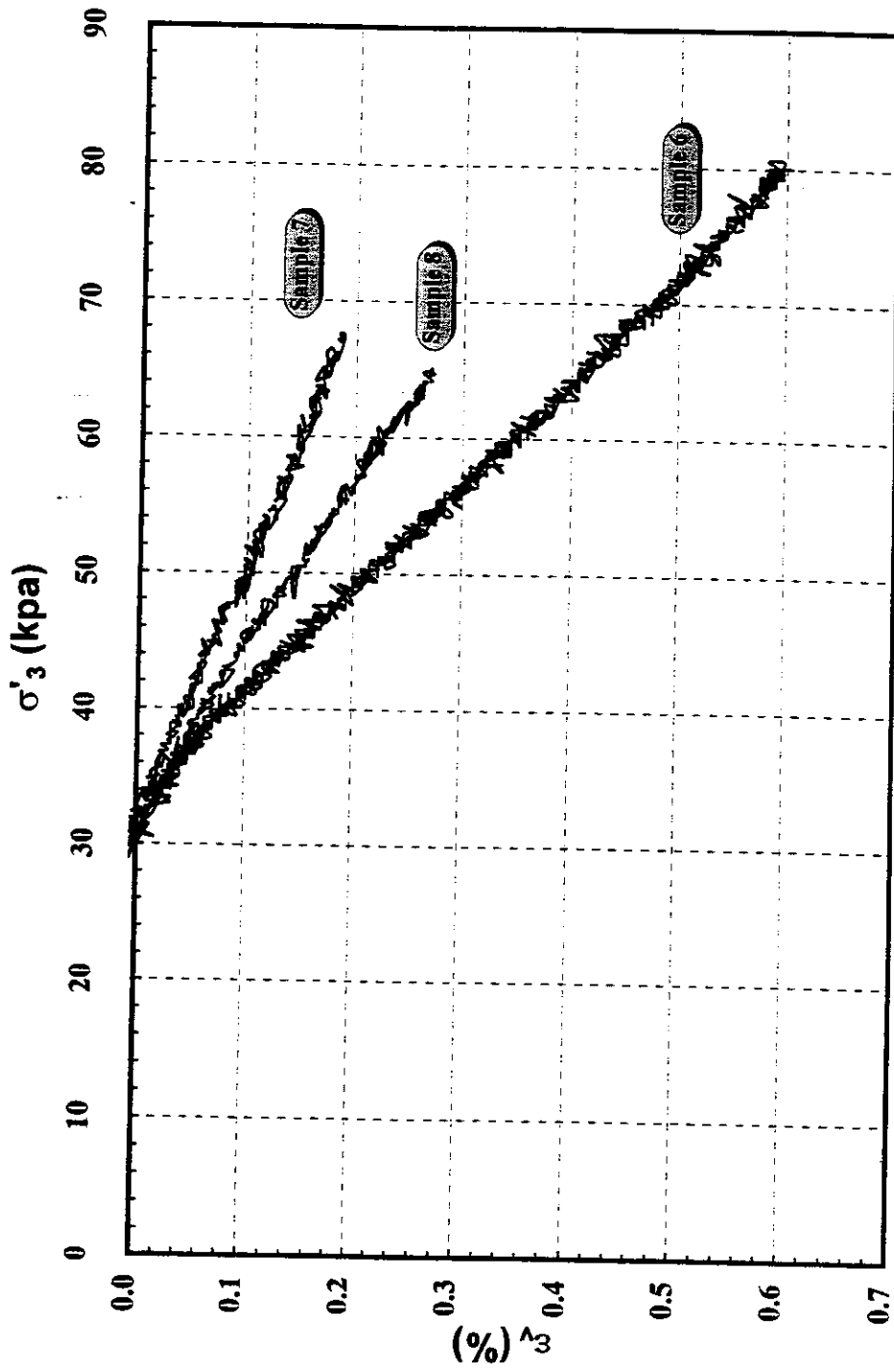


Fig. 7.15 Isotropic Consolidation Curves.

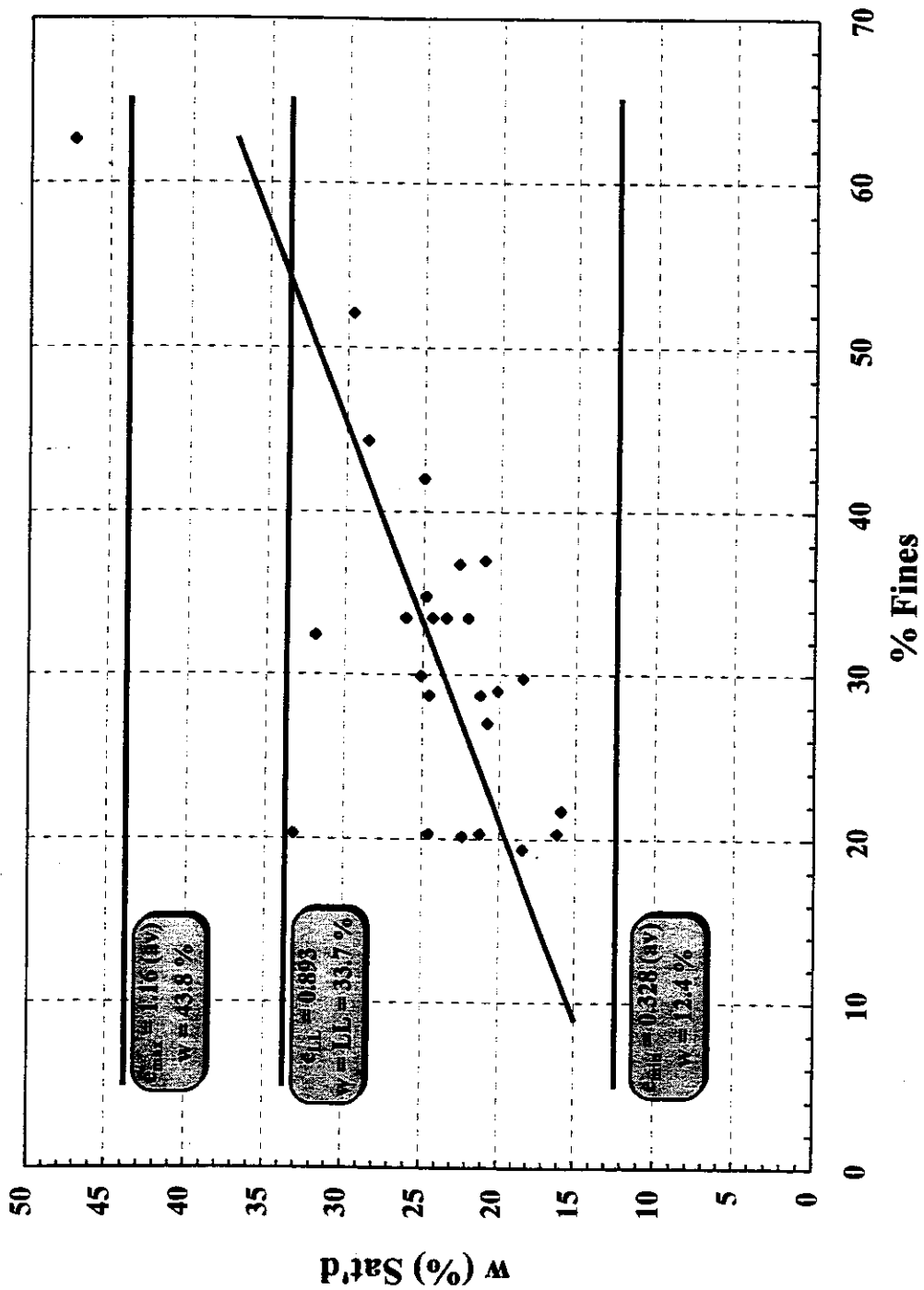


Fig. 7.16 Correlation Between Standard Water Content or Void Ratio and Percent Fines.

Chapter 8

Lab and Field Permeability Test Results

8.1. Overview

As discussed in Chapters 2 and 3, lab triaxial permeability tests (using GDS controllers across a specimen maintained at a particular stress state), CPT cone dissipations, and slug and bailing field tests were all performed in order to assess hydraulic conductivities. In addition, permeability was backcalculated from the standard consolidation test.

8.2. Lab Tests

In total, eight vertical triaxial and two horizontal triaxial test permeabilities were assessed. The vertical triaxial permeabilities were obtained under isotropic stresses, under different levels of deviatoric stress (staged σ_d loading), and for a condition of K_0 consolidation. However, after learning that there were differences in orders of magnitude in permeability from one sample to the next due to variability in the material, and only variation within a single order of magnitude as a function of stress state (isotropic consolidation, K_0 consolidation, staged σ_d loading), stress state dependency became a minor issue.

While the authors tried to account for material variability through consideration of differences in void ratio, fines content and uniformity coefficient, such attempts didn't provide any logical relationship. Table 8.1 provides a summary of order of magnitude permeabilities by sample, sample location and sample properties (e , fines and C_u) for triaxial test samples 1 - 11. Note that no permeability was assessed for sample 3 (an undrained test) or sample 12 (the stress path test). Samples 7, 8 (both at 20 % fines) and 11 (at 38 % fines) are the reconstituted samples whose permeability will be discussed in a separate section. Samples 9 and 10 are the undisturbed samples tested under horizontal flow conditions (Fig 3.1b). sample 12 is the stress path test sample whose permeability was not assessed. Also included is the standard consolidation test sample where permeability was back calculated from time rate of consolidation (C_v) readings.

Permeabilities are separated as vertical and horizontal. Field test results are also listed in Table 8.1 for the sake of comparison. Note that field bailing and slug tests are listed as providing horizontal permeability and the CPT dissipations as mixed. The field values reflect different effective lengths (2 and 4 ft. for the wells used in the slug tests and 10 ft. for the bailing test). Discussion of the field tests follows in the next section.

Most discouraging were the results from triaxial test samples 5, 6, 9, and 10 which were from 9.5 ft. and 10.5 ft. depth at Pz2 location, i.e. two with a common

trimmed end at 9.5 ft. (one above, one below 9.5 ft.) and the other two with a common end at 10.5 ft. They show some variation in void ratio and fines content (even percent fines in the upper versus the lower half of the same sample) but there are two orders of magnitude difference in permeability. What is worse, one might even expect such difference by direction due to layering (horizontal greater than vertical), but not that difference in the same direction (10^{-5} versus 10^{-7} cm/sec horizontally) and certainly not with the sample with the lower percent fines (though it does have a lower void ratio) yielding the lower permeability (by two orders of magnitude).

There is no clear pattern to the undisturbed lab test sample values. To add further insult, the one standard consolidation test (sample 1-D) yielded the lowest permeability (10^{-9} cm/sec). Given the dependency of permeability ($k = C_v \frac{a_v}{1 + e_o} \gamma_w$) upon the coefficient of consolidation (C_v) and the compressibility ($a_v = \frac{C_c}{2.3\bar{\sigma}}$), the low value of k obtained was most affected by C_c . But the one order of magnitude difference in C_c of the consolidation curves of samples 5 and 6 versus sample 1-D (the standard consolidation test) would not account for the three to four orders of magnitude difference in vertical permeability between 5 and 6 versus 1-D. Therefore a second standard consolidation test on an undisturbed sample from a 9.5 ft. depth at Pz2 was undertaken. This sample was obtained from

a separate NDOT sampling operation on 9/11/96, one year after the completion of piezometer readings. It has been held for just such an emergency. See Appendix 10 for the boring log. Note that SPT blow counts were obtained (with equalized water levels) immediately above and below the Shelby tube sample. Such N values agree very well with N values at Pz3 location (unequal water levels) prior to construction of the fill.

8.3. Field Tests

The difficulty in assessing a meaningful in situ permeability at the Zolezzi Lane site relates to the level of facies changes that occur laterally and the structuring that occurs vertically in this alluvial deposit. Cone penetration dissipation reflect in situ permeability as assessed very locally around the piezocone tip and using the Roberston and Campenella (1984) correlations yielded a lower estimate of permeability (10^{-7} cm/sec). Part of this phenomena is likely the distortion and smearing of the very thin horizontal seams/partings due to cone insertion and the consequent restriction in flow this might have caused.

Most faith should be placed in the bailing and slug tests because they reflect the response of a larger volume of material. Even so, there is variability over the larger volume as shown for instance in Fig 8.1 which is an attempt to delineate differences based on the CPT logs which used sensor readings to reflect switches

from cohesionless to "silt-clay" soils. While such soil classifications were not born out in the lab, they still reflect a variation of the (same) material that may be worth characterizing. As shown, the two and the four foot effective lengths of the slug test wells have a center (10 ft. depth) in the same material but the longer effective length has ends in the more permeable material (cohesionless versus the shaded finer grained soil according to the CPT logs). Even so, the permeability of the shorter length section in supposedly finer grained material was greater, not less than that of the other.

The authors fully recognized that bedding can play a significant role in permeability results. Usually horizontal permeability is much less affected by the presence of relatively thin impervious partings than vertical permeability as discussed in Chapter 3. Some attempt was made to account for this by assessing differences in percent fines of the upper and lower halves of the triaxial test specimens. However, what the authors did not expect was the presence and random orientation of root holes or micropores in samples at 10 ft. depth. Such open root holes/micropores were only noticed upon oven or air drying the failed or discarded lab test samples. While the soil survey indicated the presence of such micropores, the authors had assumed that they would be restricted to the upper organic mat, or at most to the 5 ft. depth of the soil survey report, but not to 10 ft. and possibly greater depth.

It is interesting to read from Terzaghi, Peck and Mesri (1996) these words of wisdom regarding field and lab permeability:

The accurate determination of the permeability of soil strata of any kind on the basis of the results of soil tests is impracticable, because the permeability depends on structural details of the strata that cannot be detected by any method of soil exploration. However, if the method for investigating the permeability is selected judiciously and used intelligently, fairly reliable limiting values can be obtained under almost any circumstances. The difference between the limiting values and the real average value cannot be determined, but for many practical purposes only a knowledge of the limiting values is needed.

Natural deposits are never homogeneous. The water percolates through them along more or less tortuous lines following lenses and layers composed of the coarsest constituents, and their permeability in a vertical direction is usually much smaller than that in a horizontal one. Therefore, laboratory investigations of any kind cannot be expected to disclose more than the order of magnitude of the permeability of the deposit even if the tests are performed by causing the water to flow through undisturbed samples separately in horizontal and vertical directions. Furthermore, the cores are never continuous. A single seam of silt located between two adjoining samples of sand may have a radical influence on the ratio of horizontal to vertical permeability. The occurrence of such seams is not uncommon.

For these reasons the use of undisturbed samples for permeability tests is hardly justified. Results no less reliable can be obtained by testing reconstituted samples. The estimates and test results on reconstituted samples can be adjusted to take into account the difference between the relative density of the remolded and the in-place material.

Elaborate investigations of this nature are rarely justified economically. The determination of the

permeability of natural deposits below the water table by in situ permeability tests is always more reliable than that by laboratory tests. In a falling-head test in a drill hole it is likely that fines suspended in the water may form a filter skin over the walls and bottom of the hole in the previous material; consequently, the observed permeability may be too small. The error may be avoided by bailing the water from the casing until the water level is below that of the pervious stratum and by measuring the elevation of the water level various times as it rises toward its equilibrium position. The results of such tests are little more than an indication of the order of magnitude of the coefficient of permeability. More reliable information is obtained from pumping tests on test wells.

8.4. Lab Tests on Reconstituted Samples and General Conclusions

Based on the comments above, three sets of permeabilities were assessed on reconstituted samples at $e = 0.560$ (samples 7 and 8) and $e = 0.605$ (sample 11). Such samples, while tested vertically are expected to reflect an isotropic value of permeability. Samples 7 and 8 contained 20% fines while sample 11 contained 38% fines. Such lab tests at the lower fines content (samples 7 and 8) gave values that reflected the bailing test permeability corresponding to an $e = 0.559$ to 0.874 over a 10 ft. depth at Pz2, i.e. 10^{-4} cm/sec. This is one order of magnitude higher than that obtained on sample 11 at the higher fines content (but higher void ratio) that reflected the field value from the slug test results (10^{-5} cm/sec corresponding to $e = 0.435$ to 0.647 at 10 ± 1 or 2 ft. at Pz3).

Given this agreement in range (excluding CPT dissipations) of permeability (10^{-4} to 10^{-5} cm/sec) between field and reconstituted lab test results, the authors feels that this is the most representative of the site as a whole. Standard or sophisticated lab tests on undisturbed samples involving primarily vertical permeability are not worth the effort and are potentially misleading. However, some consolation can be had if one considers the range in permeability as seen in Fig 8.2 from Lambe and Whitman (1969) for the silty sand (soil 3) line at the lower end of the void range (e) for the Zolezzi lane silty sand, up to that of the natural silt (soil 21) which traverses the higher void ratio range encountered at Zolezzi. (Realize that this natural silt, soil 21, is likely to have root holes.) These two materials that reflect the silty sand at the site (the material) and its structure (root holes) span the same 10^{-4} to 10^{-8} cm/sec permeability range we encountered in Table 8.1.

8.5. Discussion

For the successful evaluation of groundwater flow conditions, one must establish the horizontal, and to a lesser degree, the vertical permeabilities of various units comprising the flow regime. In the current project it was envisioned that permeabilities would change due to fill construction and the consequent differential compression of void space of the various units beneath and to the side

of the fill. The greater amount of consolidation at shallow depths in the upper portion of the soil profile would therefore require initial assessment of permeability via corrected field and lab tests followed by additional permeability tests on K_0 or stress path consolidated lab samples to reflect changes that would occur subsequent to fill construction.

The unexpected finding in the current project was that seasonally adjusted flow conditions would not change because there would be no particular compression of this medium dense to dense silty sand material. In fact, the only discernible change was the short lived drop in certain piezometers during construction due to the suppressed dilatant expansion of the material resulting from shear loading with the increase in fill height. This negative excess porewater pressure dissipated quickly (5 weeks) within the time of construction.

Another unexpected development was the inability of the authors to more accurately establish in situ permeability given the constancy of the material (it did not change due to fill construction) and the various means employed to assess permeability: CPT dissipations, slug and bailing tests, laboratory assessed horizontal and vertical permeability of Shelby tube samples and of reconstituted samples of different percent fines, and back calculation from time rate readings from the consolidation test.. The reader should take to heart the comments provided by Terzaghi, Peck and Mesri (1996). In that regard, note that while field

pumping tests are recommended, preliminary evaluation indicated they would not be successful given the lower expected permeability ($<10^{-4}$ cm/sec). The bailing test was used instead.

It is the authors opinion that the effective permeability for basically horizontal flow at Zolezzi (both before and after fill construction) is 10^{-4} to 10^{-5} cm/sec. This range derives from the bailing and slug tests and is supported by lab tests on reconstituted samples. It is felt that the reconstituted samples reflect a reasonable "average" homogenous condition while flow in the field occurs in torturous paths (see Fig 8.1) through the more permeable material.

Table 8.1 Permeability Results

Sample	Location		e	% Fines upper/lower	C _u	k _v cm/sec	k _h cm/sec
	Piezometer	Depth (ft)					
1	Pz3	6.0	-	20	-	10 ⁻⁶	
2	Pz3	8.0	0.496	19	7	10 ⁻⁶	
3	Pz3	3.0	0.746	32	10	-	-
4	Pz5	3.0	0.642	31/65	10	10 ⁻⁷	
5	Pz2	10.5	0.661	32/29	11	10 ⁻⁵	
6	Pz2	10.5	0.585	65/26	30	10 ⁻⁶	
7	Reconstituted		0.560	20	9	10 ⁻⁴	
8	Reconstituted		0.560	20	9	10 ⁻⁴	
9	Pz2	9.5	0.577	36/56	6		10 ⁻⁵
10	Pz2	9.5	0.524	26/27	10		10 ⁻⁷
11	Reconstituted		0.605	38		10 ⁻⁵	
12	Pz2	10.0	0.654	37		-	-
1-D	Pz3	7.0	0.637	-	-	10 ^{-9*}	
Bailing	Pz2	0-10	0.559-0.847	-	6-30		10 ⁻⁴
Slug	Pz3	9-11 8-12	0.435-0.796	-	10-13		10 ⁻⁵
CPT Dissipations	Pz3	35537.0					10 ⁻⁷

* A second standard consolidation test (e = 0.607) on a sample from Pz2 at 9.5 ft. yielded a vertical permeability of 10⁻⁷ cm/sec corresponding to a C_c slope of 0.083

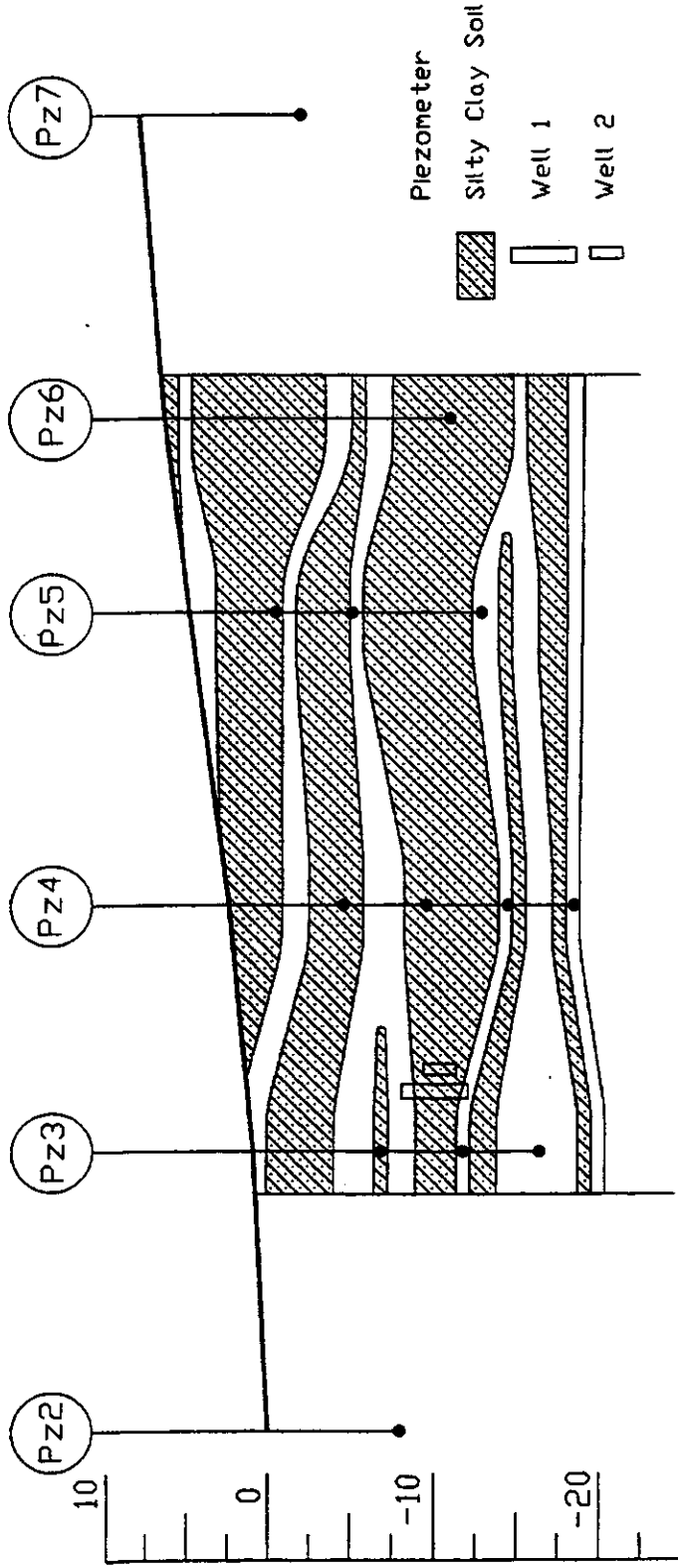


Fig 8.1 Possible Material Variation Based on CPT Log Interpretation

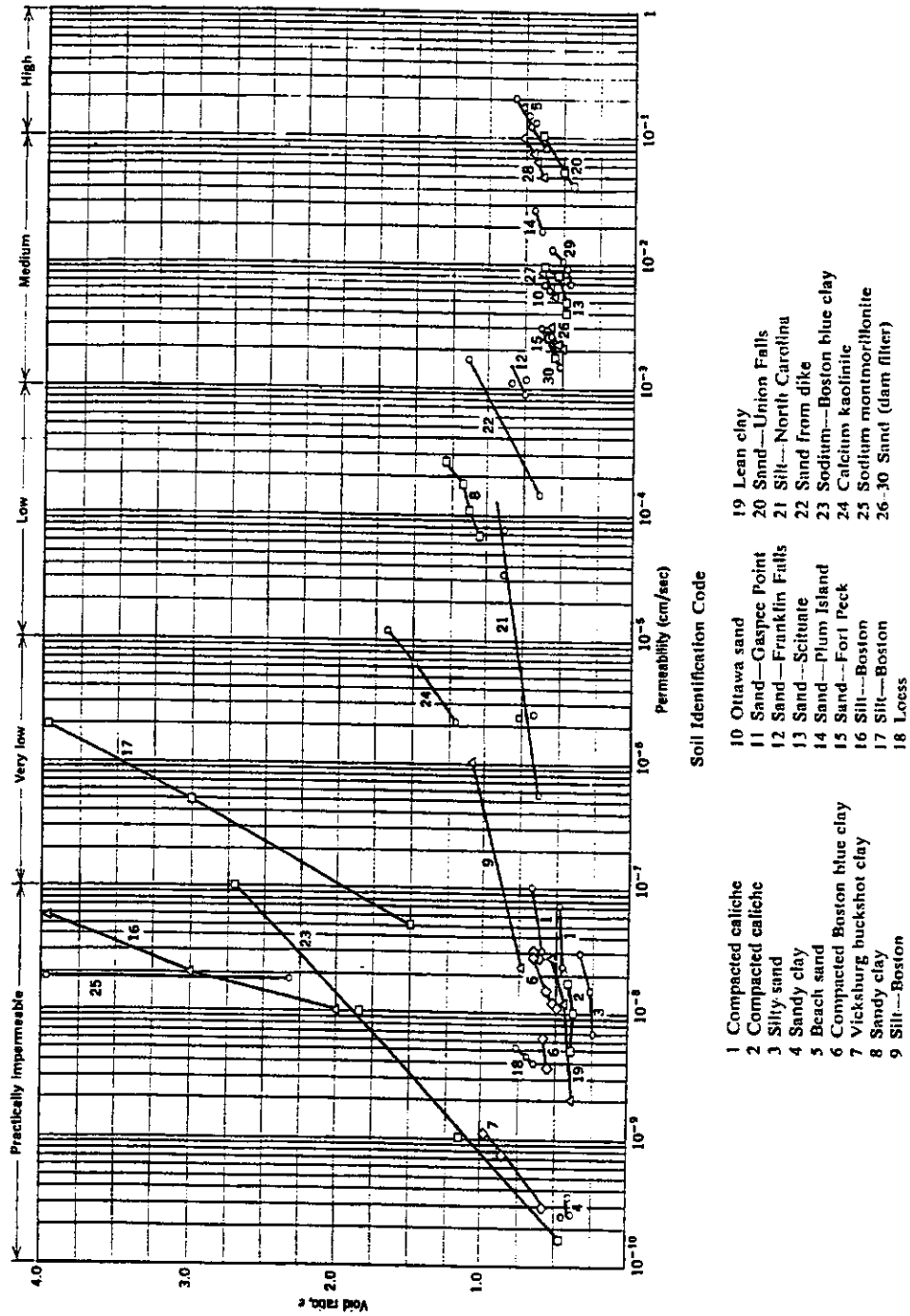


Fig 8.2 Permeability Test Data from Lambe and Whitman (1969)

Chapter 9

Finite Element and Stress Path Analysis

9.1. Overview

This chapter deals with the finite element analysis of the undrained and the drained stress state induced by fill construction. It also discuss the stress path triaxial test loading used to simulate stress changes, so assessed, in order to evaluate the induced porewater pressure and the undrained strains followed by the drained strains as the excess porewater pressure is allowed to dissipate. Recall that in the field a negative porewater pressure of approximately 6 kPa (or 2 ft. of water) developed in certain piezometers (see Fig 6.22) corresponding to an (assumed) undrained dilatant response. It is the purpose in this chapter to see if that might be reasonably simulated via finite element modeling and triaxial test stress path testing.

9.2. Finite Element

Chapter 5 dealt with the FEADAM84 model used to characterize subsurface and embankment layers. Basically, recommended values of input parameters from Duncan et al (1984) were used for all but the two upper in situ layers. Choice of

such parameter input required only general information regarding the soil units, which was obtained from NDOT borings B1 and B2 (see Fig 2.7) and classification of the highway embankment fill as GW soil. Originally the two upper in situ layers, that are the flow region of concern, were characterized as a medium dense silty sand (SM) with $\phi = 33^\circ$ (and $K_0 = 1 - \sin \phi$) largely based on blow count interpretations at Pz3, Pz4 and Pz5 (see Table 7.3). CPT data was ignored given that the CPT mistakenly classified this soil as fine grained silt-clay soil in large part. Using the initial stress conditions for the static water case (water level at 4 ft. depth and assuming a $\gamma = 120$ pcf), the drained stress state after loading was assessed, but only for the purpose of picking confining pressures and K_0 consolidation stress levels to be used in standard triaxial test strength evaluations discussed in Chapter 7. (Permeability was also assessed in the course of these tests.) Such was the basis for the choice of the range in isotropic consolidation ($\bar{\sigma}_3 = 45, 50, 60, 65, 80$ kPa) and K_0 consolidation ($\bar{\sigma}_3 = 60$ and 77 kPa) confining pressures used in the triaxial tests on undisturbed samples 1-6, 9 and 10. (Note that all such $\bar{\sigma}_3$ pressures exceeded the horizontal effective stress at the associated sample's preconsolidation pressure and, therefore, satisfied SHANSEP testing conditions, once the applied σ_d was increased to its K_0 level.) The test on sample 3 was an undrained test while all other tests on the undisturbed samples were drained. Two tests, one drained and one undrained, on reconstituted

samples (7 and 8) were carried out at $\bar{\sigma}_3 = 30$ kPa after first isotropically consolidating them to a $\bar{\sigma}_3 = 65$ kPa (and, therefore, an OCR = 2). (Due to operator error, no data was obtained from undrained failure of a third reconstituted sample, i.e. sample 11.)

Once the results of all these strength tests were used to establish Fig 7.2, it was recognized that the ϕ of 33° for the upper silty sand region was too conservative. Likewise, K_0 tests of samples 5 and 9 confirmed the OCR = 2 obtained from the standard consolidation test (1-D) but yielded a K_0 of 0.3 and 0.4 (for normally consolidated conditions at $\bar{\sigma}_3 = 60$ and 77 kPa). For the average void ratio of $e = 0.605$ from Pz2, Pz3, Pz4 and Pz5 sample data in Table 2.5, values of $\phi = 41^\circ$ (from Fig 7.2), $K_0 = 0.5$ (for OCR = 2) and $\gamma = 125$ pcf were taken as the adjusted values to use for the silty sand (SM) of the upper two in situ finite element layers (the flow region of concern) above the artesian layer.

Sensitivity studies were also undertaken to ascertain the effect of using the initial stresses calculated based on static versus steady-state flow porewater pressure conditions and the influence of a K_0 of 0.3, 0.4 or 0.5 for the silty sand. Such influences had little effect on the calculated drained effective stress state after fill construction. (However, they do have an effect on the initial stress state and, therefore, for triaxial test purposes, how we should condition the sample prior to loading to final stresses.)

FEADAM84 runs were also obtained for assumed initial undrained conditions in the upper sand using separate S_u values of 1, 2 and 5 ksf (based on results from tests on samples 3 and 8) and a bulk modulus as per Byrne et al (1987) suggestions. The results for the $S_u = 5$ ksf are used here for discussion purposes. It should be noted that the $S_u = 1$ ksf case yielded several elements at an undrained stress level of one (failure).

As important as the choice of S_u for the upper silty sand, so is the treatment of in situ layers below the artesian layer (GM). In one instance, such layers were treated as drained using the input values previously discussed. In a second instance, these lower layers were also treated as if they were undrained over the time of fill construction. In that instance, they were given the same S_u and input parameters as the upper silty sand. In all cases, the fill (which is above groundwater level) and the artesian layer were treated as drained.

Note that since initial effective stresses are used as input to FEADAM84, the computed stresses that result from undrained loading represent apparent effective stresses (P), i.e. total stress (σ) minus static or steady-state porewater pressure (u_s) which is also the effective stress ($\bar{\sigma}$) plus any undrained excess porewater pressure (Δu), i.e.

$$P = \sigma - u_s = \bar{\sigma} + \Delta u$$

This is what Lambe and Whitman (1969) call the $(T-u_s)$ stress state (i.e. total stress minus static or steady-state porewater pressure). Along a stress path, the horizontal difference between the P or $(T-u_s)$ stress path and the effective stress path (ESP) is Δu .

Appendices 8 and 9 contain a portion of the output of the stresses for these two different undrained cases (i.e. undrained upper layers with undrained versus drained layers beneath the artesian layer). Rather than study the difference in response of all elements of the silty sand atop the artesian layer, we will focus on conditions at a representative location. Further, we will conduct our stress path triaxial test using stresses calculated at this location to assess undrained or excess porewater pressure buildup due to shear, Δu_d (and, therefore, pore pressure parameter $\bar{A} = \Delta u_d / (\Delta \sigma_1 - \Delta \sigma_3)$), undrained strains, and then drained strains, once the excess porewater pressure is released and the applied stresses are adjusted to reflect the drained upper layer FEADAM results.

If the stress path triaxial test yields the same undrained and then drained strains for this location as predicted in the FEADAM84 undrained and drained outputs, then the finite element modeling and stress path testing are simultaneously successful at this early stage. However, if the strains are significantly different, then the FEADAM input parameters for the silty sand would need to be changed to reflect what was observed in the stress path test or the lab triaxial test stress-strain-

pore pressure response further corrected for disturbance effects, or a combination of both employed. Ideally, differential settlement measurements from field instrumentation yielding vertical strains would provide a measure of guidance as to how to proceed. Of course, if the changed FEADAM input parameters yield significantly different applied stresses for the undrained and drained cases, then there might be a need to repeat the triaxial stress path test and, hence, cause further iteration.

Please note that these first undrained and drained FEADAM runs were made with just the Duncan and Byrne recommended input parameters for stress-strain response using the lab assessed undrained S_u and drained ϕ values for the silty sand. (No attempt was made to use any specific triaxial test stress-strain curve information from samples 1-10.)

9.3. Stresses

The representative location chosen for consideration is at Pz4 location at a depth of 10 ft. Note that Pz4A, Pz4B and Pz4C all showed the previously noted negative porewater pressure change (see Fig 6.22) and Pz4A and Pz4-B are at 7 and 12 ft. depths, respectively. As shown in Fig 9.1, averaging the stresses representing conditions at the center of elements 302 and 303 yields the stresses at 5.5 ft. depth directly above the point of interest, and averaging those for elements

248 and 249 yields the stresses at a depth of 16.75 directly below it. The stresses at Pz4 at 10 ft. depth can then be assessed from linear interpolation of the stresses at 5.5 and 16.75 ft.

Values of stresses (and strains) at this location assessed from FEADAM for the undrained loading case are

$$P_1 = \sigma_1 - u_s = 4.50 \text{ ksf} = 225 \text{ kPa} \quad \epsilon_1 = 0.078\%$$

$$P_3 = \sigma_3 - u_s = 1.30 \text{ ksf} = 65 \text{ kPa} \quad \epsilon_3 = -0.074\%$$

$$\sigma_d = P_1 - P_3 = 3.20 \text{ ksf} = 160 \text{ kPa}$$

for static water conditions (water at 4 ft. depth), $S_u = 5 \text{ tsf}$ ($=250 \text{ kPa}$) in the upper silty sand, and assumed drained response of the layers beneath the artesian layer.

Alternatively, for similar undrained response of the layers below the artesian layer, these same stresses (and strains) are

$$P_1 = \sigma_1 - u_s = 4.54 \text{ ksf} = 226 \text{ kPa} \quad \epsilon_1 = 0.051\%$$

$$P_3 = \sigma_3 - u_s = 1.70 \text{ ksf} = 85 \text{ kPa} \quad \epsilon_3 = -0.047\%$$

$$\sigma_d = P_1 - P_3 = 2.84 \text{ ksf} = 140 \text{ kPa}$$

Therefore, average values of

$$P_1 = 225 \text{ kPa}$$

$$P_3 = 75 \text{ kPa}$$

$$\sigma_d = 150 \text{ kPa}$$

were adopted for stress path triaxial testing. Likewise values at this location for drained loading for an assumed $\phi = 41^\circ$, $K_0 = 0.5$ and static water conditions in the upper silty sand are

$$\bar{\sigma}_1 = P_1 = \sigma_1 - u_s = 225 \text{ kPa}$$

$$\bar{\sigma}_3 = P_3 = \sigma_3 - u_s = 70 \text{ kPa}$$

$$\sigma_d = 155 \text{ kPa}$$

Note that in the undrained case the FEADAM stresses represent

$$P_1 = \sigma_1 - u_s = \bar{\sigma}_1 + \Delta u$$

$$P_3 = \sigma_3 - u_s = \bar{\sigma}_3 + \Delta u$$

while for the drained case they are effective stresses, i.e.

$$P_1 = \sigma_1 - u_s = \bar{\sigma}_1 \quad ; \Delta u = 0$$

$$P_3 = \sigma_3 - u_s = \bar{\sigma}_3 \quad ; \Delta u = 0$$

Figure 9.2 shows the initial stresses at this depth, i.e.

$$P_{10} = (\sigma_1 - u_s)_0 = \bar{\sigma}_{10} = 50 \text{ kPa}$$

$$P_{30} = \bar{\sigma}_{30} = K_0 \bar{\sigma}_{10} = 25 \text{ kPa}$$

$$\sigma_{d0} = 25 \text{ kPa}$$

Therefore, in going from these initial stresses to the undrained stresses for fill loading, the undrained porewater pressure generated is (Skempton, 1954)

$$\Delta u = B \Delta \sigma_3 + \bar{A} (\Delta \sigma_1 - \Delta \sigma_3)$$

which, in the present notation, is also

$$\Delta u = \Delta P_3 + \bar{A}(\sigma_d - \sigma_{d0}) \quad ; B = 1$$

(Note that there has been no rotation in major and minor principal stress directions.) Alternatively,

$$\Delta u = \Delta u_b + \Delta u_d$$

where

$$\Delta u_b = \Delta \sigma_3 = \Delta P_3 \quad ; B = 1$$

is due to the isotropic change in confining pressure, and

$$\Delta u_d = \bar{A}(\sigma_d - \sigma_{d0})$$

is due to the undrained change in the deviatoric stress.

For a cohesive soil that is normally consolidated or has a low OCR (e.g. 2), Δu is positive. In fact, for K_0 loading (i.e. horizontal strain $\varepsilon_h = \varepsilon_3 = 0$, as in the standard consolidation test) of any saturated soil ($B = 1$, $\nu = 1/2$)

$$\varepsilon_3 = \frac{\Delta \sigma_3}{E} - \nu \frac{\Delta \sigma_3}{E} - \nu \frac{\Delta \sigma_1}{E} = 0$$

$$\Delta \sigma_3 = \frac{\nu}{1-\nu} \Delta \sigma_1$$

$$\Delta \sigma_3 = \Delta \sigma_1 \quad ; \nu = 1/2$$

whereby

$$\Delta u = \Delta \sigma_3 + \bar{A}(\Delta \sigma_1 - \Delta \sigma_3)$$

$$\Delta u = \Delta u_b = \Delta \sigma_3 \quad ; \Delta u_d = \bar{A}(\Delta \sigma_1 - \Delta \sigma_3) = 0$$

Therefore, there must be some lateral distortion, $\epsilon_h = \epsilon_3 \neq 0$ (and $\Delta\sigma_3 < \Delta\sigma_1$), for a dilatant material ($\bar{A} < 0$) to yield a Δu less than $\Delta\sigma_3$. Fig 9.2 shows the possible position of the effective stress circle for fill loading (where there is lateral strain such that $\Delta\sigma_3 < \Delta\sigma_1$) in association with different possible values of Δu_d and, hence, $\Delta u = \Delta u_b + \Delta u_d = \Delta\sigma_3 + \Delta u_d$. Note below the figure of the circles there are line diagrams of Δu_d and Δu values for cases A ($\Delta u_d > 0$, $\bar{A} > 0$, Δu between $\Delta\sigma_1$ and $\Delta\sigma_3$), B ($\Delta u_d = 0$, $\bar{A} = 0$, $\Delta u = \Delta\sigma_3$), C ($\Delta u_d < 0$, $\bar{A} < 0$, $\Delta u < \Delta\sigma_3$ but $\Delta u > 0$), D ($\Delta u_d = \Delta\sigma_3$, $\bar{A} = -1/(\Delta\sigma_1 / \Delta\sigma_3 - 1)$, $\Delta u = 0$), and our assumed case E ($\Delta u_d < -\Delta\sigma_3$, $\bar{A} < -1/(\Delta\sigma_1 / \Delta\sigma_3 - 1)$, $\Delta u < 0$).

For the representative location, $\Delta P_3 = 75 - 25 = 50$ kPa and $(\sigma_d - \sigma_{do}) = (150 - 25) = 125$ kPa. Therefore, while we expect

$$\Delta u = -6 \text{ kPa}$$

(for the approximate recorded 2 ft. drop in piezometer water levels in the dilatant region shown in Fig 6.22) this is due to

$$\begin{aligned} \Delta u &= \Delta u_b + \Delta u_d = \Delta P_3 + \bar{A}(\sigma_d - \sigma_{do}) \\ &= 50 + \bar{A}(125) \end{aligned}$$

For $\Delta u = -6$ kPa,

$$\Delta u_d = \bar{A}(125) = -56$$

$$\bar{A} = -56/125 = -0.45$$

Of course, the above assumes the 6 kPa drop is a fully undrained value. In fact, it may be a partially drained value, in which case Δu_d and \bar{A} would be even greater negative values.

Figure 9.3a shows the associated Mohr circles, while Fig 9.3b shows the undrained components of the total volumetric strain, i.e.

$$\varepsilon_v = \varepsilon_{v\text{iso}} + \varepsilon_{v\text{shear}} = 0$$

which must be zero for undrained conditions of this saturated soil. Consequently

$$\varepsilon_{v\text{shear}} = -\varepsilon_{v\text{iso}}$$

where $\varepsilon_{v\text{iso}}$ is the volumetric strain (compression) associated with the undrained change in $\bar{\sigma}_3$ from 25 to 81 kPa and $\varepsilon_{v\text{shear}}$ is the equal and opposite (dilatant) component of volumetric strain due to the change in deviatoric stress from $\sigma_{d0} = 25$ kPa at $\bar{\sigma}_3 = 25$ kPa to $\sigma_d = 150$ kPa at $\bar{\sigma}_3 = 81$ kPa.

Note that in the above discussion,

$$\begin{aligned} \bar{\sigma}_3 &= P_3 - \Delta u \quad \text{or} \\ &= 75 - (-6) = 25 - (-56) \\ &= 81 \text{ kPa} \end{aligned}$$

and

$$\begin{aligned} \bar{\sigma}_1 &= P_1 - \Delta u = \bar{\sigma}_3 - \Delta u + \sigma_d \quad \text{or} \\ &= 225 - (-6) = 25 - (-56) + 150 \end{aligned}$$

$$= 231 \text{ kPa}$$

As indicated, Δu_d must be a large negative value (-56 kPa) to overcome $\Delta u_b = \Delta P_3 (= 50 \text{ kPa})$ to get a net value of $\Delta u = -6 \text{ kPa}$ and the effective stress (ES) state shown in Fig 9.3a.

While volumetric strain $\varepsilon_v = 0$ during undrained loading, there is distortion. For the plane strain conditions ($\varepsilon_2 = 0$) of FEADAM,

$$\varepsilon_v = \varepsilon_1 + \varepsilon_2 + \varepsilon_3 = 0$$

$$\varepsilon_3 = -\varepsilon_1$$

Of course, the strain outputs do not exactly reflect this condition because ν can not be taken equal to $\frac{1}{2}$ in the FEADAM analysis (i.e. computational instability results).

By contrast, the stress path test will reflect undrained triaxial compression conditions, i.e. $\varepsilon_2 = \varepsilon_3$ and, therefore, $\varepsilon_v = 0$ requires

$$\varepsilon_3 = -\frac{1}{2} \varepsilon_1$$

In truth, the field problem is neither a plane strain problem, because of the cross section's proximity to the abutment of the Zolezzi Lane overcrossing (see Fig 2.1), nor triaxial, because of its plane strain confinement in the opposite direction. Accordingly, a less sophisticated three-dimensional elastic analysis such as Newmark's chart (see e.g. p 174 of DM-7.1, 1982) might have been as accurate as the finite element analysis. On the other hand, neither this nor the finite element

analysis have been modified to account for the surface grass acting as an equivalent geotextile fabric to redistribute the load.

9.4. Settlement

If one were to integrate or sum the undrained vertical strains, ϵ_1 , of the FEADAM output over the depth of the deposit, the result would yield the immediate settlement, ρ_i , at ground surface, i.e.

$$\rho_i = \int_0^{75 \text{ ft}} \epsilon_1 dz = \sum_{i=1}^N (\epsilon_1 \Delta H)_i$$

where N is the number of in situ layers. By contrast, if one were to do the same for the drained ϵ_1 strains, the resulting total settlement ρ would be a combination of immediate (ρ_i) and consolidation (ρ_c) settlement, i.e.

$$\rho = \rho_i + \rho_c$$

and, therefore, the consolidation settlement would be

$$\rho_c = \rho - \rho_i$$

Such evaluation has been made (see Table 9.1) and ρ_i and ρ_c values (in inches) for the 75 ft. deep deposit characterized are

Element 299	Element 300
$\rho_i = 0.827$, say 0.8	0.837, say 0.8

$$\begin{aligned} \rho_c &= 7.476 - 0.827 & 7.640 - 0.838 \\ &= 6.649, \text{ say } 6.6 & 6.802, \text{ say } 6.8 \end{aligned}$$

inches along two vertical lines (through the center of elements 299 and 300 of Fig 5.2b) on either side of centerline. If the layers beneath the artesian are treated as drained during fill construction then

Element 299	Element 300
$\rho_i = 6.435, \text{ say } 6.4$	$6.491, \text{ say } 6.5$
$\rho_c = 7.476 - 6.435$	$7.640 - 6.491$
$= 1.04, \text{ say } 1.0$	$1.149, \text{ say } 1.1$

inches. Of course the time span between ρ_i and ρ_c , i.e. the dissipation of Δu , occurs in a very short period (during construction) at Zolezzi. Hence, for design purposes, we would normally assume or evaluate just the drained response of this silty sand and call the resulting drained settlement the immediate settlement (i.e. it occurs as fast as the construction rate of loading). However, for the present purpose of predicting the observed negative pore pressure change, the above distinction holds. Note that such values reflect plane strain conditions which are not exactly what exist at the site.

Such evaluations should be checked against recorded field behavior but since such settlement instrumentation was not provided, it should at least be

compared with other methods to get a feel for its accuracy and, therefore, for FEADAM's capability to accurately simulate behavior.

Note that the undrained immediate settlement might also be calculated more traditionally (p 23 of Duncan and Buchignani, 1987) as

$$\rho_i = \frac{qB}{E} (1 - \nu^2) I_1 I_o$$

using $\nu = 1/2$ and an undrained Young's modulus $E = K_u S_u$ with S_u from an undrained triaxial test. Sample 8 (a reconstituted sample) was tested undrained after first being consolidated to $\bar{\sigma}_3 = 65$ kPa, to simulate the mean effective stress under the preconsolidation pressure, and then rebounded to $\bar{\sigma}_3 = 30$ kPa, corresponding to the mean effective stress at an OCR = 2 of the average or representative location. Using $E = 1000 S_u$ (i.e. $K_u = 1000$ from p 26 of Duncan and Buchignani for $PI < 30$ and OCR = 2), then $E = 1000 (260 \text{ kPa})$, $q = 1/2 (29+36.5) (130) = 4258 \text{ psf} = 4.26 \text{ ksf} = 213 \text{ kPa}$, $(1-\nu^2)I_1 = 0.1$ for $H/B = 75/(148+279)/2 = 0.35$ and $I_o = 1$ ($D = 0$), the calculated ρ_i is 0.21 inches. This average value can be corrected to the center by multiplying by a factor (Table 7, p 25 of Duncan and Buchignani) of 1.3, i.e. $1.3 (0.21) = 0.27$ inches. While 0.27 in. is considerably less than the 0.83 in. from the FEADAM solution, most of the FEADAM ρ_i derives from drained deformation of the artesian layer. Therefore, if we subtract this and proportion the difference ($[0.827 - 0.662] \times 75/(75 - 15) = 0.206$) there is much better agreement between the values, i.e. 0.27 versus 0.21

inches. Realize, of course, we would expect the 0.83 in. to develop, i.e. the traditional calculation does not account for a good portion of the full value.

In the same vein, Schmertmann's method for the (drained) settlement of sand can be used to assess the total or final settlement ρ as

$$\rho = C_1 C_2 q \sum \frac{I_z \Delta z}{x q_c}$$

Note that $x q_c$ is the Young's modulus E as assessed from CPT cone tip resistance, q_c (or Q_c in previous notation). Factor $x = 2.5$ or 3.5 , depending on whether the problem is axisymmetric (e.g. triaxial) or plane strain (e.g. FEADAM). In this instance we can use an intermediate value to better reflect actual conditions (or use 3.5 to compare with the FEADAM drained solution). Note that ρ is really the integration $\int \varepsilon_1 dz$ where

$$\varepsilon_1 = \frac{\Delta \bar{\sigma}_1}{E} - \nu \frac{\Delta \bar{\sigma}_2}{E} - \nu \frac{\Delta \bar{\sigma}_3}{E}$$

or in triaxial conditions (where $\bar{\sigma}_1 = \bar{\sigma}_3 + \sigma_{d1}$, $\bar{\sigma}_2 = \bar{\sigma}_3 + \sigma_{d2}$)

$$\varepsilon_1 = \frac{1}{E} (\Delta \bar{\sigma}_3 + \Delta \sigma_{d1}) - \frac{\nu}{E} (\Delta \bar{\sigma}_3 + \Delta \sigma_{d2}) - \frac{\nu}{E} \Delta \bar{\sigma}_3$$

For an axisymmetric axial compression case, $\sigma_{d2} = 0$, i.e. $\Delta \sigma_2 = \Delta \sigma_{d2} = 0$, this becomes

$$\varepsilon_1 = \frac{\Delta \sigma_{d1}}{E} + \frac{(1-2\nu)}{E} \Delta \bar{\sigma}_3$$

In our drained case $\Delta\sigma_{d1} = \sigma_d - \sigma_{d0} = 155 - 25 = 130$ kPa, $\Delta\bar{\sigma}_3 = 70 - 25 = 45$ kPa. If ν , by shear dilatancy (not undrained behavior), were to reach a value of 0.5, then ε_1 would equal

$$\varepsilon_1 = \frac{\Delta\sigma_{d1}}{E} = \frac{\Delta\sigma_1 - \Delta\sigma_3}{E}$$

and be due entirely to shear loading (with no contribution from confining pressure change, $\Delta\bar{\sigma}_3$, i.e. $(1 - 2\nu)\Delta\bar{\sigma}_3 = 0$).

In fact, Schmertmann's equation is really a characterization of $\int \varepsilon_1 dz$ for a condition of $\nu = 1/2$, as shown below:

$$\rho_i = \sum \varepsilon_1 \Delta z$$

$$\rho_i = \sum \frac{(\Delta\sigma_1 - \Delta\sigma_3)}{E} \Delta z$$

$$\rho_i = \sum q \frac{I_z}{E} \Delta z \quad \text{where } \Delta\sigma_1 - \Delta\sigma_3 = qI_z$$

$$\rho_i = q \sum \frac{I_z}{E} \Delta z$$

Additional factors, C_1 and C_2 , are for embedment and creep effects which in our case are equal to unity ($C_1 = C_2 = 1$). One will note, therefore, that Schmertmann's I_z triangle (see p 51 of Schmertmann, 1977) multiplied by q is the $\Delta\sigma_1 - \Delta\sigma_3$ or $\Delta\sigma_d$ variation due to the imposed fill load. It reaches a peak of approximately $0.6 q$ at a depth $B/2$ (and diminishes to zero at $2 B$) for the axisymmetric or triaxial case, or a depth B (and diminishes to zero at $4 B$) for the

plane strain case ($L > 10 B$). Looking at this $(\Delta\sigma_1 - \Delta\sigma_3) = q I_z$ triangle in the vicinity of the representative location, it suggests that at $z = 10$ ft. or $z/B = 10/214 = 0.05$, $\Delta\sigma_1 - \Delta\sigma_3$ should be between 0.1 (axisymmetric) and 0.2 (plane strain) of q ($= 4.26$ ksf) or 21 to 42 kPa (0.426 to 0.852 ksf), not the $\sigma_d - \sigma_{d0}$ ($= 155 - 25$) drained value of 130 kPa predicted by FEADAM. In fact, the vertical strain at this representative location,

$$\varepsilon_1 = \frac{\Delta\sigma_1 - \Delta\sigma_3}{E} = \frac{\Delta\sigma_1 - \Delta\sigma_3}{xq_c}$$

should be between

$$\frac{0.213 \text{ to } 0.426 \text{ tsf}}{2.5 \text{ to } 3.5 (25 \text{ tsf})} = 0.0024 \text{ to } 0.0068 = 0.24 \text{ to } 0.68 \%$$

using an average q_c at Pz3, Pz4, Pz5 and Pz6 (see Appendix 2) of say 25 tsf. The drained FEADAM value of 0.41% (see Table 9.1 drained case ε_y value) falls in the middle of this range. Therefore, while the value of the drained strain from FEADAM agrees, the $\Delta\sigma_1 - \Delta\sigma_3$ or $\sigma_d - \sigma_{d0}$ due to the fill load does not.

Alternatively, the full settlement can be calculated by Hough's method as outlined in the Soils and Foundation Workshop Manual (1993) on pages 169-170.

This K_0 or consolidometer type settlement is

$$\rho = \frac{C_c}{1+e_0} H \log \frac{\bar{\sigma}_1}{\bar{\sigma}_0} = \frac{1}{C} H \log \frac{\bar{\sigma}_1}{\bar{\sigma}_0}$$

or in our case, where there is an OCR =2,

$$\rho = \frac{1}{C_{oc}} \log \frac{P'_p}{\bar{\sigma}_{1o}} + \frac{1}{C'} \log \frac{\bar{\sigma}_1}{P'_p}$$

If vertical strain ε_1 is again sought, then at the representative location,

$$\varepsilon_1 = \frac{\Delta H}{H} = \frac{1}{C_{oc}} H \log \frac{P'_p}{\bar{\sigma}_{1o}} + \frac{1}{C'} H \log \frac{\bar{\sigma}_1}{P'_p}$$

Using the average of $\frac{1}{C} = C_{\varepsilon c}$ of 0.0243 and 0.0365 or 0.0309 as obtained from K_0 consolidation tests on samples 5 and 9 (see Fig 7.13) and $\bar{\sigma}_1 = 225$ kPa from FEADAM, $\bar{\sigma}_{1o} = 50$ kPa, $P'_p = 100$ kPa, and $\frac{1}{C_{oc}}$ of say 0.2 of $\frac{1}{C}$, then

$$\varepsilon_1 = 0.0127 = 1.27 \%$$

Note that $C' = 32$ ($= 1/0.0309$) which agrees reasonably well with the value of 50 on p 170 of the Soils and Foundations Workshop Manual for well graded fine to medium silty sand for an $N_1 = 16$ (for $N = 12$ at Pz4 at 11-12.5 ft. from Table 7.3 and $C_N = 1.3$ as assessed from p 169). By contrast, the standard consolidation test $C' = \frac{1}{C_{oc}}$ of 260 would require an associated N_1 in excess of 100 for this same material. This indicates that the 1-D consolidation test response (and C_c) was too stiff.

This value of ε_1 is three times the drained value (0.41%) obtained by FEADAM at this representative location. Note that we could have used a value of

$\bar{\sigma}_1 = \bar{\sigma}_{10} + \Delta\sigma_v$ where $\Delta\sigma_v$ is calculated from the elastic abutment chart on p 165 of the Soils and Foundation Workshop Manual (i.e. $b = 107$ ft., $h = 32.75$ ft., distance from middle of the abutment slope = 140 ft. as per Fig 2.2), but $\Delta\sigma_v$ at Pz4 at 10 ft. could only be assessed to be between 0.5 and 1.0 times γh ($= 4258$ psf) or, say, 3000 psf = 150 kPa. Therefore, $\bar{\sigma}_1$ would be $150+50$ or 200 kPa. Alternatively, $\Delta\sigma_v$ from the plane strain embankment chart on p 170 of DM-7.1 (see p 172 for an example of its use) yields a $\Delta\sigma_v$ of $0.95 \gamma h$ or 4045 psf = 202 kPa and, therefore, a drained $P_1 = \bar{\sigma}_1 = 252$ kPa.

Regardless of the variation in $\Delta\sigma_1 - \Delta\sigma_3$ (130 kPa from FEADAM to $21 - 42$ kPa from Schmertmann's CPT analysis), $\Delta\sigma_v$ (175 kPa from FEADAM to $150 - 200$ kPa from elastic embankment charts) or $\bar{\sigma}_1$ (225 kPa from FEADAM to $200 - 252$ kPa from embankment charts), ρ_j (0.83 inches from FEADAM to 0.27 inches from undrained elastic settlement) or drained ε_1 (0.41 % from FEADAM versus $0.24 - 0.68$ % from the CPT and Schmertmann versus 1.27 % from consolidation type behavior), the resultant effect on volume change and, hence, permeability of the soil will still be negligible. For instance, if we accept the larger value of final or drained strain of 1.27 %, this Hough value is for K_0 conditions ($\varepsilon_v = \varepsilon_1$, $\varepsilon_3 = 0$) and, therefore, this volumetric strain

$$\varepsilon_v = \frac{\Delta e}{1 + e_o} = 0.0127$$

yields

$$\Delta e = 0.0127(1 + e_o)$$

which equals 0.02 for $e_o = 0.60$. Therefore, an e of 0.60 might reduce to 0.58. Furthermore, as shall be seen from the stress path triaxial test, the resulting volume change may be of the opposite sense (expansive) rather than the compressive value indicated in all these prior calculations. In fact, we might conclude here, that if we get a negative undrained pore pressure buildup, followed by a net expansive volume change in the lab, that our finite element and elastic based computations of volumetric strains are misleading. They predict, at best, zero volume change as v approaches $\frac{1}{2}$; and they blow up as v is taken equal to $\frac{1}{2}$ or close to it (> 0.49). Recall that for the undrained FEADAM plane strain results, $\varepsilon_v = 0$ requires that $\varepsilon_3 = -\varepsilon_1$, but FEADAM gives values that only approximate this condition.

Therefore, it may be that finite element or other analyses might only serve to give approximate stresses (not truly correct if v is limited to $\frac{1}{2}$), and that only stress path tests will be capable of accounting for such dilatant volume change ($v > \frac{1}{2}$).

9.5. Stress Path Testing

Figure 9.4a shows the ES and P (i.e. TS- u_s) Mohr circles for the original level ground state, the presumed undrained fill loading state (using the negative field porewater pressure), followed by the drained fill loading case. Fig 9.3 portrays the corresponding equal and opposite effective stress volumetric responses ($\epsilon_{v\text{iso}} = -\epsilon_{v\text{shear}}$) due to $\Delta\bar{\sigma}_3$ (i.e. $\epsilon_{v\text{iso}}$) and $\Delta\sigma_1 - \Delta\sigma_3$ (i.e. $\epsilon_{v\text{shear}}$) that occur during undrained loading (Norris et al, 1997). Note that considerable undrained vertical strain ($\epsilon_1 = \epsilon_{1\text{iso}} + \epsilon_{1\text{shear}}$; $\epsilon_{1\text{iso}} = 1/3 \epsilon_{v\text{iso}}$) and displacement may occur even though total volumetric strain ($\epsilon_v = \epsilon_{v\text{iso}} + \epsilon_{v\text{shear}}$) is zero and volume is preserved. Accordingly, there will be lateral distortion ($\epsilon_3 = -\epsilon_1$ in plane strain or $\epsilon_3 = -1/2 \epsilon_1$ in triaxial or axisymmetric strain). Such strains will be followed by additional strains equivalent to the opening of the drainage valve in the stress path triaxial test and dissipation of the undrained porewater pressure (Δu) at pretty much the same applied stresses (i.e. P_1 and P_2). Based on the characterization shown in Fig 9.3b, Fig 9.4b (with Fig 9.3b reproduced as points x to y) shows the possible volumetric expansion that might result from such drainage (going from point y to z). It is these responses that stress path testing is intended to record.

However, before embarking on such stress path testing, the undisturbed stress path test sample (sample 12 from Pz2 at 10 ft. depth, $e = 0.654$) must first be

reloaded to its initial stress condition corresponding to the average element (OCR = 2). While the end state is important, the changes to be recorded will probably be more a function of how we condition the sample in getting it to the initial (level ground) stress condition. Originally a reconstituted sample (at say, $e = 0.60$) was to be employed in stress path testing, but it was felt that the bedded structure of the natural sample would dramatically affect the pore pressure and the resulting undrained effective stress path. However, in lieu of testing an undisturbed sample at higher pressures to overcome disturbance effects, the authors decided to reload the specimen in a fashion similar to that envisioned for conditioning a reconstituted sample.

Figure 9.5 shows the stress path loading used to get to the initial stress state. First, the specimen is back pressure saturated at an effective confining pressure of 25 kPa. The sample is then isotropically consolidated to 40 kPa and with $P_3 = \bar{\sigma}_3$ held at this value, the sample is sheared with $\sigma_d = 60$ kPa yielding a $P_1 = \bar{\sigma}_1 = 100$ kPa, to simulate the preconsolidation pressure P'_p of 100 kPa (OCR = 2) for a $K_0 = 40/100 = 0.4$ at 10 ft. depth. The sample is then unloaded in shear to zero, yielding the isotropic pressure $P_3 = \bar{\sigma}_3 = 40$ kPa. Thereafter, the confining pressure is reduced to $P_3 = \bar{\sigma}_3 = 25$ kPa before being sheared (while holding $\bar{\sigma}_3 = 25$ kPa) to $\sigma_d = 25$ kPa or $P_1 = \bar{\sigma}_1 = 50$ kPa.

Fig 9.6 shows the various responses

$$\sigma_d - \varepsilon_1$$

$$\varepsilon_v - \varepsilon_1$$

$$\varepsilon_v - \bar{\sigma}_3$$

$$\sigma_d - \varepsilon_v$$

during drained conditioning of sample 12. In particular, note that a cumulative volumetric strain of $\varepsilon_v = 0.55\%$ results. (This causes a negligible change in e .) Of a special interest is the volumetric strain that occurs in shear unloading (point 3 to point 4) in the $\varepsilon_v - \varepsilon_1$ plot.

At this point the sample is ready for application of the undrained stress changes due to fill loading followed by the drained changes as indicated in Fig 9.4. Of course the undrained ES circle shown is for the presumed $\Delta u = -6$ kPa as obtained from piezometric readings, and the question here is whether or not stress path testing will yield the same response.

Fig 9.7 shows the all important responses during undrained loading. Note that this loading was carried out by first increasing P_3 (25 to 75 kPa) while maintaining $\sigma_d = 25$ kPa (point 6 to 7) and then shearing from $\sigma_d = 25$ to 150 kPa at constant P_3 (= 75 kPa). As can be seen, a considerable amount of axial (ε_1) and lateral (ε_3) strain developed, much much more than the values predicted by FEADAM ($\pm 0.078\%$, $\pm 0.051\%$). Of course, one needs to convert triaxial strains to

equivalent plane strain values to compare with the plane strain FEADAM results ($\varepsilon_1 = -\varepsilon_3$, $\varepsilon_2 = 0\%$), i.e.

triaxial	equivalent plane strain
$\varepsilon_1 = \frac{\sigma_{d_1}}{E} = 3.1\%$	$\varepsilon_1 = \frac{\sigma_{d_1}}{E} - \nu \frac{\sigma_{d_2}}{E} = 3.1 - \frac{1}{2} \left(\frac{1}{2} 3.1 \right) = 2.3\%$
$\varepsilon_2 = \varepsilon_3$	$\varepsilon_2 = -\nu \frac{\sigma_{d_1}}{E} + \frac{\sigma_{d_2}}{E} = 0$
$\varepsilon_3 = -\nu \frac{\sigma_{d_1}}{E} = -1.5\% \left(\nu = \frac{1}{2} \right)$	$\sigma_{d_2} = \frac{1}{2} \sigma_{d_1} \left(\nu = \frac{1}{2} \right)$
$\varepsilon_v = 0\% \text{ (0.04 \% recorded)}$	$\varepsilon_3 = -\nu \frac{\sigma_{d_1}}{E} - \nu \frac{\sigma_{d_2}}{E} = -\frac{1}{2} (3.1) - \frac{1}{2} \left(\frac{1}{2} 3.1 \right)$
	$= -2.3\%$
	$\varepsilon_v = 0\%$

While this large disagreement in values ($\varepsilon_1 = 2.3\%$ versus 0.078%) is partly the disturbance effect on the stress path response of the undisturbed sample (even after the conditioning phase), more of the disagreement is due to the difference in the undrained strength of 5 ksf used for the FEADAM analysis and the estimated value of 2 ksf from the projected undrained ESP from this phase of the triaxial test. More on this in a moment.

Note that contrary to expectations, the porewater pressure that resulted is a positive 35 kPa, not the -6 kPa the authors hoped would occur. As shown in Fig

9.7, \bar{A} is a dilatant -0.11 not the -0.45 expected. (By contrast, sample 8 had an $\bar{A} = \frac{\Delta u_d}{\sigma_d} = -0.3$ but this was for a lower $e = 0.560$ or $D_r = 72\%$.) Consequently the resulting ES circle is from 38 to 188 kPa and not the 81 to 225 kPa circle shown in Figs 9.3 and 9.4, and the effective confining pressure is $\bar{\sigma}_3 = 38$ kPa not 81 kPa.

If one projects this undrained ES path to the effective stress failure envelope to establish the associated undrained strength (S_u), the resulting value is 92.5 kPa or approximately 1 tsf = 2 ksf as shown in Fig 9.8. (Note this projection is based on the actual measured ϕ of 41.6° obtained at the conclusion of the drained fill loading phase to be described later. More importantly, it assumes that the undrained resistance will not increase by ES path movement up the failure envelope.) This means that the undrained stress level (SL) of the representative location is 81 %, not the low value of 75/260 or 29 % as implied in the FEADAM analysis.

If the results from the FEADAM analysis for the $S_u = 2$ ksf undrained case are considered instead, the resulting representative location stresses and strains are

$$\begin{array}{ll} P_1 = 224 \text{ kPa} & \varepsilon_1 = 0.10 \% \\ P_3 = 80 \text{ kPa} & \varepsilon_3 = -0.095 \% \\ \sigma_d = 144 \text{ kPa} & \end{array}$$

at a stress level of $(144/2)/100$ or 72 %. If one considers the stress path test strains obtained at this earlier or smaller undrained stress level (0.72 instead of 0.81), the equivalent plane strain values of ± 2.3 % will be considerably reduced, but not down to the level of ± 0.1 % from FEADAM.

For further contrast, the corresponding values from the FEADAM undrained $S_u = 1$ ksf computer run,

$P_1 = 223$ kPa	$\epsilon_1 = 0.9$ %
$P_3 = 112$ kPa	$\epsilon_3 = -0.4$ % (note)
$\sigma_d = 112$ kPa	SL \rightarrow 1

yield strains that are be in reasonable agreement with the adjusted stress path values, but it would seems that this is not a fair basis for comparison, i.e. $S_u = 1$ ksf instead of the stress path test projected $S_u = 2$ ksf. Note, however, from the ES path for the undrained test on sample 8 in Fig 7.10, that undrained resistance of a dense sand ($e = 0.560$) will increase via dilatant movement along the failure envelope. (On the other hand, it will be limited for a loose sand, $e = 0.746$, as in sample 3's ES path.) But this increased undrained resistance requires considerable additional strain (as shown in Fig 7.9) for the dilatant porewater pressure (see Fig 7.4) to develop, thereby, causing $\bar{\sigma}_3$ and the effective stress resistance

$(\sigma_d = \bar{\sigma}_3 \left[\tan^2 \left(45 + \frac{\phi}{2} \right) - 1 \right])$ to increase progressively. As seen in Fig 7.9, the stress - strain curve for such response (sample 8) is not the nice hyperbolic shape corresponding to that of loose sand (sample 3) whose ES path basically terminates once the ES failure line (see Fig 7.10) is first reached. Since recommended FEADAM input parameters for undrained response are modeled after clay, and clay's stress - strain curve is characteristic of the shape of the loose sand (sample 3), not the strain hardening curve of dense / dilatant sand (sample 8), it should be expected that strains predicted by FEADAM will be very low¹. However, if we assume a fictitiously lower undrained strength (i.e. $S_u = 1$ ksf) for such dilatant material then we are, in effect, better modeling the steeper initial portion of the material's stress - strain curve (e.g. up to $\epsilon_1 = 2\%$ for sample 8's curve in Fig 7.9) in our FEADAM analysis². If we don't, the FEADAM strains will be very low as compared to actual behavior. On the other hand, such FEADAM modeling will not permit the dilatant strain hardening that we see in sample 8 once stresses reach this fictitious strength. Therefore, successful modeling of the undrained response

¹ Likewise, $E = K S_u$ in the undrained settlement (ρ_i) calculation considered earlier will be way too stiff, because $K = 1000 S_u$ corresponds to clay's response.

² We might do the same for the immediate settlement calculation, i.e. keep $E = 1000 S_u$ but consider a fictitious $S_u = 1$ ksf

of a dilatant sand requires arbitrary adjustment of FEADAM strength values. Furthermore, we cannot automatically assume the stress path test stress - strain response we observe in the lab is necessarily correct. In other words, the lab recorded response exhibits, to some agree, the effects of sample disturbance, and without differential settlement measurements in the upper portion of the deposit we can not know the strains that actually developed during undrained fill loading.

Next Let us compare the stress path drained or end state response versus that obtained from drained FEADAM analysis. Recognize that while the undrained stress path response is needed to try to simulate the dilative porewater pressure response recorded, such response is short lived and we traditionally just consider loading of such soil as drained (relative to construction rates of loading). Given that the sample survives the undrained stress path load state, the cumulative undrained and drained strains from the triaxial test should be comparable to the FEADAM solution for $\phi = 41^\circ$ (Table 9.1).

To undertake such triaxial test loading, the back pressure from the CKC volume change device must first be raised to match the internal sample porewater pressure (i.e. with the $\Delta u = 35$ kPa) before the drainage valve to the volume change device is opened. Thereafter, the stresses applied to the sample, P_1 and P_3 ,

and the effective stresses ($\bar{\sigma}_3 = P_3$ and $\bar{\sigma}_1 = P_1$) are adjusted to match the drained FEADAM values. Since backpressure is maintained constant, a drained response is obtained.

The effective stresses of $\bar{\sigma}_3 = 38$, $\bar{\sigma}_1 = 188$ kPa ($\sigma_d = 150$ kPa) in undrained loading are raised to those of the drained loading case ($\bar{\sigma}_3 = 70$ and $\bar{\sigma}_1 = 225$, $\sigma_d = 155$ kPa) by first raising the effective confining pressure ($\bar{\sigma}_3$) from 38 to 70 kPa at a constant $\sigma_d = 150$ kPa as shown in Fig 9.9. For this change an $\varepsilon_{1ISO} = 0.03$ % and $\varepsilon_{VISO} = 0.08$ % were recorded. The sample is then sheared at a constant $\bar{\sigma}_3 = 70$ kPa as in a standard drained test. A point 10 corresponding to the fill drained loading condition was achieved during the course of this response. Fig 9.10 shows the drained loading to failure ($\phi = 41.6^\circ$). Note that the volume change curve that resulted was very flat just like that of sample 2 (see Fig 7.6). The corresponding strains (ε_1 and ε_v) from $\sigma_d = 150$ to 155 kPa corresponding to the mobilization of the drained loading condition (point 10) were negligible.

Collectively the cumulative strains from level ground to drained fill loading from the stress path test were

$\varepsilon_1 = 3.1$	$\varepsilon_3 = -1.5$	Undrained
$= 0.03$	$= 1/2 (0.08 - 0.03)$	Drained $\bar{\sigma}_3$ change
$= 0$	$= 0$	Drained σ_d change
<hr/>	<hr/>	<hr/>
3.1 %	-1.5 %	Total

most of which occurred during undrained loading. These correspond to plane strain values of 2.3 and -2.3 % respectively. If we compare these latter values with those from the drained FEADAM loading case ($\phi = 41^\circ$) from Table 9.1 (i.e. ± 0.41 %), we see that there is considerable difference. Recall that the Schmertmann method gave $\varepsilon_1 = 0.24$ to 0.68 % and the Hough method, $\varepsilon_1 = 1.27$ %, by comparison.

If one considers, instead, stress path drained fill loading strains as evaluated from purely drained triaxial test response, rather than the stress path undrained followed by the drained response, then different final strains may result. No purely drained stress path test was undertaken, though drained tests on samples 5 and 6 can be used as good approximations. Sample 5 was the K_0 consolidated sample ($e = 0.661$) that was then sheared to failure ($\phi = 40.5^\circ$, $\bar{\sigma}_3 = 77$ kPa), while sample 6 ($e = 0.585$) was isotropically consolidated to $\sigma_{3c} = 80$ kPa and then sheared to failure ($\phi = 40.7^\circ$). Recall that both samples exhibited $\varepsilon_1 = \varepsilon_v =$

0.9% at a K_0 condition ($\sigma_d = 120$ kPa) and yielded additional ϵ_1 and ϵ_v strains as σ_d was raised at a constant $\bar{\sigma}_3$. Given that the 30 kPa forming pressure for samples 5 and 6 is approximately the mean pressure for the in situ level ground condition of Fig 9.4, and we adjust the results to reflect the desired drained fill loading condition of Fig 9.4 ($\bar{\sigma}_3 = 70$, $\sigma_d = 155$ kPa), then an estimate of ϵ_1 and ϵ_v for purely drained conditions can be obtained from these tests. Note that the desired stress ratio for fill loading is $225/70 = 3.21$; therefore, for the same stress ratio, $\bar{\sigma}_1 = 3.21 (77) = 247$, $\sigma_d = 247 - 77 = 170$ kPa for sample 5 and $\bar{\sigma}_1 = 3.21 (80) = 257$, $\sigma_d = 257 - 80 = 147$ kPa for sample 6. In going from the K_0 condition ($\sigma_d = 120$ kPa, $\epsilon_1 = \epsilon_v = 0.9\%$) in both these tests, to the respective adjusted σ_d values, one obtains an additional ϵ_1 of 0.4% in both tests, and an additional ϵ_v of 0.2% in sample 5 and 0.15% in sample 6. Accordingly, the total drained strains are $\epsilon_1 = 1.3\%$ (i.e. $0.9 + 0.4$) and $\epsilon_v = 1.1\%$ (i.e. $0.9 + 0.2$ or 0.15) and $\epsilon_3 = \frac{1}{2} (\epsilon_v - \epsilon_1) = -0.1\%$. (A similar treatment of the sample 4 response ($e = 0.642$, $\phi = 42.5^\circ$, $\sigma_{3c} = 65$ kPa) yields a total drained $\epsilon_1 = 1.3\%$ but $\epsilon_v = 1.5\%$ and, therefore, $\epsilon_3 = +0.1\%$.) The corresponding equivalent plane strain value is 1.0%.

It is anticipated that such strains would have been obtained on the conditioned stress path test sample ($e = 0.654$) had it been subjected to the same

purely drained conditions. Therefore, a great deal of the stress path test sample's ϵ_1 strain of 3.1% arises from the much lower effective confining pressure ($\bar{\sigma}_3 = 38$ kPa) and higher effective stress ratio ($38+150/38 = 4.95$, rather than $225/70 = 3.21$) that results during undrained loading, prior to dissipation of the net positive value of pore pressure (i.e. $50-13 = 37$ kPa), and the establishment of final effective stresses. In fact, if we consider the drained axial strain from the test on the reconstituted sample 7 ($\bar{\sigma}_3 = 30$ kPa, $e = 0.560$, $\phi = 43.6^\circ$) at this stress ratio (i.e. $\bar{\sigma}_1 = 4.95 (30) = 148$, $\sigma_d = 148-30 = 118$ kPa), the axial strain (ϵ_1) is 3.0%, very close to the 3.1% in undrained stress path response at $\bar{\sigma}_3 = 38$ kPa.

Therefore, it remains as an unresolved question as whether the undrained - drained stress path test (2.3 %), the drained triaxial test (1 %) or the drained FEADAM results (0.4 %) best predicts the drained strains that occurred in the field at the average element location after dissipation of any excess porewater pressure. Note that the stress path test result is dominated by the undrained strain but for sample 12's void ratio of 0.654 only a small negative pore pressure developed (i.e. $\bar{A} = -0.1$). If we consider the undrained test on sample 8 ($e = 0.560$) instead, an $\epsilon_1 = 2$ % develops at $\sigma_d = 150$ kPa corresponding to a $\Delta u_d = -15$ kPa ($\bar{A} = -15/150 = -0.1$; even though \bar{A} later rises to -0.3). The equivalent plane strain ϵ_1 is,

therefore, 1.5 % which is lower than the 2.3 % from the stress path test ($e = 0.654$). A sample that would yield an $\bar{A} = -0.45$ would, of course, experience an ϵ_1 value much close to the FEADAM drained response (since undrained $\bar{\sigma}_3$ would be higher, 81 kPa, than for the drained state $\bar{\sigma}_3 = 70$ kPa). Given that sample disturbance probably affected the stress path test sample response, while the absence of layering in the reconstituted sample 8 caused its similar smaller negative pore pressure, a value of $\bar{A} = -0.45$, in keeping with the recovered -6 kPa ($50-56 = -6$ kPa) should have been expected of this material in situ.

9.6. Discussion

While stress path testing is usually employed on clays, the silty sand of the flow regime of interest had enough fines to hold the undisturbed samples and layers together via capillary tension. Consequently, stress path testing for the Zolezzi lane soil was attempted. Unfortunately the conditioning cycle employed was not sufficient to overcome the large amount of sample disturbance to such soils. (Normally only reconstituted samples of sand are tested.) Therefore, the strains obtained to simulate undrained and drained loading were very large as

compared to the values predicted from the finite element analysis. Of course, the FEADAM results could not be calibrated against field strains since no settlement measurements were taken. Therefore, such results had to be calibrated against other values of predicted undrained and drained settlements.

It is expected that the FEADAM undrained response is best characterized based on an equivalent fictitious undrained strength (S_u) of 1 ksf. Such a fictitious strength value is required in order to better model the resulting stiffer portion of the undrained stress - strain curve of such dilatant material.

Note that the only way to provide prediction that a dilative pore pressure should be expected from such undrained fill loading was through the stress path or the standard undrained triaxial tests. Certainly, there was negative pore pressure ($\bar{A} < 0$) generated during shear loading, i.e. $\bar{A} = -0.1$ during the stress path test ($e = 0.654$) and -0.3 during the later stage of the standard undrained test on sample 8 ($e = 0.560$). However, a value of -0.45 would have been required to overcome the positive porewater pressure increase due to $\Delta\sigma_3$ to yield a net negative value of 6 kPa corresponding to the 2 ft. drop indicated in the highlighted piezometers of Fig 6.22. While an $\bar{A} = -0.3$ for $e = 0.560$ ($D_r = 70\%$) might indicate that such a value of -0.45 is possible (at higher D_r) in tests on undisturbed samples, the range

in values of D_r as established from void ratios (i.e. water contents) of Table 7.5 indicate this might only occur (i.e. $D_r > 70\%$) at Pz3 location. However, sample disturbance in the present tests most likely loosened the undisturbed sample and caused it to lose dilatant behavior. Therefore we can argue that such response is possible but not definitively proven. Freezing the soil in situ, before taking undisturbed samples, would reduce disturbance, but such effort would be prohibitively expensive.

Table 9.1 Undrained and Drained Strains and Settlements

Settlement Calculations for Undrained Case (all layers except the artesian undrained) (c=5 ksf)												
Soil Type	Element No.	Element Ht		ϵ_y	Settlement		Element No.	Element Ht		ϵ_y	Settlement	
		ft	in		ft	in		ft	in		ft	in
Above the	299	11.85	0.04	0.005	0.057	300	11.60	0.041	0.005	0.057	0.005	0.057
Artesian	245	11.68	0.04	0.005	0.056	246	11.63	0.04	0.005	0.056	0.005	0.056
Artesian	191	15.00	0.368	0.055	0.662	192	15.00	0.374	0.056	0.673	0.056	0.673
Below the	137	12.00	0.017	0.002	0.024	138	12.00	0.017	0.002	0.024	0.002	0.024
Artesian	81	11.00	0.012	0.001	0.016	82	11.00	0.012	0.001	0.016	0.001	0.016
	29	13.50	0.007	0.001	0.011	30	13.50	0.007	0.001	0.011	0.001	0.011
				0.069	0.827				0.070	0.838		

Settlement Calculations for Undrained Case (only layer above the artesian undrained) (c=5 ksf)												
Soil Type	Element No.	Element Ht		ϵ_y	Settlement		Element No.	Element Ht		ϵ_y	Settlement	
		ft	in		ft	in		ft	in		ft	in
Above the	299	11.85	0.054	0.006	0.077	300	11.60	0.054	0.006	0.075	0.006	0.075
Artesian	245	11.68	0.098	0.011	0.137	246	11.63	0.101	0.012	0.141	0.012	0.141
Artesian	191	15.00	0.47	0.071	0.846	192	15.00	0.483	0.072	0.869	0.072	0.869
Below the	137	12.00	1.467	0.176	2.112	138	12.00	1.467	0.176	2.112	0.176	2.112
Artesian	81	11.00	1.098	0.121	1.449	82	11.00	1.098	0.121	1.449	0.121	1.449
	29	13.50	1.119	0.151	1.813	30	13.50	1.138	0.154	1.844	0.154	1.844
				0.536	6.435				0.541	6.491		

Settlement Calculations for Drained Case (all layers) ($\phi=41^\circ$)												
Soil Type	Element No.	Element Ht		ϵ_y	Settlement		Element No.	Element Ht		ϵ_y	Settlement	
		ft	in		ft	in		ft	in		ft	in
Above the	299	11.85	0.405	0.048	0.576	300	11.60	0.41	0.048	0.571	0.048	0.571
Artesian	245	11.68	0.405	0.047	0.567	246	11.63	0.414	0.048	0.578	0.048	0.578
Artesian	191	15.00	0.515	0.077	0.927	192	15.00	0.515	0.077	0.927	0.077	0.927
Below the	137	12.00	1.487	0.178	2.141	138	12.00	1.53	0.184	2.203	0.184	2.203
Artesian	81	11.00	1.118	0.123	1.476	82	11.00	1.168	0.128	1.542	0.128	1.542
	29	13.50	1.104	0.149	1.788	30	13.50	1.123	0.152	1.819	0.152	1.819
				0.623	7.476				0.637	7.640		

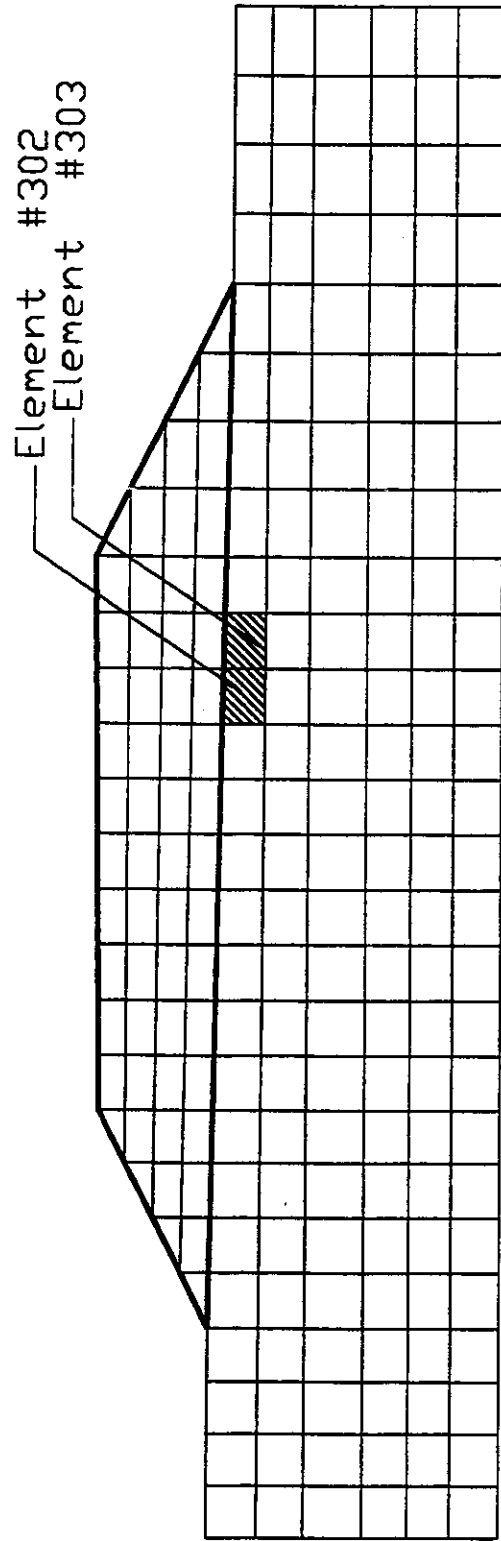


Fig 9.1 Location of Elements 302 and 303 within the Finite Element Mesh

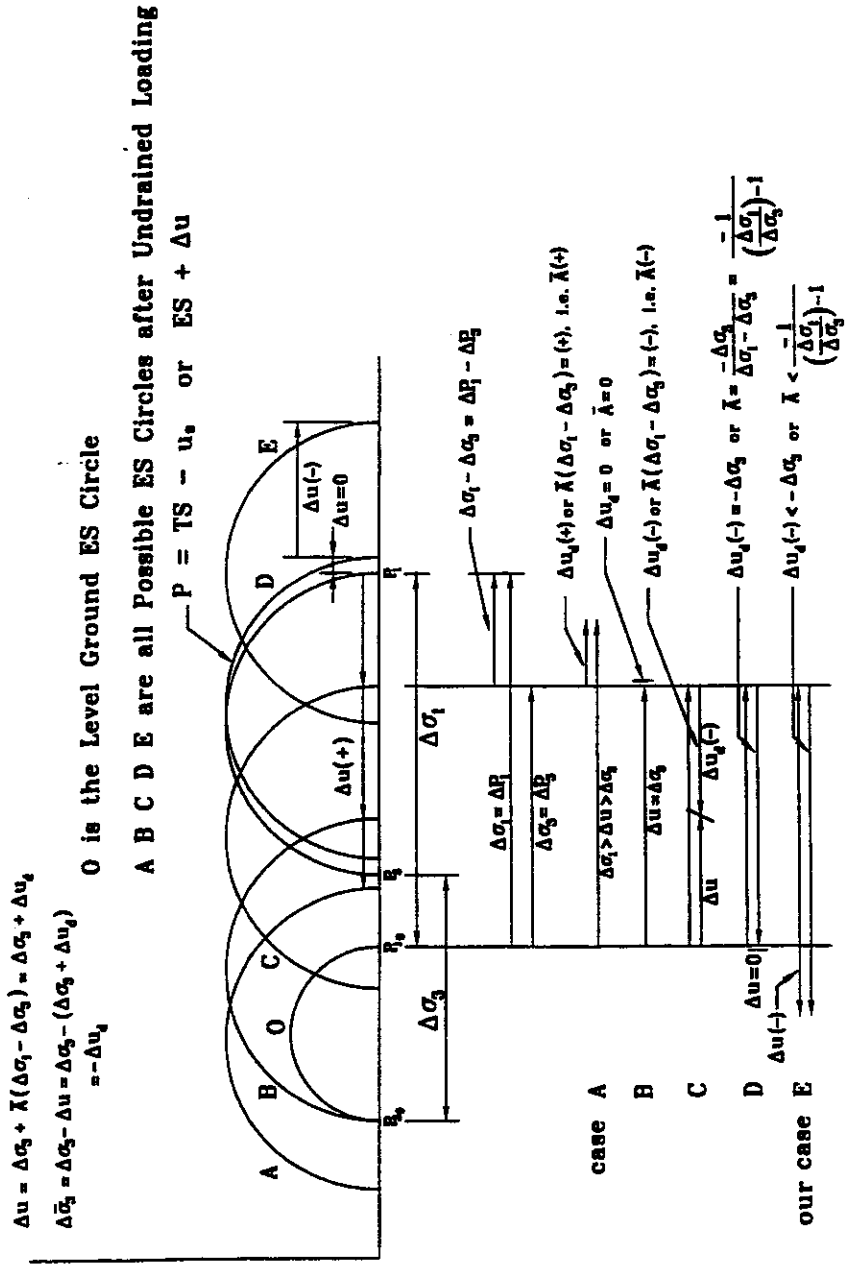


Fig 9.2 Possible Pore Pressures and Undrained Effective Stress Circles

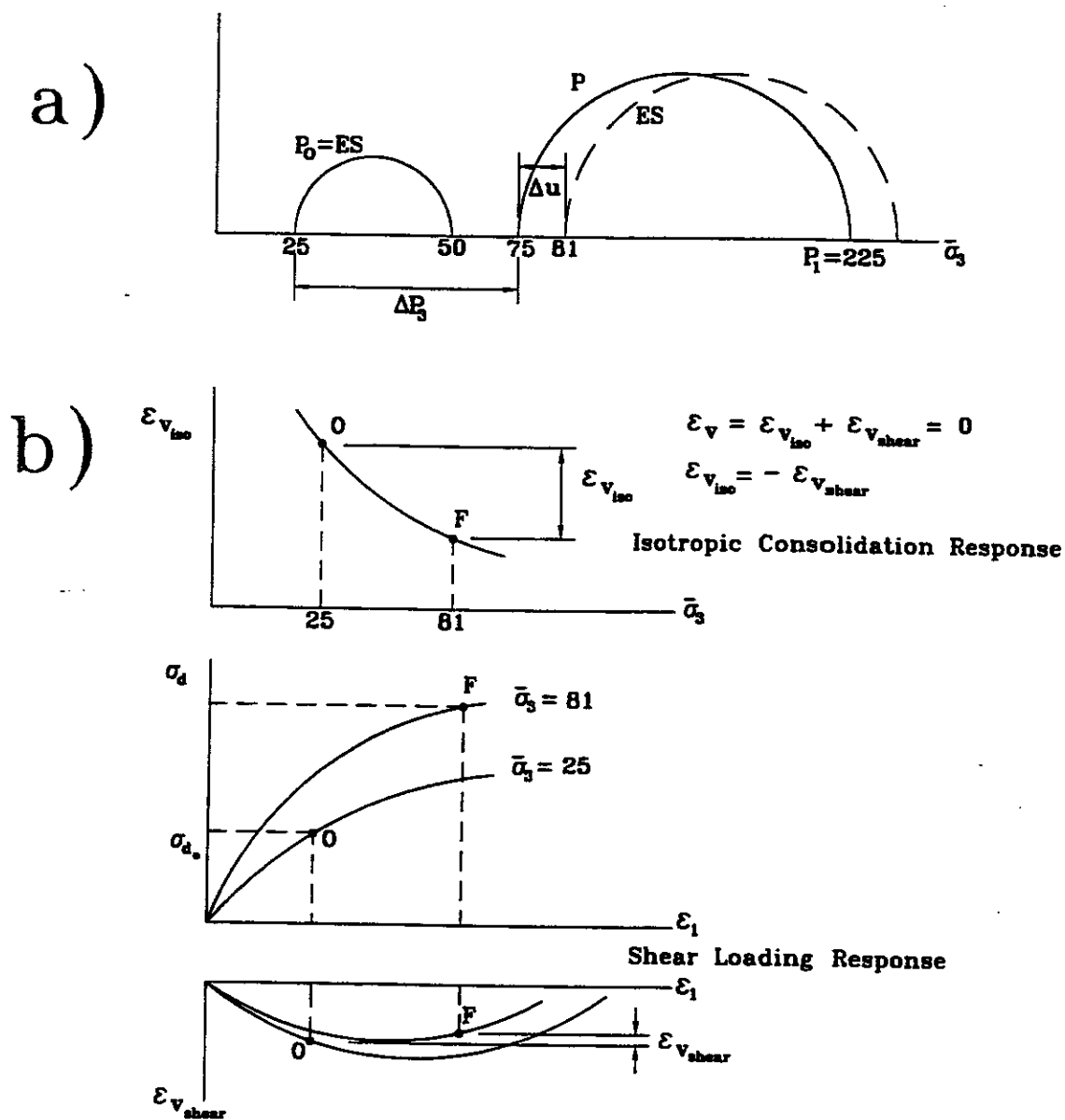


Fig 9.3 Presumed a) Stress and b) Counteracting Volume Change Responses (Pz4 at 10 ft.) due to undrained fill loading.

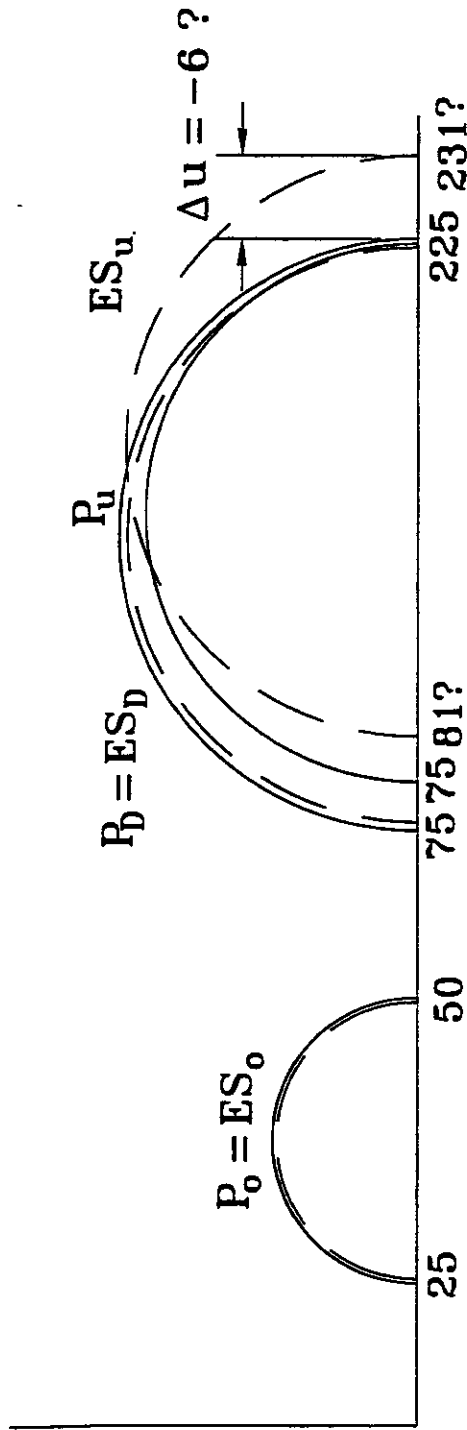
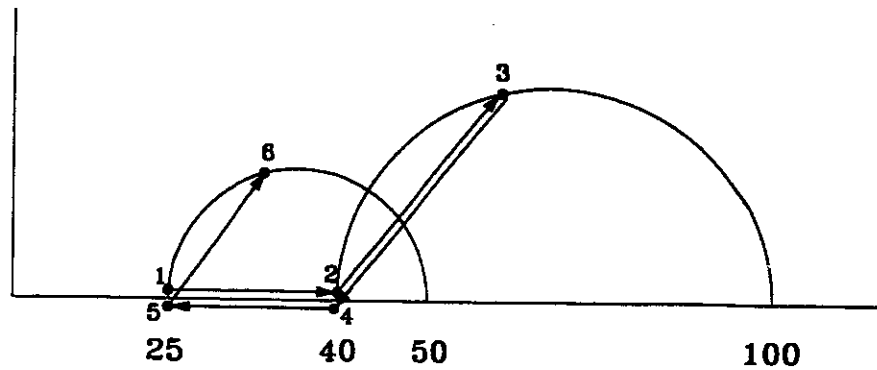


Fig 9.4 Presumed stress Changes going from Initial (Level Ground) to the Undrained to the Drained Fill Loading Case at Pz4 at 10 ft.



$$P_p = 100 \text{ kPa}$$

$$\text{OCR} = \frac{100}{50} = 2$$

$$K_o = \frac{40}{100} = 0.4 \text{ at } \bar{\sigma}_3 = 40 \text{ kPa}$$

$$K_o = \frac{25}{50} = 0.5 \text{ at } \bar{\sigma}_3 = 25 \text{ kPa}$$

Fig 9.5 Drained Conditioning of the Undisturbed Sample 12 Prior to Undrained Testing

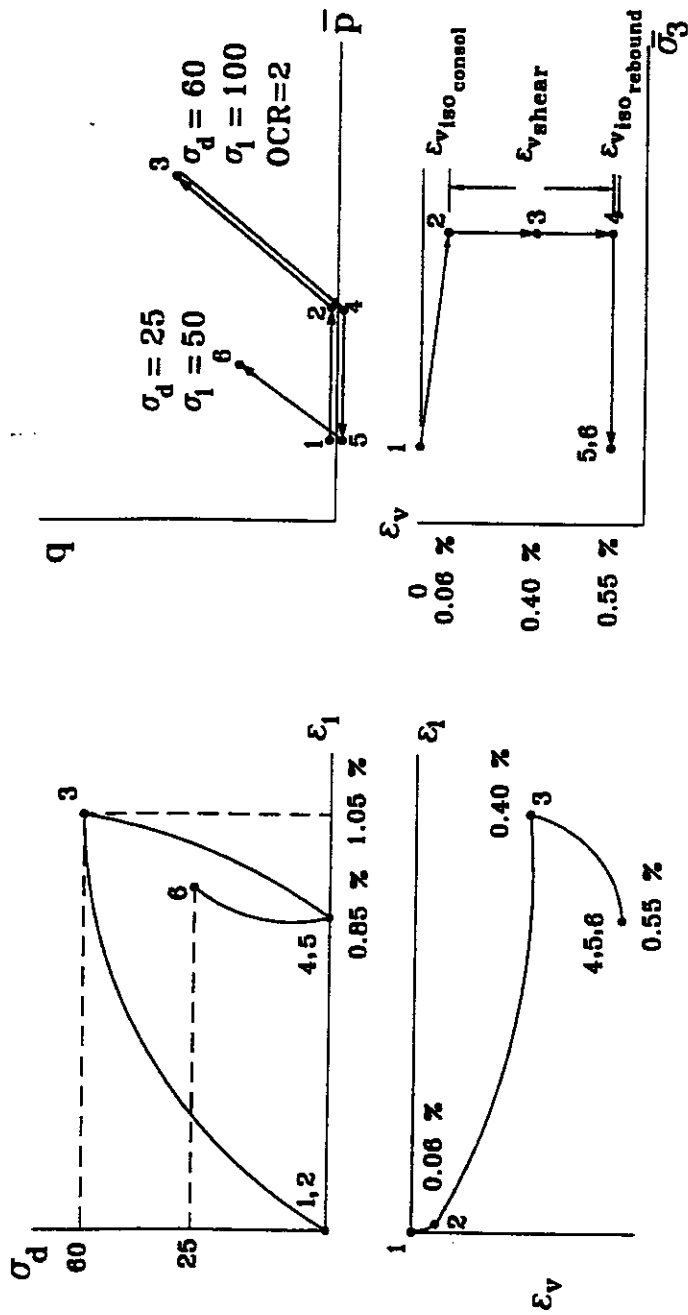


Fig 9.6 Stress Path Sample Response During Conditioning Phase

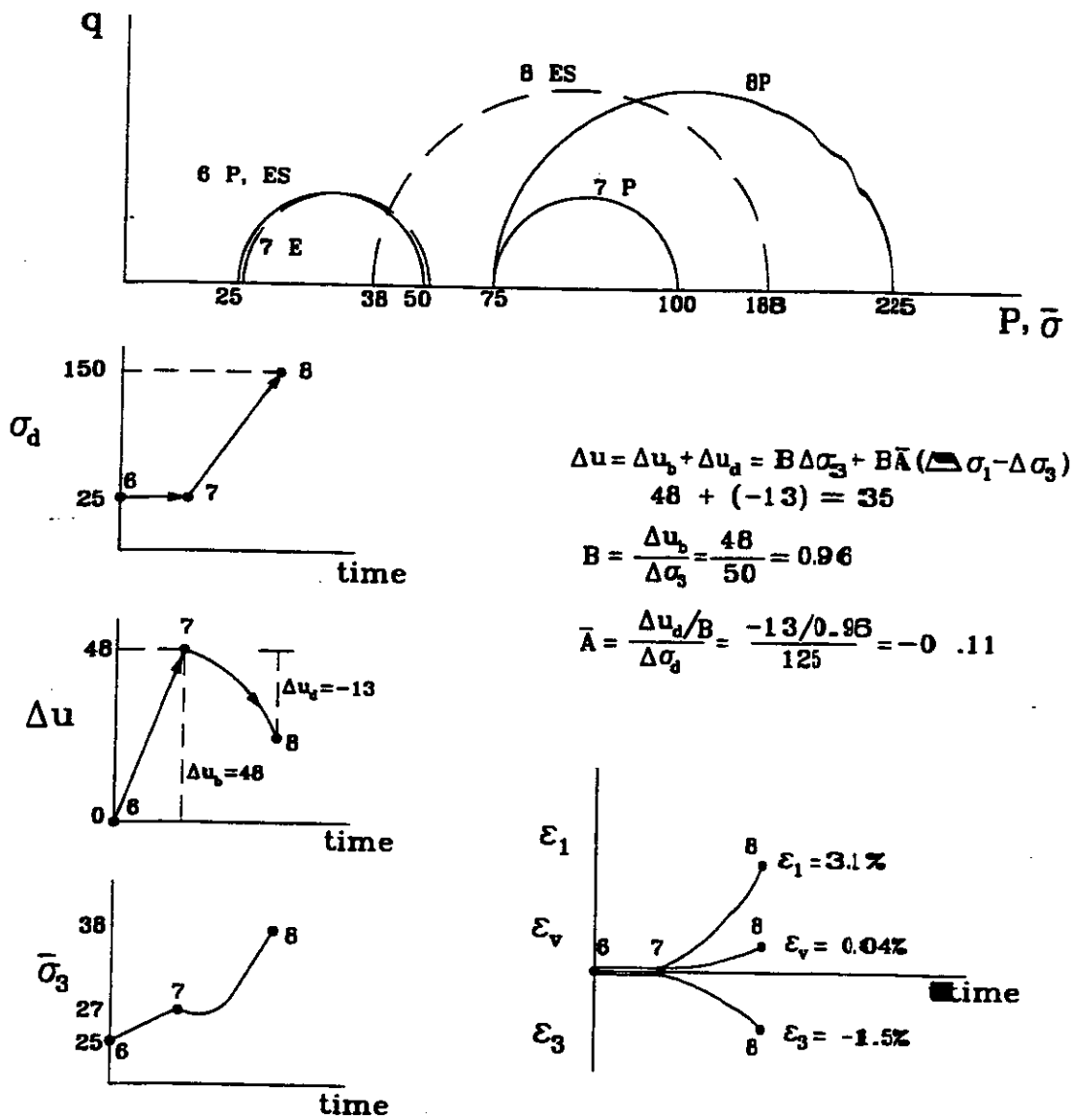


Fig 9.7 Stress Path Sample Response During Undrained Loading

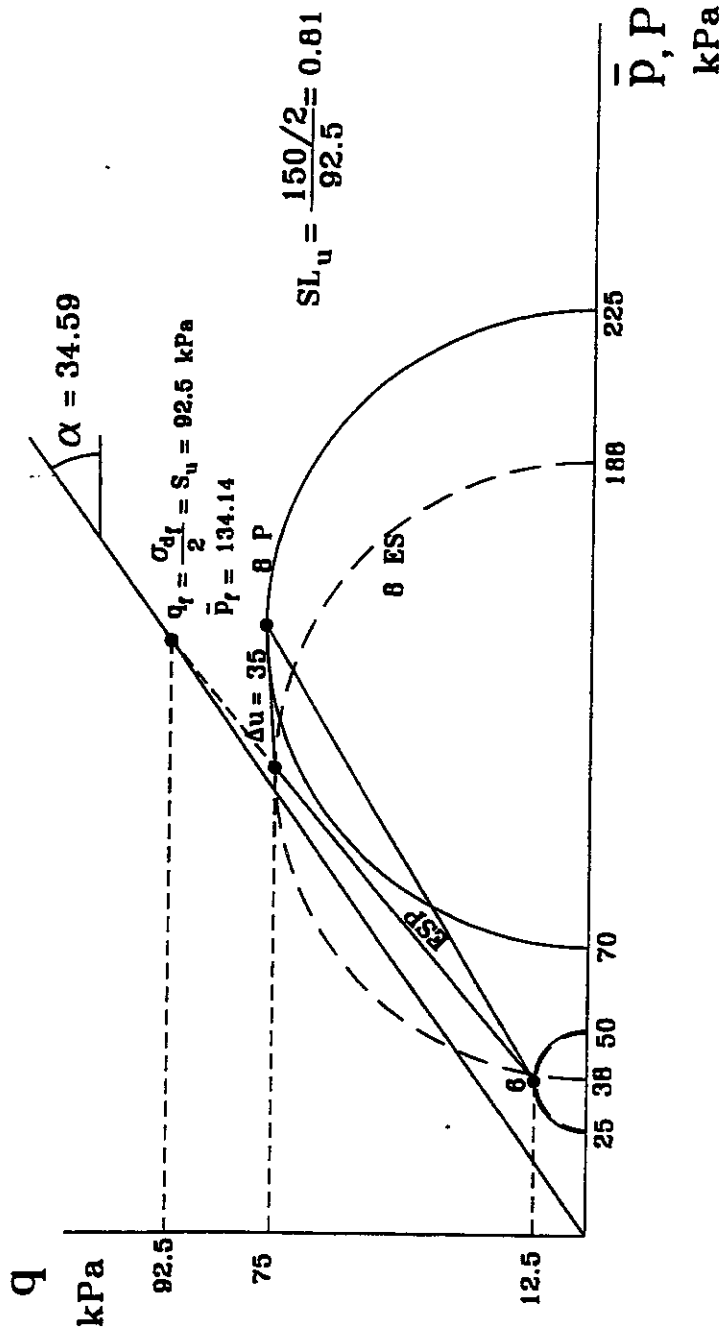


Fig 9.8 Undrained Strength and Stress Level

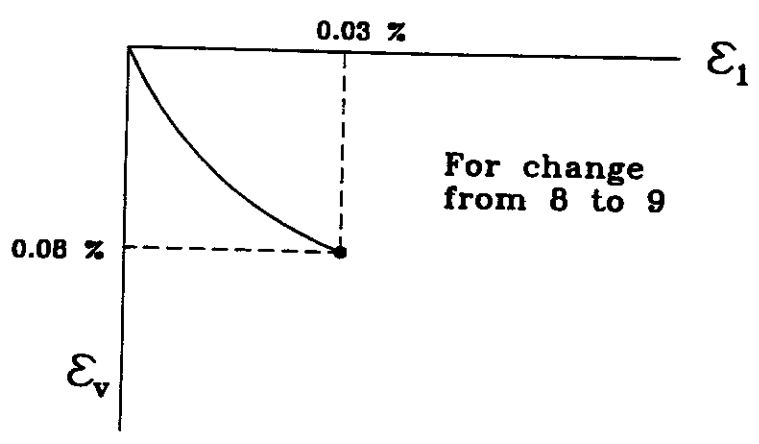
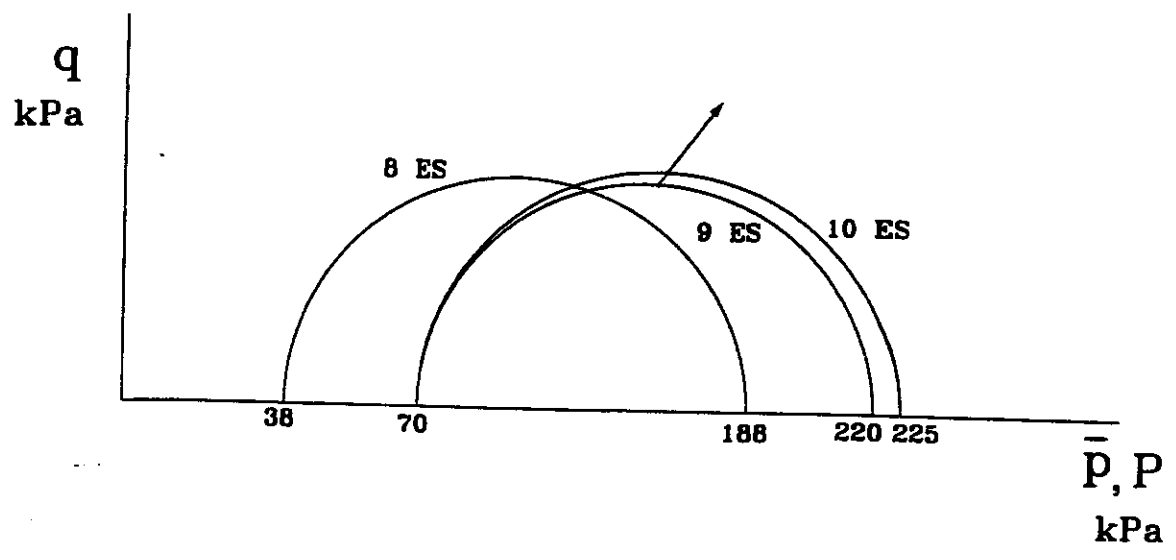


Fig 9.9 Undrained to Drained Fill Loading

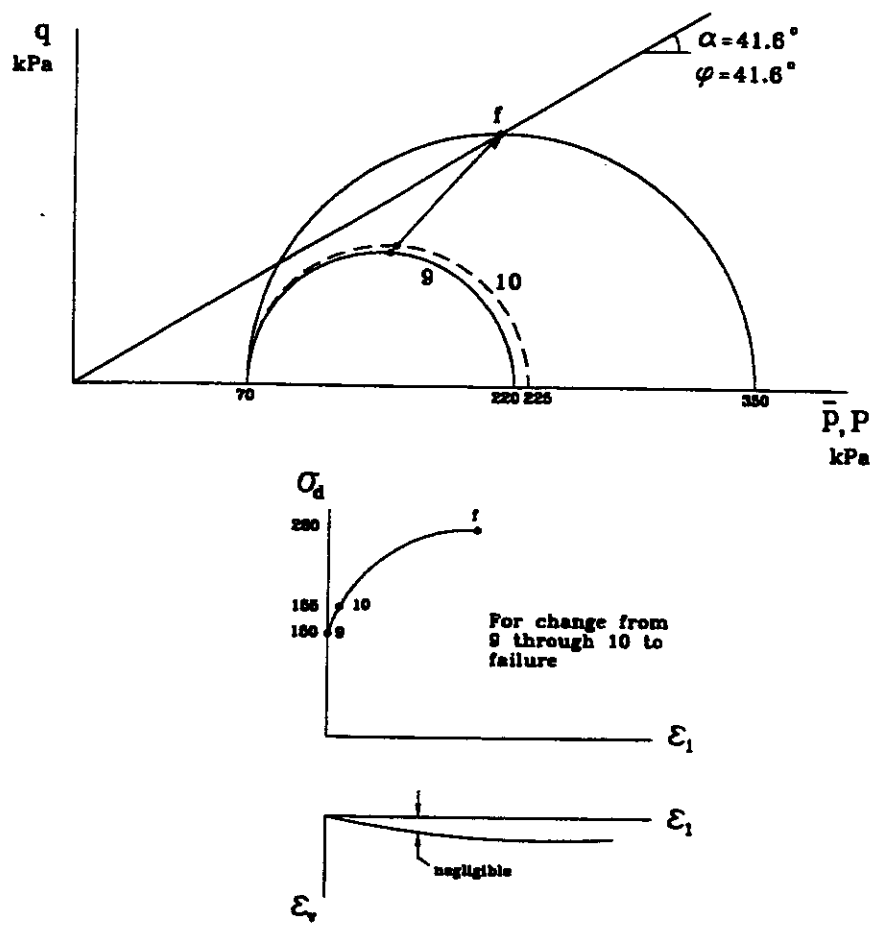


Fig 9.10 Drained Loading to Failure

Chapter 10

Conclusions and Recommendations

10.1. Project Response at a Glance

The good news relative to the question of possible changes in groundwater flow conditions due to fill construction is that at an alluvial deposit such as the Zolezzi Lane site, that despite lower blow counts of 6 to 12 in the upper 17 ft. (and > 20 between 17 and 21 ft.), that the construction of a 30 ft. high fill caused no volume change or change in permeability in this upper silty sand sitting on top of the artesian layer (starting at 21 ft. depth). As shown by the piezometer readings, there were no significant jumps from the seasonal variation in water flow over the two years of readings. If anything, there was a small dilatant water level or porewater pressure drop. Therefore, all the fears of a significant compression of this material leading to a damming up of water and loss of downstream flow were unfounded.

However, these conclusions are specific to the medium dense to dense silty sand (SM) at Zolezzi that contained root holes to greater than 10 ft. depth. Whether this would be true of a looser sand has not been answered. Certainly, had this site been a clay site, this fear might have materialized.

10.2. Lessons Learned

There were several lessons that the authors learned as a result of this research project. First of all, do not believe all of what you read (geologic maps) or receive (CPT interpretations). Contrary to what we thought going into the project, the soil at this site was cohesionless ($PI = 0 - 5$). The fact that it had 35 % or greater fines means that by the AASHTO soil classification system (not the Unified) it might be classified as a silt-clay soil, but it was a silty sand of negligible plasticity.

If CPT results are obtained, they need to be checked against the actual soil (grain size and Atterberg limits results). Certainly if a piezo cone is used, one should pay particular attention to any dilative (negative) porewater pressure data, both in terms of what material is present and what to expect in porewater pressure changes (negative not positive) when it is loaded.

Certainly a very easy and very beneficial task that the NDOT field crew should routinely undertake is to obtain numerous water content samples from the split spoon sampler because they can be used to assess $e (= w G_s)$ for samples from below the water table ($S = 1$). Likewise, $e_{max} (\gamma_{dmin})$ and $e_{min} (\gamma_{dmax})$ values should be determined in the lab so that relative density can be established directly to compare with interpreted values from blow counts. Where possible, blow counts should be assessed after first equalizing the water in the hole with that

outside it, then there will be no question of any loosening effect.

Note that undisturbed samples and reconstituted samples plotted along the same strength relationship (ϕ versus e , Fig 7.2). Therefore, for this young medium to dense sand with this high percentage of fines, sample disturbance did not seem to have a significant effect of the drained friction angle. Further, such strength results proved to be much less conservative than commonly used correlations (see Fig 7.12) and yet fit nicely with other data (see Fig 7.3). It is the senior author's personal experience (Norris, 1977) that strength is much better correlated with e than D_r .

If standard drained strength tests are undertaken, the volume change curve will be extremely helpful in ascertaining whether dilatant behavior is to be expected in the field. Note, also, that we start at the K_0 condition in the field and, therefore, near the bottom of the volume change curve (see Fig 7.8), such that any shear above K_0 conditions will likely generate dilatancy (provided the volume change curve starts to ascend).

Definitely, one should undertake grain size analysis (i.e. get D_{50} and C_u) or save labeled samples so that such information can be obtained at a later time if needed.

Permeability determinations are a very humbling experience. Definitely the comments of Terzaghi, Peck and Mesri (1996) should be taken to heart. It may be

that a study of the orientation and density of root holes might have helped explain the large variation in permeability, but this is not assured. Certainly, the field results (excluding CPT dissipations) are more likely the correct values for interpretation of field behavior (i.e. flow on the large scale and predominantly in the horizontal direction). Absent of this, tests on reconstituted samples are in as good or better agreement with field results as stress-path triaxial tests on undisturbed samples.

Strains and settlements predicted on the basis of finite element analyses should be calibrated against observed behavior where possible or against more traditional empirical or semi-empirical calculations. Sample disturbance will preclude the evaluation of FEADAM stress - strain parameters from stress path tests on undisturbed samples. However, triaxial tests should be undertaken to establish realistic rather than overly conservative strength (ϕ) values in cases where that might lead to a more economical design. Specialized K_0 and stress path tests don't provide any information that can't be ascertained from standard (isotropically consolidated) drained and undrained tests. More specifically, one needs such standard tests to reason away behavior (volume and porewater pressure changes) observed in the more "sophisticated" tests. In fact, there exists a very great need to better characterize the standard undrained test stress - strain response of such dilatant sands as per Norris et al (1977) procedures based on drained tests

with volume change measurements; because most of the undrained strength increase that occurs is due to the material's dilatant ES path travel along the Mohr - Coulomb failure envelope (see sample 8's path in Fig 7.10) with consequent large strains (see Fig 7.9). Currently employed / recommended hyperbolic finite element stress - strain curve parameters for undrained response characterization are based on tests on clay where such dilatant strain hardening is not present. Therefore, FEADAM or other finite element evaluations of undrained strains and deformations of dilatant sands will remain poor until such improvements are made.

As far as analysis is concerned, no finite element or elastic solution that is limited to $\nu < \frac{1}{2}$ is capable of accurately determining volume change behavior of a dilatant material. Therefore, stress path tests, or better yet, reasoning in light of the response from standard triaxial tests is required to forecast the unusual water level drop in piezometers encountered at Zolezzi. Finite element analyses are only good in assessing approximate stress changes for use in stress path testing. Realize that some consideration should be taken of the membrane effect of the grass mat that acts as equivalent geotextile fabric.

Recognize that stress path tests require appropriate conditioning of the sample leading up to the initial stress state. Volumetric strains evaluated from stress path or standard tests may be used to evaluate void ratio changes due to fill loading. Some idea of the effect of such change on the material's permeability can

be obtained from standard permeability tests on reconstituted material where void ratio is varied.

10.3. Implementation at Future Sites

If future sites (e.g. through the Carson Valley) involve alluvial deposits of a similar character (medium to dense silty sand), then it is likely that it too will be dilative and there will be no net volumetric compression and therefore, no effect on the groundwater flow condition through these near surface soils. Therefore, as such sites are encountered, water contents and void ratios of samples from below the water table should be assessed as well as blow counts. Strength tests on natural samples and reconstituted samples correlated with void ratio should be undertaken to see if such dilatant behavior can be expected. The only analytical analysis that would be required be that needed to assess stress changes for planning lab tests.

If sites involve loose sands or loose silty sands, then the work undertaken by the authors for the Army Corps of Engineers should be consulted (Norris, et al, 1997). Work at sites involving cohesive soils that are compressive rather than dilative will require an effort as originally planned for the Zolezzi Lane site.

Certainly, if there is a question as to the likelihood of any change in groundwater flow conditions, it is recommended that piezometers be installed (maybe only a few) and that seasonal readings be taken one year ahead to one year

after construction. While this may involve a considerable number of man hours, this cost should be weighed against simply having to pay off on a legal settlement should such supporting evidence not to be taken or obtained. Likewise, it might be advisable to install a single vertical line of settlement monitors through the depth of the soil of concern. These "spiders" are relatively simply to install and can be easily read in the same visit that piezometers are read. However, large vertical movements, in and of themselves, do not necessarily indicate compressive volume change. A slope indicator at the toe of the embankment may also be needed to establish lateral distortion so that volume change (net compressive or net dilative / expansive) can be judged.

References

- Bishop, A. W. and Wesley, L. D. (1975), "A Hydraulic Triaxial Apparatus for Controlled Stress Path Testing," *Geotechnique*, Vol. 25, No. 4, p. 657-670.
- Boast, C. W. and Kirkham, D. (1971), "Auger Hole Seepage Theory," *Soil Science Society of America Proceedings*, Vol. 35, No. 3, pp. 365-373.
- Byrne, P. M., Cheung, H. and Yan, L. (1987), "Soil Parameters for Deformation analysis of Sand Masses," *Canadian Geotechnical Journal*, Vol. 24, pp.366-376.
- Cheney, R. S. and Chassie, R.G. (1993), "Soils and foundation Workshop Manual," Publication No. *FHWA HI-88-009*, National Highway Institute.
- Duncan, J. M. and Buchignani, A. L. (1976), "An Engineering Manual for Settlement Studies," *Department of Civil Engineering, Institute of Transportation and Traffic Engineering*, University of California, Berkeley, California.
- Duncan, J. M., Byrne, P., Wong, K. S., Mabry, P. (1980), "Strength Stress-Strain and Bulk Modulus parameters for Finite Element analyses of Stresses and Movements in Soil Masses," *Report No. UCB/GT/80-01*, University of California, Berkeley, California.
- Duncan, J. M., Seed, R. B., Wong, K. S. and Ozawa, Y. (1984), "FFEADAM 84: A Computer Program for Finite Element analysis of Dam," *Geotechnical Engineering Research*, Virginia Tech., Blacksburg, VA.
- Gates, W. and Watters, R., (1992), "Geology of Reno and Truckee Meadows, Nevada, United Sates of America," *Bulletin of AEG*, Vol. XXIX, No. 3, pp. 229-298.
- Ladd, C. C. and Foote, R. (1974), "New Design Procedure for Stability of Soft Clay," *Journal of Geotechnical Engineering*, ASCE, Vol. 100, No. GT7, pp. 763-786.
- Lambe, T. W. and Whitman, R. V. (1969), "Soil Mechanics," *John Wiley & Sons, Inc.*, New York.
- Li, X. S., Chan, C. K. and Shen, C. K. (1988), "An Automated Triaxial Testing System," *Advanced Triaxial Testing of Soil and Rock*, ASTM STP 977, pp.95-106

- Nevada Bureau of Mines and Geology (1976), "Reno Folio," *Environmental Folio Series, Reno Quadrangle*.
- Nevada Bureau of Mines and Geology, Geologic Map, Mt Rose NE Quadrangle, 1983.
- Norris, G. M. (1977), "The Drained Shear Strength of Uniform Quartz Sand as Related to Particle Size and Natural Variation in Particle Shape and Surface Roughness," *Ph.D. Thesis*, University of California, Berkeley, California.
- Norris, G. M., Zafir, M. and Siddharthan, R. (1997), "Liquefaction and Residual Strength of Sands from Drained Triaxial Tests," *Journal of Geotechnical and Geoenvironmental Engineering*, Vol. 123, No. 3, pp. 220-228.
- Parry, R. H. (1971), "Stress-Strain Behavior of Soils," *Proceedings of the Roscoe Memorial Symposium*, Cambridge University, pp. 600-631.
- Peck, R. B., Hanson, W. E. and Thornburn, T.H. (1974), "Foundation Engineering," *John Wiley & Sons, Inc.*, New York.
- Robertson, P. K. and Campanella, R. G., (1984), "Guidelines for Use & Interpretation of the Electronic Cone Penetration Test," *Hogentogler & Co., Inc.*, Maryland.
- Seed, H. B. and Lee, K. L. (1967), "Undrained Strength Characteristics of Cohesionless Soils," *Journal of Soil Mechanics and Foundation Division*, ASCE, Vol. 93, No. SM6, pp. 333-360.
- Schmertmann, J. H. (1978), "Guidelines for CPT Performance and Design," *Federal Highway Administration*, US. Department of Transportation, TS-78-209, pp. 51.
- Seed, H. B. et al (1975), "The Slides in the San Fernando Dams during the Earthquake of February 9, 1971," *Journal of the Geotechnical Engineering Division*, ASCE, Vol. 101, No. GT7, Proceedings paper 11449, pp. 651-688.
- Seed, H. B., Wong, R. T., Idriss, I. M. and Tokimatsu, K. (1984), "Moduli and Damping Factors for Dynamic Analyses of Cohesionless Soils," *Report No. UCB/EERC-84/14, Earthquake Engineering Research Institute*, University of California, Berkeley, California.

Skempton, A. W. 1954, "The Pore-pressure Coefficients A and B," *Geotechnique*, Vol. II, No. 4, pp. 143-147

Soil Conservation Service, (1983), "Soil Survey of Washoe County, Nevada, South Part", *USDA*.

Terzaghi, K., Peck, R. B. and Mesri, G. (1996), "Soil Mechanics in Engineering Practice," *John Wiley & Sons, Inc.*, New York.

U.S. Navy, NAVFAC DM 7.1 (1986), Design Manual: Soil Mechanics, *Department of Navy*, Washington, D.C.

Appendix 1

Boring Logs for the Eight Holes Logged by

NDOT



EXPLORATION LOG

START DATE: 10/11/93 SHEET 1 OF 1
 END DATE: 10/11/93
 JOB DESCRIPTION: HIGHWAY 395 RESEARCH STATION: "H"557+00
 LOCATION: IFR 580 @ M.P. WA 17.27 OFFSET: 350' Right
 BORING: PZ-1 ENGINEER: _____
 E.A. #: _____ EQUIPMENT: _____
 GROUND ELEV.: FT OPERATOR: _____
 DRILLING METHOD: HOLLOW STEM AUGER
 HAMMER DROP SYSTEM: _____ BACKFILLED: _____ DATE: _____

GROUNDWATER LEVEL		
DATE	DEPTH	ELEV.

ELEV. (m)	DEPTH (m)	SAMPLE			LAB TESTS	USCS Group	MATERIAL DESCRIPTION	REMARKS
		NO.	TYPE	BLOWS/300mm / Recovery (%)				
	1					SM	SILTY FINE SAND brown	550 psi down
	2	A	CS			SC	1.68 SILTY CLAYEY SAND with GRAVEL gravel to 1"	
	2	B	CS			SM	2.13 SILTY SAND wet, gray brown	900 psi down; wet
	3						3.05 B.O.H.	Piezo installed @ 9' w/350' of lead
	4							
	5							
	6							
	7							
	8							
	9							

EXP-EM 385R 01/12/97



START DATE: 10/11/93

EXPLORATION LOG

SHEET 1 OF 1

END DATE: 10/11/93

JOB DESCRIPTION: HIGHWAY 395 RESEARCH

STATION: "H" 557 + 00

LOCATION: IR 580 @ M.P. WA 17.27

OFFSET: 250' Right

BORING: PZ-2

ENGINEER:

E.A. #:

EQUIPMENT:

GROUND ELEV.: m

GROUNDWATER LEVEL

OPERATOR:

DATE	DEPTH	ELEV.

DRILLING METHOD:

HAMMER DROP SYSTEM

BACKFILLED

DATE

ELEV. (m)	DEPTH (m)	SAMPLE			LAB TESTS	USCS Group	MATERIAL DESCRIPTION	REMARKS
		NO.	TYPE	BLOWS/300mm Recovery (%)				
1						SM SILTY SAND brown	600 psi - held for steady feed	
2		A	CS			ML 1.48 some gravel SANDY SILT brown, some organic		
3		B	CS			wet 2.99 B.O.H.	wet Piezo installed @ 8' w/250' lead	
4								
5								
6								
7								
8								
9								

EXP. 395R 0/12/07



EXPLORATION LOG
 START DATE: 10/13/93 SHEET 1 OF 1
 END DATE: 10/13/93
 JOB DESCRIPTION: HIGHWAY 395 RESEARCH STATION: "H" 557+00
 LOCATION: IR 580 @ M.P. WA 17.27 OFFSET: 150' Right
 BORING: PZ-3-18 ENGINEER: _____
 E.A. #: _____ EQUIPMENT: _____
 GROUND ELEV.: m OPERATOR: _____
 DRILLING METHOD: HOLLOW STEM AUGER
 HAMMER DROP SYSTEM: _____ BACKFILLED: _____ DATE: _____

GROUNDWATER LEVEL		
DATE	DEPTH	ELEV.

ELEV. (m)	DEPTH (m)	SAMPLE			LAB TESTS	USCS Group	MATERIAL DESCRIPTION	REMARKS
		NO.	TYPE	BLOWS/300mm Recovery (%)				
	0.61					ML	SANDY SILT brown	
1	1.22	A	SH			ML	SANDY SILT loose, brown	200-250 psi down
	1.68	B	SPT	8				
	2.201							
	2.62	C	SH			SM	SILTY SAND medium dense, wet, brown	150-450 psi down
3	3.08	D	SPT	12				150-350 psi down
	3.54	E						
4	4.15	F	SH					
	4.60	G	SPT	11				
5	5.06							
	5.67	H	SH					sample settled 6" into soil Piezo installed @ 17.4' in 2" sand, 3' pellets, and ben/cem grout
6							B.O.H.	
7								
8								
9								

EXP. EM. 395R 01/12/97



EXPLORATION LOG

SHEET 1 OF 1

START DATE: 10/13/93

END DATE: 10/13/93

JOB DESCRIPTION: HIGHWAY 395 RESEARCH

LOCATION: IR 580 @ M.P. WA 17.27

BORING: PZ-3-13

E.A. #

GROUND ELEV. m

HAMMER DROP SYSTEM

STATION: *H*557+00

OFFSET: 150' Right

ENGINEER

EQUIPMENT

OPERATOR


DRILLING METHOD: HOLLOW STEM AUGER

BACKFILLED DATE

GROUNDWATER LEVEL		
DATE	DEPTH	ELEV.

ELEV. (m)	DEPTH (m)	SAMPLE			LAB TESTS	USCS Group	MATERIAL DESCRIPTION	REMARKS
		NO.	TYPE	BLOWS/300mm / Recovery (%)				
						no info		
1								
2								
3								
4						3.96 B.O.H.	Piezo installed @ 12.7'	
5								
6								
7								
8								
9								

EXP-EM 388R 0/12/97

		EXPLORATION LOG				SHEET 1 OF 1													
START DATE: 10/19/93		END DATE: 10/19/93		JOB DESCRIPTION: HIGHWAY 395 RESEARCH		STATION: _____													
LOCATION: IR 580 @ M.P. WA 17.27		BORING: FZ-4		E.A. # _____		ENGINEER: _____													
GROUND ELEV. m _____		HAMMER DROP SYSTEM _____		<table border="1" style="font-size: small;"> <tr><th colspan="3">GROUNDWATER LEVEL</th></tr> <tr><th>DATE</th><th>DEPTH</th><th>ELEV.</th></tr> <tr><td> </td><td> </td><td> </td></tr> <tr><td> </td><td> </td><td> </td></tr> </table>		GROUNDWATER LEVEL			DATE	DEPTH	ELEV.							EQUIPMENT: _____	
GROUNDWATER LEVEL																			
DATE	DEPTH	ELEV.																	
				OPERATOR: _____		DRILLING METHOD: <u>HOLLOW STEM AUGER</u>													
				BACKFILLED: _____		DATE: _____													

ELEV. (m)	DEPTH (m)	SAMPLE			LAB TESTS	USCS Group	MATERIAL DESCRIPTION	REMARKS
		NO.	TYPE	BLOWS/300mm / Recovery (%)				
	1							
	1.22							
	1.83	A	SH	25				
	2							0-250 psi
	2.29	B	SPT	6				
	2.74							
	3							
	3.35	C	CS	100				no tube w/catcher
	3.81	D	SPT	12				
	4							disturbed
	4.27							
	5							
	5.49	E	CS	100				
	5.94							
	6.10	F	SPT	17			pebbles in SPT	
							gravel	
	6.71	G	CS	100				piezo installed @ 21'; 2' sand, 2' pellets, 10' grout
	7						6.71 B.O.H.	
	8							
	9							

EXP. 614.388R 01/2007



EXPLORATION LOG

SHEET 1 OF 1

START DATE: 10/14/93

END DATE: 10/18/93

JOB DESCRIPTION: HIGHWAY 395 RESEARCH

LOCATION: IR 580 @ M.P. WA 17.27

BORING: FZ-5-18

E.A. #

GROUND ELEV. m

HAMMER DROP SYSTEM

STATION

OFFSET

ENGINEER

EQUIPMENT

OPERATOR

DRILLING METHOD: HOLLOW STEM AUGER

BACKFILLED DATE

GROUNDWATER LEVEL		
DATE	DEPTH	ELEV.

ELEV. (m)	DEPTH (m)	SAMPLE				LAB TESTS	USCS Group	MATERIAL DESCRIPTION	REMARKS
		NO.	TYPE	BLOWS/300mm	Recovery (%)				
	0.61						SILTY SAND with GRAVEL brown		
1	1.22	A	SH					250 psi	
	1.68	B	SPT	6					
2	2.13								
	2.74	C	SH						
3	3.20	D	SPT	11				300 psi	
	3.66								
4	4.27	E	SH				0 psi (weight of head) no return		
	4.88	F	SH				0 psi first foot; 100 psi second foot no return		
5	5.33	G	SPT	19					
						5.49			
6							B.O.H.	Piezo installed @ 18'	
7									
8									
9									

EXP-EM 388R 6/12/07

NEVADA DEPARTMENT OF AGRICULTURE GEOLOGICAL ENGINEERING		START DATE: <u>10/18/93</u>				EXPLORATION LOG				SHEET 1 OF 1	
		END DATE: <u>10/18/93</u>				JOB DESCRIPTION: <u>HIGHWAY 395 RESEARCH</u>				STATION: _____	
		LOCATION: <u>IR 580 @ M.P. WA 17.27</u>				BORING: <u>PZ-5-10</u>				ENGINEER: _____	
		E.A. #: _____				GROUNDWATER LEVEL				EQUIPMENT: _____	
		GROUND ELEV.: <u>m</u>				DATE				OPERATOR: _____	
		HAMMER DROP SYSTEM: _____				DEPTH				DRILLING METHOD: <u>HOLLOW STEM AUGER</u>	
						ELEV.				BACKFILLED: _____	
										DATE: _____	
ELEV. (m)	DEPTH (m)	SAMPLE			LAB TESTS	USCS Group	MATERIAL DESCRIPTION	REMARKS			
		NO.	TYPE	BLOWS/ 300mm Recovery (%)							
	1					no info					
	2										
	3										
	3.19					B.O.H.	Piezo installed @ 10'				
	4										
	5										
	6										
	7										
	8										
	9										

EXP EM 365R 8/12/87

ELEV. (m)		DEPTH (m)		SAMPLE		LAB TESTS	USCS Group	MATERIAL DESCRIPTION	REMARKS
NO.	TYPE	BLOWS/300mm	Recovery (%)						
1								no info	
2									
3									
4									
5									
6							5.49	B.O.H.	Piezo installed @ 17.4'
7									
8									
9									

EXP. EM 388R 01/2007



EXPLORATION LOG SHEET 1 OF 1

START DATE: 10/14/93 END DATE: 10/14/93

JOB DESCRIPTION: HIGHWAY 395 RESEARCH STATION: "H"557+00

LOCATION: IR 580 @ M.P. WA 17.27 OFFSET: 130' Left

BORING: PZ-6 ENGINEER: _____


E.A. #: _____ EQUIPMENT: _____

GROUND ELEV.: m OPERATOR: _____

HAMMER DROP SYSTEM: _____ DRILLING METHOD: HOLLOW STEM AUGER

BACKFILLED: _____ DATE: _____

GROUNDWATER LEVEL		
DATE	DEPTH	ELEV.



EXPLORATION LOG

SHEET 1 OF 1

START DATE: 10/13/93
 END DATE: 10/13/93
 JOB DESCRIPTION: HIGHWAY 395 RESEARCH
 LOCATION: IR 580 @ M.P. WA 17.27
 BORING: PZ-7
 E.A. #: _____
 GROUND ELEV. m
 HAMMER DROP SYSTEM: _____

GROUNDWATER LEVEL		
DATE	DEPTH	ELEV.

STATION: _____
 OFFSET: _____
 ENGINEER: _____
 EQUIPMENT: _____
 OPERATOR: _____
 DRILLING METHOD: HOLLOW STEM AUGER
 BACKFILLED: _____ DATE: _____

ELEV. (m)	DEPTH (m)	SAMPLE		LAB TESTS	USCS Group	MATERIAL DESCRIPTION	REMARKS
		NO.	TYPE				
1		A	CS			no info	900 psi w/restricted feed
2		B	CS				
3					3.05	B.O.H.	Piezo installed @ 9.8'
4							
5							
6							
7							
8							
9							

EXP. EN. 505R 6/12/87



EXPLORATION LOG
 START DATE: 10/13/93
 END DATE: 10/13/93
 JOB DESCRIPTION: HIGHWAY 395 RESEARCH
 LOCATION: IR 580 @ M.P. WA 17.27
 BORING: PZ-B
 E.A. #: _____
 GROUND ELEV. ft: _____
 HAMMER DROP SYSTEM _____

SHEET 1 OF 1

STATION _____
 OFFSET _____
 ENGINEER _____
 EQUIPMENT _____
 OPERATOR _____
 DRILLING METHOD: HOLLOW STEM AUGER
 BACKFILLED _____ DATE _____

GROUNDWATER LEVEL		
DATE	DEPTH	ELEV.

ELEV. (m)	DEPTH (m)	SAMPLE		BLOWS/300mm	Recovery (%)	LAB TESTS	USCS Group	MATERIAL DESCRIPTION	REMARKS
		NO.	TYPE						
1		A	CS				SM	SILTY SAND brown	800 psi w/ restricted feed
2		B	CS					wet	
3							3.05	B.O.H.	Piezo installed @ 9.5'
4									
5									
6									
7									
8									
9									

EXP. EM. 388R 8/12/97

Appendix 2

Interpreted Logs for the CPT Readings

TONTO ENVIRONMENTAL DRILLING

Engineer U.N.R.
On Site Loc: CPT-P3
Job No. : U.N.R.
Tot. Unit Wt. (avg) : 115 pcf

CPT Date : 12/22/93 09:57
Cone Used : 465
Water table (meters) : 3

DEPTH (meters)	DEPTH (feet)	Qc (avg) (tsf)	Ps (avg) (tsf)	Rf (avg) (%)	SIGV' (tsf)	SOIL BEHAVIOUR TYPE	E _q - Dr (%)	PHI deg.	SPT N	Su tsf
0.25	0.82	52.74	0.85	1.61	0.02	silty sand to sandy silt	>90	>48	17	UNDEFINED
0.50	1.64	10.14	0.41	4.00	0.07	clay	UNDFND	UNDFND	10	.6
0.75	2.46	3.36	0.10	2.90	0.12	clay	UNDFND	UNDFND	3	.2
1.00	3.28	3.56	0.09	2.54	0.17	clay	UNDFND	UNDFND	3	.2
1.25	4.10	22.08	0.44	1.99	0.21	sandy silt to clayey silt	UNDFND	UNDFND	8	1.4
1.50	4.92	47.48	1.05	2.21	0.26	sandy silt to clayey silt	UNDFND	UNDFND	18	3.1
1.75	5.74	50.50	0.92	1.83	0.31	silty sand to sandy silt	60-70	42-44	16	UNDEFINED
2.00	6.56	45.10	0.64	1.43	0.35	silty sand to sandy silt	50-60	42-44	14	UNDEFINED
2.25	7.38	35.88	0.22	0.60	0.40	silty sand to sandy silt	50-60	40-42	11	UNDEFINED
2.50	8.20	14.90	0.20	1.32	0.45	sandy silt to clayey silt	UNDFND	UNDFND	6	.9
2.75	9.02	30.32	0.33	1.09	0.50	silty sand to sandy silt	40-50	38-40	10	UNDEFINED
3.00	9.84	53.14	0.44	0.82	0.54	silty sand to sandy silt	50-60	40-42	17	UNDEFINED
3.25	10.66	22.96	0.38	1.64	0.58	sandy silt to clayey silt	UNDFND	UNDFND	9	1.4
3.50	11.48	28.06	0.63	2.25	0.60	sandy silt to clayey silt	UNDFND	UNDFND	11	1.8
3.75	12.30	26.82	0.36	1.33	0.62	sandy silt to clayey silt	UNDFND	UNDFND	10	1.7
4.00	13.12	56.02	0.37	0.66	0.64	sand to silty sand	50-60	40-42	13	UNDEFINED
4.25	13.94	14.06	0.20	1.40	0.66	sandy silt to clayey silt	UNDFND	UNDFND	5	.8
4.50	14.76	16.16	0.52	3.25	0.68	silty clay to clay	UNDFND	UNDFND	10	1.0
4.75	15.58	72.82	1.19	1.63	0.71	silty sand to sandy silt	60-70	40-42	23	UNDEFINED
5.00	16.40	107.10	1.15	1.07	0.73	sand to silty sand	70-80	42-44	26	UNDEFINED
5.25	17.22	89.24	1.13	1.27	0.75	sand to silty sand	60-70	40-42	21	UNDEFINED
5.50	18.04	85.60	0.51	0.59	0.77	sand to silty sand	60-70	40-42	20	UNDEFINED
5.75	18.86	98.08	1.98	2.01	0.79	silty sand to sandy silt	60-70	40-42	31	UNDEFINED
6.00	19.69	73.64	1.00	1.36	0.81	silty sand to sandy silt	60-70	40-42	24	UNDEFINED
6.25	20.51	34.24	0.73	2.14	0.84	sandy silt to clayey silt	UNDFND	UNDFND	13	2.2
6.50	21.33	103.36	1.64	1.59	0.86	silty sand to sandy silt	60-70	40-42	33	UNDEFINED
6.75	22.15	22.82	0.56	2.45	0.88	clayey silt to silty clay	UNDFND	UNDFND	11	1.4
7.00	22.97	43.02	1.22	2.83	0.90	sandy silt to clayey silt	UNDFND	UNDFND	16	2.7
7.25	23.79	72.10	1.26	1.74	0.92	silty sand to sandy silt	50-60	38-40	23	UNDEFINED
7.50	24.61	149.20	2.85	1.91	0.94	silty sand to sandy silt	70-80	42-44	48	UNDEFINED

Dr - All sands (Janiolkowski et al. 1985)

PHI - Robertson and Campanella 1983

Su: NR= 15

**** Note: For interpretation purposes the PLOTTED CPT PROFILE should be used with the TABULATED OUTPUT from CPTINTRI (v 3.04) ****

1 TONTO ENVIRONMENTAL DRILLING

Engineer U.N.R.
 On Site Loc:CPT-P4
 Job No. :U.N.R.
 Tot. Unit Wt. (avg) : 115 pcf

CPT Date :12/22/93 12:32
 Cone Used :465
 Water table (meters) : 3

DEPTH (meters)	DEPTH (feet)	Qc (avg) (tsf)	Fs (avg) (tsf)	Rf (avg) (%)	SIGV' (tsf)	SOIL BEHAVIOUR TYPE	Eq - Dr (%)	PHI deg.	SPT N	Su tsf
0.25	0.82	22.38	0.35	1.57	0.02	sandy silt to clayey silt	UNDFND	UNDFND	9	1.4
0.50	1.64	18.02	0.10	0.58	0.07	sandy silt to clayey silt	UNDFND	UNDFND	7	1.1
0.75	2.46	10.02	0.00	0.04	0.12	sensitive fine grained	UNDFND	UNDFND	5	.6
1.00	3.28	16.46	0.10	0.58	0.17	sandy silt to clayey silt	UNDFND	UNDFND	6	1.0
1.25	4.10	30.22	0.32	1.05	0.21	silty sand to sandy silt	50-60	42-44	10	UNDEFINED
1.50	4.92	70.06	1.17	1.67	0.26	silty sand to sandy silt	70-80	44-46	22	UNDEFINED
1.75	5.74	24.92	0.27	1.07	0.31	sandy silt to clayey silt	UNDFND	UNDFND	10	1.6
2.00	6.56	17.08	0.44	2.59	0.35	clayey silt to silty clay	UNDFND	UNDFND	8	1.1
2.25	7.38	14.88	0.26	1.76	0.40	clayey silt to silty clay	UNDFND	UNDFND	7	.9
2.50	8.20	39.68	0.66	1.66	0.45	sandy silt to clayey silt	UNDFND	UNDFND	15	2.6
2.75	9.02	87.22	0.74	0.84	0.50	sand to silty sand	70-80	42-44	21	UNDEFINED
3.00	9.84	56.46	0.79	1.40	0.54	silty sand to sandy silt	50-60	40-42	18	UNDEFINED
3.25	10.66	65.54	0.53	0.80	0.58	sand to silty sand	60-70	40-42	16	UNDEFINED
3.50	11.48	46.38	0.99	2.13	0.60	sandy silt to clayey silt	UNDFND	UNDFND	18	3.0
3.75	12.30	31.22	0.82	2.64	0.62	sandy silt to clayey silt	UNDFND	UNDFND	12	2.0
4.00	13.12	22.94	0.40	1.73	0.64	sandy silt to clayey silt	UNDFND	UNDFND	9	1.4
4.25	13.94	14.02	0.05	0.37	0.66	sandy silt to clayey silt	UNDFND	UNDFND	5	.8
4.50	14.76	19.50	0.51	2.59	0.68	clayey silt to silty clay	UNDFND	UNDFND	9	1.2
4.75	15.58	31.32	0.69	2.19	0.71	sandy silt to clayey silt	UNDFND	UNDFND	12	2.0
5.00	16.40	34.26	0.92	2.68	0.73	sandy silt to clayey silt	UNDFND	UNDFND	13	2.2
5.25	17.22	92.52	1.75	1.89	0.75	silty sand to sandy silt	60-70	40-42	30	UNDEFINED
5.50	18.04	84.94	2.08	2.45	0.77	sandy silt to clayey silt	UNDFND	UNDFND	33	5.5
5.75	18.86	97.68	1.16	1.18	0.79	sand to silty sand	60-70	40-42	23	UNDEFINED
6.00	19.69	64.82	1.31	2.02	0.81	silty sand to sandy silt	50-60	40-42	21	UNDEFINED
6.25	20.51	116.50	3.52	3.02	0.84	sandy silt to clayey silt	UNDFND	UNDFND	45	7.6
6.50	21.33	149.26	3.41	2.29	0.86	silty sand to sandy silt	80-90	42-44	48	UNDEFINED

Dr - All sands (Janiołkowski et al. 1985)

PHI - Robertson and Campanella 1983

Su: N= 15

**** Note: For interpretation purposes the PLOTTED CPT PROFILE should be used with the TABULATED OUTPUT from CPTINR1 (v 3.04) ****

1 TONTO ENVIRONMENTAL DRILLING

Engineer U.N.R.
On Site Loc:CPT-P5
Job No. :U.N.R.
Tot. Unit Wt. (avg) : 115 pcf

CPT Date :12/22/93 14:54
Cone Used :465
Water table (meters) : 3

DEPTH (meters)	DEPTH (feet)	Qc (avg) (tsf)	Ps (avg) (tsf)	Rf (avg) (%)	SIGV' (tsf)	SOIL BEHAVIOUR TYPE	Eq - Dr (%)	PHI deg.	SPT N	Su tsf
0.25	0.82	38.02	0.47	1.25	0.02	silty sand to sandy silt	>90	>48	12	UNDEFINED
0.50	1.64	25.94	0.13	0.50	0.07	silty sand to sandy silt	60-70	46-48	8	UNDEFINED
0.75	2.46	15.90	0.21	1.29	0.12	sandy silt to clayey silt	UNDFND	UNDFND	6	1.0
1.00	3.28	15.12	0.28	1.82	0.17	clayey silt to silty clay	UNDFND	UNDFND	7	.9
1.25	4.10	23.38	0.58	2.46	0.21	clayey silt to silty clay	UNDFND	UNDFND	11	1.5
1.50	4.92	17.86	0.19	1.07	0.26	sandy silt to clayey silt	UNDFND	UNDFND	7	1.1
1.75	5.74	23.36	0.20	0.88	0.31	sandy silt to clayey silt	UNDFND	UNDFND	9	1.5
2.00	6.56	41.26	0.63	1.53	0.35	silty sand to sandy silt	50-60	40-42	13	UNDEFINED
2.25	7.38	19.94	0.54	2.71	0.40	clayey silt to silty clay	UNDFND	UNDFND	10	1.3
2.50	8.20	20.84	0.41	1.96	0.45	sandy silt to clayey silt	UNDFND	UNDFND	8	1.3
2.75	9.02	33.40	0.82	2.46	0.50	sandy silt to clayey silt	UNDFND	UNDFND	13	2.1
3.00	9.84	32.48	0.77	2.36	0.54	sandy silt to clayey silt	UNDFND	UNDFND	12	2.1
3.25	10.66	66.32	0.51	0.76	0.58	sand to silty sand	60-70	40-42	16	UNDEFINED
3.50	11.48	36.92	1.00	2.72	0.60	sandy silt to clayey silt	UNDFND	UNDFND	14	2.4
3.75	12.30	35.70	0.68	1.90	0.62	sandy silt to clayey silt	UNDFND	UNDFND	14	2.3
4.00	13.12	38.78	0.77	1.99	0.64	sandy silt to clayey silt	UNDFND	UNDFND	15	2.5
4.25	13.94	13.82	0.21	1.54	0.66	clayey silt to silty clay	UNDFND	UNDFND	7	.8
4.50	14.76	24.24	0.72	2.96	0.68	clayey silt to silty clay	UNDFND	UNDFND	12	1.5
4.75	15.58	23.44	0.57	2.42	0.71	clayey silt to silty clay	UNDFND	UNDFND	11	1.5
5.00	16.40	37.42	1.34	3.57	0.73	clayey silt to silty clay	UNDFND	UNDFND	18	2.4
5.25	17.22	34.08	1.04	3.05	0.75	clayey silt to silty clay	UNDFND	UNDFND	16	2.2
5.50	18.04	70.06	1.22	1.74	0.77	silty sand to sandy silt	60-70	40-42	22	UNDEFINED
5.75	18.86	66.98	1.37	2.04	0.79	silty sand to sandy silt	50-60	40-42	21	UNDEFINED
6.00	19.69	53.24	1.06	1.99	0.81	sandy silt to clayey silt	UNDFND	UNDFND	20	3.4
6.25	20.51	162.76	1.78	1.10	0.84	sand to silty sand	80-90	42-44	39	UNDEFINED
6.50	21.33	90.62	2.17	2.39	0.86	silty sand to sandy silt	60-70	40-42	29	UNDEFINED

Dr - All sands (Janioikowski et al. 1985)

PHI - Robertson and Campanella 1983

Su: N= 15

**** Note: For interpretation purposes the PLOTTED CPT PROFILE should be used with the TABULATED OUTPUT from CPTINTR1 (v 3.04) ****

1
TONTO ENVIRONMENTAL DRILLING

Engineer U.N.R.
 On Site Loc: CPT-P6
 Job No. : U.N.R.
 Tot. Unit Wt. (avg) : 115 pcf

CPT Date : 12/22/93 17:44
 Cone Used : 465
 Water table (meters) : 3

DEPTH (meters)	DEPTH (feet)	Qc (avg) (tsf)	Ps (avg) (tsf)	Rf (avg) (%)	SIGV' (tsf)	SOIL BEHAVIOUR TYPE	Eq - Dr (%)	PHI deg.	SPT N	Su tsf
0.25	0.82	22.00	0.52	2.35	0.02	clayey silt to silty clay	UNDFND	UNDFND	11	1.4
0.50	1.64	28.42	0.29	1.01	0.07	silty sand to sandy silt	60-70	46-48	9	UNDEFINED
0.75	2.46	6.48	0.05	0.83	0.12	sensitive fine grained	UNDFND	UNDFND	3	.4
1.00	3.28	8.72	0.01	0.07	0.17	sensitive fine grained	UNDFND	UNDFND	4	.5
1.25	4.10	16.20	0.03	0.21	0.21	sandy silt to clayey silt	UNDFND	UNDFND	6	1.0
1.50	4.92	35.38	1.00	2.82	0.26	sandy silt to clayey silt	UNDFND	UNDFND	14	2.3
1.75	5.74	30.96	0.68	2.21	0.31	sandy silt to clayey silt	UNDFND	UNDFND	12	2.0
2.00	6.56	27.18	0.55	2.02	0.35	sandy silt to clayey silt	UNDFND	UNDFND	10	1.7
2.25	7.38	30.48	0.58	1.89	0.40	sandy silt to clayey silt	UNDFND	UNDFND	12	2.0
2.50	8.20	26.22	0.77	2.93	0.45	clayey silt to silty clay	UNDFND	UNDFND	13	1.7
2.75	9.02	22.52	0.47	2.11	0.50	sandy silt to clayey silt	UNDFND	UNDFND	9	1.4
3.00	9.84	19.98	0.37	1.83	0.54	sandy silt to clayey silt	UNDFND	UNDFND	8	1.2
3.25	10.66	44.34	0.15	0.33	0.58	sand to silty sand	50-60	38-48	11	UNDEFINED
3.50	11.48	28.90	0.16	0.54	0.60	silty sand to sandy silt	<40	36-38	9	UNDEFINED
3.75	12.30	18.44	0.39	2.14	0.62	clayey silt to silty clay	UNDFND	UNDFND	9	1.1
4.00	13.12	49.60	0.75	1.51	0.64	silty sand to sandy silt	50-60	38-40	16	UNDEFINED
4.25	13.94	44.42	0.70	1.58	0.66	silty sand to sandy silt	48-50	38-40	14	UNDEFINED
4.50	14.76	22.06	0.40	1.79	0.68	sandy silt to clayey silt	UNDFND	UNDFND	8	1.4
4.75	15.58	19.64	0.47	2.38	0.71	clayey silt to silty clay	UNDFND	UNDFND	9	1.2
5.00	16.40	42.44	0.88	2.07	0.73	sandy silt to clayey silt	UNDFND	UNDFND	16	2.7
5.25	17.22	47.62	1.31	2.74	0.75	sandy silt to clayey silt	UNDFND	UNDFND	18	3.1
5.50	18.04	30.58	0.60	1.97	0.77	sandy silt to clayey silt	UNDFND	UNDFND	12	1.9
5.75	18.86	29.18	0.89	3.06	0.79	clayey silt to silty clay	UNDFND	UNDFND	14	1.8
6.00	19.69	43.08	1.40	3.24	0.81	clayey silt to silty clay	UNDFND	UNDFND	21	2.7
6.25	20.51	34.92	1.10	3.16	0.84	clayey silt to silty clay	UNDFND	UNDFND	17	2.2
6.50	21.33	82.62	2.87	3.48	0.86	sandy silt to clayey silt	UNDFND	UNDFND	32	5.4
6.75	22.15	114.18	2.04	1.79	0.88	silty sand to sandy silt	70-80	42-44	36	UNDEFINED
7.00	22.97	31.96	0.76	2.36	0.90	sandy silt to clayey silt	UNDFND	UNDFND	12	2.0
7.25	23.79	30.46	0.76	2.48	0.92	sandy silt to clayey silt	UNDFND	UNDFND	12	1.9
7.50	24.61	94.16	2.70	2.86	0.94	sandy silt to clayey silt	UNDFND	UNDFND	36	6.1

Dr - All sands (Janioikowski et al. 1985)

PHI - Robertson and Campanella 1983

Su: Nk= 15

**** Note: For interpretation purposes the PLOTTED CPT PROFILE should be used with the TABULATED OUTPUT from CPTINTER1 (v 3.04) ****

Appendix 3

**Sample Test Data of the In Place Hydraulic
Conductivity Tests**

Well # 1

Eff. Length	L (in)	48
Inner Dia.	2r (in)	2
Dia. of Hole	2R (in)	9.25

Date	27-Jul-95		Permeability (K) <i>cm/sec</i>
Water Level	71.5		
Time (min)	Reading	Notes	
0	0		
0.5	2		5.810E-05
1	3.5		4.468E-05
1.5	5		4.568E-05
2	6.5		4.672E-05
3	9.8		5.334E-05
4	12.5		4.581E-05
6	18		5.006E-05
8	22.5		4.496E-05
10	26		3.793E-05
15	35		4.496E-05
20	41		3.668E-05
Average			4.627E-05

Well # 2

Eff. Length	L (in)	24
Inner Dia.	2r (in)	2
Dia. of Hole	2R (in)	9.25

Date	17-Jun-94		Permeability (K) <i>cm/sec</i>
Water Level	110		
Time (min)	Reading	Notes	
0	0		
2	5.75		3.869E-05
4	10.5		3.361E-05
6	14.5		2.957E-05
10	21.75		2.844E-05
15	28		2.117E-05
25	38.25		1.922E-05
0	0		
0	0		
Average			2.845E-05

Appendix 4

**A Complete Logging Description of the
Continuous Clear Tube Sample Obtained
from Pz4 Location at a Depth of 8 to 21 ft.**

Depth		Description
From	To	
8.8 ft	9.9 ft	Clayey to SL clayey fine to medium sand, few subangular coarse sand, trace of fine gravel. A pocket of clayey fine sand SC was found at depth of 9.0 ft
9.9 ft	10.5 ft	Medium sand, trace of non plastic fines, brown. A pocket of fine to medium silty sand was found at a depth of 10.0 ft
10.5 ft	10.8 ft	Fine sand, few non plastic fines, light brown. A pocket of clayey fine sand, medium plasticity fines, red brown, moderately cemented was found.
14.7 ft	16.0 ft	Fine to medium silty sand, brown.
16.0 ft	16.4 ft	Silty fine sand, light brown, estimated fines 10 %.
16.4 ft	16.8 ft	Silty fine sand, fewer fines than the layer above.
16.8 ft	17.3 ft	Silty fine sand but have two colors, light and dark brown.
19.7 ft	20.5 ft	Gravelly clayey sand, gravel is coarse to fine subrounded, sand is fine, fines are low plasticity, brown.
20.5 ft	21.0 ft	Clayey fine sand to fine sandy clay, fines are medium to high plasticity, red brown.
21.0 ft	21.5 ft	Sandy clay, sand fine, medium plasticity, brown.

Appendix 5

Mathematical Proof for the Equation Used in Calculating the Horizontal Hydraulic Conductivity

Test with Falling Headwater and Rising Tailwater

For axial flow:

$$k = \frac{a_{in} * a_{out}}{a_{in} + a_{out}} \frac{L}{A t} \frac{dh}{h}$$

where

a_{in} is a calibration factor for water going into the sample (cc/cm)

a_{out} is a calibration factor for water coming out of the sample (cc/cm)

L is the height of the sample (cm)

t is the time (sec)

h is the head applied to the specimen (cm)

Reference: Daniel, D. E. "A Note in Falling Headwater and Rising Tailwater Permeability Tests," *Geotechnical Testing Journal*, Vol. 12, No. 4, Dec. 1989, pp. 308-310

Considering radial flow, where the area, A , from which water flows is

$$A = 2\pi r L$$

also, the hydraulic head, i , radial across the sample is

$$i = \frac{h}{dr}$$

Therefore

$$k = \frac{a_{in} * a_{out}}{a_{in} + a_{out}} \frac{dh}{dt} \frac{dr}{h} \frac{1}{2\pi r L}$$

Integration yields

$$k = \frac{a_{in} * a_{out}}{a_{in} + a_{out}} \frac{1}{2\pi L t} \ln\left(\frac{h_1}{h_2}\right) \ln\left(\frac{R}{r_o}\right)$$

where

h_1 is the head applied in the center of the specimen (cm)

h_2 is the head applied at the edge of the specimen (cm)

R is the outer radius of the specimen (cm)

r_o is the radius of the hole (cm)

Isotropic state

Cell Pressure 300 kpa
 Back Pressure 270 kpa
 Effective stress 30 kpa
 Deviator stress 0 kpa

σ_3' 30 kpa
 σ_1' 30 kpa

Head Pressure 280 kpa
 Tail Pressure 270 kpa

Time	H. Read	T. Read	H. Diff	T. Diff	W. In	W. Out	Delta H	Av. Flow	K(hz)
min	cm	cm	cm	cm	cc	cc	cm	cc/sec	cm/sec
0.0	73.30	53.60					121.60		
1.0	72.90	54.20	-0.40	0.60	-7.99	12.07	120.60	0.17	2.33E-05
2.0	72.20	54.70	-0.70	0.50	-13.98	10.06	119.40	0.20	2.82E-05
4.0	71.40	55.50	-0.80	0.80	-15.97	16.10	117.80	0.13	1.90E-05
6.0	70.50	56.50	-0.90	1.00	-17.97	20.12	115.90	0.16	2.29E-05
9.0	69.00	57.75	-1.50	1.25	-29.95	25.15	113.15	0.15	2.25E-05
11.0	68.25	58.50	-0.75	0.75	-14.98	15.09	111.65	0.13	1.88E-05
14.0	67.00	59.70	-1.25	1.20	-24.96	24.15	109.20	0.14	2.08E-05
16.0	66.25	60.50	-0.75	0.80	-14.98	16.10	107.65	0.13	2.01E-05
19.0	65.15	61.70	-1.10	1.20	-21.96	24.15	105.35	0.13	2.03E-05
24.0	63.50	63.50	-1.65	1.80	-32.95	36.22	101.90	0.12	1.88E-05
29.0	61.80	65.00	-1.70	1.50	-33.94	30.18	98.70	0.11	1.80E-05
34.0	60.20	66.50	-1.60	1.50	-31.95	30.18	95.60	0.10	1.80E-05
44.0	57.50	69.50	-2.70	3.00	-53.91	60.37	89.90	0.10	1.73E-05
49.0	56.00	70.60	-1.50	1.10	-29.95	22.14	87.30	0.09	1.65E-05

Average 2.03E-05

K_n State

Cell Pressure 329 kpa
Back Pressure 270 kpa
Effective stress 59 kpa
Deviator stress 141 kpa

 σ_3' 59 kpa
 σ_1' 200 kpa

Head Pressure 280 kpa
Tail Pressure 270 kpa

Time	H. Read	T. Read	H. Diff	T. Diff	W. In	W. Out	Delta H	Av. Flow	K(hz)
min	cm	cm	cm	cm	cc	cc	cm	cc/sec	cm/sec
0.0	74.80	52.25					124.45		
1.0	74.50	52.60	-0.30	0.35	-5.99	7.04	123.80	0.11	1.47E-05
2.0	74.00	52.90	-0.50	0.30	-9.98	6.04	123.00	0.13	1.83E-05
4.0	73.50	53.50	-0.50	0.60	-9.98	12.07	121.90	0.09	1.27E-05
6.0	72.90	54.10	-0.60	0.60	-11.98	12.07	120.70	0.10	1.39E-05
9.0	72.00	55.00	-0.90	0.90	-17.97	18.11	118.90	0.10	1.41E-05
11.0	71.50	55.50	-0.50	0.50	-9.98	10.06	117.90	0.08	1.19E-05
14.0	70.60	56.40	-0.90	0.90	-17.97	18.11	116.10	0.10	1.44E-05
16.0	70.10	56.90	-0.50	0.50	-9.98	10.06	115.10	0.08	1.22E-05
19.0	69.50	57.50	-0.60	0.60	-11.98	12.07	113.90	0.07	9.84E-06
24.0	68.25	58.75	-1.25	1.25	-24.96	25.15	111.40	0.08	1.25E-05
29.0	67.20	59.80	-1.05	1.05	-20.97	21.13	109.30	0.07	1.07E-05
34.0	66.70	60.50	-0.50	0.70	-9.98	14.09	108.10	0.04	6.22E-06
39.0	65.40	61.50	-1.30	1.00	-25.96	20.12	105.80	0.08	1.21E-05
44.0	64.50	62.25	-0.90	0.75	-17.97	15.09	104.15	0.06	8.85E-06
49.0	63.60	63.10	-0.90	0.85	-17.97	17.10	102.40	0.06	9.55E-06
59.0	62.10	64.50	-1.50	1.40	-29.95	28.17	99.50	0.05	8.09E-06
68.0	60.90	66.00	-1.20	1.50	-23.96	30.18	96.80	0.05	8.61E-06

Average 1.77E-05

Appendix 6

A Trial to Separate the Horizontal from the Vertical Hydraulic Conductivity using the Falling Head Test Data

$$k = \left(\frac{r^2}{2L} \right) \ln \left(\frac{mL}{R} \right) \frac{\ln \left(\frac{H}{H_2} \right)}{t_2 - t_1}$$

where

$$m = \sqrt{\frac{k_h}{k_v}}$$

where

L = Length of the screen

r = Radius of the tube

R = Radius of the hole

Reference: U.S. Navy, NAVFAC DM 7.1 (1986), Design Manual: Soil Mechanics, *Department of Navy*, Washington, D.C., pp. 104

<u>Well #1</u>	<u>Well #2</u>
L = 48.0 in.	L = 24.0 in.
r = 1.0 in.	r = 1.0 in.
R = 4.625 in.	R = 4.625 in.
At H ₁ = 63.75 in.	At H ₁ = 60.75 in.
H ₂ = 51.75 in.	H ₂ = 56.75 in.
T ₁ = 0 min.	T ₁ = 0 min.
T ₂ = 10 min.	T ₂ = 10 min.

$$k_1 = 0.000217 * (\ln m + 2.3397) \quad k_1 = 0.000116 * (\ln m + 1.6466)$$

$$k_1 = k_2 = k_{\text{mean}}$$

$$0.000217 * (\ln m + 2.3397) = 0.000116 * (\ln m + 1.6466)$$

$$1.8707 * (\ln m + 2.3397) = (\ln m + 1.6466)$$

$$0.8707 * \ln m = -2.7303$$

$$m = 0.0435$$

Therefore,

$$k_{\text{mean}} = -1.728e-4 \text{ in/min}$$

of course, this negative number is not realistic

Appendix 7

Initial Stress Conditions for various Elements for The Two Different Groundwater Conditions

Element #	X ft	Y ft	depth ft	σ_y (total) ksf	P.W.P. (Static) ksf	σ_y (effective) ksf	P.W.P. (Steady S) ksf	σ_y (effective) ksf
1	7.25	6.75	70.75	9.14	4.17	4.98	4.60	4.54
2	21.75	6.75	70.75	9.14	4.17	4.98	4.60	4.54
3	36.25	6.75	70.75	9.14	4.17	4.98	4.60	4.54
4	50.75	6.75	70.75	9.14	4.17	4.98	4.60	4.54
5	65.25	6.75	70.75	9.14	4.17	4.98	4.60	4.54
6	79.75	6.75	70.75	9.14	4.17	4.98	4.60	4.54
7	94.25	6.75	70.75	9.14	4.17	4.98	4.60	4.54
8	108.75	6.75	70.75	9.14	4.17	4.98	4.60	4.54
9	123.25	6.75	70.75	9.14	4.17	4.98	4.60	4.54
10	137.75	6.75	70.75	9.14	4.17	4.98	4.60	4.54
11	152.25	6.75	70.75	9.14	4.17	4.98	4.60	4.54
12	166.75	6.75	70.75	9.14	4.17	4.98	4.60	4.54
13	181.25	6.75	70.75	9.14	4.17	4.98	4.60	4.54
14	195.75	6.75	70.75	9.14	4.17	4.98	4.60	4.54
15	210.25	6.75	70.75	9.14	4.17	4.98	4.60	4.54
16	224.75	6.75	70.75	9.14	4.17	4.98	4.60	4.54
17	239.25	6.75	70.75	9.14	4.17	4.98	4.60	4.54
18	253.75	6.75	70.75	9.14	4.17	4.98	4.60	4.54
19	268.25	6.75	70.75	9.14	4.17	4.98	4.60	4.54
20	282.75	6.75	70.75	9.14	4.17	4.98	4.60	4.54
21	297.25	6.75	70.60	9.12	4.16	4.97	4.59	4.53
22	311.75	6.75	70.31	9.09	4.14	4.95	4.57	4.51
23	326.25	6.75	70.02	9.05	4.12	4.93	4.56	4.50
24	340.75	6.75	69.73	9.02	4.10	4.91	4.54	4.48
25	355.40	6.75	69.44	8.98	4.08	4.90	4.52	4.46
26	370.20	6.75	69.15	8.94	4.07	4.88	4.50	4.44
27	385.00	6.75	68.86	8.91	4.05	4.86	4.48	4.42
28	399.80	6.75	68.57	8.87	4.03	4.84	4.47	4.40
29	414.60	6.75	68.27	8.83	4.01	4.82	4.45	4.39
30	429.40	6.75	67.98	8.80	3.99	4.80	4.43	4.37

Note that, $K_0 = 0.5$, i.e. $\sigma_h = 0.5 * \sigma_y$

Element #	X ft	Y ft	depth ft	σ_y (total) ksf	P.W.P (Static) ksf	σ_y (effective) ksf	P.W.P (Steady S) ksf	σ_y (effective) ksf
31	444.20	6.75	67.69	8.76	3.97	4.79	4.41	4.35
32	459.00	6.75	67.40	8.72	3.96	4.77	4.39	4.33
33	473.80	6.75	67.11	8.69	3.94	4.75	4.37	4.31
34	488.60	6.75	66.82	8.65	3.92	4.73	4.36	4.29
35	505.13	6.75	66.49	8.61	3.90	4.71	4.34	4.27
36	523.38	6.75	66.14	8.57	3.88	4.69	4.31	4.25
37	541.63	6.75	65.78	8.52	3.86	4.67	4.29	4.23
38	559.88	6.75	65.43	8.48	3.83	4.64	4.27	4.21
39	578.13	6.75	65.25	8.46	3.82	4.63	4.26	4.20
40	596.38	6.75	65.25	8.46	3.82	4.63	4.26	4.20
41	614.63	6.75	65.25	8.46	3.82	4.63	4.26	4.20
42	632.88	6.75	65.25	8.46	3.82	4.63	4.26	4.20
43	651.13	6.75	65.25	8.46	3.82	4.63	4.26	4.20
44	669.38	6.75	65.25	8.46	3.82	4.63	4.26	4.20
45	687.63	6.75	65.25	8.46	3.82	4.63	4.26	4.20
46	705.88	6.75	65.25	8.46	3.82	4.63	4.26	4.20
47	724.13	6.75	65.25	8.46	3.82	4.63	4.26	4.20
48	742.38	6.75	65.25	8.46	3.82	4.63	4.26	4.20
49	760.63	6.75	65.25	8.46	3.82	4.63	4.26	4.20
50	778.88	6.75	65.25	8.46	3.82	4.63	4.26	4.20
51	797.13	6.75	65.25	8.46	3.82	4.63	4.26	4.20
52	815.38	6.75	65.25	8.46	3.82	4.63	4.26	4.20
53	833.63	6.75	65.25	8.46	3.82	4.63	4.26	4.20
54	851.88	6.75	65.25	8.46	3.82	4.63	4.26	4.20
55	7.25	19.00	58.50	7.55	3.40	4.15	3.84	3.71
56	21.75	19.00	58.50	7.55	3.40	4.15	3.84	3.71
57	36.25	19.00	58.50	7.55	3.40	4.15	3.84	3.71
58	50.75	19.00	58.50	7.55	3.40	4.15	3.84	3.71
59	65.25	19.00	58.50	7.55	3.40	4.15	3.84	3.71
60	79.75	19.00	58.50	7.55	3.40	4.15	3.84	3.71

Element #	X ft	Y ft	depth ft	σ_y (total) ksf	P.W.P (Static) ksf	σ_y (effective) ksf	P.W.P (Steady S) ksf	σ_y (effective) ksf
61	94.25	19.00	58.50	7.55	3.40	4.15	3.84	3.71
62	108.75	19.00	58.50	7.55	3.40	4.15	3.84	3.71
63	123.25	19.00	58.50	7.55	3.40	4.15	3.84	3.71
64	137.75	19.00	58.50	7.55	3.40	4.15	3.84	3.71
65	152.25	19.00	58.50	7.55	3.40	4.15	3.84	3.71
66	166.75	19.00	58.50	7.55	3.40	4.15	3.84	3.71
67	181.25	19.00	58.50	7.55	3.40	4.15	3.84	3.71
68	195.75	19.00	58.50	7.55	3.40	4.15	3.84	3.71
69	210.25	19.00	58.50	7.55	3.40	4.15	3.84	3.71
70	224.75	19.00	58.50	7.55	3.40	4.15	3.84	3.71
71	239.25	19.00	58.50	7.55	3.40	4.15	3.84	3.71
72	253.75	19.00	58.50	7.55	3.40	4.15	3.84	3.71
73	268.25	19.00	58.50	7.55	3.40	4.15	3.84	3.71
74	282.75	19.00	58.50	7.55	3.40	4.15	3.84	3.71
75	297.25	19.00	58.35	7.53	3.39	4.14	3.83	3.70
76	311.75	19.00	58.06	7.50	3.37	4.12	3.81	3.69
77	326.25	19.00	57.77	7.46	3.36	4.10	3.79	3.67
78	340.75	19.00	57.48	7.42	3.34	4.09	3.77	3.65
79	355.40	19.00	57.19	7.39	3.32	4.07	3.76	3.63
80	370.20	19.00	56.90	7.35	3.30	4.05	3.74	3.61
81	385.00	19.00	56.61	7.31	3.28	4.03	3.72	3.59
82	399.80	19.00	56.32	7.28	3.26	4.01	3.70	3.58
83	414.60	19.00	56.02	7.24	3.25	3.99	3.68	3.56
84	429.40	19.00	55.73	7.20	3.23	3.98	3.66	3.54
85	444.20	19.00	55.44	7.17	3.21	3.96	3.65	3.52
86	459.00	19.00	55.15	7.13	3.19	3.94	3.63	3.50
87	473.80	19.00	54.86	7.09	3.17	3.92	3.61	3.48
88	488.60	19.00	54.57	7.06	3.16	3.90	3.59	3.47
89	505.13	19.00	54.24	7.02	3.14	3.88	3.57	3.45
90	523.38	19.00	53.89	6.97	3.11	3.86	3.55	3.42

Element #	X ft	Y ft	depth ft	σ_y (total) ksf	P. W. P (Static) ksf	σ_y (effective) ksf	P. W. P (Steady S) ksf	σ_y (effective) ksf
91	541.63	19.00	53.53	6.93	3.09	3.84	3.53	3.40
92	559.88	19.00	53.18	6.88	3.07	3.82	3.51	3.38
93	578.13	19.00	53.00	6.86	3.06	3.80	3.49	3.37
94	596.38	19.00	53.00	6.86	3.06	3.80	3.49	3.37
95	614.63	19.00	53.00	6.86	3.06	3.80	3.49	3.37
96	632.88	19.00	53.00	6.86	3.06	3.80	3.49	3.37
97	651.13	19.00	53.00	6.86	3.06	3.80	3.49	3.37
98	669.38	19.00	53.00	6.86	3.06	3.80	3.49	3.37
99	687.63	19.00	53.00	6.86	3.06	3.80	3.49	3.37
100	705.88	19.00	53.00	6.86	3.06	3.80	3.49	3.37
101	724.13	19.00	53.00	6.86	3.06	3.80	3.49	3.37
102	742.38	19.00	53.00	6.86	3.06	3.80	3.49	3.37
103	760.63	19.00	53.00	6.86	3.06	3.80	3.49	3.37
104	778.88	19.00	53.00	6.86	3.06	3.80	3.49	3.37
105	797.13	19.00	53.00	6.86	3.06	3.80	3.49	3.37
106	815.38	19.00	53.00	6.86	3.06	3.80	3.49	3.37
107	833.63	19.00	53.00	6.86	3.06	3.80	3.49	3.37
108	851.88	19.00	53.00	6.86	3.06	3.80	3.49	3.37
109	7.25	30.50	47.00	6.06	2.68	3.37	3.12	2.94
110	21.75	30.50	47.00	6.06	2.68	3.37	3.12	2.94
111	36.25	30.50	47.00	6.06	2.68	3.37	3.12	2.94
112	50.75	30.50	47.00	6.06	2.68	3.37	3.12	2.94
113	65.25	30.50	47.00	6.06	2.68	3.37	3.12	2.94
114	79.75	30.50	47.00	6.06	2.68	3.37	3.12	2.94
115	94.25	30.50	47.00	6.06	2.68	3.37	3.12	2.94
116	108.75	30.50	47.00	6.06	2.68	3.37	3.12	2.94
117	123.25	30.50	47.00	6.06	2.68	3.37	3.12	2.94
118	137.75	30.50	47.00	6.06	2.68	3.37	3.12	2.94
119	152.25	30.50	47.00	6.06	2.68	3.37	3.12	2.94
120	166.75	30.50	47.00	6.06	2.68	3.37	3.12	2.94

Element #	X ft	Y ft	depth ft	σ_y (total) ksf	P.W.P (Static) ksf	σ_y (effective) ksf	P.W.P (Steady S) ksf	σ_y (effective) ksf
121	181.25	30.50	47.00	6.06	2.68	3.37	3.12	2.94
122	195.75	30.50	47.00	6.06	2.68	3.37	3.12	2.94
123	210.25	30.50	47.00	6.06	2.68	3.37	3.12	2.94
124	224.75	30.50	47.00	6.06	2.68	3.37	3.12	2.94
125	239.25	30.50	47.00	6.06	2.68	3.37	3.12	2.94
126	253.75	30.50	47.00	6.06	2.68	3.37	3.12	2.94
127	268.25	30.50	47.00	6.06	2.68	3.37	3.12	2.94
128	282.75	30.50	47.00	6.06	2.68	3.37	3.12	2.94
129	297.25	30.50	46.85	6.04	2.67	3.36	3.11	2.93
130	311.75	30.50	46.56	6.00	2.66	3.34	3.09	2.91
131	326.25	30.50	46.27	5.96	2.64	3.33	3.07	2.89
132	340.75	30.50	45.98	5.93	2.62	3.31	3.06	2.87
133	355.40	30.50	45.69	5.89	2.60	3.29	3.04	2.85
134	370.20	30.50	45.40	5.85	2.58	3.27	3.02	2.83
135	385.00	30.50	45.11	5.82	2.57	3.25	3.00	2.82
136	399.80	30.50	44.82	5.78	2.55	3.24	2.98	2.80
137	414.60	30.50	44.52	5.75	2.53	3.22	2.97	2.78
138	429.40	30.50	44.23	5.71	2.51	3.20	2.95	2.76
139	444.20	30.50	43.94	5.67	2.49	3.18	2.93	2.74
140	459.00	30.50	43.65	5.64	2.47	3.16	2.91	2.73
141	473.80	30.50	43.36	5.60	2.46	3.14	2.89	2.71
142	488.60	30.50	43.07	5.56	2.44	3.13	2.87	2.69
143	505.13	30.50	42.74	5.52	2.42	3.11	2.85	2.67
144	523.38	30.50	42.39	5.48	2.40	3.08	2.83	2.65
145	541.63	30.50	42.03	5.43	2.37	3.06	2.81	2.62
146	559.88	30.50	41.68	5.39	2.35	3.04	2.79	2.60
147	578.13	30.50	41.50	5.37	2.34	3.03	2.78	2.59
148	596.38	30.50	41.50	5.37	2.34	3.03	2.78	2.59
149	614.63	30.50	41.50	5.37	2.34	3.03	2.78	2.59
150	632.88	30.50	41.50	5.37	2.34	3.03	2.78	2.59

Element #	X ft	Y ft	depth ft	σ_x (total) ksf	P.W.P (Static) ksf	σ_x (effective) ksf	P.W.P (Steady S) ksf	σ_x (effective) ksf
151	651.13	30.50	41.50	5.37	2.34	3.03	2.78	2.59
152	669.38	30.50	41.50	5.37	2.34	3.03	2.78	2.59
153	687.63	30.50	41.50	5.37	2.34	3.03	2.78	2.59
154	705.88	30.50	41.50	5.37	2.34	3.03	2.78	2.59
155	724.13	30.50	41.50	5.37	2.34	3.03	2.78	2.59
156	742.38	30.50	41.50	5.37	2.34	3.03	2.78	2.59
157	760.63	30.50	41.50	5.37	2.34	3.03	2.78	2.59
158	778.88	30.50	41.50	5.37	2.34	3.03	2.78	2.59
159	797.13	30.50	41.50	5.37	2.34	3.03	2.78	2.59
160	815.38	30.50	41.50	5.37	2.34	3.03	2.78	2.59
161	833.63	30.50	41.50	5.37	2.34	3.03	2.78	2.59
162	851.88	30.50	41.50	5.37	2.34	3.03	2.78	2.59
163	7.25	44.00	33.50	4.26	1.84	2.42	2.28	1.98
164	21.75	44.00	33.50	4.26	1.84	2.42	2.28	1.98
165	36.25	44.00	33.50	4.26	1.84	2.42	2.28	1.98
166	50.75	44.00	33.50	4.26	1.84	2.42	2.28	1.98
167	65.25	44.00	33.50	4.26	1.84	2.42	2.28	1.98
168	79.75	44.00	33.50	4.26	1.84	2.42	2.28	1.98
169	94.25	44.00	33.50	4.26	1.84	2.42	2.28	1.98
170	108.75	44.00	33.50	4.26	1.84	2.42	2.28	1.98
171	123.25	44.00	33.50	4.26	1.84	2.42	2.28	1.98
172	137.75	44.00	33.50	4.26	1.84	2.42	2.28	1.98
173	152.25	44.00	33.50	4.26	1.84	2.42	2.28	1.98
174	166.75	44.00	33.50	4.26	1.84	2.42	2.28	1.98
175	181.25	44.00	33.50	4.26	1.84	2.42	2.28	1.98
176	195.75	44.00	33.50	4.26	1.84	2.42	2.28	1.98
177	210.25	44.00	33.50	4.26	1.84	2.42	2.28	1.98
178	224.75	44.00	33.50	4.26	1.84	2.42	2.28	1.98
179	239.25	44.00	33.50	4.26	1.84	2.42	2.28	1.98
180	253.75	44.00	33.50	4.26	1.84	2.42	2.28	1.98

Element #	X ft	Y ft	depth ft	σ_x (total) ksf	P.W.P (Static) ksf	σ_x (effective) ksf	P.W.P (Steady S) ksf	σ_y (effective) ksf
181	268.25	44.00	33.50	4.26	1.84	2.42	2.28	1.98
182	282.75	44.00	33.50	4.26	1.84	2.42	2.28	1.98
183	297.25	44.00	33.35	4.24	1.83	2.41	2.27	1.98
184	311.75	44.00	33.06	4.21	1.81	2.39	2.25	1.96
185	326.25	44.00	32.77	4.17	1.80	2.38	2.23	1.94
186	340.75	44.00	32.48	4.14	1.78	2.36	2.21	1.92
187	355.40	44.00	32.19	4.10	1.76	2.34	2.20	1.90
188	370.20	44.00	31.90	4.06	1.74	2.32	2.18	1.88
189	385.00	44.00	31.61	4.03	1.72	2.30	2.16	1.87
190	399.80	44.00	31.32	3.99	1.70	2.28	2.14	1.85
191	414.60	44.00	31.02	3.95	1.69	2.27	2.12	1.83
192	429.40	44.00	30.73	3.92	1.67	2.25	2.10	1.81
193	444.20	44.00	30.44	3.88	1.65	2.23	2.09	1.79
194	459.00	44.00	30.15	3.84	1.63	2.21	2.07	1.78
195	473.80	44.00	29.86	3.81	1.61	2.19	2.05	1.76
196	488.60	44.00	29.57	3.77	1.60	2.18	2.03	1.74
197	505.13	44.00	29.24	3.73	1.58	2.16	2.01	1.72
198	523.38	44.00	28.89	3.69	1.55	2.13	1.99	1.70
199	541.63	44.00	28.53	3.64	1.53	2.11	1.97	1.67
200	559.88	44.00	28.18	3.60	1.51	2.09	1.95	1.65
201	578.13	44.00	28.00	3.58	1.50	2.08	1.93	1.64
202	596.38	44.00	28.00	3.58	1.50	2.08	1.93	1.64
203	614.63	44.00	28.00	3.58	1.50	2.08	1.93	1.64
204	632.88	44.00	28.00	3.58	1.50	2.08	1.93	1.64
205	651.13	44.00	28.00	3.58	1.50	2.08	1.93	1.64
206	669.38	44.00	28.00	3.58	1.50	2.08	1.93	1.64
207	687.63	44.00	28.00	3.58	1.50	2.08	1.93	1.64
208	705.88	44.00	28.00	3.58	1.50	2.08	1.93	1.64
209	724.13	44.00	28.00	3.58	1.50	2.08	1.93	1.64
210	742.38	44.00	28.00	3.58	1.50	2.08	1.93	1.64

Element #	X ft	Y ft	depth ft	σ_y (total) ksf	P.W.P (Static) ksf	σ_y (effective) ksf	P.W.P (Steady S) ksf	σ_y (effective) ksf
211	760.63	44.00	28.00	3.58	1.50	2.08	1.93	1.64
212	778.88	44.00	28.00	3.58	1.50	2.08	1.93	1.64
213	797.13	44.00	28.00	3.58	1.50	2.08	1.93	1.64
214	815.38	44.00	28.00	3.58	1.50	2.08	1.93	1.64
215	833.63	44.00	28.00	3.58	1.50	2.08	1.93	1.64
216	851.88	44.00	28.00	3.58	1.50	2.08	1.93	1.64
217	7.25	57.99	19.51	2.44	0.97	1.47	1.34	1.10
218	21.75	57.97	19.54	2.44	0.97	1.47	1.34	1.10
219	36.25	57.94	19.56	2.44	0.97	1.47	1.34	1.10
220	50.75	57.92	19.58	2.45	0.97	1.48	1.34	1.10
221	65.25	57.90	19.60	2.45	0.97	1.48	1.35	1.10
222	79.75	57.87	19.63	2.45	0.98	1.48	1.35	1.11
223	94.25	57.85	19.65	2.46	0.98	1.48	1.35	1.11
224	108.75	57.83	19.67	2.46	0.98	1.48	1.35	1.11
225	123.25	57.80	19.70	2.46	0.98	1.48	1.35	1.11
226	137.75	57.78	19.72	2.47	0.98	1.48	1.36	1.11
227	152.25	57.76	19.74	2.47	0.98	1.49	1.36	1.11
228	166.75	57.73	19.77	2.47	0.98	1.49	1.36	1.11
229	181.25	57.71	19.79	2.47	0.99	1.49	1.36	1.11
230	195.75	57.69	19.81	2.48	0.99	1.49	1.36	1.11
231	210.25	57.66	19.84	2.48	0.99	1.49	1.36	1.12
232	224.75	57.64	19.86	2.48	0.99	1.49	1.37	1.12
233	239.25	57.62	19.88	2.49	0.99	1.49	1.37	1.12
234	253.75	57.60	19.91	2.49	0.99	1.50	1.37	1.12
235	268.25	57.57	19.93	2.49	0.99	1.50	1.37	1.12
236	282.75	57.55	19.95	2.49	1.00	1.50	1.37	1.12
237	297.25	57.53	19.83	2.48	0.99	1.49	1.36	1.11
238	311.75	57.50	19.56	2.45	0.97	1.47	1.35	1.10
239	326.25	57.48	19.29	2.41	0.95	1.46	1.33	1.08
240	340.75	57.46	19.03	2.38	0.94	1.44	1.31	1.07

Element #	X ft	Y ft	depth ft	σ_y (total) ksf	P.W.P (Static) ksf	σ_y (effective) ksf	P.W.P (Steady S) ksf	σ_y (effective) ksf
241	355.40	57.43	18.76	2.34	0.92	1.42	1.30	1.05
242	370.20	57.41	18.49	2.31	0.90	1.41	1.28	1.03
243	385.00	57.39	18.22	2.28	0.89	1.39	1.26	1.02
244	399.80	57.36	17.95	2.24	0.87	1.37	1.24	1.00
245	414.60	57.34	17.69	2.21	0.85	1.36	1.23	0.98
246	429.40	57.31	17.42	2.18	0.84	1.34	1.21	0.97
247	444.20	57.29	17.15	2.14	0.82	1.32	1.19	0.95
248	459.00	57.27	16.88	2.11	0.80	1.31	1.17	0.94
249	473.80	57.24	16.61	2.08	0.79	1.29	1.16	0.92
250	488.60	57.22	16.35	2.04	0.77	1.27	1.14	0.90
251	505.13	57.19	16.05	2.01	0.75	1.25	1.12	0.89
252	523.38	57.16	15.72	1.97	0.73	1.23	1.10	0.87
253	541.63	57.14	15.40	1.92	0.71	1.21	1.08	0.85
254	559.88	57.11	15.07	1.88	0.69	1.19	1.06	0.83
255	578.13	57.08	14.92	1.87	0.68	1.18	1.05	0.81
256	596.38	57.05	14.95	1.87	0.68	1.19	1.05	0.82
257	614.63	57.02	14.98	1.87	0.69	1.19	1.05	0.82
258	632.88	56.99	15.01	1.88	0.69	1.19	1.06	0.82
259	651.13	56.96	15.04	1.88	0.69	1.19	1.06	0.82
260	669.38	56.93	15.07	1.88	0.69	1.19	1.06	0.82
261	687.63	56.90	15.10	1.89	0.69	1.19	1.06	0.82
262	705.88	56.87	15.13	1.89	0.69	1.20	1.07	0.83
263	724.13	56.84	15.16	1.89	0.70	1.20	1.07	0.83
264	742.38	56.81	15.19	1.90	0.70	1.20	1.07	0.83
265	760.63	56.79	15.22	1.90	0.70	1.20	1.07	0.83
266	778.88	56.76	15.24	1.91	0.70	1.20	1.07	0.83
267	797.13	56.73	15.27	1.91	0.70	1.21	1.08	0.83
268	815.38	56.70	15.30	1.91	0.71	1.21	1.08	0.83
269	833.63	56.67	15.33	1.92	0.71	1.21	1.08	0.84
270	851.88	56.64	15.36	1.92	0.71	1.21	1.08	0.84

Element #	X ft	Y ft	depth ft	σ_y (total) ksf	P.W.P (Static) ksf	σ_y (effective) ksf	P.W.P (Steady S) ksf	σ_y (effective) ksf
271	7.25	70.99	6.51	0.81	0.16	0.66	0.40	0.42
272	21.75	70.97	6.54	0.82	0.16	0.66	0.40	0.42
273	36.25	70.94	6.56	0.82	0.16	0.66	0.40	0.42
274	50.75	70.92	6.58	0.82	0.16	0.66	0.40	0.42
275	65.25	70.90	6.60	0.83	0.16	0.66	0.41	0.42
276	79.75	70.87	6.63	0.83	0.16	0.66	0.41	0.42
277	94.25	70.85	6.65	0.83	0.17	0.67	0.41	0.42
278	108.75	70.83	6.67	0.83	0.17	0.67	0.41	0.42
279	123.25	70.80	6.70	0.84	0.17	0.67	0.41	0.42
280	137.75	70.78	6.72	0.84	0.17	0.67	0.41	0.43
281	152.25	70.76	6.74	0.84	0.17	0.67	0.42	0.43
282	166.75	70.73	6.77	0.85	0.17	0.67	0.42	0.43
283	181.25	70.71	6.79	0.85	0.17	0.67	0.42	0.43
284	195.75	70.69	6.81	0.85	0.18	0.68	0.42	0.43
285	210.25	70.66	6.84	0.85	0.18	0.68	0.42	0.43
286	224.75	70.64	6.86	0.86	0.18	0.68	0.42	0.43
287	239.25	70.62	6.88	0.86	0.18	0.68	0.43	0.43
288	253.75	70.60	6.91	0.86	0.18	0.68	0.43	0.44
289	268.25	70.57	6.93	0.87	0.18	0.68	0.43	0.44
290	282.75	70.55	6.95	0.87	0.18	0.68	0.43	0.44
291	297.25	70.45	6.90	0.86	0.18	0.68	0.43	0.44
292	311.75	70.28	6.78	0.85	0.17	0.67	0.42	0.43
293	326.25	70.12	6.66	0.83	0.17	0.67	0.41	0.42
294	340.75	69.95	6.54	0.82	0.16	0.66	0.40	0.41
295	355.40	69.78	6.41	0.80	0.15	0.65	0.39	0.41
296	370.20	69.61	6.29	0.79	0.14	0.64	0.39	0.40
297	385.00	69.44	6.17	0.77	0.14	0.64	0.38	0.39
298	399.80	69.27	6.05	0.76	0.13	0.63	0.37	0.39
299	414.60	69.10	5.92	0.74	0.12	0.62	0.36	0.38
300	429.40	68.93	5.80	0.73	0.11	0.61	0.35	0.37

Element #	X ft	Y ft	depth ft	σ_y (total) ksf	P.W.P (Static) ksf	σ_y (effective) ksf	P.W.P (Steady S) ksf	σ_y (effective) ksf
301	444.20	68.76	5.68	0.71	0.10	0.61	0.35	0.36
302	459.00	68.59	5.56	0.69	0.10	0.60	0.34	0.36
303	473.80	68.42	5.44	0.68	0.09	0.59	0.33	0.35
304	488.60	68.25	5.31	0.66	0.08	0.58	0.32	0.34
305	505.13	68.06	5.18	0.65	0.07	0.57	0.31	0.34
306	523.38	67.86	5.03	0.63	0.06	0.56	0.30	0.33
307	541.63	67.65	4.88	0.61	0.05	0.56	0.29	0.32
308	559.88	67.45	4.73	0.59	0.05	0.55	0.28	0.31
309	578.13	67.33	4.67	0.58	0.04	0.54	0.29	0.30
310	596.38	67.30	4.70	0.59	0.04	0.54	0.29	0.30
311	614.63	67.27	4.73	0.59	0.05	0.55	0.29	0.30
312	632.88	67.24	4.76	0.60	0.05	0.55	0.29	0.30
313	651.13	67.21	4.79	0.60	0.05	0.55	0.29	0.30
314	669.38	67.18	4.82	0.60	0.05	0.55	0.30	0.31
315	687.63	67.15	4.85	0.61	0.05	0.55	0.30	0.31
316	705.88	67.12	4.88	0.61	0.05	0.55	0.30	0.31
317	724.13	67.09	4.91	0.61	0.06	0.56	0.30	0.31
318	742.38	67.06	4.94	0.62	0.06	0.56	0.31	0.31
319	760.63	67.04	4.97	0.62	0.06	0.56	0.31	0.31
320	778.88	67.01	4.99	0.62	0.06	0.56	0.31	0.31
321	797.13	66.98	5.02	0.63	0.06	0.56	0.31	0.32
322	815.38	66.95	5.05	0.63	0.07	0.57	0.31	0.32
323	833.63	66.92	5.08	0.64	0.07	0.57	0.32	0.32
324	851.88	66.89	5.11	0.64	0.07	0.57	0.32	0.32

Appendix 8

**Portion of FEADAM Output of The stresses
for The Undrained Case (i.e. All Layers Are
Undrained Except for The Artesian)**

Appendix 9

**Portion of FEADAM Output of The stresses
for The Undrained Case (i.e. Only The Layer
Above The Artesian Is Undrained)**

Appendix 10

Boring Log for The NDOT Sampling

Operation Done on 9/11/96



Kenny C. Guinn, Governor

Nevada Department of Transportation
Tom Stephens, P.E. Director
Prepared by Research Division
Alan Hilton, Research Manager
(775) 888-7803
ahilton@dot.state.nv.us
1263 South Stewart Street
Carson City, Nevada 89712



Kenny C. Guinn, Governor

Nevada Department of Transportation
Tom Stephens, P.E. Director
Prepared by Research Division
Alan Hilton, Research Manager
(775) 888-7803
ahilton@dot.state.nv.us
1263 South Stewart Street
Carson City, Nevada 89712